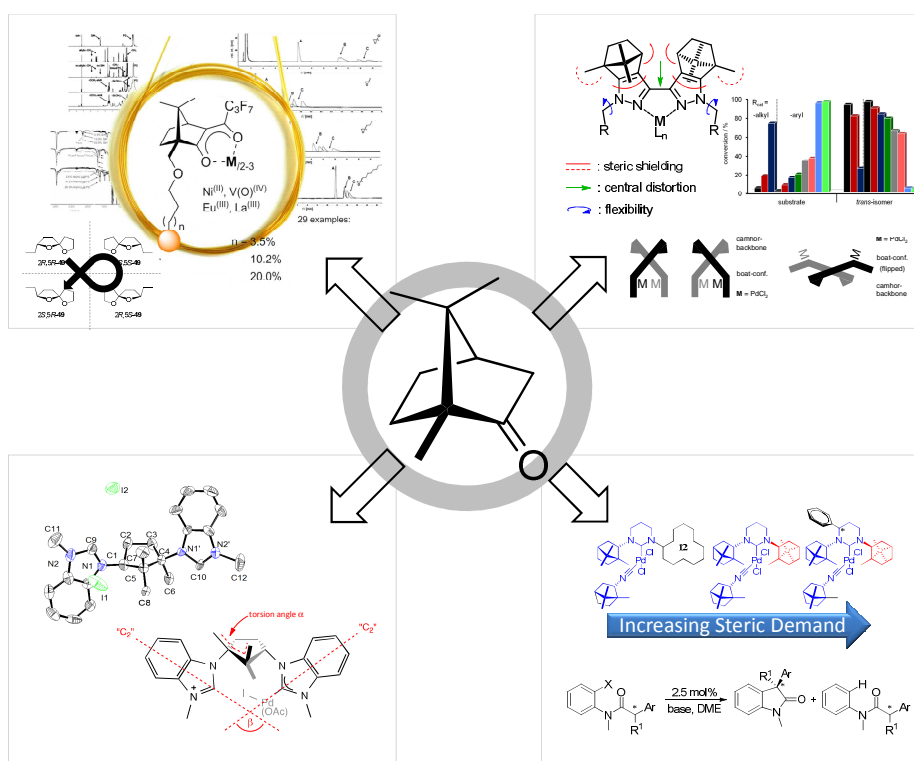


Camphor as Chiral Motif in Ligand Design

Applications in Catalysis and Complexation Gas-Chromatography



DISSERTATION

MARKUS JÜRGEN SPALLEK

2012

INAUGURAL-DISSERTATION

zur

Erlangung der Doktorwürde

der

Naturwissenschaftlich-Mathematischen

Gesamtfakultät

der

Ruprecht-Karls-Universität

zu Heidelberg

vorgelegt von

M. Sc. Chem. Markus Jürgen Spallek

aus Mering

Tag der mündlichen Prüfung: 20.04.2012

Camphor as Chiral Motif in Ligand Design

Applications in Catalysis and Complexation Gas-Chromatography

Dekan: Prof. Dr. A. Stephen K. Hashmi

Gutachter: Prof. Dr. Oliver Trapp

Prof. Dr. A. Stephen K. Hashmi

dedicated to my family

Angelika, Jürgen and Martin

Quos irrupta tenet copula, nee, malis

Divulsus quserimoniis,

Suprema citius solvet amor die.

Quintus Horacius Flaccus (C. 1, 13, 17).

(Happy, happy, happy they

Whose living love, untroubled by all strife

Binds them till the last sad day,

Nor parts asunder but with parting life!)

Acknowledgement

I want to express my sincere gratitude and appreciation to my PhD supervisor and mentor Prof. Dr. Oliver Trapp for his generous support during the time of my research, his consistent interest in the progress of my work as well as valuable suggestions and valuable discussions. Especially, I enjoyed the excellent working conditions and literally no wishes were left unfulfilled with the plenty of top, first-class equipment available. This allowed me not only having fun doing my research studies but also allowed me to get a broad, profound knowledge in analytical and surface chemistry (beside the synthetic parts of my work). Furthermore, I want to thank Prof. Dr. Oliver Trapp for an overall pleasant atmosphere, the fruitful discussions and his anytime accessibility! I enjoyed my scientific freedom very much, which was only limited to the use of camphor related systems. Overall, this opportunity to choose the topics and course of my research studies by myself and the stimulating environment made it possible being curious and creative on a daily basis.

Prof. Dr. A. Stephen K. Hashmi is gratefully acknowledged for refereeing this thesis.

The Graduate College 850 “Modeling of Molecular Properties” granted me with a Doctoral Fellowship that allowed me to focus on my studies, for which I am very grateful.

I thank the SFB 623 “Molecular Catalysts – Structure and Functional Design” for financial support of my research.

I thank Prof. Dr. M. Enders for fruitful discussions and high resolution nuclear magnetic resonance measurements in the analytical department of inorganic chemistry.

This thesis would have not been possible without ideas, suggestions and discussions with colleagues and friends. In particular, I would like to thank Christian Lothschütz and Dominic Riedel and for fruitful discussions, the overall pleasant atmosphere, the confidence and exchanging ideas.

The students performing their bachelor and master theses and advanced research internships under my supervision, especially Golo Storch and Skrollan Stockinger as well as Constantin Böhling, Alexandra S. Burk, Sylvie C. Drayss, Mike Guericke and Jan J. König are acknowledged.

I also thank my colleagues in Heidelberg, in particular Alexander, Andrea, Caro, Frank, Johannes, Kerstin, Matthias, Simone, Sylvie and Ute for their generous support.

The members of the analytical service departments at the University of Heidelberg, namely Dr. Jürgen Gross, Doris Lang, Iris Mitsch, Norbert Nieth (MS), Dr. Jürgen Graf (NMR), Frank Rominger, Frank Dallmann (X-Ray), and Dr. Richard Goddard (X-Ray) at the Max-Planck-Institut für Kohlenforschung in Mülheim an der Ruhr are acknowledged for their continuous support and service.

I thank the Gesellschaft Deutscher Chemiker (GDCh) for travel grants and additional support during my work for the Jungchemikerforum in Heidelberg.

The Synchrotron Light Source ANKA for measuring time at the beamline is gratefully acknowledged.

A lot of thanks to all my friends in particular Basti, Bettina, Blob, Erik, Liu, Mathias, Matthias, Micha, Michael, Niko, Pascal and Romi.

I am deeply grateful for the consistent and strong support of my beloved family, Angelika, Jürgen & Martin, and for their support of my academic career. Devoid their faith and loving care my present goals would not have been reached at all!

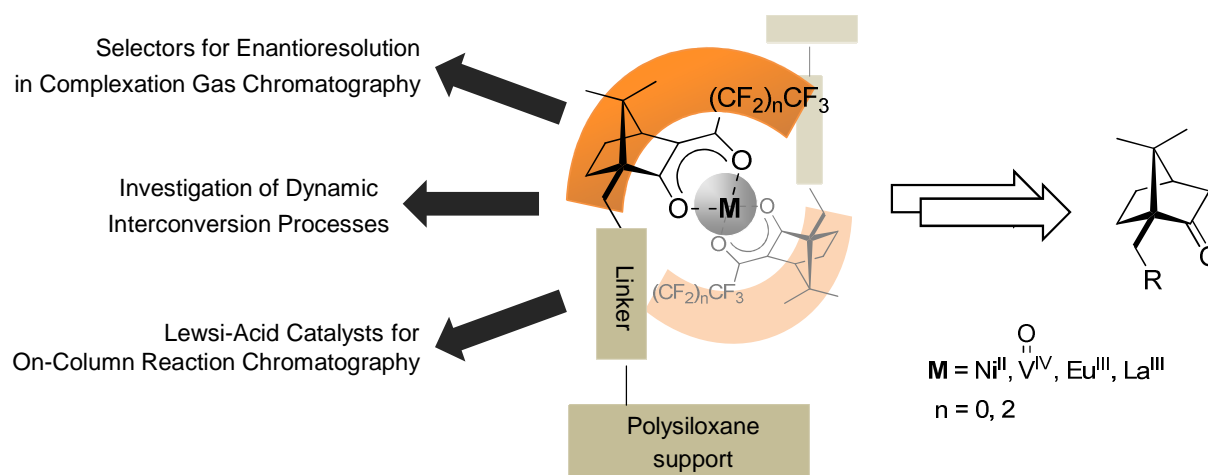
Abstract

Natural *d*-(+)-camphor represents a privileged and structural versatile motif originating from the chiral pool and is often employed for the development of novel ligands and catalysts, which are broadly applicable in asymmetric synthesis, catalysis and separation science. Besides their use as chiral auxiliaries, as lewis-acid catalysts and as *N*-heterocyclic ligands in asymmetric transformations they are known to be powerful selectors for the separation of enantiomers and stereoisomers of various compounds. Discrimination of enantiomers can be realized in homogeneous and heterogeneous systems. Camphor-based NMR-shift reagents are well established auxiliaries for enantiomer analysis in the liquid-liquid phase, but camphor derivatives can also be employed for chromatographic separations in gas-liquid (GC, CGC), liquid-liquid phases (LC) and super-critical-phases (SFC). This thesis is intended to further extend the scope of camphor and camphor-derived building blocks in the synthesis of chiral ligands, catalysts and selectors, their successful application in catalysis and in enantioseparation sciences.

The thesis is divided into four chapters each focusing on the development of novel camphor-based compounds and their application as catalysts or selectors. A short introduction is given in each chapter dealing with recent progress in the field of interest as well as providing essential basics of the affected chemistry, like Pd-catalysis, polymer and separation science.

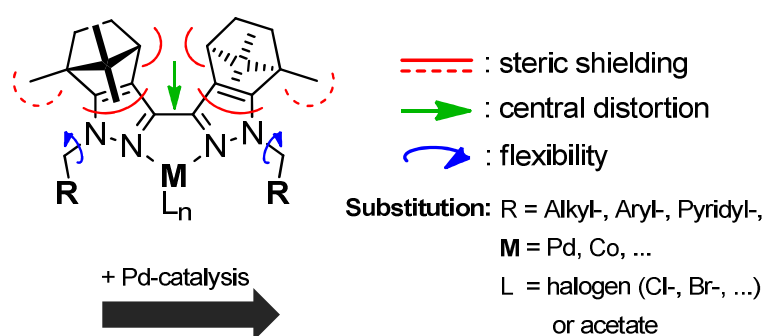
In chapter 1, after an introduction about general aspects of chiral stationary phases (CSPs) and their application in complexation gas chromatography (CGC), the total synthesis of novel, extended CSPs derived from 1*S*-(+)-camphorsulfonic acid is presented. The developed *Chirasil-Metal-OC*₃ phases are synthesized with overall high yield in only six steps. Two different approaches towards *Chirasil-Metals* featuring either an oxypropyl- or propylsulfanyl linker is presented. Furthermore, a new protocol for the fluoroacylation, which is one of the key steps in synthesis of 3-(perfluoroalkanoyl)-(1*R*)-camphorate metal complexes, is presented to improve the isolation and overall yield. Besides synthesis of the polysiloxane CSPs, this chapter focuses on the immobilization step furnishing the polymer-supported chiral ligand. Therefore, a detailed study for three different selector-concentrations on the polymer is given for the immobilization step and for the metal incorporation to the target metal-selectors using IR- and NMR spectroscopy. Overall seven different *Chirasil-Metal* polymers with different separation capabilities are reported by metal-incorporation of nickel(II), oxovanadium(IV), europium(III), lanthanum(III) and variation of the amount of ligand content

on the polymer (3.5%, 10.2% and 20.0%). Their performance in enantioselective complexation gas chromatography (CGC) is studied in terms of selector-type, selector-concentration, polymer film thickness, polymer composition and column length. Superior activity and separation of 29 small-sized compounds, encompassing *inter alia* epoxides, derivatized alkenes and alkynes as well as alcohols and amides, is presented, throughout with high separation factors α . The thermal stability and the broad applicability, synthetic versatility and efficiency of the newly derived *Chirasil-Metal-OC₃* phase is reported. Furthermore, the separation of enantiomers and epimers of the four stereoisomers of chalcogran, the principle component of the aggregation pheromone of the bark beetle *pityogenes chalcographus*, is reported and the kinetic data (ΔG^\ddagger , ΔH^\ddagger and ΔS^\ddagger) for the interconversion barrier for the epimerization process of chalcogran obtained by temperature-dependent measurements using dynamic complexation gas chromatography (DCGC) is presented. By comparison with results obtained by dynamic inclusion GC on *Chirasil- β -Dex* stationary phases an explanation for the differences in activation parameters is given. Moreover, a unique, novel approach to an efficient assignment of enantiomer configuration and determination of enantiomeric excesses via on column gas chromatography (*dynamic elution profiles by CSP-coupling*) is developed and presented. The advantages of this approach concerning sample purity, injection quantities and accessibility to enantiopure compounds is discussed. Furthermore, the separation of the major components of an interconversion plateau into separated peak areas by coupling of different separation columns is presented. Finally, the synthetic value and versatility of the camphor building block is demonstrated by a two-step procedure with stereoselective introduction of two new chiral centers (*S*-, *R*-) by coupling of two camphor molecules – an approach towards the development of acyclic chiral stationary phases (*cf.* Scheme 1).



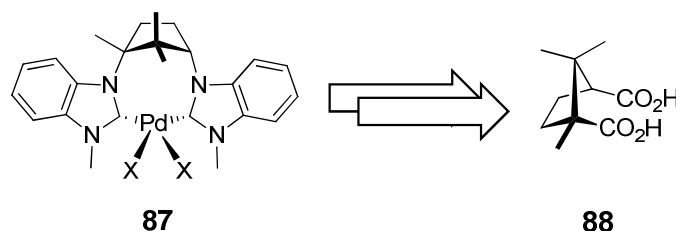
Scheme 1 Development of novel, immobilized CSPs from camphor and their application in complexation gas chromatography.

The 2nd chapter deals with the synthesis of a novel bidentate *N,N*-heterocyclic ligand motif derived from *d*-(+)-camphor. After a short introduction into isomerization reactions and the Wacker-oxidation of olefins, the synthesis and structural analysis of overall 11 new ligands is reported and the coordination to palladium, copper and cobalt is investigated. As the synthesis initially involves the preparation of diastereopure chiral camphortetraketones the focus was set on the investigation of the isomer distribution and configuration thereof, giving evidence for a new proto-chelate type, keto-enol tautomerism supported by X-ray crystallographic and VT proton NMR analysis. The preparation and the molecular structure of two, chiral bihomometallic transition-metal(I) complexes is described as well. The performance of three representative palladium catalysts exhibiting different electronic properties in the palladium-catalyzed copper-free Wacker oxidation of different alkenes is described and the obtained results are discussed in detail. A detailed study of all 11 Pd-catalysts in the selective isomerization of a series of substituted terminal arylpropenoids is presented. The influence of catalyst loading and the impact of acid and base additives is addressed. An extensive solvent, catalyst and finally substrate screening is undertaken and the results are discussed concerning steric and electronic effects of the ligands and employed solvents. The reaction mechanism involved is studied in detail using deuterium labeled solvents and substrates and the reaction rate orders of catalyst, substrate and solvent are determined by GC, GC-MS and NMR measurements. The integrity and stability of the catalyst system is demonstrated by multiple addition reaction cycles, successive filtration and isolation experiments. Finally, an extension of the bidentate 3,3'-bipyrazole ligand pattern to furnish 2nd generation tetradentate ligands and their palladium-complexes featuring either pyridine or methylpyridine as wingtip substituents is presented and their structural characteristics (atropisomerism) are discussed (*cf.* Scheme 2).



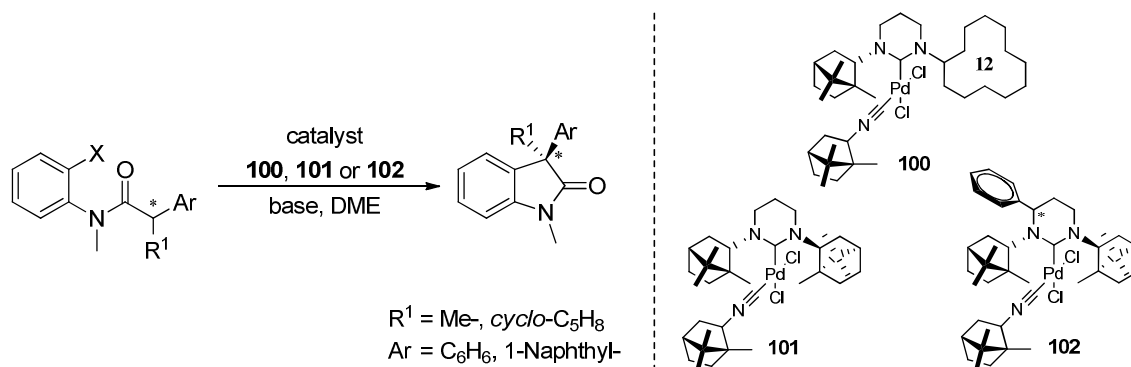
Scheme 2 Synthesis and catalytic application of novel camphor derived, bidentate 3,3'-bipyrazole palladium complexes.

Chapter 3 of this thesis focuses on the synthesis of a chiral NHC-pincer ligand derived from camphoric acid as the chiral building block. The preparation is presented in overall five steps in moderate to good overall yield. Two NHC-pincer ligands with differing counter ions and one dibenzotriazole ligand are described. The developed procedure allows the regioselective monosubstitution of the central chiral building block as validated by NMR spectroscopic and X-Ray crystallographic analysis. The molecular structures of the NHC- and triazole pincer ligand is presented and the structural characteristics are discussed in detail. The results are supported by X-ray crystallographic measurements and an explanation for the observed coordination properties is given (*cf.* Scheme 3).



Scheme 3 Target palladium pincer-complex **78** derived from camphoric acid.

Chapter 4 of this thesis focuses on the structure-reactivity relationship in the asymmetric intramolecular oxindole synthesis using Pd-NHC isonitrile catalysts (**100** – **102**) featuring increasing steric demand while maintaining the same chiral substitution pattern (camphor). After a short introduction into chiral NHCs used for these transformations, three six-membered hexahydropyrimidine core based, camphor-derived (bornylamine) NHC-Pd-isonitrile complexes are presented and their application in the enantioselective α -amide arylation to form 3,3-disubstituted oxindoles is described. The preparation of five different substrates bearing benzyl- and naphthyl-substituents and *N*-alkylation and the influence of the NHC-substitution pattern on enantioselectivity in the asymmetric α -arylation of amides is reported. Different enantioselectivities and a change in the reaction profile is observed. The results are discussed taking steric effects at the catalyst metal-center and steric demand of the substrates into account (*cf.* Scheme 4).



Scheme 4 Asymmetric oxindole synthesis using Pd-isonitrile complexes **100** – **102**.

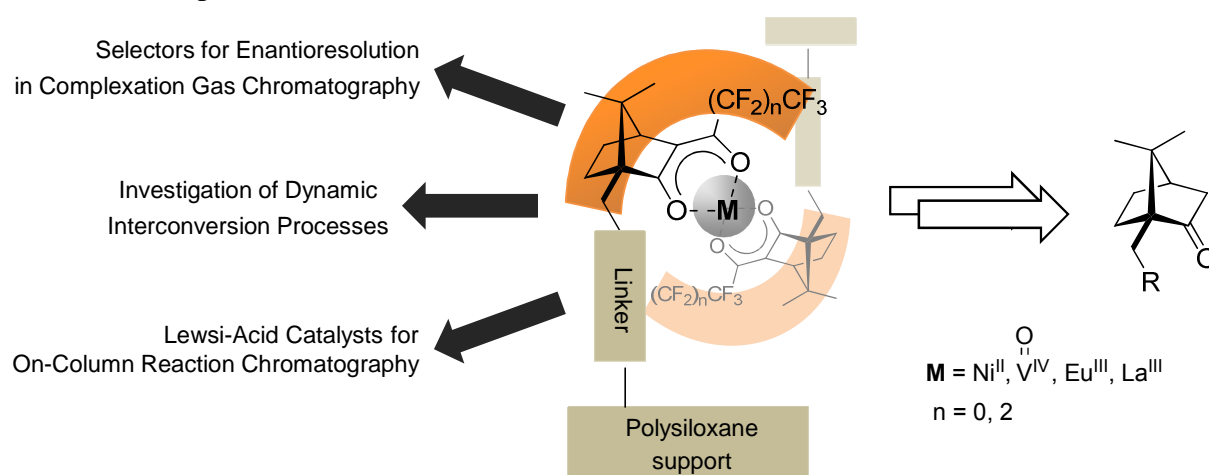
Zusammenfassung

Natürlicher *d*-(+)-Campher stellt – dem chiralen Pool entnommen – ein privilegiertes und strukturell vielseitiges Motiv dar. Es wird für die Entwicklung von neuen Liganden und Katalysatoren verwendet und besitzt ein breites Einsatzspektrum in der asymmetrischen Synthese, Katalyse und in der Enantiomerentrennung. Neben der Verwendung als chirales Auxiliär, als Lewis-Säure und als Baustein für *N*-heterozyklische Liganden findet es auch Einsatz in Form potenter Selektoren in homogenen und heterogenen Systemen. In der flüssig-flüssig Phase haben sich Campher-basierte NMR-shift Reagenzien für die Enantiomerenanalytik erfolgreich etabliert und einige Derivate sind ebenfalls in der gas-flüssig (GC, CGC), flüssig-flüssig (LC) und überkritischen Phase (SFC) einsetzbar. Die vorliegende Arbeit beschäftigt sich auf der Grundlage von Campher mit der Entwicklung neuer chiraler Liganden, Katalysatoren und Selektoren sowie deren Anwendung in der Katalyse und Trennanalytik.

Die vorliegende Arbeit ist in vier Kapitel unterteilt, von denen sich jedes mit der Entwicklung neuer Campher basierter Zielstrukturen sowie deren Einsatz als Katalysatoren oder Selektoren beschäftigt. Zu Beginn eines jeden Kapitels wird dabei auf den Stand aktueller Entwicklungen und die notwendigen Grundlagen der betreffenden Themengebiete, beispielsweise der Palladium-Katalyse, der Polymerwissenschaft und der Trennanalytik eingegangen.

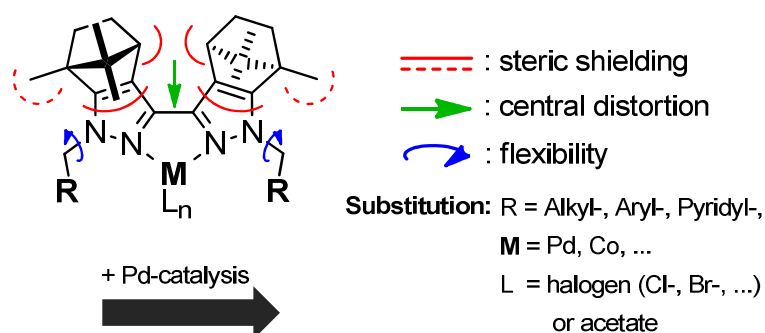
In Kapitel 1 wird, nach einer kurzen Einleitung die Grundlagen chiraler Stationärphasen (CSPs) und deren Anwendung in der Komplexierungs-Gaschromatographie betreffend, die Totalsynthese einer neuen CSP ausgehend von 1*S*-(+)-Camphersulfonsäure präsentiert. Die so genannten „*Chirasil-Metall-OC₃*“ Phasen sind in hohen Gesamtausbeuten über sechs Stufen zugänglich. Insgesamt werden zwei Vorgehensweisen für die *Chirasil-Metall* Phasen, basierend entweder auf einem oxypropyl- oder einem propanylsulfanyl Linker, vorgestellt. Für den Schlüsselschritt in der Synthese – eine Fluoracylierung – wird ein neues Verfahren vorgestellt, welches eine entscheidende Verbesserung der bestehenden Routen darstellt. Neben der Synthese der Polysiloxan CSPs liegt ein Hauptaugenmerk auf der Immobilisierung des Selektors am Polymer. Mittels IR- und NMR spektroskopischen Untersuchungen wird die Immobilisierung anhang dreier variierender Liganden-Konzentrationen auf dem Polymer sowie der Metalleinbau zu den fertigen Selektoren verfolgt und eine detaillierte Studie dargelegt. Mit der Wahl der Selektorkonzentration auf dem Polymer (3.5%, 10.2% und 20.0%) sowie dem Einbau von Nickel(II), Oxovanadium(II), Europium(III) und Lanthan(III) werden insgesamt sieben *Chirasil-Metall* Phasen mit unterschiedlichen Trenneigenschaften

vorgestellt. Der Einfluß des Metalls, der Selektorkonzentration, der Säulenlänge sowie der Schichtdicke und der Zusammensetzung des Polymers auf die Effizienz in der Komplexierungs-Gaschromatographie wird untersucht. Anhand der Auftrennung von 29 kleinen Substraten, bestehend aus derivatisierten Epoxiden, Alkenen, Alkinen, Alkoholen und Amiden wird die hohe Effizienz der neuen chiralen Stationärphasen aufgezeigt. Die thermische Belastbarkeit, das breite Einsatzspektrum der Phasen und die vielfältigen Möglichkeiten in der Synthese neuer CSPs wird dabei erläutert. Darüber hinaus wird die Auftrennung der Enantiomere und Epimere der vier Stereoisomeren von Chalcogran, dem Hauptbestandteil des Aggregationspheromons des Borkenkäfers *pitogenes chalcographus*, vorgestellt und die kinetischen Daten (ΔG^\ddagger , ΔH^\ddagger and ΔS^\ddagger) der Interkonversionsbarriere für den Epimerisationsprozess von Chalcogran durch temperaturabhängige Messungen mittels dynamischer Komplexierungs-Gaschromatographie (DCGC) ermittelt. Die erhaltenen Daten werden mit den Ergebnissen der Chalcograntrennung mittels dynamischer Einschluß-Gaschromatographie auf *Chirasil- β -Dex* verglichen und eingehend diskutiert. Weiterhin wird eine einzigartige, neu entwickelte Methode zur effizienten Konfigurationsbestimmung von Enantiomerenpaaren sowie optional der Ermittlung des Enantiomerenüberschusses einer konfiguratив unbekannt Probe mittels on-column Gaschromatographie vorgestellt. Die Generierung dynamischer Elutionsprofile durch Kupplung chiraler Stationärphasen vereint hierbei Vorteile der Gaschromatographie (kleine Probenvolumina, Analyse verunreinigter Proben und Schnelligkeit) mit der Möglichkeit der Enantiomerdifferenzierung in einer Methode und erlaubt erstmals eine reale, physikalische Trennung der einzelnen Bestandteile eines Interkonversionsprofils (Plateaus) in zeitlich separierte Peakflächen. Am Ende des Kapitels wird die stereoselektive Synthese eines Campherdimers durch selektive Einführung zweier chiraler Zentren (*S*-, *R*-) und dessen Verwendung als azyklische chirale Stationärphase für die GC besprochen (s. Schema 1).



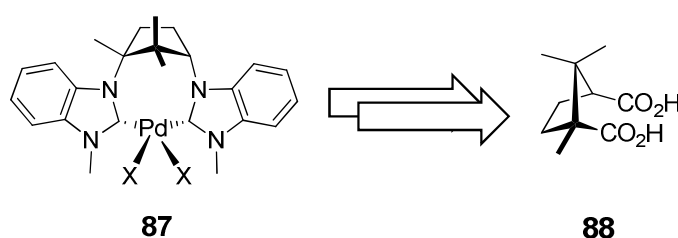
Schema 1 Entwicklung neuer, angebundener, chiraler Stationärphasen ausgehend von Campher und deren Anwendung in der Komplexierungsgaschromatographie.

Das zweite Kapitel der vorliegenden Arbeit hat die Synthese einer neuen, bidentaten *N,N*-heterozyklischen Ligandenklasse ausgehend von *d*-(+)-Campher zum Ziel. Nach einer kurzen Einleitung zu Isomerisierungsreaktionen und der Wacker-Oxidation von Olefinen wird die Synthese und Strukturanalyse von insgesamt 11 neuen Liganden beschrieben und die Komplexierungseigenschaften zu Palladium, Kupfer und Kobalt untersucht. Die Darstellung diastereomerenreiner, chiraler Camphertetraketone stellt dabei den ersten Schritt in der Synthese dar, weshalb zu Beginn speziell auf die Isomerenverteilung sowie auf die Isolierung und Identifizierung der generierten Diastereomere und deren Konformation eingegangen wird. Hierbei zeigt sich ein dynamisches Verhalten, welches durch temperaturabhängige Protonen NMR Spektroskopie und Kristallstruktur gestützte Analysen Hinweis auf eine neue Art von Protonen-Chelat Keto-Enol Tautomerie gibt. Auf die Darstellung zweier bihomometallischer Übergangsmetallkomplexe des chiralen Tetraketons ist ebenfalls hingewiesen. Nach erfolgreich fortgeführter Synthesen werden repräsentativ drei Palladium Komplexe der neuen Ligandenklasse ausgewählt und auf ihre Effizienz in der kupferfreien Wackeroxidation hin untersucht und die Ergebnisse diskutiert. Eine weitaus detailliertere Studie zur Palladium katalysierten Isomerisierung terminaler Arylpropanoide wird anschließend präsentiert. Hierzu werden insgesamt 11 Palladium Katalysatoren eingesetzt und der Einfluß von Säuren und Basen als Additive in der Reaktion untersucht. Ein ausführliches Screening von Lösungsmitteln, Substraten und Katalysatoren gibt Aufschluss über den Mechanismus und den Einfluß von Sterik und elektronischen Faktoren der Liganden auf die Katalyse. Mittels GC-, GC-MS- und NMR- sowie Deuterium Markierungsexperimenten werden die Reaktionsordnungen bezüglich Katalysator, Substrat und Lösungsmittel ermittelt und ein plausibler Isomerisierungsmechanismus postuliert. Die Integrität und Stabilität des Katalysatorsystems ist anhand multipler Substratzugaben, Feinfiltration und Isolierungsexperimenten adressiert. Im letzten Teil des Kapitels wird die 3,3-Bipyrazol basierte, bidentate Ligandenklasse durch Einführung von Pyridin und Methylpyridinsubstituenten zu einer tetradentate Ligandenklasse ausgebaut, deren Palladiumkomplexe dargestellt und deren strukturellen Charakteristika (Atropisomerismus) diskutiert (s. Schema 2).



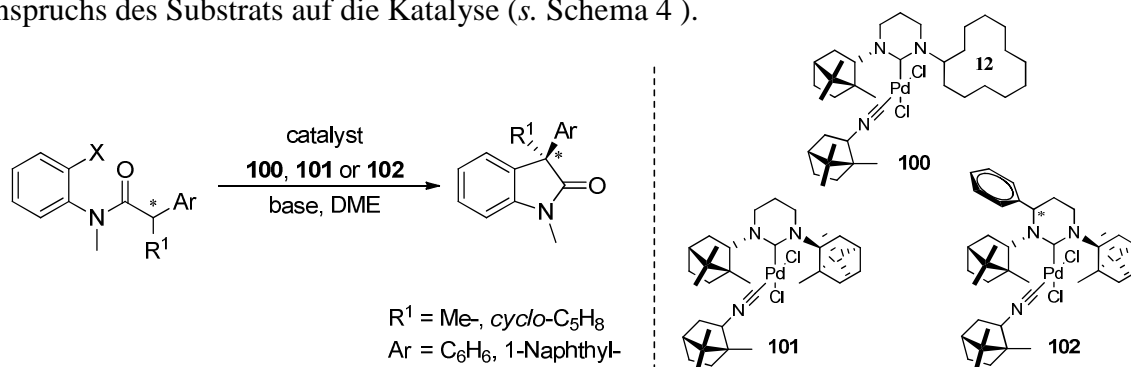
Schema 2 Synthese von neuen Palladium 3,3'-Bipyrazol Komplexen und deren katalytische Aktivität.

Das dritte Kapitel der Arbeit beschreibt die Synthese neuer chiraler NHC-pincer Liganden basierend auf Camphersäure als zentralen Brückenkopf, welche in moderaten bis guten Ausbeuten in 5 Stufen zugänglich sind. Zwei NHC-Liganden mit unterschiedlichen Gegenionen und zusätzlich ein Dibenzotriazol-Ligand werden präsentiert. Die entwickelte Syntheseroute erlaubt dabei die regioselektive Monosubstitution des zentralen chiralen Campher motifs, was sowohl durch NMR spektroskopische Messungen als auch durch Kristallstrukturanalyse aufgezeigt wird. Weiterhin wird die molekulare Struktur des NHC-pincer Liganden sowie die des Dibenzotriazol-Liganden aufgeklärt und eingehend diskutiert. Die Ergebnisse der Strukturen und die der Synthesevorläufer liefern hierbei eine plausible Erklärung für die beobachteten Komplexierungseigenschaften (s. Schema 3).



Schema 3 Palladium-Pincer Zielkomplex **78** ausgehend von Camphersäure.

Im vierten Kapitel der vorliegenden Arbeit werden Struktur-Reaktivitätsbeziehungen in der asymmetrischen, intramolekularen Oxindolsynthese mittels Pd-NHC Isonitril Katalysatoren untersucht, welche bei gleichbleibendem chiralen Muster (Campher) einen Anstieg des sterischen Anspruchs aufweisen. Nach einer kurzen Einführung chiraler NHCs, welche Verwendung in dieser Katalyse finden, wird die Synthese sechsgliedriger Hexahydropyrimidine NHC-Pd Katalysatoren ausgehend von Campher (Bornylamin) und deren Anwendung als Katalysatoren für die enantioselektive Synthese von 3,3-disubstituierten Oxindolen beschrieben. Die Synthese von fünf unterschiedlichen *N*-alkylierten Substraten (Benzyl-, Naphthyl-substituiert) und der Einfluß des Substitutionsmusters in der enantioselektiven, asymmetrischen α -Arylierung von Amiden wird untersucht. Eine Veränderung der Enantioselektivitäten und eine Änderung des Reaktionsprofils gibt dabei Aufschluss über den Einfluß sterischer Beladung des Katalysators als auch des sterischen Anspruchs des Substrats auf die Katalyse (s. Schema 4).



Schema 4 Asymmetrische Oxindolsynthese mit Pd-Isonitril Komplex **100** – **102**

Publications

Refereed Publications

M. J. Spallek, S. Stockinger, R. Goddard, F. Rominger and O. Trapp*, *Eur. J. Inorg. Chem.* **2011**, 32, 5014 – 5024, full paper. Novel Bulky and Modular 3,3'-Bipyrazoles as Ligands – Synthesis, Characterization and Catalytic Activity of the Pd Complexes.

M. J. Spallek, D. Riedel, A. S. K. Hashmi, O. Trapp*, *Organometallics* **2012**, full paper, accepted (ASAP). Six-membered, chiral NHCs derived from Camphor – Structure-Reactivity Relationship in Asymmetric Oxindole Synthesis.

M. J. Spallek, S. Stockinger, R. Goddard, O. Trapp*, *Adv. Synth. Catal.* **2012**, full paper, accepted. Modular Palladium Bipyrazoles for the Isomerization of Allylbenzenes – Insights into Catalyst Design and Activity, Role of Solvent pH Effects and Mechanistic Considerations.

M. J. Spallek, G. Storch, O. Trapp*, *Eur. J. Org. Chem.* **2012**, full paper, submitted. Straightforward Synthesis of Immobilized 3-(Perfluoroalkanoyl)-(1*R*)-camphorate Metal Complexes and their Application in Enantioselective Complexation Gas Chromatography.

M. J. Spallek, S. K. Weber and O. Trapp*, **2012**, full paper, submitted. Metathese in ionischen Flüssigkeiten: Ursache der außergewöhnlichen Stabilisierung des Katalysators; Metathesis in ionic liquids: Reason for the remarkable stabilization of the catalyst.

Poster Presentations

M. J. Spallek, C. Lang, J. Troendlin, O. Trapp*, 5th Heidelberger Forum of Molecular Catalysis **2009**, Heidelberg, Germany. High-Throughput Screening of Ligand Libraries in Catalysis.

M. J. Spallek, S. Sandel, O. Trapp*, Colloquium of the Graduate College 850 **2009**, Heidelberg, Germany. Design of Water-Soluble Metathesis Catalysts and Investigations on Pd Nanoparticle Catalyzed C-C Coupling Reactions.

M. J. Spallek, R. Goddard, O. Trapp*, 6th Heidelberger Forum of Molecular Catalysis **2010**, Heidelberg, Germany. Chiral 3,3'-Bicamphorpyrazoles as Ligands.

M. J. Spallek, R. Goddard, O. Trapp*, Modeling of Molecular Properties **2011**, Heidelberg, Germany. Structure Dynamics of Chiral Tetraketones – Selective Synthesis of Defined Rh(I) and Ir(I) Lewis-Acid Catalysts.

M. J. Spallek, R. Goddard, O. Trapp*, 23rd International Symposium on Chiral Discrimination (Chirality) **2011**, Liverpool, UK. Chiral 3,3'-Bicamphorpyrazoles (bcpz) as Ligands – Synthesis, Structure, Solution Dynamics and Catalytic Activity.

M. J. Spallek, G. Storch, F. Rominger, O. Trapp*, 23rd International Symposium on Chiral Discrimination (Chirality) **2011**, Liverpool, UK. Norbornane-based Chiral Lewis Acids (CLAs) – First Evidence for Stable Chelate-type Tautomers by X-ray Crystallographic Analysis & Selective Formation of One Single Isomer upon Complexation.

Table of Contents

Acknowledgement.....	i
Abstract	iii
Zusammenfassung.....	vii
Publications	xi
Table of Contents	xiii
List of Abbreviations.....	xvi
Chapter 1 Camphor-Derived Stationary Phases in Complexation Gas Chromatography	1
1.1 Introduction.....	2
1.1.1 Separation of Enantiomers on Chiral Stationary Phases (CSP) in Chromatography.....	2
1.1.2 Complexation Gas Chromatography.....	6
1.1.3 Immobilization of Selectors and Choice of Supports in GC.....	8
1.2 Objectives.....	15
1.3 Results and Discussion.....	17
1.3.1 Selector Synthesis and Immobilization.....	17
1.3.2 Preparation of <i>Chirasil-Metal</i> Phases	23
1.3.3 Enantioselective Complexation Gas Chromatography	29
1.3.3.1 Selector Concentration in the Discrimination of Chiral Epoxides.....	29
1.3.3.2 <i>Chirasil(hfpc)_x@PS</i> of Ni(II), Eu (III), La (III) and Oxovanadium(IV).....	30
1.3.3.3 Extending the Scope of <i>Chirasil-Ni(hfpc)₂@PS</i> – Separation of Enantiomers using Compound Libraries with Differing Functional Groups.....	33
1.3.4 Resolution of Chalcogran on <i>Chirasil-Europium-/Lanthanum-</i> and <i>Nickel-OC₃</i> by Dynamic Complexation GC (DCGC)	39
1.3.5 Dynamic Elution Profiles by CSP-Coupling – A Novel Approach Towards Efficient Assignment of Enantiomer Configurations via On-Column GC.....	49
1.3.6 Camphordimers with Two Centers of Chirality – Towards New Acyclic, Metal-free Selectors for (CB)CSPs	60
1.4 Conclusion	65

Chapter 2	Bi- and Tetradentate Pd-Bicamphorpyrazole Heterocycles (bcpz) – Synthesis, Characterization and Their Application in Catalysis	67
2.1	Introduction – Wacker Oxidation and Isomerization of Olefins.....	68
2.2	Objectives.....	76
2.3	Results and Discussion.....	77
2.3.1	Synthesis and Structural Dynamics of Chiral Tetraketones and Their Metal Complexes.....	77
2.3.2	Palladium-bipyrazoles derived from Camphortetraketones.....	84
2.3.2.1	Synthesis and Characterization	84
2.3.2.2	Wacker-Oxidation of Terminal Olefins	89
2.3.2.3	Isomerization of Allylbenzenes – Insights into Catalyst Design and Activity, Role of Solvent, pH Effects and Mechanistic Considerations	91
2.3.2.4	2 nd -Generation (Tetradentate) Camphorbipyrazole Ligands and Their Palladium Complexes.....	107
2.4	Conclusion	112
Chapter 3	Chiral, <i>N</i> -heterocyclic Carbene (NHC) Pincer Ligands using Camphoric Acid as Chiral Building Block	115
3.1	Introduction – <i>N</i> -heterocyclic Carbene (NHC) Pincer Ligands.....	116
3.2	Objectives.....	117
3.3	Results and Discussion.....	118
3.4	Conclusion	124
Chapter 4	Six-Membered, Chiral Pd-NHCs Derived from Camphor – Structure-Reactivity Relationship in the Asymmetric Oxindole Synthesis	127
4.1	Introduction – NHC-Palladium Catalysts in Asymmetric Oxindole Synthesis	128
4.2	Objectives.....	130
4.3	Results and Discussion.....	131
4.3.1	Six-Membered, Chiral Pd-NHC-Camphorisonitrile Complexes	131
4.3.2	Asymmetric Oxindole Synthesis.....	134
4.4	Conclusion	137

Experimental Section	138
General Methods and Materials	138
Experimental Section – Chapter 1	139
Experimental Section – Chapter 2.....	162
Experimental Section – Chapter 3.....	191
Experimental Section – Chapter 4.....	198
References	211
Appendix	138
Academic Teachers	232

List of Abbreviations

ΔG^\ddagger	Gibbs activation energy
ΔH^\ddagger	activation enthalpy
ΔS^\ddagger	activation entropy
9-BBN	9-borabicyclo[3.3.1]nonane
ACSP	acyclic chiral stationary phase
Ar	aryl
<i>n</i> -BuLi	<i>n</i> -butyl lithium
^t Bu	<i>tert</i> -butyl
cat.	catalytic
<i>Chirasil-β-Dex</i>	octamethylen-permethyl-β-cyclodextrin-poly(dimethylsiloxane)
<i>Chirasil-Ni(hfc)₂</i>	nickel(II)-bis[(3-heptafluorobutanoyl)-(1 <i>R</i>)-camphorate] dissolved in poly(dimethylsiloxane)
<i>Chirasil-Ni(II)</i> ,	nickel(II)-bis[(3-heptafluorobutanoyl)-(1 <i>S</i>)-10-methylenecamphorate]-poly(dimethylsiloxane)
<i>Chirasil-Eu(III)</i>	europium(III)-tris[(3-heptafluorobutanoyl)-(1 <i>S</i>)-10-methylenecamphorate]-poly(dimethylsiloxane)
<i>Chirasil-V(O)(IV)</i>	oxovanadium(IV)-bis[(3-heptafluorobutanoyl)-(1 <i>S</i>)-10-methylenecamphorate]-poly(dimethylsiloxane)
<i>Chirasil-Europium-OC₃ X%</i> ,	
<i>Chirasil-Eu(hfpc)₃@PS_{X%}</i>	europium(III)-tris[(1 <i>R</i> , 4 <i>S</i>)-3-heptafluorobutanoyl-10-propoxycamphorate] _{X%} -poly(dimethylsiloxane); (X% selector concentration on the polymer)
<i>Chirasil-Lanthanum-OC₃ X%</i> ,	
<i>Chirasil-La(hfpc)₃@PS_{X%}</i>	lanthanum(III)-tris[(1 <i>R</i> , 4 <i>S</i>)-3-heptafluorobutanoyl-10-propoxycamphorate] _{X%} -poly(dimethylsiloxane); (X% selector concentration on the polymer)

<i>Chirasil-Nickel-OC₃</i> X%,	
<i>Chirasil-Ni(hfpc)₂@PS_{X%}</i>	nickel(II)-bis[(1 <i>R</i> , 4 <i>S</i>)-3-heptafluorobutanoyl-10-propoxycamphorate] _{X%} -poly(dimethylsiloxane); (X% selector concentration on the polymer)
<i>Chirasil-Vanadyl-OC₃</i> X%,	
<i>Chirasil-V(O)(hfpc)₂@PS_{X%}</i>	oxovanadium(IV)-bis[(1 <i>R</i> , 4 <i>S</i>)-3-heptafluorobutanoyl-10-propoxycamphorate] _{X%} -poly(dimethylsiloxane); (X% selector concentration on the polymer)
CB	chemically bonded
CSP	chiral stationary phase
<i>d.e.</i>	diastereomeric excess
DIBAL	<i>di</i> isobutylaluminium hydride
<i>e.e.</i>	enantiomeric excess
ESI-MS	electron spray ionization-mass spectrometry
Et ₂ O	diethyl ether
FID	flame ionization detector
GC	gas chromatography
GC-MS	gas chromatography-mass spectrometry
h	hour(s)
hfb	heptafluorobutanoyl
hfc	3-heptafluorobutanoyl-(1 <i>R</i>)-camphorate
hfpc	(1 <i>R</i> , 4 <i>S</i>)-3-heptafluorobutanoyl-10-propoxy-camphorate
HMPA	hexamethylphosphoramide
HR	high resolution
HPLC	high performance liquid chromatography
I.D.	inner diameter
IR	infrared spectroscopy
LiAlH ₄	lithium aluminium hydride
M	metal

min	minute(s)
mol%	mol percent
MS	mass spectrometry
NHC	<i>N</i> -heterocyclic carbene
NMR	nuclear magnetic resonance
OTf	trifluoromethanesulfonyl
PDMS	poly(dimethylsiloxane)
Ph	phenyl
PS	polysiloxane
ppm	parts per million
^{<i>i</i>} Pr	<i>iso</i> -propyl
py	pyridine
<i>W.-M.</i>	<i>Wagner-Meerwein</i>
R _f	retention factor
r.t.	room temperature
sec	second(s)
<i>t</i>	time
THF	tetrahydrofuran
TMEDA	tetramethylethylenediamine
TMS	tetramethylsilane
TMSCN	trimethylsilyl cyanide
<i>t</i> _R	retention time
% V _{bur}	buried overlap volume
VT NMR	variable temperature nuclear magnetic resonance
vol%	volume percentage
wt%	weight percentage

Chapter 1

Camphor-Derived Stationary Phases

in Complexation Gas Chromatography

1.1 Introduction

1.1.1 Separation of Enantiomers on Chiral Stationary Phases (CSP) in Chromatography

Many of the biomolecules produced and processed in nature are chiral or prochiral and most metabolic transformations are stereospecific. A lot of effort is necessary for nature to introduce chirality or transfer chiral information onto a molecule or from one to another. During evolution of nature the (*L*)-configuration of small molecules (amino acids, peptides and proteins) and the (*D*)-configuration of sugars prevailed and are upon the most dominant configurations.^[1] For chiral induction enzymes are used, for instance. As most of the environs in nature are chiral, enantiomers show different effects in biological systems. For example the two enantiomers of limonene exhibit a different odor commonly known as orange aroma (*R*-limonene) or the off odor of turpentine (*S*-limonene). Especially in therapeutically medical science, drug discovery and drug evaluation, as well as present in pesticides and synthetic flavors the different effects of enantiomers in an chiral environment (as in nature) are known. In many cases the targeted effects is only limited to one enantiomer, whereas the other enantiomer shows either reduced activity or no effect at all. Different effects and considerable toxic behavior can be observed as well. This did not receive attention until the disaster with the chiral drug Thalidomide.^[2] Sold as its racemate (Contergan[®]) between 1957 and 1961 the (*S*)-enantiomer had the desired property as treatment for morning sickness for pregnant women (*cf.* Figure 1). But it turned out that the other enantiomer was teratogenic causing congenital deformations of children born from women treated with this drug. Therefore the determination of configuration of a chiral compound, the stereospecific introduction of chirality and the determination of enantiomeric excess (*e.e.*) is of great interest in pharmaceutical and related industries.^[3] Even though the need for enantiomerically pure compounds (drugs) is obvious and also increasingly forced by the legislative authority, many of the substances on the market are still sold as racemates.^[3] Reasons are high costs either due to low bioavailability of natural sources (agriculture or fermentation), their isolation or purification, as well as separation of enantiomers from their racemate by classical resolution via crystallization^[4] of diastereomeric salts or kinetic/ dynamic resolution using enzymes (or chiral catalysts).^[5] Intensive synthetic procedures^[6] and the generally time-consuming methods, necessary for their evaluation in drug regulatory affairs renders these processes challenging.

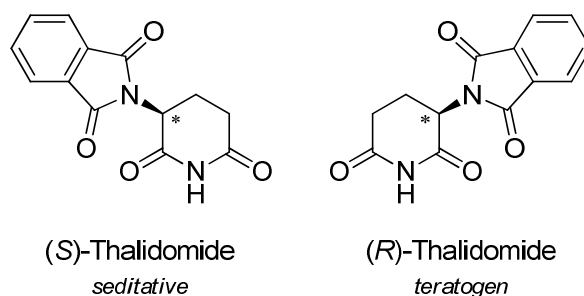


Figure 1 Thalidomide enantiomers present in Contergan[®] as sold by Grünenthal in Germany (1957 – 1961).

Efforts are made to develop novel, enantioselective analytical methods and techniques, which are fast, cheap and precise and therefore more efficient than established ones. Chromatography is beside chiroptical methods (e.g. circular dichroism) or nuclear magnetic resonance spectroscopy (NMR) utilizing shift reagents ideal combining fast analysis, flexibility and efficiency within the same method.

For the chromatographic separation of enantiomers either direct or indirect methods can be applied. By derivatization with a chiral reagent diastereomers with different physical properties are formed from the racemate, which can be separated by conventional chromatography on an achiral stationary phase (indirect method). More straightforward is the direct separation of enantiomers without derivatization of the compounds prior to separation. An additional chiral information, related to the common “key-lock-principle” in biochemistry is needed as well, but this problem is solved by application of chiral stationary phases (CSPs) in GC, SFC, HPLC, CE on which enantiomers can be separated. For HPLC and CE applications chiral additives in the eluent stream can be used as well. CSPs, the state-of-the-art technology^[5] for chromatographic separations of enantiomers, include basically five types, which are classified by the type of selector–selectand interaction (*cf.* Table 1).^[7]

The first CSP-type features protein based stationary phases, which are usually of natural origin, bonded to a silica matrix with many chiral centers present, forming strong analyte (selector–selectand) interactions. Generally, prolonged retention times are observed due to the large number of active sites (unselective contribution to retention of analyte and eluent). Also macrocyclic glycopeptides developed by Armstrong et al.^[8, 9] can be used and a high number of chiral centers and active sites combined with cavities are present within these phases, The level of intrusion into this cavities and thus the proximity to the selector is influenced by the character of selectand and eluent, which determines the magnitude of observed retention.

Table 1 Common chiral, stationary phases used for the chromatographic separation of enantiomers.

<i>class</i>		<i>type of interaction</i>	<i>common selectors</i>
I	PROTEINS	hydrophobic and polar, mesophase interactions	α_1 -acidic glycoprotein, bovine serum albumin, vancomycin
II	PIRKLE	attractive and p-p-interactions, hydrogen-bonding, charge-transfer-complex formation	various ionic or covalent bonded selectors
III	OKAMOTO (polymeric helices)	attractive interactions, selector–selectand complexes	derivatives of cellulose and amylose
IV	CAVITIES (inclusion phases)	inclusion and selector–selectand complexes	cyclodextrins, crown ethers, polyacrylamides, polymethacrylates
V	DAVANKOV (ligand-exchange)	ligand exchange, ionic interactions	amino acid-metal complexes

The second CSP-class are Pirkle-type^[10-16] stationary phases featuring only small, limited chiral centers present at the selector. Therefore, unwanted unselective contributions and retention of eluent is reduced and chiral selector-selectand selectivity become more dominant, which enhances the resolution. Okamoto-phases^[17] represent the third type of CSPs. They are based on polymeric helices of cellulose and amylose with appropriate modifications (ester, carbamate and ether derivatives).^[18-22] The fourth group of CSPs are used in inclusion GC and consist of cyclodextrins ($\alpha - \gamma$ type, depending on the ring size),^[23-25] crown ethers, polyacrylamides^[26] or polymethacrylates^[27] and derivatives thereof. The cone-shaped barrel form of cyclodextrins, the degree of substitution and the type of modification determines resolution and retention time of the analyte. More recently, also acyclic dextrans were developed and successfully applied for the separation of enantiomers. Finally, ligand-exchange chromatography introduced by Davankov^[28-31] can be used as well. The selectors consist of chiral amino acid metal complexes, like proline combined with copper, for instance. For the sake of completeness cinchona alkaloids based ionic CSPs developed by Linder et al. for the separation of (amino) acids have to be mentioned as well.

For volatile, thermally stable compounds gas chromatography is the method of choice, since determination of appropriate separation conditions is straightforward, the parameter-set is generally small, resolution and sensitivity is high and results are easily reproducible (due to the absence of solvent interactions in LC systems, for instance).^[32, 33] Today, numerous chiral stationary phases for GC are available.^[34] They are based on amino acid derivatives (diamide phases), on polysiloxane polymers and most notably on cyclodextrin derivatives. The first enantioseparation using GC was obtained with *N*-trifluoroacetyl-derivatized (*L*)-isoleucine^[35] and later with polysiloxane-based *Chirasil-Val*,^[36, 37] derived from (*S*)-valine-*tert*-butylamide, as the chiral selector in 1977. Amino acids were successfully separated by hydrogen-bonding interactions between selector and selectand. König et al. widened the scope of analytes by derivatization with isocyanates and other reagents.^[38] Another method was introduced by Schurig et al. who developed the concept of enantiomer discrimination by complexation gas chromatography^[39] (CGC) utilizing coordination interactions between selectand functionalities and chiral-metal complexes as chiral selector. Despite the early successes with polysiloxane based CPSs, cyclodextrin based CSPs developed in 1983 by Koscielski et al.^[40] (α -, β -pinene enantiomer separations in gas-liquid GC with α -CD) became impressively predominant. Inspired by these results the synthesis and successive improvement furnished a steadily growing number of cyclodextrin derivatives.^[41] Native and modified cyclodextrins, like permethylated β -cyclodextrins developed by Schurig et al.^[42-44], by König et al. (liquid cyclodextrin derivatives)^[45, 46] and Mosandl et al. (diluted modified cyclodextrins)^[47] in polysiloxanes are nowadays state-of-the-art CSPs in chiral gas chromatography (*cf.* Figure 2).

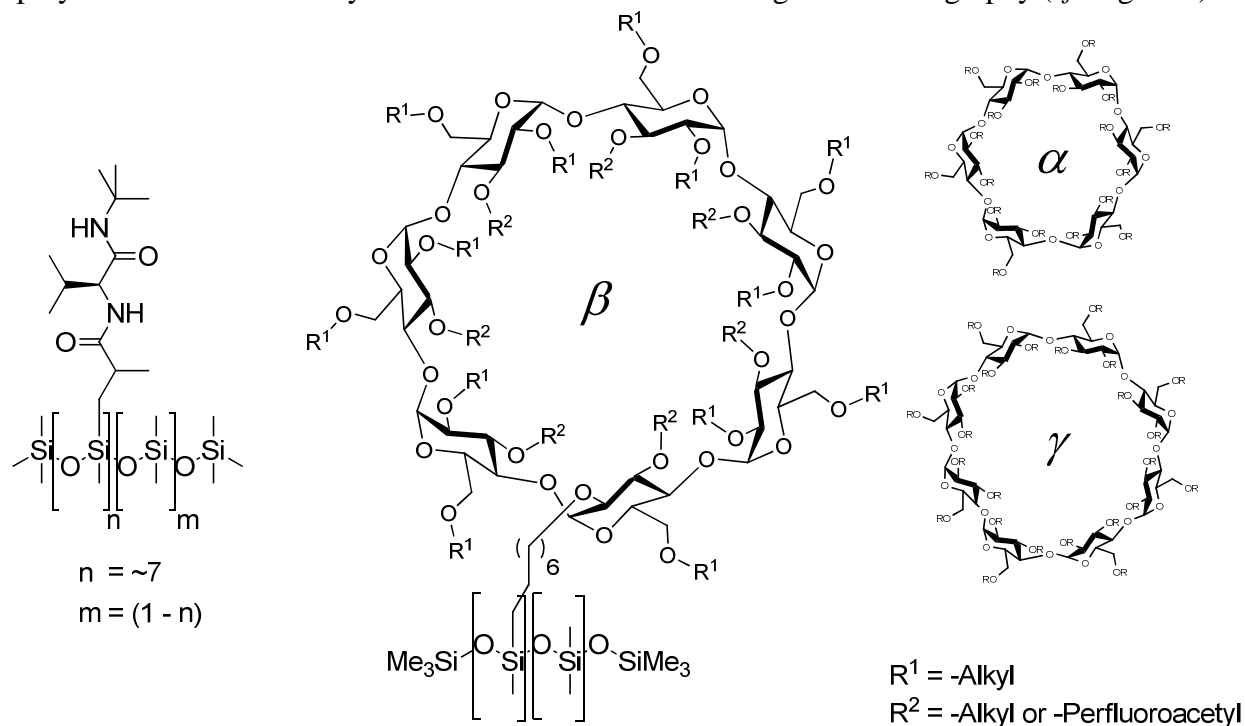


Figure 2 Polymer-supported chiral selectors for enantiodiscrimination in gas chromatography. *Chirasil-Val* (left) and *Chirasil-Cyclodextrins* ($\alpha - \gamma$, right).

1.1.2 Complexation Gas Chromatography

Despite first results in 1972, the term “*complexation GC*” was introduced by Schurig et al. in 1977.^[39] Inspired by the previous work of Gil-Av, Freibush and Charles-Siegler with amino acid alkyl esters in enantioselective GC (*cf.* Chapter 1.1.1) and their capability for hydrogen-bonding combined with the resemblance to peptide-enzyme complexes led to the development of a completely new type of selectors. Related to these selector–selectand interactions an abiotic enantioselective system displaying a metal-organic framework was considered. Key feature of the system is the coordination between the metal and an analyte exhibiting functional groups, which are prone to enantio-recognition. Therefore, the discrimination of enantiomers with CSPs by metal-organic coordination was called *enantioselective complexation gas chromatography*. As the use of silver(I)-containing CSPs utilizing π -interactions for the separation of olefins was already demonstrated decades before, the use of chiral transition metal complexes was quite intuitive.

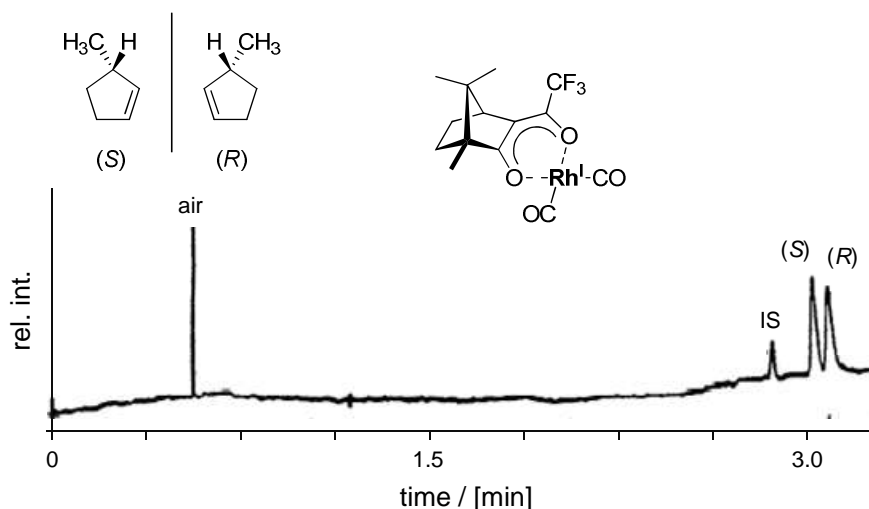


Figure 3 First example of enantiomer separation on a 200 m column by complexation GC using Rh(I)(hfc)(CO)_2 reported in 1972.

Conditions: 200 m (I.D. 500 μm) column embedded with Rh(i)(hfc)(CO)_2 . 0.04 m selector concentration in squalane at 22 $^\circ\text{C}$.

Whereas optically active phosphines and phosphites proved to be unsuccessful, complexes of chiral β -diketonates obtained from natural *d*-(+)-camphor showed promising results. Previously known as ligands for rare earth metals^[48, 49] and for their utilization as chiral shift reagents^[50] 3-trifluoroacylated *d*-(+)-camphor β -diketonate was used for this purpose. Embedded in a squalane matrix rhodium(I) 3-(trifluoroacyl)-(1*R*)-camphorate was able to separate racemic 3-methylcyclopentene demonstrating a successful discrimination of enantiomers via complexation gas chromatography for the first time (*cf.* Figure 3).^[51] This approach was limited to a number of very few, selected compounds under optimized conditions. However, as resolution of chiral unsaturated hydrocarbons, ethers and ketones

were found to be difficult, especially for small molecules, but the important applications in the field of chiral analysis became immediately apparent.

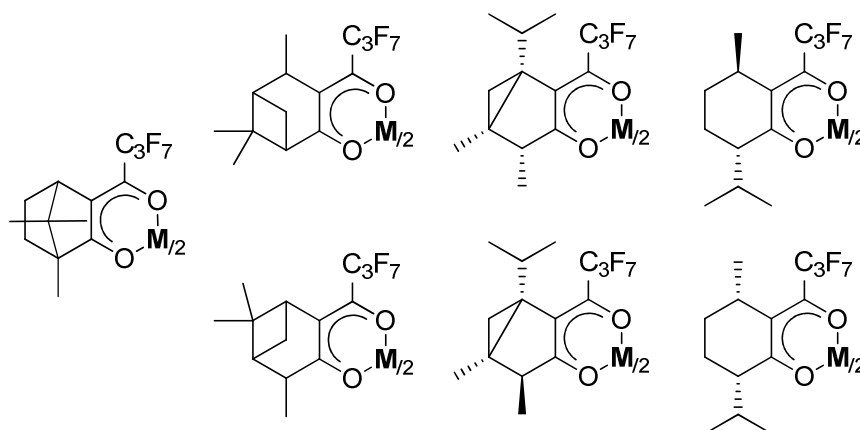


Figure 4 Mono- and bicyclic monoterpene ketones as chiral β -diketonates. Chiral building blocks (left to right and top to bottom): camphor, 3-pinone, 4-pinone, (-)- α -thujon, (-)- β -thujon, (-)-menthone, (-)-isomenthone. Metal (M): Ni(II).

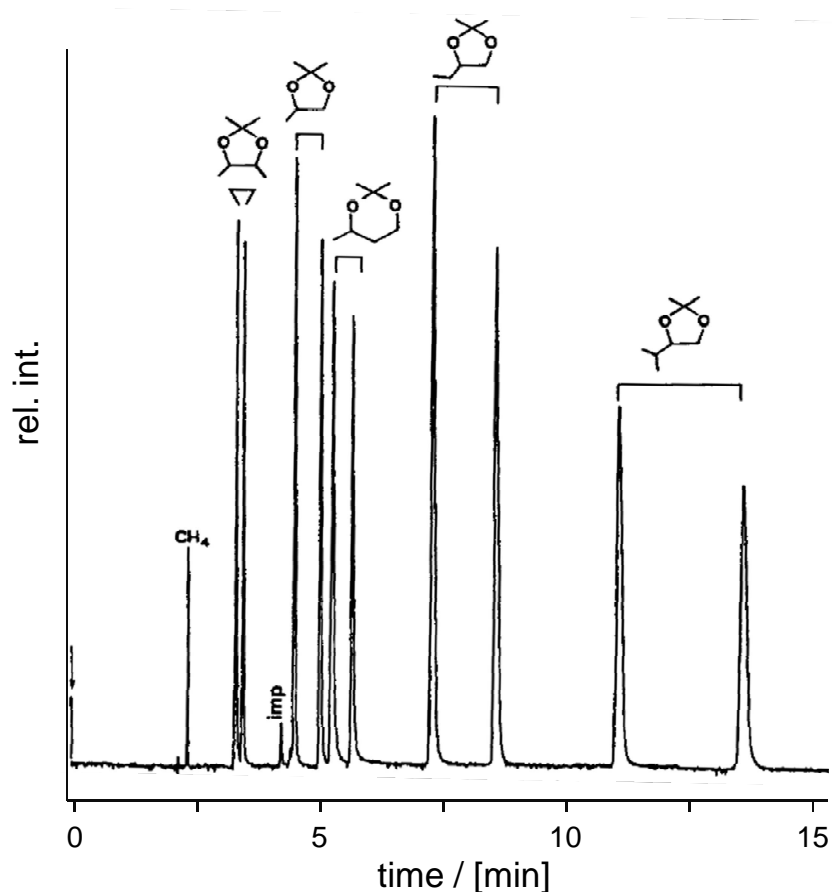


Figure 5 Enantiomer separation of aliphatic diol acetonides using diluted Ni(hfc)₂ in OV 101 by complexation GC.

Conditions: 0.17 M Ni(hfc)₂, 40 m glass capillary (I.D. 250 nm) in OV 101 at 80 °C.

Consequently, a broader approach was considered and different chiral ligand frameworks were developed and the metal-coordinated to the ligand was altered. As shown in Figure 4 natural starting materials related to camphor, pinene (nopinone), thujone and menthone were envisaged. Obtained from the chiral pool, these materials were modified to their corresponding 3-perfluoroacylated β -diketones and metals, like manganese(II),^[52] cobalt(II)^[53] and nickel (II),^[54, 55] were incorporated. Experiments showed that nickel(II)-complexes of 3-(trifluoroacyl)-(1*R*)-camphorate exhibited the best separation capability upon all metals and ligand patterns and the scope of separable compounds was extended to oxygen-, nitrogen- and sulfur containing selectands. However, oxygen-containing compounds showed good separations, whereas nitrogen- or sulfur-functionalized analytes still proved to be challenging. Utilizing this approach the type of oxygen-containing compounds was restricted to cyclic ethers and acetals,^[53] underivatized *sec*-alcohols^[56, 57] and a few ketones (*cf.* Figure 5).^[57, 58] However, the reproducibility and stability was unsatisfactory.

1.1.3 Immobilization of Selectors and Choice of Supports in GC

Several requisites have to be considered to develop new chemically-bonded chiral stationary phases for gas chromatographic applications and separation of enantiomers:^[1, 5, 34]

- thermal stability (>150 °C required) and long life-time
- broad applicability over a broad temperature range (regarding melting points)
- expanded scope of enantiorecognition and functional group tolerance
- reproducibility (separations and column preparation)
- high degree of versatility (selector-modifications)
- non-volatile selectors (column-bleeding, leaching of selector, MS-compatibility)
- high enantiopurity of the selector
- efficient selector concentration and limits (upper and lower)
- temporary interactions (selector re-liberation time)
- efficiency, retention tendency and resolution factor
- stereointegrity (aggregation and degradation tendency)
- physical properties of the (polymeric) support and selector compatibility
- synthetic value (commercial available starting materials, short synthesis and high yield)
- optional: compatibility with other separation systems, like SFC (supercritical fluid chromatography), (HP)LC ([high pressure] liquid chromatography), CE (capillary electrophoresis)

For the development and successful application of a novel (CB)CSP for the resolution of enantiomers these considerations have to be taken into account. The application of high-resolution glass and later the fused-silica column technology greatly improved the progress in (complexation) gas chromatography. Overall high thermal stability and selector integrity over a broad temperature range combined with a broad scope of enantio-recognition and a long, constant column life-time performance are upon the most critical aspects. For a suitable selector support the initially applied squalane was replaced by dimethylpolysiloxane as a unique solvent. Diluted in the polymer the selector is embedded in the matrix of the support, with the advantage of isolated selector sites (ideal case). This is beneficial for selector life-time and enantiodiscrimination, since degradation of the selector is suppressed by simple separation through space and the exposition of selector to the environment (air, moisture, carrier gas and sample impurities) is reduced. The aggregation tendency, a commonly known source for inactivation or decomposition, is decreased, the enantioselective recognition step stays intact and is not influenced by neighboring selector-selectand interactions.

A major drawback of the application of camphor- β -diketonates of rhodium(I), manganese(II) and cobalt(II) in enantioselective complexation GC is their limitation to temperatures between 25 – 90 °C and their short life-time.^[59] Leaching and degradation of the complexes were generally observed resulting in low reproducibility and reduced life-time of these columns.

Immobilization Strategies

To overcome these problems the selector has to be attached to a suitable (polymeric) support (immobilization). Overall four different basic strategies were developed, which will be discussed briefly. The compound (selector/ligand, catalyst or the preassembled metal complex) can either be attached covalently or immobilized via non-covalent interactions (entrapping, electrostatic interactions, adsorption) onto the support (*cf.* Figure 6).

Alternatively, the synthesis of the ligand can be performed on the support or the monomers of the ligand containing building blocks can be synthesized and polymerized afterwards. The latter approach enjoys the advantage of a straightforward synthesis and comfortable characterization of each product prior to polymerization. However, a controlled polymerization or copolymerization as well as the purification and characterization of the final polymer is challenging. Especially, the use of dialkoxysilane precursors, generally employed for polymerization, is not possible, since their derivatization is extremely challenging or not possible at all, due to their sensitivity to acid and base. Therefore, the synthesis of the compound for immobilization is likely to be performed in advance holding

the advantage of standard characterization techniques. In a final step immobilization can be carried out employing defined, pre-fabricated polymers of known properties.

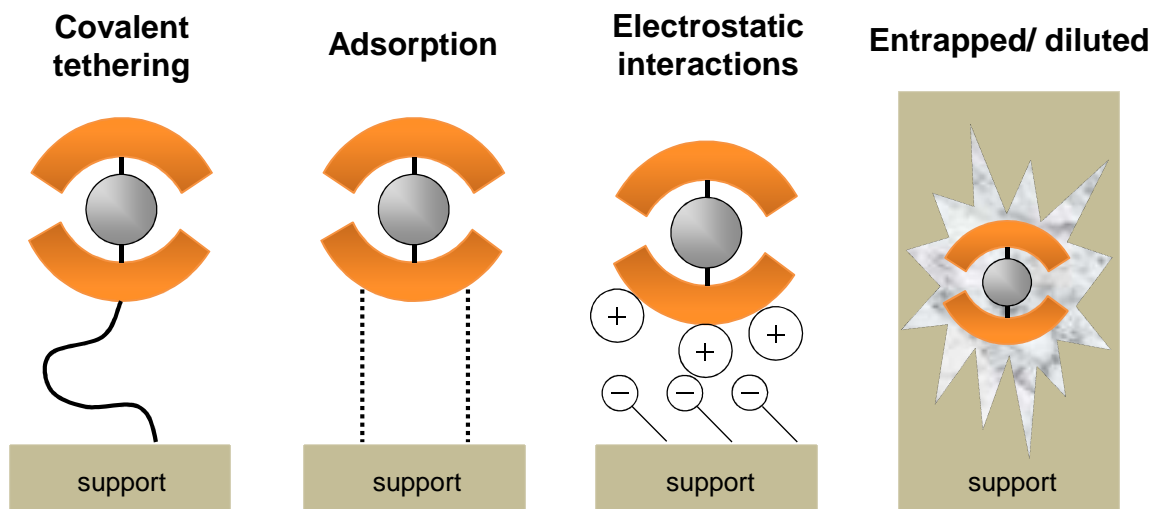


Figure 6 Basic immobilization strategies for homogeneous selector-systems.

By an immobilization approach leaching of selector can be prevented and aggregation effects are reduced. Noteworthy for chiral induction, enantio-recognition can be influenced by the geometry and electronic properties of the linker and the physical properties of the support.

For embedded or encapsulated phases, like in mesoporous materials, compounds of well-defined properties can be trapped without further modifications. Despite the ease of preparation, this approach is prone to leaching of catalyst, selector or active species during operation. For electrostatic trapping the choice of counter ions and their interactions with the environment (analytes, substrates and products, impurities and the eluting moiety) is of main interest and might change the performance. Also immobilization by simple physisorption onto a surface via *Van-der-Waals* interactions displays an attractive approach but conditions regarding the chemical environment, the interactions and the physical properties employed are crucial for success. However, the tendency to generate weakly-bound and non-stable phases is a major drawback. Finally, and doubtless most challenging is the direct, covalent linkage of the ligand or preassembled metal-complex.⁸⁵ Only few reports deal with a direct or close attachment of the compounds to the support. The predominant strategy focuses on the use of flexible linker systems (spacers) of different length. This method opens the possibility and versatility to adjust and tune the accessibility to the immobilized active sites. For this purpose the electronic and steric properties of the spacer has to be considered carefully and the choice of ligand, selector or catalyst loading and solvents employed will influence the stability and performance of the phases.^[60, 61]

Supports for Immobilization

The types of catalyst supports can be classified into solid and liquid organic materials, like organic polymers, ionic liquids and carbon nanotubes, and in inorganic materials, like mesoporous materials, inorganic polymers and silica, alumina and inorganic oxides. The physical properties of the support are very important for the application and separation performance of the chemically bonded (CB)CSPs products. Mechanical strength, thermal stability, solubility, swelling properties and the presence of functional groups have to be considered and numerous problems can arise during immobilization, which alter the desired performance profile in different ways: (i) limited selector accessibility, (ii) undesired selector-support interactions, (iii) change or reversal of enantioselectivity, (iv) reduced enantiodiscrimination and (v) stability problems within the polymeric selector-linker support, leading to decomposition or leaching. Therefore the right geometry and electronic properties of the support, the linker and the selector have to be chosen properly.

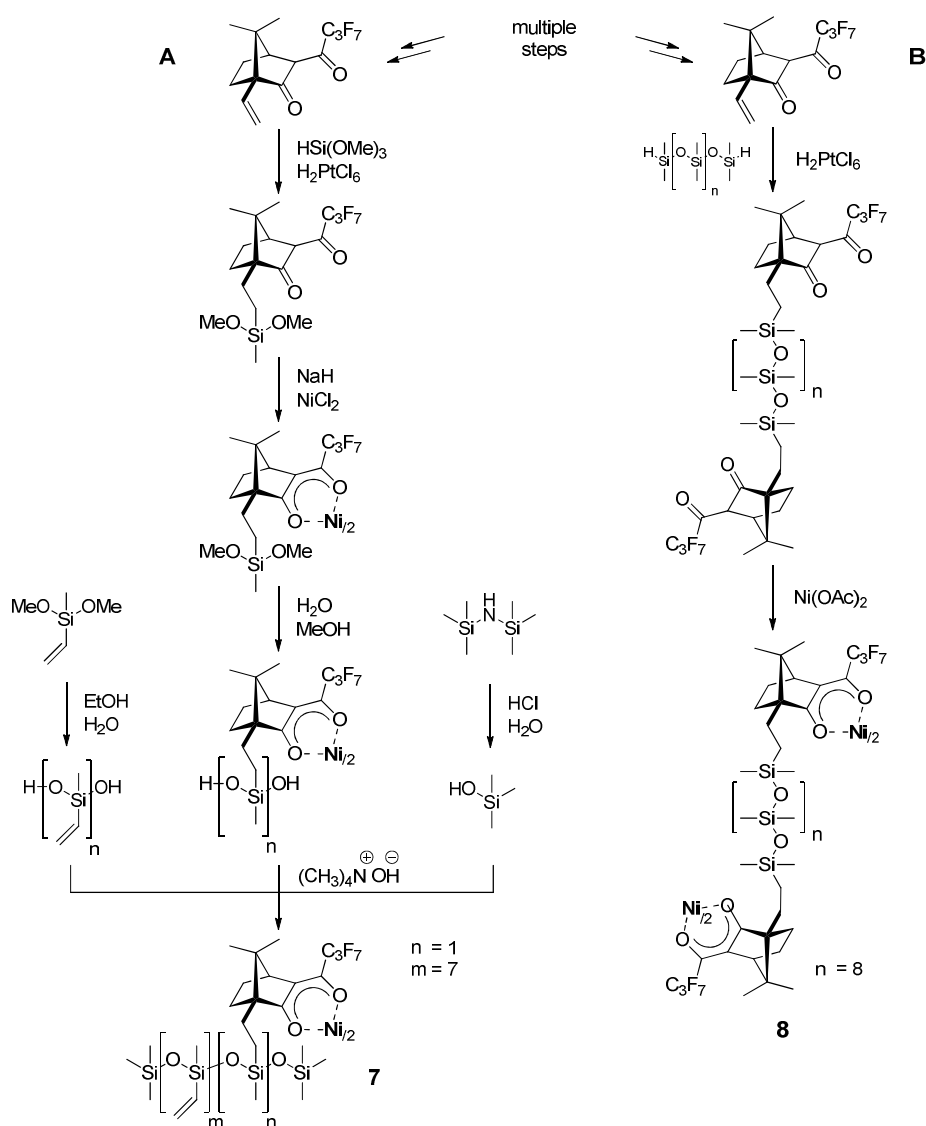
Polysiloxanes, being widely used as fluids, membranes^[62] and lubricants,^[63] showing excellent thermal (usually -100°C to $\geq 350^{\circ}\text{C}$), oxidative, biological and good chemical stability (pH 4 – 9).^[64]

Immobilization at Polysiloxanes via Hydrosilylation

Since 1990, several techniques to achieve a covalent bonding of selectors to polysiloxane backbones were developed.^[65-68] Their physical properties, like polarity and selectivity, can be tuned to furnish tailor-made chiral stationary phases in a very efficient way. However, it should be noted that the enantioseparation characteristics of polysiloxane containing diluted and linked selectors can significantly differ as shown for cyclodextrin derivatives.^[44]

A comfortable way of attaching a selector to the polysiloxane moiety is the addition of a carbon-carbon-double bond to a Si-H functionality (hydridomethyldimethylpolysiloxane, HMPS, **1**) to form an alkylsilane (**2**). This hydrosilylation reaction^[69] allows the installation of various types of residues producing polymers with defined properties. Among a large family of catalysts employed for this type of transformation (rhodium-silanols,^[70] cobalt-carbonyls,^[71] e.g.), the Pt-catalyzed hydrosilylation is most dominant.^[72] Hexachloroplatinic acid (H_2PtCl_6) in alcoholic media (*Speiers'* catalyst, **3**)^[73] can be used, but is sometimes accompanied by the precipitation of small amounts of finely dispersed Pt(0). For purpose of complete metal-free (CB)CSPs catalysts, like Pt-divinyltetramethyldisiloxane complex (**4**) (*Karstedt's* catalyst),^[74] dichlorodi(*cyclopentadienyl*)platinum(II) ($\text{Cl}_2\text{Pt}(\text{dcp})$)^[75, 76] (**5**) or the

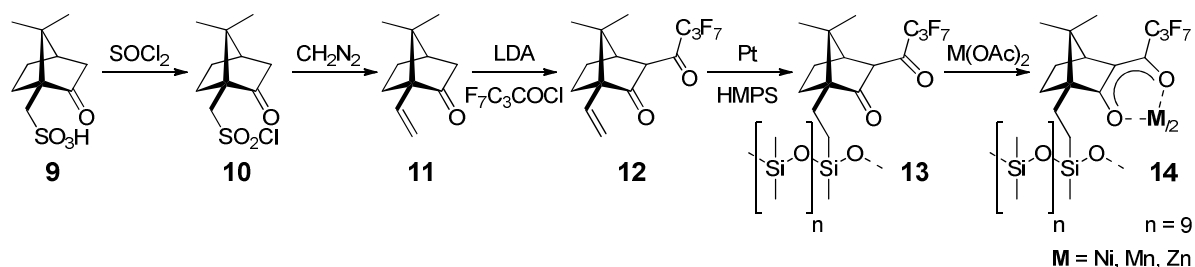
application in conventional GC was reported by Frank, Nicholson and Bayer. Linkage of the valine diamide selector, developed by Freibush and Gil-Av, to a polysiloxane support resulted in the first chiral polysiloxane containing valine phase, abbreviated as *Chirasil-Val*.^[36] This (CB)CSP proved to be efficient in the gas chromatographic resolution of amino acid enantiomers. Both antipode phases are nowadays commercially available and thermally stable up to 200 °C (*Chirasil-D/L-Val*[®]).^[79] A few related polymeric CSPs with different supports were also reported.^[80, 81] A strategy to link the chiral metal-containing selector for complexation GC to a polymeric backbone was first achieved by Schurig et al. on a hydridomethylpolysiloxane (HMPS) support by Pt-catalyzed hydrosilylation. By this approach thermal stability was improved to (100 – 120 °C), but by operation at these temperature-limits a decrease in efficiency, resolution and life-time was still observed after prolonged use!^[82-84] In particular, two main routes towards camphor-derived (CB)CSPs were pursued. Chiral polysiloxanes with metal-containing stationary phases (*Chirasil-Metals*) are obtained either by total synthesis of the chiral copolymer-block followed by copolymerization (Route A)^[85] or preferentially by synthesis on the polymer itself^[82] (*cf.* Scheme 6).



Scheme 6 Total synthesis (A) and polymer-analogous synthesis (B) of *Chirasil-Nickel 7* and **8**.

The (CB)CSPs **7** showed fast separation of 2-methyl substituted cyclic ethers. A *Chirasil-Nickel* phase, with the metal-selector as the terminating group of the polymer (**8**) was prepared as well.^[83] Unfortunately, these oligomers suffered from short chain-length (decamers) leading to aggregation, insolubility and decomposition. The use of higher molecular weight polymers was limited in this approach since the selector-concentration in the polymer (at the polymer termini), necessary for efficient resolution, is successively lowered with higher molecular weight (*cf.* Route **B**, Scheme 6).

However, besides the pioneering and inspiring work of Schurig and coworkers with *Chirasil-Metal* CSPs one major drawback of all camphor and monoterpene related (CB)CSPs prepared so far was the selector-synthesis prior to immobilization (*cf.* Scheme 7).



Scheme 7 Preparation of *Chirasil* ligand **12**, immobilization and metal incorporation step.

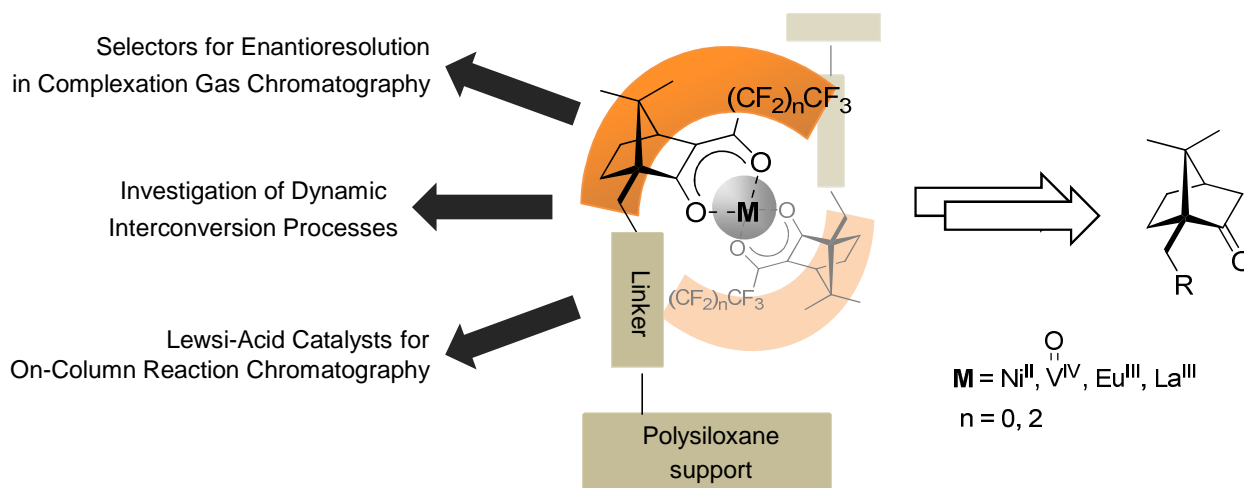
Up to now the shown synthetic procedure represents the only literature report for the preparation of chiral, metal β -diketonates useful for polymerization at a polymer backbone. For this purpose, modifications at the chiral building block are necessary and suitable functional groups have to be selected, installed and conserved during synthesis. As illustrated in Scheme 7 commercially available (1*S*)-(+)-camphorsulfonic acid was used as starting material. The olefin necessary for the hydrosilylation step was introduced using equimolar amounts of diazomethane to yield a metastable episulfone capable of sulfur dioxide elimination to yield methylenecamphor **11**.^[86, 87] Besides the need for freshly prepared cancerinogenic and potentially explosive diazomethane and the moderate yield obtained the major drawback of this route is the perfluoroacylation step to **12**.^[88] The preparation of the fluoroacylated 1,3-diketone **12** was achieved by deprotonation of the acidic α -keto proton with strong bases to form the enolate-nucleophile prior to acyl chloride addition. By using lithium diisopropylamide the yield was low (max. 35%), because of competing reactions between acyl chloride, remaining acidic camphor protons and base. The use of sodium amide and dimethoxyethane as solvent combined with higher reaction temperatures to facilitate ammonia liberation (driving force beneficial for enolate formation) slightly increased the yield up to 50% (ideal case). However, the reaction was accompanied by various side-

reactions and by-products (e.g. *O*-acylation, bisacylation and acylamide formation), which required tedious multi-step work-up procedures giving rise to low yield. The route furnished 3-heptafluorobutanoyl-10-methylencamphor **12** (prior to metal incorporation and immobilization) in yields ranging from 9% to 24% best.^{[89, 90],[91, 92]}

1.2 Objectives

Immobilized transition metal complexes derived from camphor are especially useful for asymmetric induction. Besides the use as chiral catalysts in hetero *Diels-Alder* reactions with oxovanadium(IV)^[89, 93, 94] or europium(III),^[89, 95-97] asymmetric induction in cyclopropanation reactions^[98] were reported with homogeneous as well as immobilized chiral metal β -camphordiketonates. Moreover, the immobilization of the chiral metal-complexes onto a suitable support, like polysiloxanes to produce *Chirasil-Metals* offer advantages in terms of catalyst recycling and their use as immobilized chiral stationary phases (CSP) in (gas) chromatographic applications. Being unreactive towards carbon dioxide, even application in supercritical fluid chromatography (SFC) is possible. They can be employed as stationary phases for chromatographic resolution of enantiomers as well as for catalytic active CSPs in classical bench reactions followed by recovering and re-use. Upmost, by combination of catalytic activity, separation selectivity and chromatographic analysis at the same time within the same capillary the ultimate method for determination of reaction profiles, kinetic catalyst parameters, identification and analysis of dynamic phenomena and product identification and distributions is realized. Bearing this in mind a chiral and immobilized stationary phase being either used as selectors for the resolution of enantiomers or being active catalysts themselves, by simple metal-exchange at the polymer the enormous range of applications becomes evident.

Reconsidering these opportunities and the pioneering work on chiral metal chelates this chapter focuses on the development of novel, chiral camphor-derived stationary metal phases with improved thermostability, resolution and efficiency. The use of high molecular-weight polysiloxanes ($M_w \sim 3000$ g/mol) is considered to guarantee thermal and chemical stability of the backbone and the selector. Key to an enhanced efficiency and enantioselectivity will be the development of a selector-to-support spacer of well-defined length, which has proofed to be beneficial for immobilized systems.^[99, 100] Furthermore, an straightforward, modular and high yielding access to (CB)CSPs of varying spacer-length is emphasized. The challenging fluoroacylation step and purification procedure should be improved as well (*cf.* Scheme 8).



Scheme 8 Development of novel, immobilized CSPs from camphor and their applications.

Chemically bonded chiral stationary phases (CB)CSPs incorporating different metals and their performance in the gas chromatographic resolution of compound libraries will be investigated. Furthermore, the influence on the performance of the novel camphor-derived (CB)CSPs in complexation gas chromatography will be investigated regarding:

- metal-coordination
- degree of selector perfluoruration
- selector-concentration
- selectand/ analyte composition (functional group tolerance and separation capability)
- temperature, stability and life-time
- polymer film-thickness
- polymer composition (mixed-phases)
- column length
- column conditioning

Finally, in order to revisit the great potential of metal-coordinated (CB)CSPs, the versatility of this approach and their use in asymmetric on-column reaction chromatography will be addressed and an novel approach towards a fast and efficient assignment of enantiomer configurations via dynamic complexation gas chromatography will be presented, called *dynamic elution profiles by coupling of CSPs*.

1.3 Results and Discussion

1.3.1 Selector Synthesis and Immobilization

The results obtained by Schurig and coworkers (*cf.* Chapter 1.1.2) using 10-methylidencamphor for a “direct” attachment (short linker) were promising. However, separation quality and synthesis suffered mainly from two aspects. As outlined in chapter 1.1.3 the choice of spacer (flexibility and linker-length) is crucial for the performance of the derived polymers and therefore a different approach was developed. Instead of a short two-carbon-membered linker with restricted flexibility my research focused on the design of a versatile ligand pattern allowing variation of the spacer length in the late steps of the synthesis (*cf.* Figure 7).

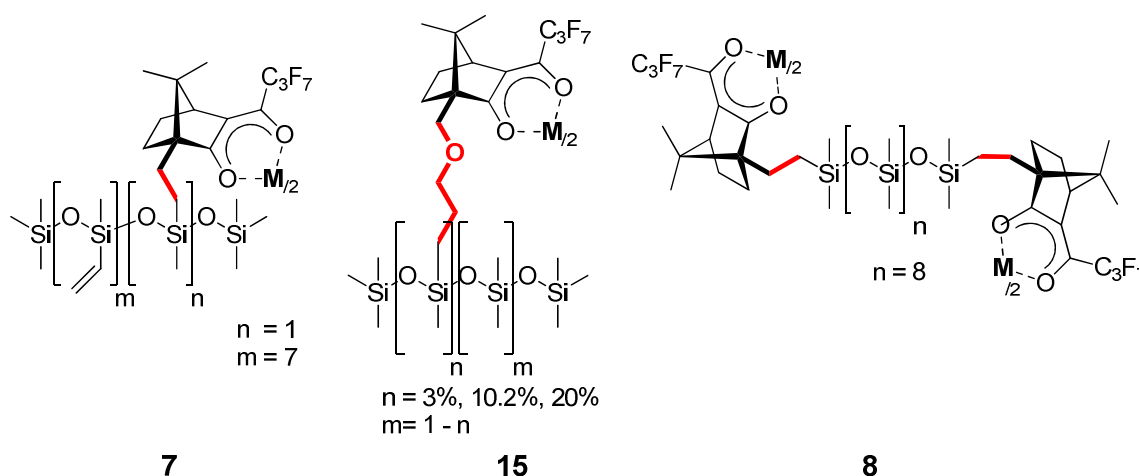


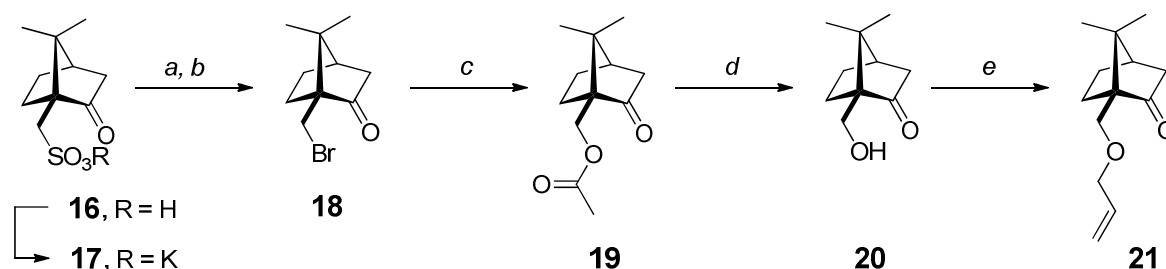
Figure 7 Camphor-derived selector pattern by Schurig (left), Fluck (right) and targeted, linker-variable selector pattern (middle).

Secondly, the synthesis of **7** and **8** give the opportunity for improvement as the need for freshly prepared cancerinogenic and potentially explosive diazomethane is unfavorable. Therefore a different synthetic approach was considered. Moreover, the challenging perfluoroacylation step had to be drastically improved regarding yield and purification procedure as outlined in chapter 1.1.3.

Synthesis of 1,3-Diketonato Camphor Ligands

Overall two different routes towards the camphor-derived chiral, fluorinated compounds prior to immobilization were developed. Starting from commercially available, enantiopure (1*S*)-(+)-camphorsulfonic acid the strategies either furnish an ether or thioether spacer, which were then subjected to immobilization onto the polysiloxane support (*cf.* Scheme 9).

For the preparation of **21** (1*S*)-(+)-camphorsulfonic acid (**16**) was first converted to its potassium sulfonate (**17**), which was reacted to its acid bromide derivative by reaction with phosphorus pentabromide, freshly prepared from phosphorus tribromide and bromine in carbon disulfide. Elimination of sulfur dioxide in *o*-xylene with catalytic amounts of calcium dichloride yielded (1*S*, 4*R*)-10-bromocamphor (**18**) in 35% yield. Further reaction with excess potassium acetate and acetic acid under molten conditions (>175 °C) resulted in the corresponding 10-acetatecamphor derivative **19** in quantitative yield (>97%). (1*R*, 4*R*)-10-hydroxycamphor (**20**) was prepared from of the acetate derivative by reaction in 10wt% methanolic solution of potassium hydroxide at reflux conditions and was obtained in good yield (92%). This route furnished (1*R*, 4*R*)-10-hydroxycamphor in four steps with an average yield of 31%. Ether synthesis to yield 10-allyloxycamphor **21** was achieved using 10-hydroxycamphor **20** and allylbromide under classical conditions (utilizing sodium hydride in tetrahydrofurane, 84% yield). With an overall yield of 10% in 6 steps synthesis had to be further improved.

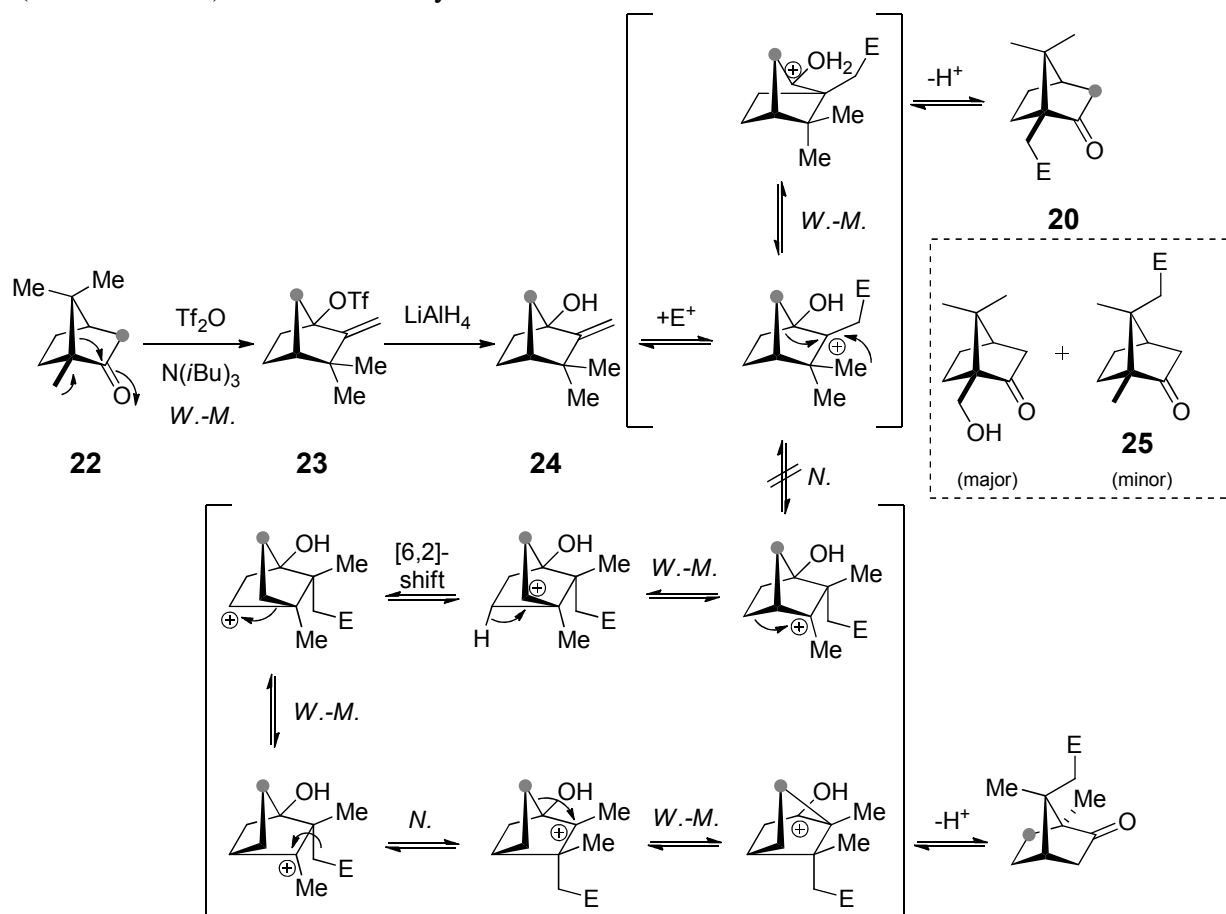


Scheme 9 Synthesis of 10-allyloxycamphor **21**.

Reaction conditions for the preparation allylether **21**: a) KOH, H₂O, r.t., quant. b) PBr₅, Et₂O, 35 °C, 48 h, 41% (**18**). c) KOAc, HOAc, 175 °C, 12 h, 93% (**19**). d) KOH, MeOH, 65 °C, 6 h, 92% (**20**). e) NaH, C₃H₅Br, THF, 0 – 50 °C, 2 h, 84% (**21**).

The preparation of enantiopure (1*R*, 4*R*)-10-hydroxycamphor by construction of a spirocyclopropanated camphor skeleton via *Diels-Alder*-reactions in 7 steps was not considered due to the use of thiophosgen and the overall low yield of 20%.^[101] An alternative enantioselective preparation of (1*R*, 4*R*)-10-hydroxycamphor **20** in a three-step synthesis starting from natural *d*-(+)-camphor via regioselective tandem-*Wagner-Meerwein* (*W.-M.*) rearrangements was quite appealing (*cf.* Scheme 10).^[102] In a first *Wagner-Meerwein* rearrangement triflic anhydride is used to furnish methylenecamphor-derivative **23** starting from *d*-(+)-camphor. This compound can be directly oxidized to their cyclopropanone diastereomers and subjected to base-induced ring-opening followed by regioselective *Wagner-Meerwein* rearrangement to enantiopure 10-hydroxycamphor **20**. Alternatively, camphen-1-yl-triflate **23** is converted into its alcohol derivative **24**, which is then subjected to cyclopropanation with *meta*-chloroperoxybenzoic acid (MCPBA) and regioselective *Wagner-*

Meerwein rearrangement. However, by following this route purification appeared challenging due to various side-products and the overall yield dropped from 70% (literature report)^[102] to 15%. Even though an access of enantiopure 10-hydroxycamphor **20** was stated by the authors and enantiopure camphor ($\geq 99\%$) was used as starting material the investigations of this approach showed that the obtained 10-hydroxycamphor was not diastereomerically pure (max. 93% *d.e.*) as determined by GC.



W.-M.: *Wagner-Meerwein* rearrangement N.: *Nametkin* migration (exo migrations) E: -OH (in case of *m*CPBA)

Scheme 10 Tandem *Wagner-Meerwein* rearrangement as reported (top), *Nametkin* migration (bottom) and observed products (dashed line).

A closer, more deeply look into literature revealed several papers^[103-119] dealing with side-products and side-reactions pointing out the need for strict temperature control and moreover the necessity of *N,N*-diisobutyl-2,4-dimethylpentylamine (DTBMP, **27**),^[108] which is nowadays not anymore commercially available. Utilizing triisobutylamine as the base, as suggested by the authors^[106] proofed to be not appropriate. This is in line with the observation that the diastereomeric distribution between camphen-1-yl-triflate **23** and camphen-4-yl-triflate **26** strongly depends on the base employed for the regioselective *Wagner-Meerwein* rearrangement (33% *d.e.* for camphen-4-yl-triflate **26** with sodium carbonate, 65% *d.e.* without base and 90% *d.e.* with DTBMP favoring camphen-1-yl-triflate **23**).^[117] With

generation of **26** *Nametkin* rearrangement becomes predominant leading to compound **25**. Furthermore, it was observed that traces of triflic acid catalyses the isomerization of camphen-1-yl-triflate in camphen-4-yl-triflate at room temperature (and at $-15\text{ }^{\circ}\text{C}$)^[117] – a second reasonable source for the observed reduced diastereoselectivity (*cf.* Figure 8, 9).

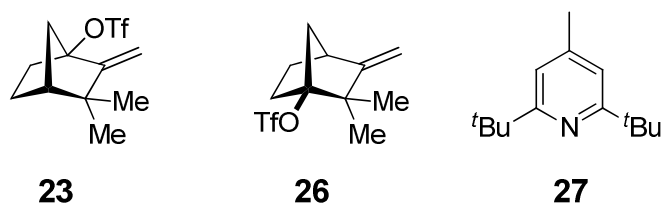


Figure 8 Camphen-1-yl-triflate (left), camphen-4-yl-triflate (middle) and *N,N*-diisobutyl-2,4-dimethylpentylamine (DTBMP, right).

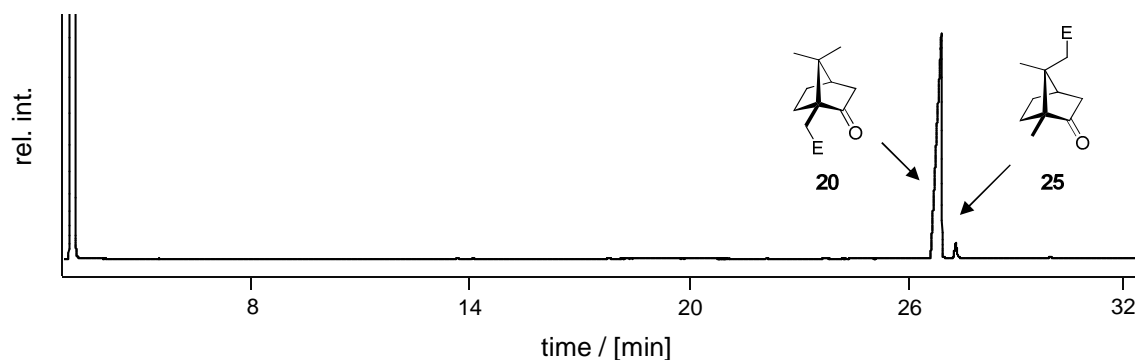
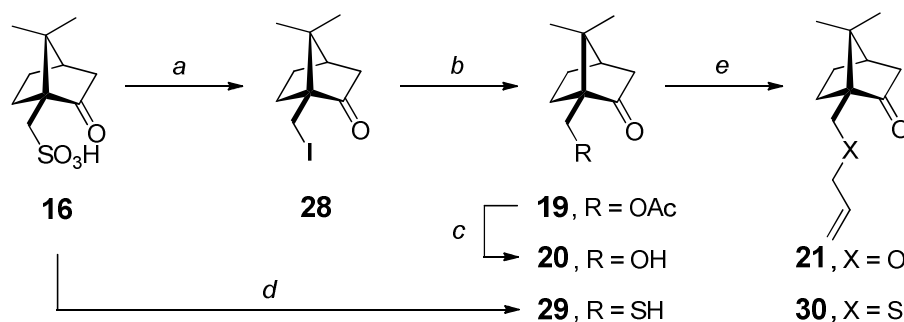


Figure 9 Gas chromatographic determination of diastereomeric purity of (1*R*, 4*R*)-10-hydroxycamphor derived in three steps by the method of Cerero and Martinez et al.¹⁰⁴ Separations were carried out after purification by flash-column chromatography using a 25 m HP-5 column (250 nm film-thickness) and helium as inert carrier gas; conditions: 50 $^{\circ}\text{C}$ to 180 $^{\circ}\text{C}$, 4K@120 kPa helium.

Finally, a change to (1*R*, 4*R*)-10-iodocamphor (**28**) proofed to be the ideal strategy. 10-iodocamphor was prepared directly from 1*S*-(+)-camphorsulfonic acid (**16**) in quantitative yield (>98%), thus saving two steps. Noteworthy, literature favors purification of 10-iodocamphor **28** by column chromatography,^[120-123] but due to involvement of triphenylphosphine and side products purification by sublimation is recommended, since high amounts of 10-iodocamphor can be readily obtained absolutely pure and in short time. Following the procedures outlined before the synthetic pathway was shortened and (1*R*, 4*R*)-10-allyloxycamphor (**21**) was prepared in overall 4 steps in very good overall yield of 73% (compared to 10%). Since the ligand pattern features an ether group as spacer and functional groups are of significant influence in complexation gas chromatography, another strategy involving a thioether moiety was considered as well. Therefore, the 10-hydroxycamphor analogue (1*S*, 4*R*)-10-thiocamphor (**29**) was prepared from 1*S*-(+)-camphorsulfonic acid (**16**) directly in a one-step procedure. Using thionylchloride and triphenylphosphine 10-

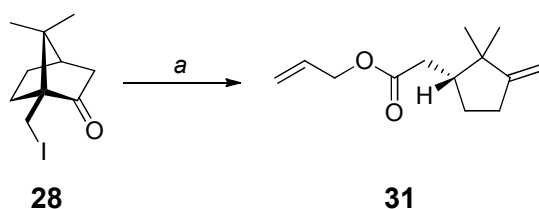
thiocamphor **29** was obtained directly in 94% yield. Following the same strategy, as applied for ether synthesis, (1*S*, 4*R*)-10-allylmercaptocamphor (**30**) was obtained in 81% yield. Utilization of this shortened two-step approach allylthiocamphor **30** was prepared in good overall yield of 76% (*cf.* Scheme 11).



Scheme 11 Improved access to (1*R*, 4*R*)-10-allyloxycamphor (**21**) and preparation of (1*S*, 4*R*)-10-allylmercaptocamphor (**30**).

Reaction conditions: a) I₂, PPh₃, toluene, 111 °C, 16 h, 98% (**18**). b) KOAc, HOAc, 175 °C, 12 h, 97% (**19**). c) KOH, MeOH, 65 °C, 6 h, 92% (**20**). d) SOCl₂, 80 °C, 4 h; PPh₃, H₂O, dioxane, 4 h, 100 °C, 94% (**29**). e) NaH, C₃H₅Br, THF, 0 – 50 °C, 2 h, 84% (**21**) and 84% (**30**).

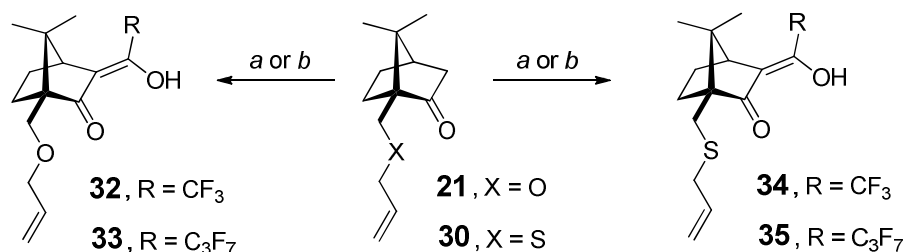
Noteworthy, during the endeavor to further shorten the synthetic pathway to 10-allyloxycamphor **21**, 10-iodocamphor **28** was directly subjected to conditions, which were intended to furnish *in situ* displacement of iodine by an allylic alcohol. Instead of the desired product **21** formation of (*R*)-all-7-yl 2-(1,2,2-trimethyl-3-methylenecyclopentyl)acetate (**31**) as the major product was detected. Early literature precedents^[124, 125] account for a transformation consisting of regioselective rearrangements initiated under basic conditions followed by *in situ* etherification. The enantiopure, newly derived product was isolated in 54% yield. This one step-procedure and related transformations may be of valuable interest in natural product synthesis (*cf.* Scheme 2)



Scheme 12 Regioselective, base induced, camphor cleavage to methylenecyclopentylester **31**.

Reaction conditions: NaH, C₃H₅OH, DMF, 80 °C, 24 h, 54%.

The key step in synthesis – the introduction of a perfluoroalkanoyl group at the selector – is a necessary prerequisite for enhanced enantioselectivity and to generate stable diketonate metal complexes. The general procedure involves deprotonation of camphor or related monoterpene derivatives at the α -carbonyl position by lithium diisopropyl amide at low temperatures ($-70\text{ }^{\circ}\text{C}$) to furnish enolate formation and suppress side-reactions. Even though low temperatures can be applied, the reaction is accompanied by side-reactions, like *O*-acylation, bisacylation, decomposition or incomplete conversions, which renders purification of the product quite challenging involving multiple-steps (*cf.* Chapter 1.1.3).^[126] Therefore different bases for enolate formation were first tested. Sodium hydride in tetrahydrofuran showed only moderate conversions over four days at reflux temperature, but remarkably no *O*-acylation and only minor side products were detected (including methyl ethers as anomalous sodium hydride reduction by-products).^[127] Encouraged by this result potassium- and lithium hydride for enolate formation were investigated. Whereas potassium hydride showed almost no conversions, lithium hydride was found to be the base of choice. Deprotonation of either 10-allyloxycamphor or 10-allylmercaptocamphor was achieved at reflux conditions (8 – 24 h) and addition of the fluorinated alkyl esters yielded the desired *C*-fluoroacylation in an unexpected, extremely clean reaction! Due to different melting points of the employed perfluorinated starting materials, purification in case of trifluoroacetylation can be achieved simply by evaporation of excess trifluoromethylester (bp. $43\text{ }^{\circ}\text{C}$) to yield the analytically pure product. By introduction of a hexafluorobutyl moiety (ethyl heptafluorobutyrate, bp. $95\text{ – }98\text{ }^{\circ}\text{C}$) the pure product can be distilled at elevated temperatures ($120\text{ }^{\circ}\text{C}$) under reduced pressure. Following this procedure (1*R*, 4*S*)-3-trifluoromethanoyl-10-allyloxycamphor (**32**, 94%), (1*R*, 4*S*)-3-heptafluorobutanoyl-10-allyloxycamphor (**33**, 75%), (1*S*, 4*S*)-3-trifluoromethanoyl-10-allylmercaptocamphor (**34**, 94%) and (1*S*, 4*S*)-3-heptafluorobutanoyl-10-allylmercaptocamphor (**35**, 77%) were obtained in very good to excellent isolated yields (colorless, viscous oils). Reasons for lower yields in case of heptafluoroacylation are observed due to distillative purification of small product quantities (*cf.* Scheme 13).



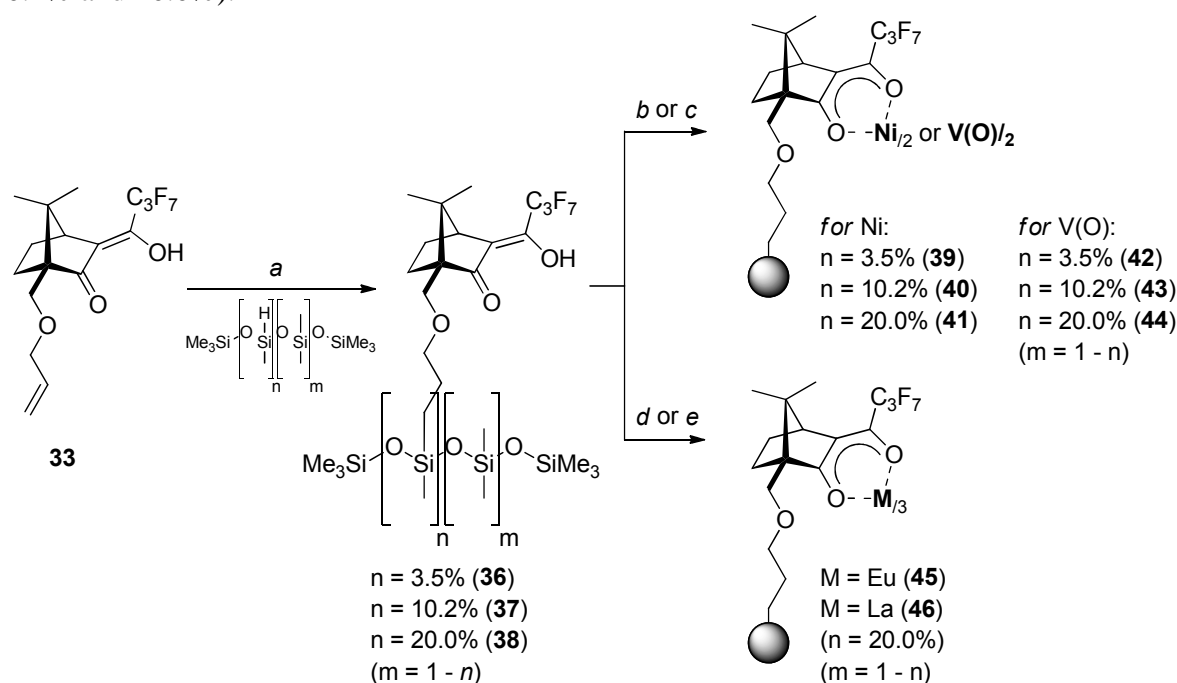
Scheme 13 Perfluoroacylation step of 10-allyloxy- and allylmercaptocamphors to furnish allylcamphor β -diketonate precursors prior to immobilization.

Reaction conditions: a) LiH, CF₃CO₂Me, THF, 0 – 67 °C, 14 h, 94% for **32**, 94% for **34**. b) LiH, C₃F₇CO₂Et, THF, 0 – 67 °C, 14 h, 75% for **33**, 77% for **35**.

1.3.2 Preparation of *Chirasil-Metal* Phases

Ligand Immobilization and Metal Incorporation

To investigate the potential of the newly derived chiral ligands (1*R*, 4*S*)-3-heptafluorobutanoyl-10-allyloxycamphor (**33**) with a high degree of perfluorination being beneficial for enantioselectivity and polysiloxanes as a suitable support (high thermal and chemical stability) were chosen. Therefore hydridomethylpolysiloxane (HMPS, $M_w \sim 3000$ g/mol) with varying content of free silane groups were synthesized, characterized and the silane content determined by NMR spectroscopic measurements (SiH content 3.5%, 10.2% and 20.0%).^[128]



Scheme 14 Synthesis of polymer-bound camphor ligands **36** – **38** and *Chirasil-Metal-OC₃* preparation by metal incorporation (**39** – **46**, M = Ni, V(O), Eu, La).

Reaction conditions: a) HMPS, *Karstedt's* cat., toluene, sonic, r.t. – 110 °C, 10 h, 88% for **36**, 73% for **37**, 73% for **38**. b) Ni(OAc)₂·4H₂O, H₂O-heptane (2:3), 100 °C, 2 h, 92% for **39**, 89% for **40**, 85% for **41**. c) V(O)SO₄·xH₂O, NEt₃, H₂O-heptane (2:3), 100 °C, 5 h, 79% for **42**, 70% for **43**, 74% for **44**. d) Eu(OAc)₃·xH₂O, NEt₃, H₂O-heptane (2:3), 100 °C, 5 h, 80% for **45**. e) La(OAc)₃·xH₂O, NEt₃, H₂O-heptane (2:3), 100 °C, 5 h, 86% for **46**.

Immobilization was achieved by platinum-catalyzed hydrosilylation reaction of 10-allyloxycamphor and HMPS using Pt-divinyltetramethyldisiloxane (*Karstedt's* catalyst)^[74] in anhydrous toluene under ultrasonication over 10 h at elevated temperatures. Purification thereof resulted in the chemical-bonded ligands with SiH contents of 3.5% (**36**, 88% yield), 10.2% (**37**, 73% yield) and 20.0% (**38**, 73% yield) in good yields along with increased

viscosity. Immobilization of (1*S*, 4*S*)-3-trifluoromethanoyl-10-allylmercaptocamphor (**34**) and (1*S*, 4*S*)-3-heptafluorobutanoyl-10-allylmercaptocamphor (**35**) failed using *Karstedt's* catalyst and hexachloroplatinic acid (H_2PtCl_6 , *Speiers'* catalyst).^[73] The results are in line with the observation that stereoelectronic properties of substituents at the reactants^[129] (and at the silicon atom)^[130] strongly influence the reactivity of the carbon-carbon double bond and account for the general more challenging hydrosilylation of allylthioethers. However, an appropriate choice of catalyst generally allows hydrosilylation reactions of thiocompounds as well.^[72, 75-77, 131]

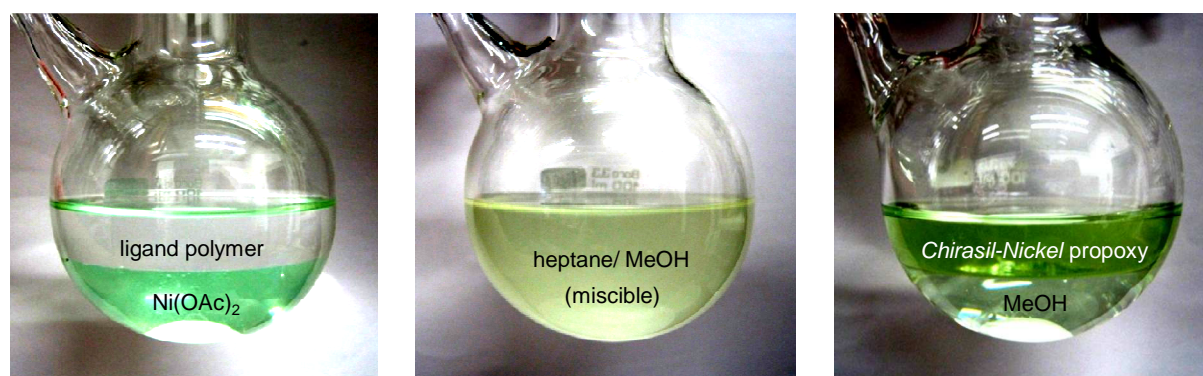


Figure 10 Color-change as observable indicator for successful metal-incorporation.

Preparation of *Chirasil-Nickel-OC*₃ **41** shown, top layer (heptane), bottom layer (methanol): $\text{Ni}(\text{OAc})_2 \times 4 \text{H}_2\text{O}$ and ligand polymer **38** prior to reaction (left), reaction mixture upon heating (middle) and *Chirasil-Nickel-OC*₃ **41** separation upon cooling (right, top layer).

Metal incorporation was accomplished using a modified procedure of Schurig and coworkers^[83]. In a two-phase liquid-liquid reaction between metal precursor and chiral polysiloxanes (*Chirasil*) takes place. For the preparation of *Chirasil-Nickel-OC*₃, nickel(II) acetate tetrahydrate dissolved in methanol and ligand polysiloxanes **36** – **38** dissolved in heptane were reacted in a two-phase mixture, which becomes miscible at elevated temperatures. Re-separation upon cooling and purification resulted in nickel(II) bis[(1*R*, 4*S*)-3-heptafluorobutanoyl-10-propoxycamphorates, hfpc] immobilized on polysiloxane as pale greenish to deep greenish oils (**39**, 3.5% $\text{Ni}(\text{hfpc})_2 @ \text{PS}$, 92% yield; **40**, 10.2% $\text{Ni}(\text{hfpc})_2 @ \text{PS}$, 89% yield; **41**, 20.0% $\text{Ni}(\text{hfpc})_2 @ \text{PS}$, 85% yield, *cf.* Scheme 14). The reaction progress can be easily monitored since the metal-precursor (green color) is only soluble in the methanolic (bottom) solvent and the colorless polymer (HMPS) is dissolved in the aliphatic heptane layer (top). Decolorization of the methanolic layer and color change of the aliphatic (heptane) layer to green is indicative for successful metal-incorporation (*cf.* Figure 10).

Incorporation of oxovanadium(IV) was achieved using oxovanadium(IV) sulfate pentahydrate and triethylamine to yield the *Chirasil-Vandyl-OC₃* polysiloxanes (**42**, 3.5% V(O)(hfpc)₂@PS, 79% yield; **43**, 10.2% V(O)(hfpc)₂@PS, 70% yield; **44**, 20.0% V(O)(hfpc)₂@PS, 74% yield) as purple-reddish oils. A change in the color-depth of the polymers is observed for varying selector-concentration and can be visualized by dissolution of small quantities in dichloromethane (*cf.* Figure 11). Following this procedure europium(III) acetate and lanthanum(III) acetate hydrate furnished *Chirasil-Europium-OC₃* (**45**, 20.0% Eu(hfpc)₃@PS, 80% yield) as a yellow and *Chirasil-Lanthanum-OC₃* (**46**, 20.0% La(hfpc)₃@PS, 86% yield) as an orange oil. (*cf.* Scheme 14).



Figure 11 Selector-content of *Chirasil-Vandyl-OC₃* visualized by dissolution of **42**, **43** and **44** in dichloromethane.
Selector concentration (left to right): 20.0%, 10.2% and 3.5% V(O)(hfpc)₂@PS.

Validation of Immobilization and Characterization of (CB)*Chirasil-Metal* phases

Immobilization of (1*R*, 4*S*)-3-heptafluorobutanoyl-10-allyloxycamphor (**33**) onto polysiloxanes and metal incorporations were monitored by IR and NMR spectroscopic measurements. This is crucial for the determination of the true nature of immobilized product and complexes present and indeed potential sources for errors or wrong conclusions. Therefore, the following detailed study is intended to contribute to this field of broad interest.^[5, 132-138]

Ligand Immobilization and Metal Incorporation Monitored by IR Spectroscopy

Immobilization of the (1*R*, 4*S*)-3-heptafluorobutanoyl-10-allyloxycamphor (**10**) on polysiloxanes can be detected and considered >99% complete by fading of the silane band at $\nu_{(\text{Si-H})} = 2160 \text{ cm}^{-1}$ and detection of two sets of bands resulting from symmetric $\nu_{(\text{C=C})}$ and $\nu_{(\text{C=O})}$ stretching frequencies and asymmetric $\delta_{(\text{OH})}$ deformations of the camphordiketone

ligand (*cf.* Figure 1). By comparison of polysiloxanes of different silane content and their hydrosilylated (CB)CSPs **14** – **16** a characteristic increase in the intensities along with higher degree of SiH content (*resp.* degree of ligand immobilization) is observed for the SiH as well as for the carbonyl-, carbon-carbon stretching and carbon-hydroxyl deformation frequencies. Finally metal incorporation of nickel(II) and oxovanadium(IV) was monitored. A pronounced change towards lower frequencies is observed for nickel(II) bis[(1*R*, 4*S*)-3-heptafluorobutanoyl-10-propoxycamphorate] on polysiloxanes [**17** – **19**, Ni(hfpc)₂@PS_{3.5-20.0%}, *Chirasil-Nickel-OC*₃], regarding the $\nu_{(C=C)}$, $\nu_{(C=O)}$ and $\nu_{(O-Metal)}$ frequencies. Disappearance of the bands at 1701 cm⁻¹ and 1642 cm⁻¹ of the diketone ligand and appearance of two new bands at 1641 cm⁻¹ and 1627 cm⁻¹ validate the successful nickel incorporation (*cf.* Figure 12).

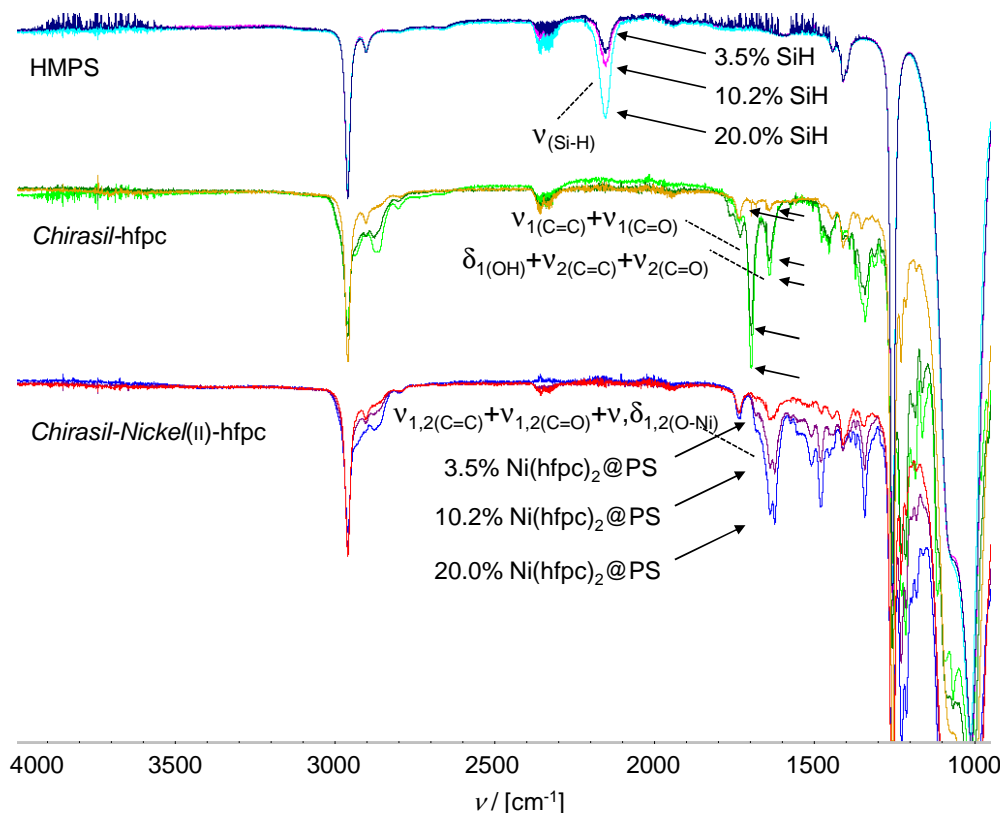


Figure 12 Immobilization of camphordiketone ligand **33** on hydridomethylpolysiloxanes with varying SiH-content and Ni(II) incorporation monitored by IR-spectroscopic measurements – *Chirasil-Nickel-OC*₃ **39**, **40** and **41**.

3.5%, 10.2%, 20.0% SiH-content; overlay of 9 spectra, characteristic absorption bands marked with arrows.

Although less pronounced, this change in frequencies is also observed for the incorporation of oxovanadium(IV) with bands at 1686 cm⁻¹ and 1635 cm⁻¹ (*Chirasil-Vanadyl*, **20** – **22**, *cf.* Figure 13). With varying ligand content in the polymer the intensities change, like discussed

for the nickel (CB)CSPs. Characteristic IR spectra for the europium and lanthanum (CB)CSPs (not shown) related to *Chirasil-Nickel-OC₃*, resp. *Chirasil-Vanadyl-OC₃*, were obtained.

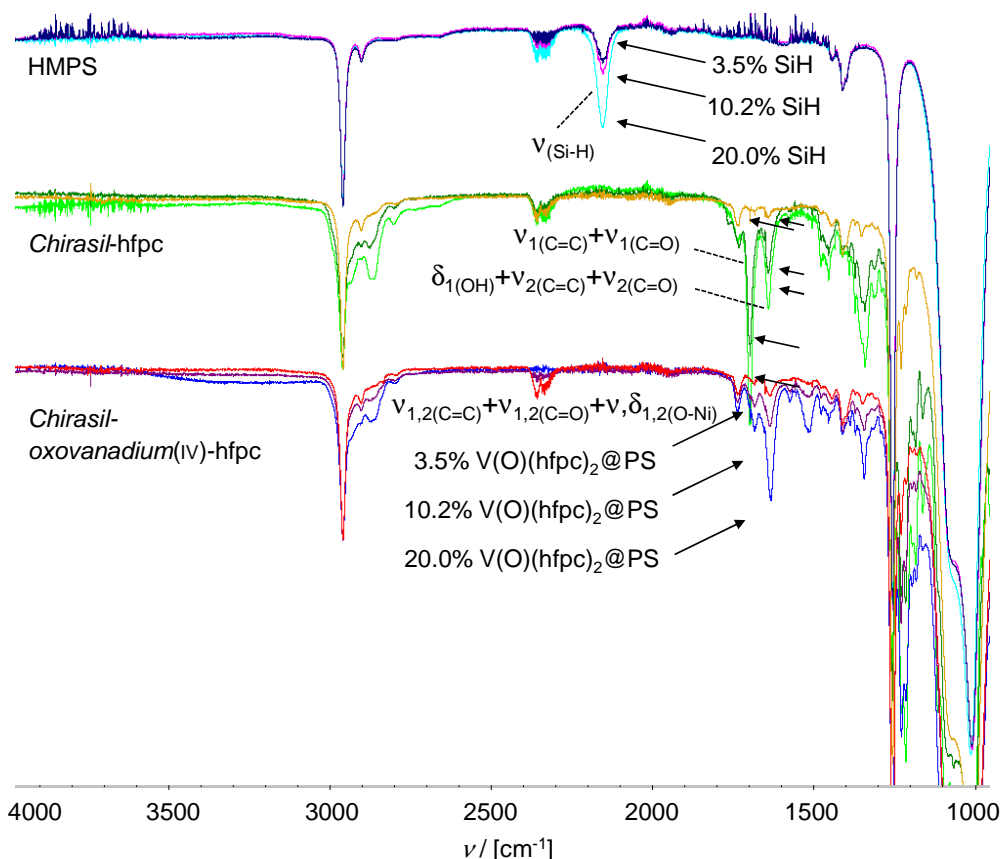


Figure 13 Immobilization of camphordiketone ligand **33** on hydridomethylpolysiloxanes with varying SiH-content and oxovanadium(IV) incorporation monitored by IR-spectroscopic measurements – *Chirasil-Vanadyl-OC₃* **42**, **43** and **44**.

3.5%, 10.2%, 20.0% SiH-content; overlay of 9 spectra, characteristic absorption bands marked with arrows.

Ligand Immobilization and Metal Incorporation Monitored by ¹H NMR Spectroscopy

The immobilization progress was also studied and verified by NMR spectroscopic measurements. Figure 14 shows the ¹H NMR spectra of starting materials, *Chirasil* and *Chirasil-Metals*. Due to detection limits only the spectra for a high silane (resp. ligand/ metal-camphorate) content of 20.0% are depicted (cf. Figure 14).

In spectrum A the signal for the silane protons at 4.68 ppm and methyl moieties of HMPS (0.2 to -0.3 ppm) can be easily detected. In B (1*R*, 4*S*)-3-heptafluorobutanoyl-10-allyloxycamphor (**33**) prior to immobilization is displayed and can be identified by its allylic protons at 5.93 – 5.86 (m, 1H), 5.28 (dd, 1H, methyleneCH_{2trans}), 5.18 (dd, 1H, methyleneCH_{2cis}) ppm and its characteristic singlets for the two C7-exomethyl groups at 1.07

and 0.96 ppm. In spectrum C immobilization onto the polysiloxane and complete conversion >99% can be verified by fading of all allylic ligand-proton signals in the range between 6.00 and 5.00 ppm as well as vanish of the silane signal of the polymer at 4.68 ppm.

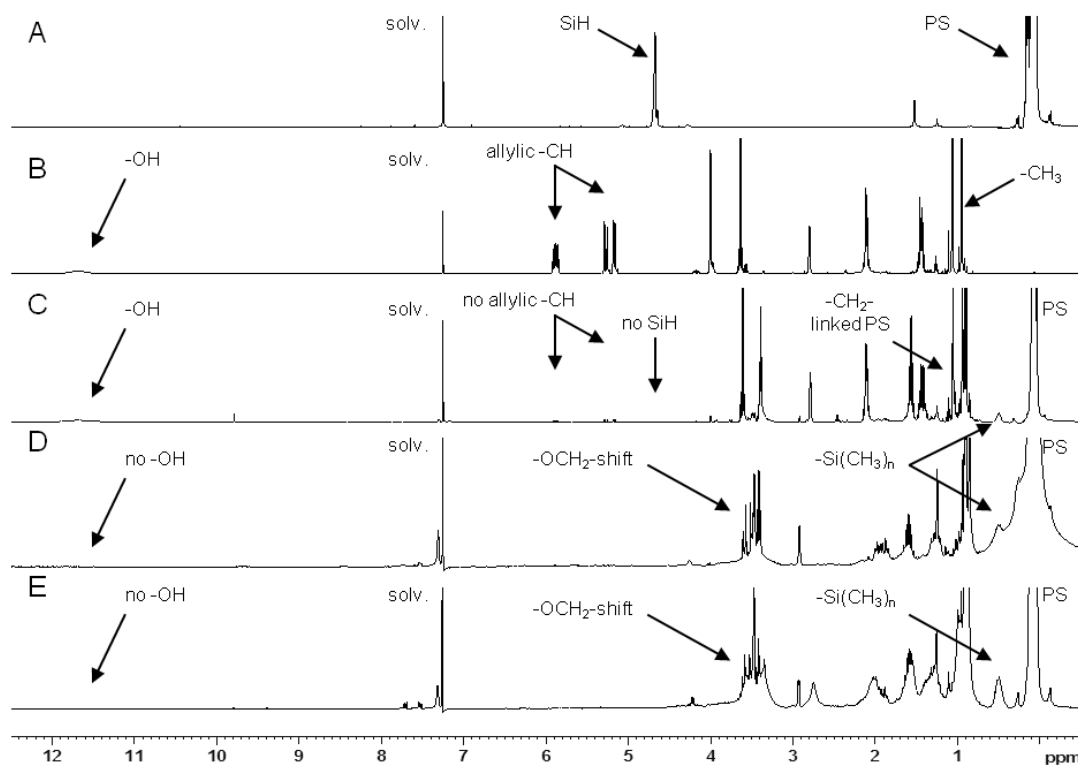


Figure 14 Immobilization of **33** on polysiloxane and incorporation of Eu(III) and La(III) monitored by ^1H NMR spectroscopy – *Chirasil-Europium/ Lanthanum-OC₃* **45** and **46**.

Characteristic signals highlighted with arrows; spectrum A) HMPs (20.0% SiH content), (B) free ligand [(1*R*, 4*S*)-3-heptafluorobutanoyl-10-allyloxycamphor (**33**)], (C) hfpc@PS (**38**) (immobilization step), (D) Eu(hfpc)₃@PS (metal incorporation step to **45**), (E) La(hfpc)₃@PS (“ to **46**).

The lack of signals in this region (5 – 6 ppm) is noteworthy, since ether-cleavage of the ligand and side reactions during hydrosilylation are possible, which makes purification as well as any further application of these polymers difficult (e.g. remaining SiH functionalities as a source for metal-reduction or remaining free complex species altering the selector performance). While these signals disappeared, the characteristic C7-methyl groups of the camphor moiety (1.07 and 0.96 ppm) and the broad singlet at 11.69 ppm for the hydroxyl group of the β -diketonate is still present, validating successful immobilization of the ligand on the polymer. Furthermore, its remarkably that it was possible to identify a triplet-signal at 0.91 ppm for the newly formed ligand-to-polymer silanomethyl bond (t, 2H, -Si-CH₂-linker) and a multiplet at 0.56 – 0.46 ppm for the silane methyl groups directly attached to the opposite location of the silicon atom where immobilization took place. Finally, metal incorporation is proven by disappearance of the hydroxyl-signal at 11.69 ppm as well as a

characteristic shift of the camphor-methylene signals between 3.1 and 3.9 ppm for *Chirasil-Europium* (**D**) and *Chirasil-Lanthanum* (**E**, cf. Figure 14). The results are in agreement with the ^{13}C and ^{19}F NMR signals obtained for the free- and immobilized hfpc-ligand **33** (not shown, cf. *Experimental Section*).

1.3.3 Enantioselective Complexation Gas Chromatography

1.3.3.1 Selector Concentration in the Discrimination of Chiral Epoxides

After characterization of the newly derived CSPs their potential was investigated in the separation of enantiomers using complexation gas chromatography. Therefore, the CSPs **17** – **24** exhibiting different hfpc-metal contents (3.5%, 10.2% and 20.0%) were coated onto the inner surface of fused-silica capillaries (0.25 mm I.D.) each using the static method described by Grob^[139] giving a defined polymer film-thickness' of 250 nm. The column-capillaries were conditioned (for conditioning of columns cf. *Experimental Section*), installed into the GC and tested. After promising first results with *Chirasil-Nickel-OC₃* in complexation GC, their potential by separation of the smallest classes of chiral compounds, namely alkyl- and halo-substituted oxiranes on this novel (CB)CSP is presented (cf. Figure 15). The prerequisite for any successful chromatographic application, in particular the stability and integrity of the selector-system, was validated. With *Chirasil-Nickel-OC₃* operating at 160 °C thermostability was proven over a period of two weeks and no loss in the quality of resolution was observed. The maximum operation temperature seems to be at higher temperature and was not probed.

Chlorhydrin, methyloxirane, butyloxirane and even octyloxirane were successfully baseline-separated. To investigate the influence of the amount of selector immobilized at the polysiloxanes on the resolution of enantiomers, all separations were conducted with capillaries of same film-thickness' under equal chromatographic conditions, but with varying hfpc-content. The results are depicted in Figure 15. On the CSP with 10.2% selector only the smallest selectand (methyloxirane) was partially separated. Chlorhydrin was separated to the baseline with a selector content of 20.0%. Methyloxirane, epoxyhexane and epoxydecane were completely separated into their enantiomers on the CSPs containing 10.2% and 20.0% selector. Retention-times as well as resolution of compounds increased with higher selector concentrations. The results are in accordance with literature,^[59] correlating prolonged chemical retention of enantiomers of the selectand with an increase of activity (concentration) of the selector (cf. Figure 15).

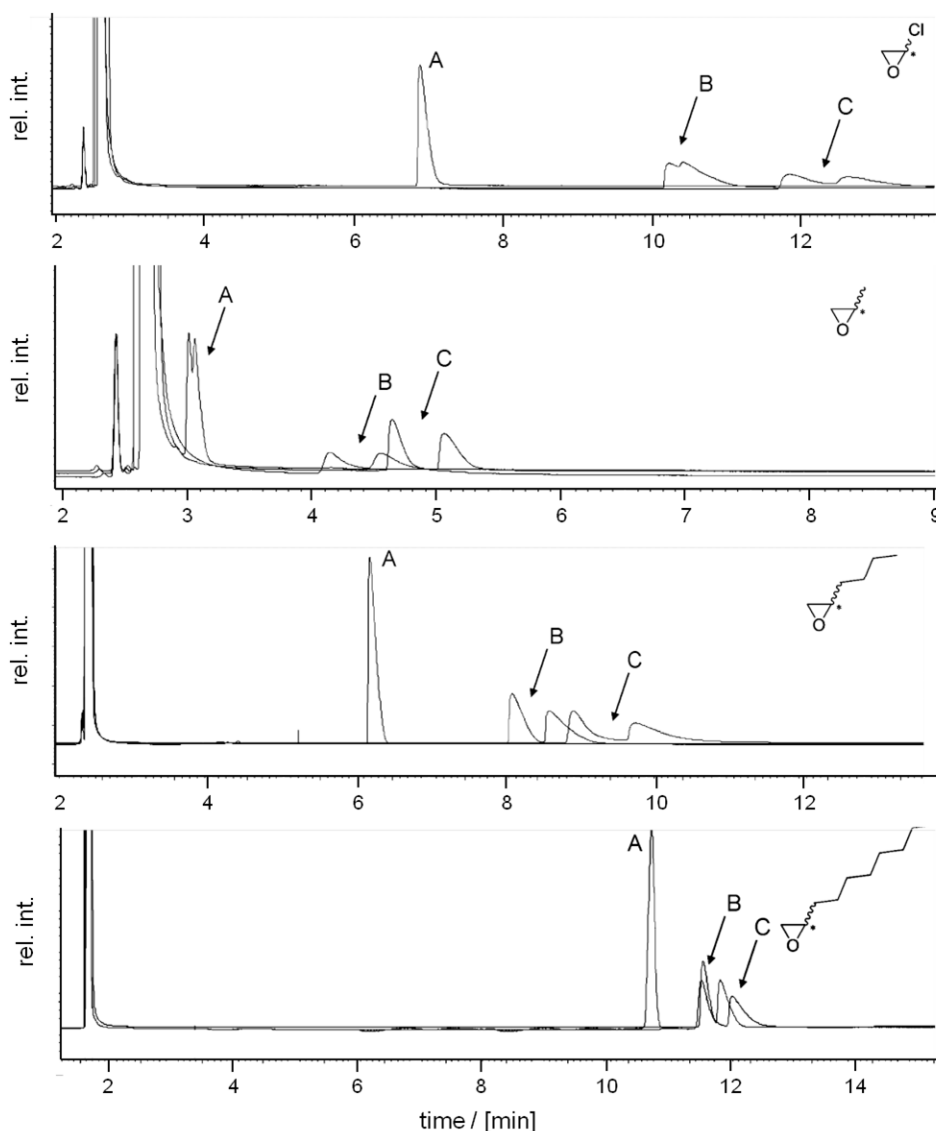


Figure 15 Resolution of oxiranes using *Chiral-Nickel-OC₃* stationary phases (**39** – **41**) with varying selector concentration.

A: 3.5% (**17**), B, 10.2% (**18**) and C: 20.0% (**19**); *enantiomeric pairs highlighted with arrows*; separations were performed using *Chiral-Nickel* coated fused-silica capillaries, 25 m, 250 nm film-thickness with helium as the inert carrier gas; conditions (top to bottom): 30 °C, 85 kPa; 40 °C, 85 kPa, 100 °C, 85 kPa and 110 °C, 120 kPa.

1.3.3.2 *Chiral(hfpc)_x@PS* of Ni(II), Eu (III), La (III) and Oxovanadium(IV)

Since enantioselectivity in complexation gas chromatography is based on metal-organic coordination, the type of metal present and the functional group of the selectand has significant influence on the chromatographic resolution. Noteworthy, there is no general relationship between strength of molecular complexation of selectands and the magnitude of enantioselectivity as proofed for related *Chiral-Nickel* stationary phases.^[126] The

enantioselectivity, $\Delta\Delta G$ and the related separation factor α only depend on the energy difference of the transient enantiomer-selector complexes. In regard to the results obtained from selector-concentration-tests with *Chirasil-Nickel-OC₃* stationary phases (**39** – **41**, cf. Chapter 1.3.3.1) the corresponding coated columns of *Chirasil-Europium-OC₃* (**45**) and *Chirasil-Lanthanum-OC₃* (**46**) were prepared containing 20.0% selector and a standard polymer film-thickness of 250 nm and 25 m length. Racemic 2-[(prop-2-yn-1-yloxy)methyl]oxirane (**47**) was chosen as model substrate for the resolution. Separation of enantiomers occurred on both (CB)CSPs but prolonged retention times were observed with *Chirasil-Lanthanum* and *Chirasil-Europium* without improvement of separation. By metal-coordination of europium(III) and lanthanum(III) the electronics as well as the coordination geometry is significantly changed. In both *Chirasil-Metals* three ligands are placed in the coordination sphere of the metal centre (two in the case of nickel and oxovanadium). Therefore, an approach of the incoming selectand is likely to be hampered and interaction via coordination is reduced on europium(III) and lanthanum(III) phases. Noteworthy, the discrimination of the enantiomers might be higher within rare earth metal-selectors considering their success as chiral shift reagents. But in fact, the detected resolution is reduced compared to *Chirasil-Nickel-OC₃* **41** (20% selector, cf. Figure 16).

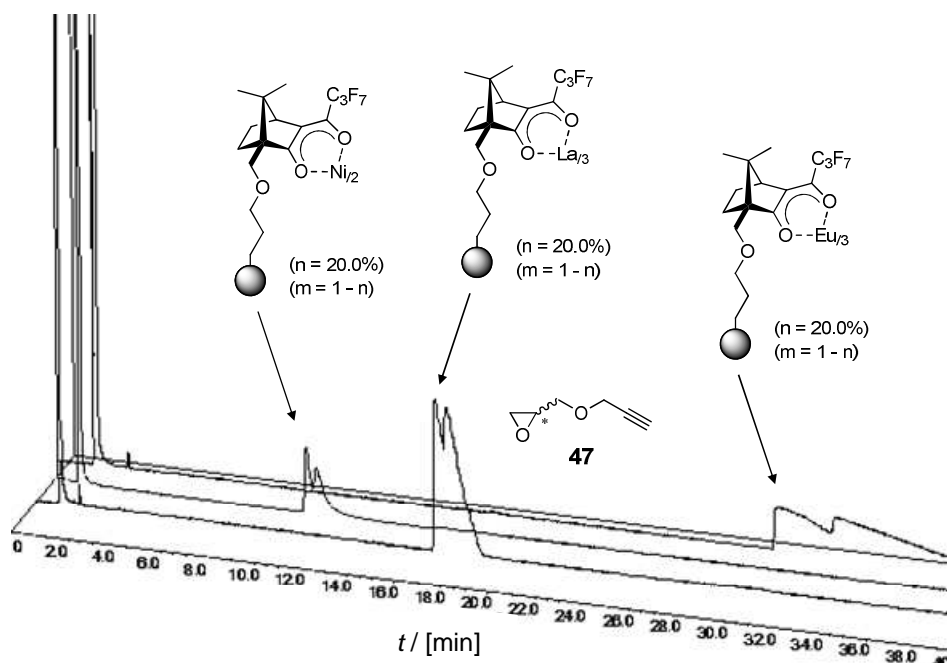


Figure 16 Influence of metal-chelate on the enantioseparation of compound **47** using Ni(hfpc)₂@PS (**41**), Eu(hfpc)₃@PS (**45**) and La(hfpc)₃@PS (**46**).

Chirasil-Metal-OC₃ columns (25 m, 250 nm film-thickness) with helium as the inert carrier gas; conditions: 80 °C, 85 kPa.

Complexation GC requires coordinative selector-selectand interactions as well as fast equilibration between mobile and coordinating analytes in the liquid polymer (and gas) phase.

The observed longer retention time for both rare-earth metal phases account for strong selector-selectand interactions with an almost doubled retention time and extensive peak-broadening on *Chirasil-Europium-OC₃*, compared to the lanthanum phase. These results are indicative for the formation of stable rare earth selector-selectand associates, which are incapable of adopting a sufficient distribution equilibria. Therefore, no enhanced enantioselectivity was obtained for europium and lanthanum (CB)CSPs and thus application of the corresponding nickel-containing (CB)CSP in complexation GC is most efficient.

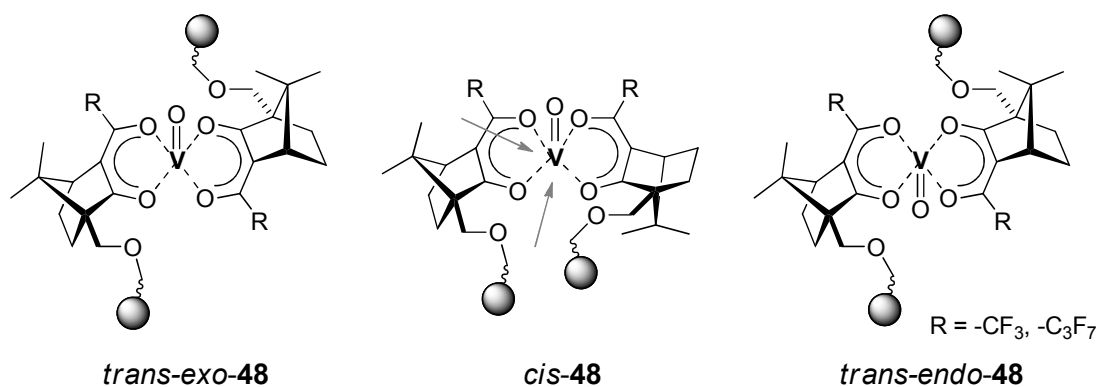


Figure 17 Possible geometries of *Chirasil-Vanadyl-OC₃* adopted in the polymer. Approach vectors for incoming substrates shown for *cis-48* and highlighted with arrows (grey).

Due to the strong coordination capability of nickel(II) weakened interactions between selector and selectand are expected by a change to oxovanadium(IV). Moreover, significant changes in enantioselectivity and complexation are reported.^[52, 93, 140, 141] By applications of *Chirasil-Vanadyl-OC₃* phases (3.5%, 10.2% and 20.0% selector content) only low separation tendencies were obtained and discrimination of enantiomers diminished completely for analytes exhibiting strong coordinative functional groups, like alcohols, amides and ketones. These observations are in agreement with the results obtained by Weber^[142] and Fluck^[83] with camphor-derived *Chirasil-Vanadyl* CSPs. Reasons for this observations may be the formation of different diastereomeric oxovanadium(IV) complex geometries and the resulting varying approach vectors for incoming selectands. For *Chirasil-Vanadyl-OC₃* the analytes are likely to enter the complex from the opposite site to the oxygen atom. Even though the real structure of the camphor selector oxovanadium-complexes at the polymer is subject of current investigations,^[50, 143] and their diastereomeric distribution is still unclear, three different complex-structures can be envisaged. The approach was shown to occur *trans* to the oxygen atom for benzaldehyde and *cis* for *N*-benzylidene-benzylamine thus proofing that different complexation geometries are possible in *Chirasil-Vanadyl* phases. (*cf.* Figure 17).^[83, 90, 93, 94]

1.3.3.3 Extending the Scope of Chirasil-Ni(hfpc)₂@PS – Separation of Enantiomers using Compound Libraries with Differing Functional Groups

As displayed in Figure 15 oxiranes were successfully baseline separated on the *Chirasil-Nickel-OC₃* phase **41** with a selector concentration of 20.0% and a polymer film-thickness of 250 nm. To further extend the scope of enantioresolutions the film-thickness was increased to 500 nm (20.0% selector) and a mixed phase consisting of 125 nm polydimethylsiloxane (GE-SE 30) and 125 nm *Chirasil-Nickel-OC₃* (20% selector) were prepared and tested in complexation GC. Screening of various racemic compounds exhibiting different functional groups showed separation of enantiomers of a broad range of compounds with overall high separation factors.

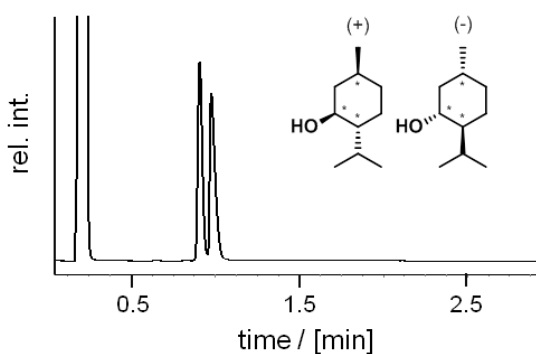


Figure 18 Baseline separation of (+/-)-menthol after <1min on 5 m of *Chirasil-Nickel-OC₃*.

Chirasil-Nickel-OC₃ column (5 m, 500 nm film-thickness, 20% selector) with helium as the inert carrier gas; conditions: 140 °C, 85 kPa.

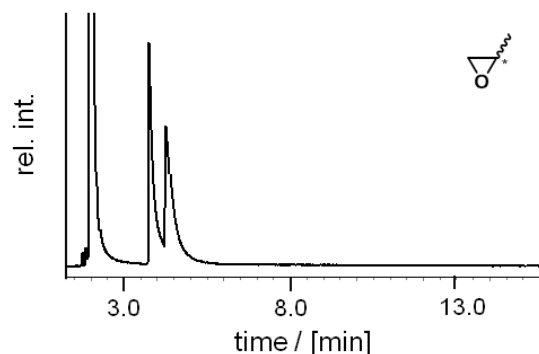


Figure 19 Nearly complete resolution of methyloxirane after 47 seconds on 25 m of *Chirasil-Nickel-OC₃* mixed CSP.

Chirasil-Nickel-OC₃ column mixed phase (25 m, 250 nm film-thickness with 50% (125 nm) polydimethylsiloxane, 20% selector) with helium as the inert carrier gas; conditions: 60 °C, 85 kPa.

The resolution includes halogen-, alkyl- and aryl substituted oxiranes, primary, secondary and tertiary alcohols, substituted internal and terminal alkenes, alkynes, cyclic ethers, ketones and allenes. Not only oxiranes but also alcohols (entries **8**, **15a** – **17a**, **28**) were successfully separated with α -values between 1.10 and 1.12 using the standard 25 m 250 nm *Chirasil-Nickel-OC₃* column were obtained. Excellent resolutions were observed for methyloxirane (entry **1c**, $\alpha = 1.32$) on the mixed phase and the highest separation-factor α was observed for the separation of TMS-alkynylbenzylalcohol enantiomers (entry **18**) with $\alpha = 1.66$ after only 6 minutes on an 8 m column (250 nm). Moreover, an extraordinary and extremely fast separation after only 47 seconds (30 sec. adjusted retention time!) was obtained using a 5 m (500 nm) *Chirasil-Nickel-OC₃* column for methyloxirane ($\alpha = 1.21$, entry **1b**, cf. Figure 19)!

(+/-)-menthol was also separated to the baseline in less than 1 min ($\alpha = 1.10$, 46 sec. adj. retention time) at 140 °C using the same column (*cf.* Figure 18). For diethyl-1,3-allene dicarboxylate (entry **29**) a high separation factor of 1.33 was obtained. By comparison of the resolution for mono-alkylated oxiranes on a standard 25 m and on a mixed 25 m *Chirasil-Nickel-OC₃-GESE-30* phase (entries **1a, 1c; 2a, 2b; 3a, 3c** and **4a, 4c**) the separation factor on both phases is decreasing along with higher oxirane-homologues (as expected). Furthermore, all four stereoisomers of chalcogran, the principal component of the aggregation pheromone of the bark beetle *pityogenes chalcographus*, consisting of a set of two interconverting epimer pairs (2*R*,5*R*-, 2*S*,5*S*-, 2*S*,5*R*- and 2*R*,5*S*-, entries **25a,b** and **26a,b**) were baseline separated as well. All columns employed, the measured and calculated values of each enantiomeric pair (A and B), like t_0 , corrected retention times $t_{R(A/B)}'$, separation factors α , resolution R_s and effective plates $N_{\text{eff}(A/B)}$ are listed in table 2. The observation of effective separations combined with the broad versatility of this novel chemically bonded *Chirasil-Nickel* phase underlines the advantage of this elegant approach (*cf.* Table 2, *shown after the following brief excursus concerning GC data evaluation for interpretation purposes*).

Interpretation of GC Data – Concise Theory, Basic Measures & Values

For comprehensive fundamentals in GC separation science reference is made to other sources in the literature.^[144-147] For sake of interpretation the basic key descriptors, following the international ASTM-standards, will be outlined.^[148] The quality of a separation of two analytes A and B depends on their net retention time t_R' (corrected by the solvent dead-time t_0 ; $t_R' = t_R - t_0$) and is expressed by the selectivity α . Generally α -values greater 1.10 afford excellent separations and values exceeding 1.20 are only occasionally reported.^[41, 53, 149]

$$\alpha = \frac{t_{R(B)}'}{t_{R(A)'}} \quad (\alpha \geq 1 \text{ and } t_{R(B)'} \geq t_{R(A)'})$$


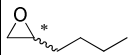
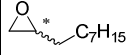
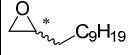
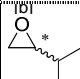
The peak profile is very important, especially the peak-width (sharpness) and is expressed by the effective plate-number N_{eff} taking the peak-width at half peak-height $W_{0.5h}$ into account (this value is more significant than the standard theoretical plate number n). High effective plate numbers are beneficial but not necessarily the determining factor for efficient separations since no measure of selector-efficiency is included. Therefore, with “good” selectors baseline-separations can be achieved even with reduced effective plate numbers.

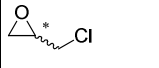
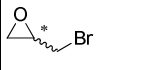
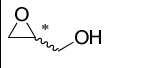

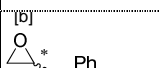


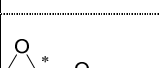
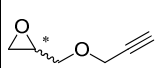
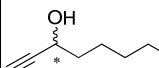
$$N = 5.545 \times \left(\frac{t_R'}{W_{0.5h}} \right)^2$$

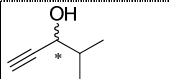
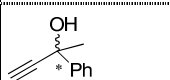
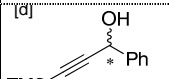
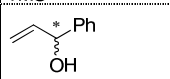
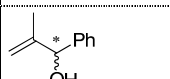
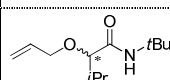
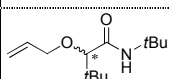
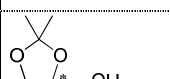
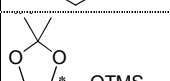
The capacity factor $k = t_R'/t_0$ is an indicator of the distribution of the analytes between the gas and liquid phase. Therefore the effective plate numbers approaches zero for analytes exhibiting a small capacity factor $k \rightarrow 0$ and no separation will be observed. The resolution R_s represents a third descriptor for the separation quality of two analytes A and B. It combines the peak-width at half peak-height $W_{0.5h}$ and the uncorrected retention times t_R of the analytes and displays another useful indicator. Noteworthy, for gaussian-shaped peaks (ideal case) a resolution $R_s = 1.00$ is sufficient for a complete baseline separation of analytes.

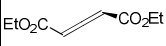
$$R_s = \left[\frac{t_R(B) - t_R(A)}{\sum(W_h)} \right]$$

Table 2 Data for baseline resolutions of enantiomers of racemic compounds using (CB)Chirasil-Nickel-OC₃ (**41**) as the CSP (column and conditions given below).^[a]

#	compound	$t_R(A)'$ /[min]	$t_R(B)'$ /[min]	$k(A)'$	$k(B)'$	α	R_s	$N_{\text{eff}}(A)$	$N_{\text{eff}}(B)$	T /[K]	p /[kPa]
1a		1.51	1.92	0.69	0.87	1.27	1.13	291	403	313	85
b	[I]	0.41	0.49	1.46	1.76	1.21	0.64	202	163	313	85
c	[9]	2.00	2.64	0.97	1.28	1.32	1.38	546	299	303	85
2a		11.86	13.6	5.76	6.61	1.15	1.40	2920	1077	363	85
b	[9]	2.93	3.38	1.53	1.77	1.15	1.47	3307	1055	353	85
3a		10.07	10.57	6.80	7.14	1.05	1.40	21058	8815	383	120
b	[e]	11.51	12.15	8.23	8.68	1.06	1.35	14730	7006	393	120
c	[9]	13.61	14.49	9.45	10.06	1.06	1.20	11942	3438	373	120
4a		35.08	36.93	23.67	24.92	1.06	1.65	24278	11422	373	120
b	[I]	10.77	11.34	56.3	59.69	1.05	0.77	6994	2180	373	120
c	[9]	28.46	30.04	19.63	20.72	1.06	1.40	23177	5952	383	120
5		10.78	12.13	3.11	3.50	1.12	0.74	1028	431	318	100

6		9.28	10.09	4.27	4.64	1.09	0.66	1247	796	313	85
7a		29.14	32.83	7.57	8.53	1.13	2.60	11792	5234	318	45
b	[e]	6.37	6.89	3.29	3.56	1.08	1.16	5189	2396	343	85
8		8.07	8.90	3.93	4.34	1.10	0.52	559	368	393	85
9a		12.72	13.21	7.40	7.68	1.04	1.43	31663	16565	363	100
b	[e]	9.62	10.00	5.95	6.18	1.04	1.90	41116	33638	383	100
c	[f]	7.17	7.56	32.91	34.69	1.05	0.90	7500	3094	343	100
d	[g]	11.28	11.59	6.78	6.96	1.03	1.00	32786	15147	363	100
10		4.17	4.37	5.06	5.31	1.05	1.00	11481	4516	373	120
11		9.59	10.12	14.13	14.91	1.06	1.15	11748	4770	373	120
12a		19.99	24.04	13.65	16.41	1.20	1.03	823	345	318	120
b	[g]	15.77	18.53	8.90	10.46	1.17	1.03	332	1374	318	120
13a		7.24	7.68	5.05	5.36	1.06	0.92	4529	3069	353	120
b	[e]	5.39	5.63	3.89	4.05	1.06	1.18	9783	5862	373	120
c	[f]	7.43	8.35	35.05	39.42	1.12	0.76	604	684	323	120
14a		9.30	9.71	4.65	4.86	1.04	0.51	3413	1579	353	85
b	[e]	6.40	6.70	3.46	3.62	1.05	0.91	7421	5071	373	85
c	[f]	6.66	7.21	31.46	34.05	1.08	0.50	998	440	323	120
15a		3.74	4.17	2.55	2.85	1.11	2.00	5711	4924	393	120
b	[e]	2.58	2.75	1.83	1.95	1.07	1.83	14773	11637	413	120

c	[l]		1.35	1.52	7.33	8.25	1.13	1.22	1983	1429	383	120
16a			0.53	0.62	0.37	0.43	1.18	1.34	983	1078	383	120
b	[e]		0.69	0.73	0.50	0.56	1.13	1.47	2171	2311	403	120
c	[g]		5.11	5.64	2.64	2.91	1.11	3.42	25717	13758	403	85
17a			11.92	13.39	8.32	9.35	1.12	1.55	2437	3112	373	120
18a	[d] 		3.13	5.25	11.94	19.83	1.66	2.16	2827	147	416	120
19a			12.85	13.73	8.88	9.49	1.07	1.37	6176	6992	383	120
b	[l]		4.78	5.28	25.43	28.10	1.11	0.99	1614	1448	368	120
20a			20.09	21.79	25.87	28.05	1.08	1.25	3791	3613	363	240
21a			9.10	9.26	5.10	5.19	1.02	0.69	28612	21594	413	100
b	[e]		21.00	21.33	11.3	11.50	1.02	0.78	47556	31048	413	85
22a			15.10	15.44	7.37	7.53	1.02	0.94	29115	26098	393	85
b	[e]		14.50	14.78	7.82	7.97	1.02	0.96	42807	35384	413	85
23a			16.13	19.34	5.59	6.70	1.20	2.78	3984	3408	403	120
24a			7.30	7.61	2.20	2.30	1.04	2.28	46167	44487	383	100
25a	(2 <i>R</i> ,5 <i>R</i>),(2 <i>S</i> ,5 <i>S</i>) -chalcogran		5.89	6.04	2.87	2.94	1.03	1.00	24656	23231	373	85
b	[l]		10.06	10.57	38.72	40.67	1.05	1.15	8981	7997	323	85
26a	(2 <i>S</i> ,5 <i>S</i>),(2 <i>S</i> ,5 <i>R</i>) -chalcogran		7.93	8.41	3.86	4.10	1.06	2.66	31663	32429	373	85
b	[l]		13.65	15.39	52.53	59.20	1.13	2.09	5179	4364	323	85
27a	(+/-)-camphor		28.23	29.87	19.91	21.06	1.06	0.96	5333	3905	353	120

b	^[g]	41.01	43.05	28.29	29.69	1.05	0.95	6489	5445	343	120
28a	(+/-)-menthol	3.73	4.16	1.78	1.99	1.12	3.05	15006	9929	413	85
b	^[e]	3.72	4.02	2.58	2.80	1.08	2.4	18145	11955	423	120
c	^[f]	0.69	0.76	3.09	3.40	1.10	1.40	3773	3224	413	85
29a	^[e] 	5.34	7.02	9.81	12.89	1.31	3.50	850	13622	393	120

^[a] Separations were carried out using a 25 m *Chirasil-Nickel-OC₃* (**41**) column (20% selector, 250 nm) unless otherwise indicated and helium as inert carrier gas.

^[b] 40 m, 250 nm *Chirasil-Nickel-OC₃* (**41**) column (20% selector, 250 nm).

^[c] 15 m, 250 nm *Chirasil-Nickel-OC₃* (**41**) column (20% selector, 250 nm).

^[d] 8 m, 250 nm *Chirasil-Nickel-OC₃* (**41**) column (20% selector, 250 nm).

^[e] 25 m, 500 nm *Chirasil-Nickel-OC₃* (**41**) column (20% selector, 500 nm).

^[f] 5 m, 500 nm *Chirasil-Nickel-OC₃* (**41**) column (20% selector, 500 nm).

^[g] 25 m, 250 nm mixed *Chirasil-Nickel-OC₃* (**41**) phase (125 nm (**19**), 20% selector and 125 nm GE-SE 30).

1.3.4 Resolution of Chalcogran on *Chirasil-Europium-/Lanthanum-* and *Nickel-OC₃* by Dynamic Complexation GC (DCGC)

Chalcogran [(2*RS*, 5*RS*)-2-ethyl-1,6-dioxaspiro[4.4]nonane] (**49**) is a spiroketal consisting of four stereoisomers^[150-152] found to be the principal component of the aggregation pheromone of the bark beetle *pitogenes chalcographus*, infesting the Norway spruce and causing serious damage to the forests. Spiroketal represents an important class of chiral compounds and are widely distributed in nature as microbacterial metabolites of antiproliferative potency, as antibiotics, cell growth inhibitors, as highly toxic metabolites of marine wildlife and as volatile pheromones for communication between insects.^[153] The stereoisomers consist of two pairs of epimers and two pairs of enantiomers (*cf.* Figure 20).

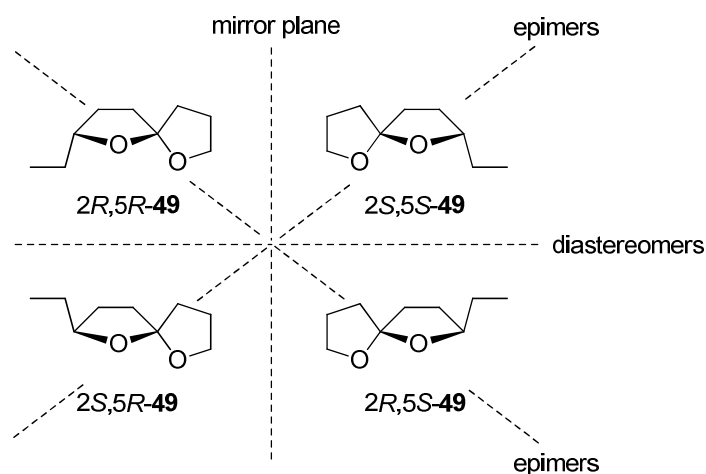


Figure 20 Epimeric, diastereomeric and enantiomeric pairs of chalcogran (**49**).

Stereochemistry indicated by dotted lines. Top left: (*Z*)-(2*R*, 5*R*)-2-ethyl-1,6-dioxaspiro[4.4]nonane; (2*R*, 5*R*)-**49**. Top right: (*Z*)-(2*S*, 5*S*)-2-ethyl-1,6-dioxaspiro[4.4]nonane; (2*S*, 5*S*)-**49**. Bottom left: (*E*)-(2*S*, 5*R*)-2-ethyl-1,6-dioxaspiro[4.4]nonane; (2*S*, 5*R*)-**49**. Bottom right: (*E*)-(2*R*, 5*S*)-2-ethyl-1,6-dioxaspiro[4.4]nonane; (2*R*, 5*S*)-**49**.

Dynamic complexation gas chromatography (DCGC) will be used to separate all four stereoisomers of chalcogran on the novel, camphor-derived *Chirasil-Metal* stationary phases of nickel, europium and lanthanum. Since chalcogran is prone to interconversion at the spiro center (tertiary carbon-atom) by zwitterionic and enolic ether/alcohol intermediates,^[154] as validated during enantio- and diastereoselective, dynamic GC on *Chirasil-β-Dex*, the novel *Chirasil*-phases will be used to determine the epimer-interconversion barriers and rate constants using the DCGC approach.

Influence of Metal-Coordination (Eu^{III} , La^{III} and Ni^{II})

Initially, the influence of the metal-incorporated at the *Chirasil*-phase was investigated using *Chirasil-Europium/Lanthanum* and *Nickel-OC₃* as the chiral stationary phase. To achieve maximum efficiency a column length of 25m with selector-concentrations of 20.0% and a standard film-thickness of 250 nm was selected and the columns prepared as described (cf. Chapter 1.3.3.1). After determination of appropriate separation conditions (100 °C, 85kPa helium) the chalcogran mixture was subjected to GC analysis. On *Chirasil-Nickel-OC₃* **41** both epimeric pairs (8.2 min, 11.5 min average value) were separated after 12 minutes. A remarkable long retention of the enantiomers of each pair was observed with the second enantiomer eluted six minutes (average time) later after the first enantiomer (operating at 100 °C!, not shown; cf. Table 2). Noteworthy, the challenge on the resolution of chalcogran stereoisomers is the structural relationship of both epimer pairs rather than the separation of each enantiomeric pair. However, a remarkably resolution of the enantiomeric pairs (2*R*, 5*R*)-**49**, (2*S*, 5*SR*)-**49** and (2*S*, 5*R*)-**49**, (2*R*, 5*S*)-**49** was possible, with (2*S*, 5*SR*)-**49** eluting 2.04 min and (2*R*, 5*S*)-**49** eluting 2.37 min later than their corresponding enantiomers at 110 °C and 85 kPa inlet pressure on *Chirasil-Nickel-OC₃* **41** (cf. Figure 21 and Table 3).

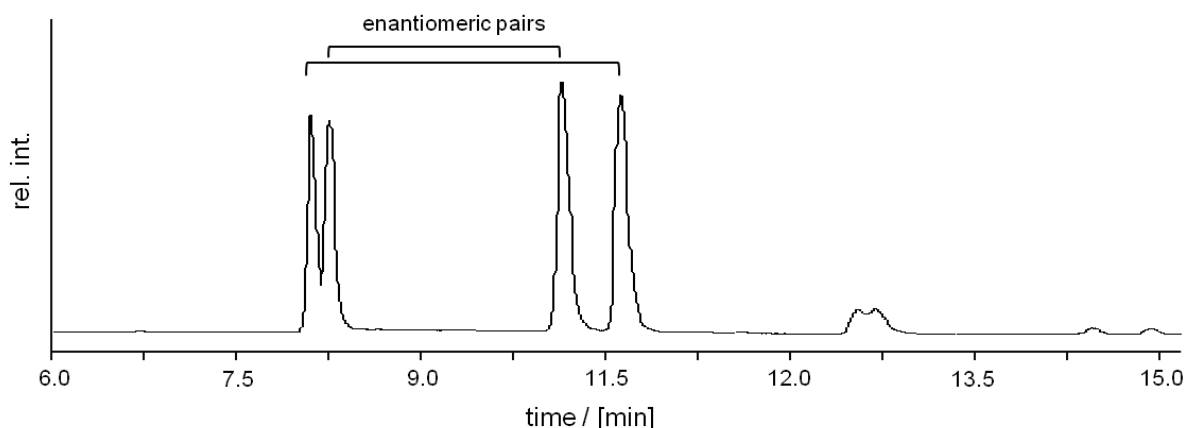


Figure 21 Stereoresolution of the epimeric and enantiomeric pairs of chalcogran (**49**). *Chirasil-Nickel-OC₃* (**41**) column (25 m, 250 nm film-thickness, 20% selector) with helium as the inert carrier gas; conditions: 110 °C, 85 kPa.

Table 3 Resolution of all four stereoisomers of chalcogran on *Chirasil-Nickel-OC₃* **41**.

#	epimer pairs	$k(\text{A})'$	$k(\text{B})'$	α	R_S	$N_{\text{eff}}(\text{A})$	$N_{\text{eff}}(\text{B})$
1	(2 <i>R</i> ,5 <i>R</i>)-, (2 <i>R</i> ,5 <i>S</i>)-chalcogran	2.87	2.94	1.03	1.00	24656	23231
2	(2 <i>S</i> ,5 <i>S</i>)-, (2 <i>S</i> ,5 <i>R</i>)-chalcogran	3.86	4.10	1.06	2.66	31663	32429

Chirasil-Nickel-OC₃ column (20% selector-content, 25 m, 250 nm film-thickness) with helium as the inert carrier gas; conditions: 110 °C, 85 kPa.

After successful resolution of all chalcogran stereoisomers on the *Chirasil-Nickel-OC₃* phase the efficiency of *Chirasil-Europium* and *Lanthanum-OC₃* as the stationary phases was investigated. Using the same conditions, regarding temperature, selector-loading, polymer film-thickness and column length, as described for the separation of the chalcogran stereoisomers with the nickel-selector, a pronounced influence of the metal was found (cf. Figure 22).

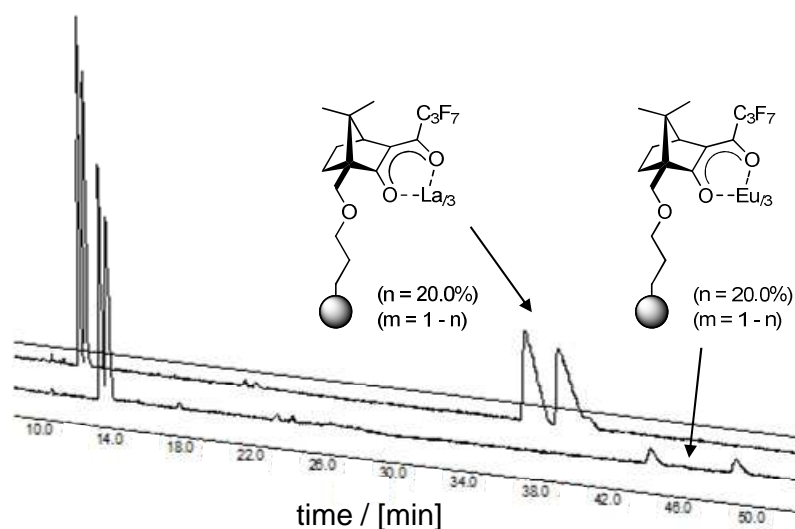


Figure 22 Prolonged enantiomer retention observed during chalcogran (**49**) resolution on *Chirasil-Lanthanum-OC₃* **46** (top) and *Chirasil-Europium-OC₃* **45** (bottom). *Chirasil*-columns (25 m, 250 nm film-thickness, 20% selector) with helium as the inert carrier gas; conditions: 100 °C, 85 kPa.

Whereas, all components were eluted within eleven minutes on the *Chirasil-Nickel-OC₃* phase the epimeric pair was retained on the column eluting 25 min later on the lanthanum and even 31 min later on the europium-phase. This effect is remarkably, bearing in mind that the enantiomers are eluted with a time-gap of 25, respectively 31 minutes. There is only one single report of an enantiomer retention over a period of 30 minutes. An extraordinary high separation-factor of $\alpha \sim 10$ was observed for resolution of the methanol-decomposition product of the inhalational anesthetic sveoflurane by GC on Lipodex E (pentylated γ -cyclodextrin derivative) dissolved in polysiloxane (5 m column, 26 °C, 120 kPa hydrogen).^[149] This represents also the highest separation-factor α observed so far. No retention in this order of magnitude was ever reported for chalcogran isomers. On *Chirasil-Europium* as derived by Schurig^[83] (cf. Chapter 1.1.3) exhibiting a C2-linker the retention time for the chalcogran epimers almost doubled (10 m, 87 °C, 1000 kPa helium). As a common phenomenon longer retention times are accompanied by peak broadening. With the novel (CB)CSPs of lanthanum and europium this effect was also observed. However, peak

broadening did not exceed elution over a period of 1.5 minutes – an order of magnitude that was also observed with *Chirasil-Europium* by Schurig and coworkers (overloaded conditions and reduced mobile-phase flow rates did not account for this observation).^[183, 155] Besides these remarkable results with the novel (CB)CSPs the observations are in agreement with the explanations given in chapter 1.3.3.2 for the role of the coordinated metal. Europium(III) exhibits the strongest selector-selectand complexation properties compared to lanthanum(III) and nickel(II) within the novel CSPs and therefore prolonged retention times and peak-broadening is observed on *Chirasil-Europium-OC₃* **45**. Furthermore, the second epimeric pair of chalcogran, eluted after 44 min and 49 min, is likely to be separated more efficiently on the europium-based than on the lanthanum-based (CB)CSPs (*cf.* Chapter 1.3.3.2 and Figure 22).

Resolution of Chalcogran Stereoisomers on *Chirasil-Nickel-OC₃* – Influence of Selector-Loading, Temperature, Polymer Film-thickness and Composition

As *Chirasil-Nickel-OC₃* proofed to be the ideal, chiral stationary phase for the separation of chalcogran stereoisomers, columns with varying selector-concentrations (3.5%, 10.2% and 20.0%) and 250 nm film-thickness were selected to investigate the influence of selector-loading on the quality of separation. By application a pressure of 85 kPa the operating temperature was raised to 110 °C to force peak-overlap. The second epimer pair of chalcogran is generally more easily separated on the *Chirasil-Nickel-OC₃* phase. Even with selector-

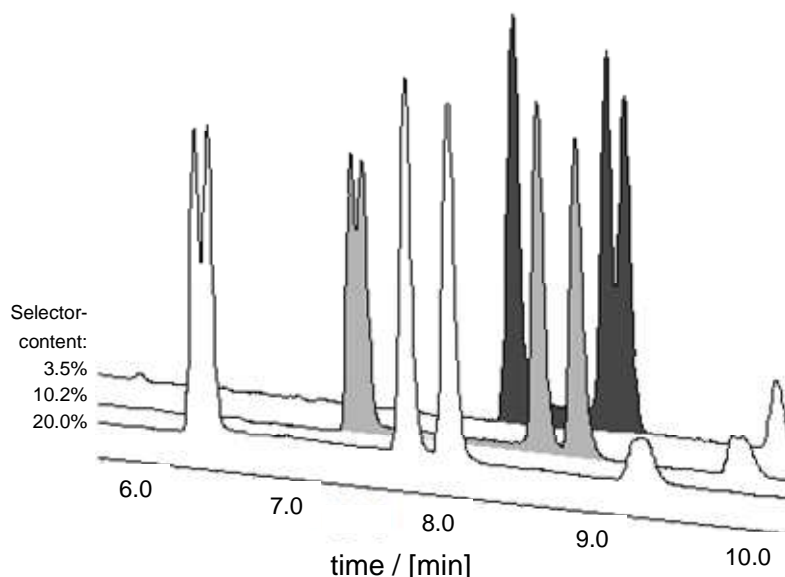


Figure 23 Chalcogran separation on *Chirasil-Nickel-OC₃* with varying selector concentration. *Chirasil*-columns (25 m, 250 nm film-thickness, 3.5 –20.0% selector content) with helium as the inert carrier gas; conditions: 110 °C, 85 kPa.

loadings of 3% partial separation of these peaks was observed. Although different selector-concentrations were employed, retention times of the stereoisomers were almost equal and faster elution on columns exhibiting less selector-concentration was not observed. Selector concentrations of 10.2% were sufficient to baseline separate the second epimeric pair and partial resolution of the first pair. The resolution-factor R_s drastically improved from 0.75 to 1.83 (3.5% → 10.2% selector-loading). With 20.0% metal-selector the resolution of the first epimeric pair was further improved as can be seen from the chromatogram, by change of the α -values from 1.01 to 1.02 and improvement of the resolution-factor R_s from 0.64 to 0.70 for each epimeric pair (*highlighted with arrows*, entries 2a, 3a, 2b, 3b; cf. Figure 23 and Table 4).

Table 4 Influence of the selector-concentration on the quality of epimer-resolution.

#	epimer pairs	$k(A)'$	$k(B)'$	α	R_s	$N_{\text{eff}}(A)$	$N_{\text{eff}}(B)$
1a	(2 <i>R</i> ,5 <i>R</i>),(2 <i>R</i> ,5 <i>S</i>) -chalcogran	2.26	-	-	-	20269	-
b	(2 <i>S</i> ,5 <i>S</i>),(2 <i>S</i> ,5 <i>R</i>) -chalcogran	2.52	2.57	1.02	0.75	21804	21186
2a	(2 <i>R</i> ,5 <i>R</i>),(2 <i>R</i> ,5 <i>S</i>) -chalcogran	2.00	2.02	1.01	0.64	29403	20723
b	(2 <i>S</i> ,5 <i>S</i>),(2 <i>S</i> ,5 <i>R</i>) -chalcogran	2.51	2.62	1.04	1.83	28300	29587
3a	(2 <i>R</i> ,5 <i>R</i>),(2 <i>R</i> ,5 <i>S</i>) -chalcogran	2.00	2.03	1.02	0.70	18389	16753
b	(2 <i>S</i> ,5 <i>S</i>),(2 <i>S</i> ,5 <i>R</i>) -chalcogran	2.66	2.80	1.05	1.99	25292	24794

Epimeric pairs connected with arrows for resolution factor α and resolution R_s . Separations were carried out using a 25 m *Chirasil-Nickel-OC₃* column (250 nm film-thickness) at 110 °C and 85 kPa helium as inert carrier gas (selector-concentrations: 3.5%, entry 1; 10.2%, entry 2 and 20.0%, entry 3).

The observation that selector-concentrations of 20.0% *Chirasil-Nickel-OC₃* still improve separation quality is very important for further developments of *Chirasil-Metal-OC₃* derived chiral stationary phases! This is noteworthy, since selector-selector interactions might lead to reduced efficiency by the formation of unselective complex-species and decomposition products. Therefore, complexation GC is more sensitive to selector-content than inclusion GC. For permethylated- β -cyclodextrin dissolved in OV-1701 (cyanopropylphenyl methylpolysiloxane) the selector-concentration was limited to a maximum of 25%. Exceeding this concentration did not lead to any further increase in the separation factor, resp. quality of

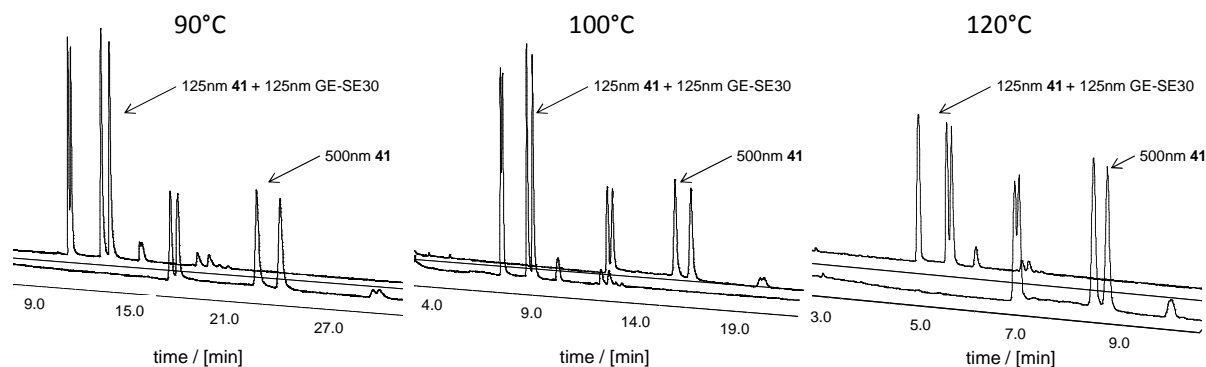


Figure 24 Influence of film-thickness and temperature on the enantio- and epimerresolution of chalcogran isomers (**49**) using *Chirasil-Nickel-OC₃*.

(A) 25 m *Chirasil-Nickel-OC₃* (**41**) phase (20% selector, 500 nm); (B) 25 m mixed *Chirasil-Nickel-OC₃* phase (125 nm **41**, 20% selector and 125 nm GE-SE 30).

resolution, because of crystallization of the selector resulting in low selector concentration accessible for analytes.^[156] After the findings that a nickel-selector content of 20.0% is still beneficial for the quality of resolution, the polymer-film-thickness and composition was altered. Separation columns (20.0% selector-concentration) of 250 nm, 500 nm and a mixed

Table 5 Quality of stereoresolution of chalcogran isomers on a 500 nm *Chirasil-Nickel-OC₃* phase.

#	epimer	α	R_S	$N_{\text{eff}}(\text{A})$	$N_{\text{eff}}(\text{B})$
1a	(2 <i>R</i> ,5 <i>R</i>), (2 <i>R</i> ,5 <i>S</i>)	1.03	1.74	60635	53614
b	(2 <i>S</i> ,5 <i>S</i>), (2 <i>S</i> ,5 <i>R</i>)	1.06	4.07	56688	58643
2a	(2 <i>R</i> ,5 <i>R</i>), (2 <i>R</i> ,5 <i>S</i>)	1.02	1.33	50642	43063
b	(2 <i>S</i> ,5 <i>S</i>), (2 <i>S</i> ,5 <i>R</i>)	1.06	3.19	48246	48296
3a	(2 <i>R</i> ,5 <i>R</i>), (2 <i>R</i> ,5 <i>S</i>)	1.02	0.78	33905	27588
b	(2 <i>S</i> ,5 <i>S</i>), (2 <i>S</i> ,5 <i>R</i>)	1.04	2.33	50571	52295

Conditions: 25 m *Chirasil-Nickel-OC₃* (**41**, 500 nm, 20% selector) column at 90 °C (entry 1), 100 °C (entry 2) and 120 °C (entry 3) and 85 kPa helium.

Table 6 Separation quality of chalcogran isomers on a mixed *Chirasil-Nickel-OC₃*/ polydimethylsiloxane phase.

#	epimer	α	R_S	$N_{\text{eff}}(\text{A})$	$N_{\text{eff}}(\text{B})$
1a	(2 <i>R</i> ,5 <i>R</i>), (2 <i>R</i> ,5 <i>S</i>)	1.02	1.03	40452	42090
b	(2 <i>S</i> ,5 <i>S</i>), (2 <i>S</i> ,5 <i>R</i>)	1.05	2.58	42547	39619
2a	(2 <i>R</i> ,5 <i>R</i>), (2 <i>R</i> ,5 <i>S</i>)	1.01	0.73	34647	26128
b	(2 <i>S</i> ,5 <i>S</i>), (2 <i>S</i> ,5 <i>R</i>)	1.04	2.10	38776	38856
3a	(2 <i>R</i> ,5 <i>R</i>), (2 <i>R</i> ,5 <i>S</i>)	-	-	9303	24132
b	(2 <i>S</i> ,5 <i>S</i>), (2 <i>S</i> ,5 <i>R</i>)	1.03	1.12	21364	26128

Conditions: 25 m *Chirasil-Nickel-OC₃* (**41**, 125 nm, 20% selector) and 125 nm GE-SE30 column at 90 °C (entry 1), 100 °C (entry 2) and 120 °C (entry 3) and 85 kPa helium.

phase consisting of 125 nm *Chirasil-Nickel-OC₃* and 125 nm polydimethylsiloxane (GE-SE 30) were prepared. Three different temperatures (120 °C, 100 °C and 90 °C) were applied. For comparison, the results obtained for the mixed and the *Chirasil-Metal* phase with 500 nm polymer thickness are displayed (constant helium pressure of 85 kPa; cf. Figure 24, Table 5 and Table 6). Throughout good separations were observed on all phases and temperatures applied, especially for the second epimeric pair even at 120 °C. The 500 nm *Chirasil-Nickel-OC₃* phase showed the best results observed so far for the separation of chalcogran isomers!^[154] With respect to a four times lower selector-concentration of the mixed phase (app. 5% selector-content) compared to 20.0% in the 500 nm column the results obtained with the mixed (CB)CSP at all temperatures are remarkable since almost no separation was achieved on the pure phase with 3.5% selector-concentration at 100 °C (as elucidated for the investigations regarding selector-loading). The effective plates are reduced from $N_{\text{eff}} = 60\text{k}/56\text{k}$ to $40\text{k}/43\text{k}$ (entries 1a and b), but are still high considering four times lower selector-concentrations. Therefore, the presence of selector-free polymer within the *Chirasil-Metal* phase is beneficial for separation quality. This observation becomes plausible, if complexation GC is reconsidered as an discriminating process between free selectands, selector-selectand complex formation and selectand-liberation. After injection all analytes will be present in the liquid polymer phase 99% of the time competing for and interacting with the selector bound to the polymer. The presence of selector-free polymer might therefore add unselective contribution to separation by offering free space for incoming selectands and thus guaranteeing selection and fast equilibration between complexation and liberated substrates. This approach is not uncommon and in fact are many stationary phases for gas chromatographic applications are polymer-diluted or mixed phases consisting of different compounds.^[5, 144, 149, 157]

Determination of the Interconversion Barriers of Chalcogran by Dynamic Complexation Gas Chromatography (DCGC) on *Chirasil-Nickel-OC₃*

The epimerization of chalcogran during dynamic diastereo- and enantioselective DCGC gives rise to two independent interconversion peak profiles, each featuring a plateau between the epimer pairs being currently interconverted. Reason for this observation is the time-dependend interconversion and thus change of the physical properties of each epimer within the chiral environment (CSP). Therefore, either a prolonged retention or an accelerated elution of a certain amount of epimers is detected during experiment. By overlay of both contributions (areas) of each interconverted epimers a plateau is formed and superposition of both interconversion processes leads to a characteristic peak-profile, as illustrated in Figure 25.

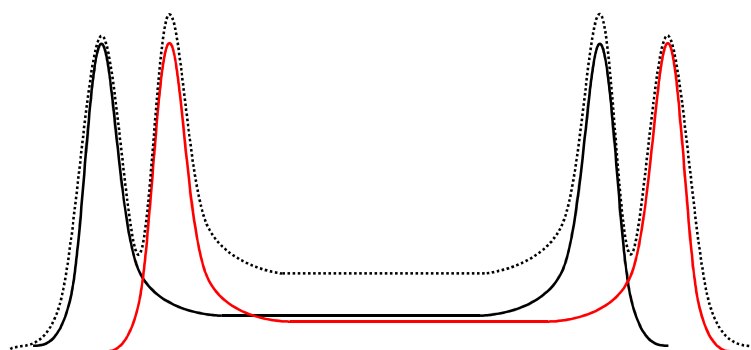


Figure 25 Schematic representation of the interconversion peak profile of chalcogran on *Chirasil-β-Dex*.

Isolated interconversion processes (black and red) and observed overall peak-profile (dotted line).

The rate-constants for the epimerization process (k_{app}) by DCGC were obtained by consecutive measurements at temperatures between 90 °C and 130 °C on *Chirasil-Nickel-OC₃* (cf. Figure 26). A constant, standard inlet pressure of 85 kPa was chosen, since the observed interconversion process will be influenced by the metal-complex on the CSP and therefore has

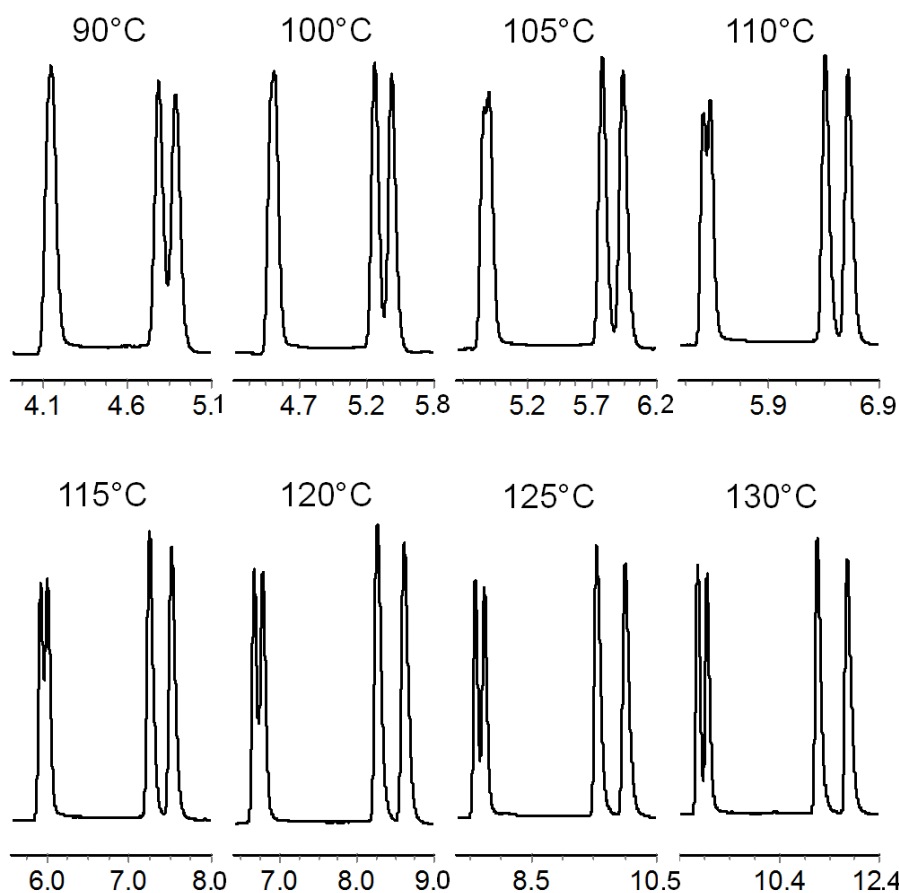


Figure 26 Epimerization of chalcogran (**49**) at different temperatures.^[a]

Experimental chromatograms as obtained on a 25 m *Chirasil-Nickel-OC₃* (**41**, 250 nm, 20% selector) column between 90 °C and 130 °C at 85 kPa helium.

to be considered to be catalytic. Therefore, conversion will depend on the retention time of the analytes on the CSP and thus depend on the probability of being present at the catalytic center, which is strongly influenced by the internal pressure – a significant difference to the determination of interconversion barriers by inclusion GC on *Chirasil-β-Dex*.^[154] The pressure-dependency and therefore the influence of the *Chirasil-Metal* phase on the interconversion process was validated as different reaction-rate-constants k_{app} were observed at constant temperature with varying inlet pressures (85 – 180 kPa, cf. Table 7, Figure 27).

Table 7 Pressure depended interconversion of chalcogran epimers.^[a]

p [kPa]	k_{app} [s ⁻¹]	p [kPa]	k_{app} [s ⁻¹]
85	4.98×10^{-4}	140	4.35×10^{-4}
100	4.69×10^{-4}	160	4.20×10^{-4}
120	4.36×10^{-4}	180	3.63×10^{-4}

Reaction-rate-constants k_{app} observed at 413.15 K for varying helium inlet pressures on a 25 m *Chirasil-Nickel-OC₃* (**41**, 250 nm, 20% selector) column.

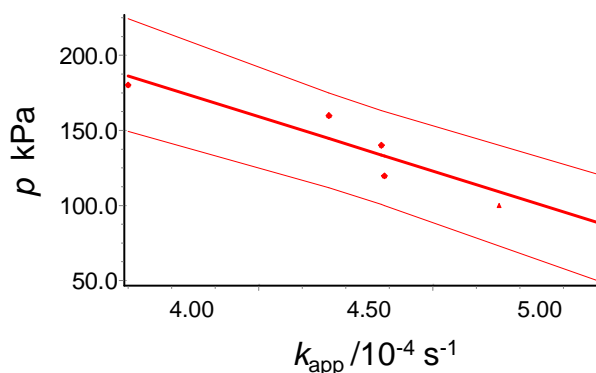


Figure 27 Graphic representation of pressure-dependent chalcogran epimerization (plotted data from table 7).

The reaction-rate-constant k_{app} and activation parameters (ΔG^\ddagger , ΔH^\ddagger , ΔS^\ddagger) at constant pressure of 85 kPa were obtained by data evaluation using kinetic models and the *Unified Equation* approach as previously described by Trapp et al.^[158-164] The activation enthalpy ΔH^\ddagger was obtained from the slope and the activation entropy ΔS^\ddagger from the y-axis intercept of the Eyring plot [$\ln(k_{app}/T)$] as a function of $1/T$ (cf. Figure 28) at constant pressure. The standard deviation of the activation parameters ΔH^\ddagger and ΔS^\ddagger has been calculated by error band analysis with a level of confidence of $r = 99\%$ and a residual deviation of 10%, regarding the error band. The Eyring activation parameters of the experimental interconversion profiles between 100 and 120 °C in the presence of *Chirasil-Nickel-OC₃* **41** were determined to be:

$$\Delta G^\ddagger (289.15 \text{ K}, 85 \text{ kPa}) = 107.7 \text{ kJ/mol}$$

$$\Delta H^\ddagger = 66.7 \pm 7.9 \text{ kJ/mol}$$

$$\Delta S^\ddagger = -137.4 \pm 52.2 \text{ kJ/mol}$$

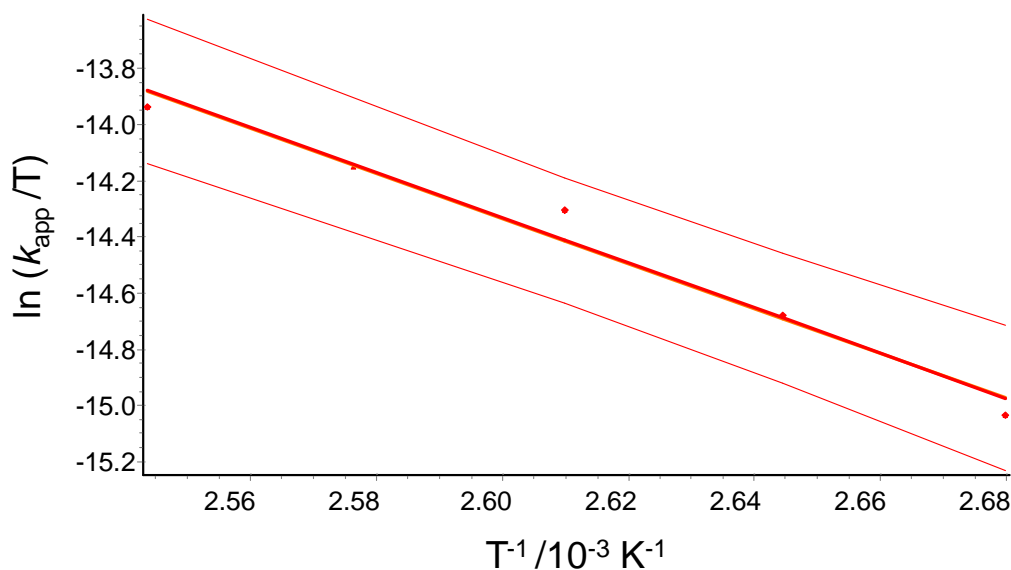
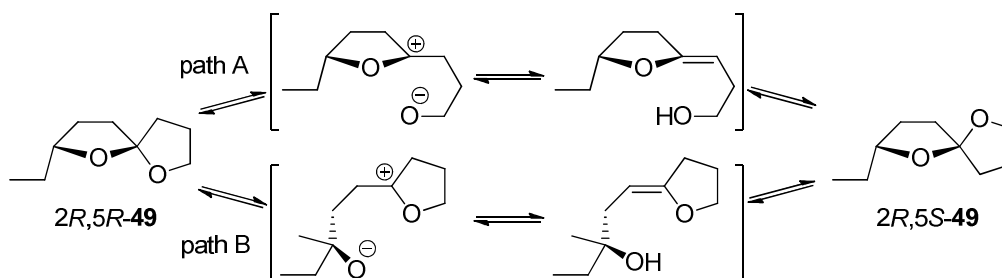


Figure 28 Eyring plot [$\ln(k_{\text{app}}/T)$] as function of $1/T$ for the epimerization of chalcogran on *Chirasil-Nickel-OC₃*.

Conditions: 25 m *Chirasil-Nickel-OC₃* (**49**, 250 nm, 20% selector) column between 100 °C and 120 °C at 85 kPa helium.

By comparison of the results obtained by literature reports on the interconversion barrier of chalcogran on *Chirasil-β-Dex* using dynamic gas chromatography (DGC, inclusion chromatography) a reasonable explanation for and interpretation of the results obtained from DGC and DCGC-experiments was possible. The overall activation Gibbs free energies, standardized to 298.15 K using either complexation or inclusion gas chromatography is almost equal (0.6 kJ/mol deviation). However, the parameters for the activation enthalpy ΔH^\ddagger and activation entropy ΔS^\ddagger differ significantly and can be directly interpreted in this case. The overall highly negative activation entropies ΔS^\ddagger observed in both cases account for a highly ordered state for the epimerization process. A dissociative mechanism involving bond breakage at the spiro center at C5 and formation of a zwitterions/enol ether/alcohol structure was stated and supported by computational chemistry (*cf.* Scheme 15).^[154]



Scheme 15 Interconversion mechanism of the empimeric pair (2R, 5R)-**49**/ (2R, 5S)-**49** via a zwitterions/enol ether/alcohol intermediates.

Considering the strong electrostatic attractions present at intermediate structures, both pathways represent a highly ordered system thus accounting for the highly negative value of the activation entropy ΔS^\ddagger . As the activation free Gibbs energies are almost equal a similar reaction-pathway can tentatively be envisaged. As shown in Table 8, the entropy of the epimerization process at 20 °C increases by 66.5 kJ/mol on *Chirasil-Nickel-OC₃* compared to *Chirasil- β -Dex*, thus implying a more ordered structure during epimerization. Being still highly negative ($\Delta S^\ddagger = -137.4$) an ordered-structure featuring electrostatic interactions and the coordination to the chiral selector, in close proximity to the metal-center, may be envisaged and account for this decrease in order by 66.5 kJ/mol. As a matter of fact, reconsidering the Gibbs free activation energies, the enthalpy is raised to a certain extend (+19.2 kJ/mol) – a phenomenon related to enthalpy–entropy compensation. It represents a fundamental principle ubiquitously found in the chemistry of living systems, but hardly attracted interest in literature.^[165] The message of “Win some, lose some”(enthalpy \leftrightarrow entropy), as stated by Dunitz,^[166] applies for the observations made for the epimerization process of chalcogran on different CSPs as validated with *Chirasil-Nickel-OC₃* and *Chirasil- β -Dex* CSPs exhibiting the same polymer-backbone (polysiloxane).

Table 8 Activation parameters at 298.15 K (ΔG^\ddagger , ΔH^\ddagger , ΔS^\ddagger) for chalcogran epimerization in DGC and DCGC.

#	stationary phase (CSP)	ΔG^\ddagger	ΔH^\ddagger	ΔS^\ddagger	$\Delta\Delta G^\ddagger$ [b]	$\Delta\Delta H^\ddagger$ [b]	$\Delta\Delta S^\ddagger$ [b]
1	<i>Chirasil-β-Dex</i>	108.3	47.6	-203.5	-0.6	+19.2	+66.5
2	<i>Chirasil-Nickel-OC₃</i>	107.7	66.7	-137.4			

Data in kJ/mol; entry 1: 50 m *Chirasil- β -Dex* (300 nm) column between 70 °C and 120 °C; entry 2: 25 m *Chirasil-Nickel-OC₃* (19, 250 nm, 20% selector) column between 100 °C and 120 °C at 85 kPa helium. [b] $\Delta\Delta X^\ddagger = \Delta X^\ddagger_{(Chirasil-Nickel-OC_3)} - \Delta X^\ddagger_{(Chirasil-\beta-Dex)}$

1.3.5 Dynamic Elution Profiles by CSP-Coupling – A Novel Approach Towards Efficient Assignment of Enantiomer Configurations via On-Column GC

Chiral compounds are throughout present in nature and are highly important compounds for global industry, including the pharmaceutical and agricultural sectors, for instance (*cf.* Chapter 1.1.1). As a prerequisite for any research in this area, the structure and the enantiomer configuration has to be identified. A lot of effort is necessary to determine the enantiomeric composition (enantiomeric excess, *e.e.*) either from racemic, enantiomer enriched or impure

mixtures. Therefore, the compounds are initially produced in their racemic forms, followed by enantioselective synthesis of each enantiomer, extraction from natural sources or selective crystallization, for instance. The necessity of having the racemate and both enantiomers in their isolated forms at hand, renders this approach economically unfavorable. Therefore, the development of new techniques for an efficient determination and assignment of enantiomer configurations is and will be pursued on a continuous basis.^[1]

For this purpose a new process using a gas chromatographic dynamic on-column approach by coupling of chiral-stationary phases was developed. The idea is based on the principles of discrimination of enantiomers by chromatography. Enantiomers exhibit, while present in a symmetric environment identical chemical and physical properties (except optical activity). However, by introduction of additional chiral information, like with chiral-stationary phases, marked differences regarding retention-times, peak shape, distribution or reactivity of the enantiomers can be observed because each enantiomer now interacts differently with its environment. Therefore, the question, which led to the development of this method, arised:

“What happens by a change of the chiral information present in the environment during an enantiodiscriminating step?”

(instead of varying the chiral information of the analyte by derivatization or by displacement of the chiral environment to another after each successive *run*, for instance).

Two different, chiral stationary phases combining the separation strategies of complexation and inclusion gas chromatography were chosen to answer this question. The novel, camphor-derived (CB)CSP *Chirasil-Nickel-OC₃* (complexation GC) and a standard cyclodextrin phase (*Chirasil-β-Dex*, inclusion GC) were selected. Initially, the efficiency of the CSPs in the stereoresolution of chalcogran isomers was evaluated. For this purpose, chalcogran was injected on both phases (5 m column length each). The obtained chromatograms are displayed in Figure 29. Besides the extraordinary resolution on the novel, polysiloxane diluted (mixed) *Chirasil-Nickel-OC₃* phase, the chromatograms shows that all stereoisomers tend to separate on the *Chirasil-β-Dex* phase as well (*cf.* Figure 29).

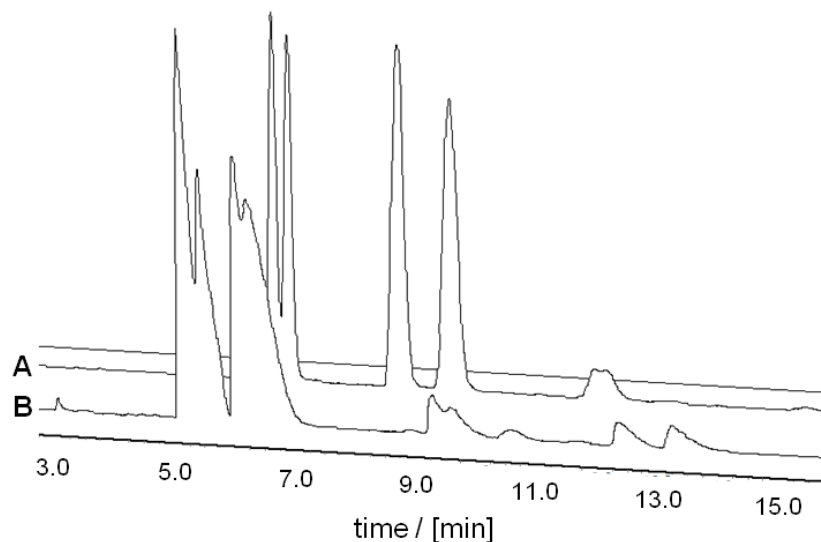


Figure 29 Chalcogran resolution on *Chirasil-Nickel-OC₃* (**A**) and *Chirasil-β-Dex* (**B**).

Separations were carried out either using (A) 5 m *Chirasil-Nickel-OC₃* (**41**) column (125 nm, 20% selector and 125 nm GE-SE 30) and (B) 5 m *Chirasil-β-Dex* column (500 nm film-thickness) at 60 °C and 85 kPa helium as inert carrier gas.

A temporary *change of the chiral environment* during the separation process was achieved by direct coupling of both phases within one gas chromatograph. For a maximum effect the column length was increased to 25 m each to furnish a “fused” 50 m separation column of unique properties. First, the stereoseparation of chalcogran was performed on each single *Chirasil* column. The temperature was raised to 90 °C and the pressure to 110 kPa to force a faster elution of the analytes. The single chromatograms (**A** and **B**) show distinct interconversion profiles of chalcogran depending on the chiral, stationary phase employed. By injection of chalcogran onto the coupled phase a further temperature increase of 10 °C to 100 °C was found to be sufficient enough for elution of all analytes within appropriate times (30 min) on the 50 m column. The obtained chromatograms showed distinct peak-profiles, which have never been reported before. Besides a plateau formation, due to interconversion of chalcogran epimers, as outlined in 1.3.4, two additional “hump-shaped” peak areas were observed, with one located in front and one at the end of some peaks. Measurements were repeated and the same results showing this characteristic pattern were obtained. Furthermore, by reverse coupling of the (CB)CSPs a different peak-pattern exhibiting these additional fronting/retracing peak areas was observed. The corresponding chromatograms are depicted in the following (*cf.* Figure 30, Figure 31).

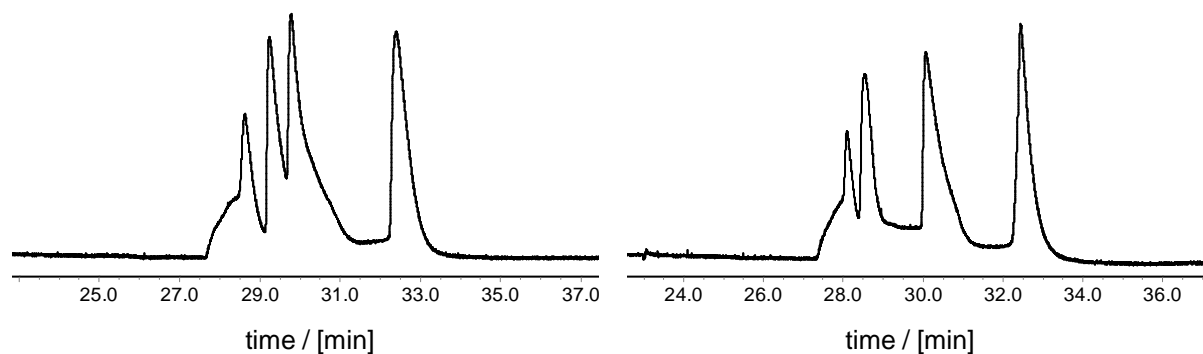


Figure 30 Distinct interconversion profiles for chalcogran stereoisomers observed on coupled CSPs of *Chirasil-β-Dex* and *Chirasil-Nickel-OC₃*.

Separations were carried out using coupled, fused silica capillaries of *Chirasil-β-Dex* (500 nm film-thickness) and *Chirasil-Nickel-OC₃* (**41**, 125 nm, 20% selector and 125 nm GE-SE 30) with an overall column length of 50 m at 100 °C and 100 kPa helium; (A) 25 m *Chirasil-β-Dex* coupled to 25 m *Chirasil-Nickel-OC₃* (left) and (B) 25 m *Chirasil-Nickel-OC₃* coupled to 25 m *Chirasil-β-Dex* (right).

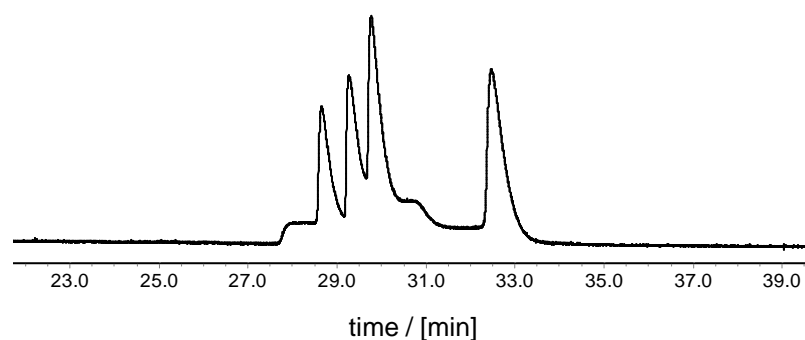


Figure 31 Interconversion profiles for chalcogran observed on *Chirasil-β-Dex* and *Chirasil-Nickel-OC₃*.

Separations were carried out either using (A) 25 m *Chirasil-β-Dex* column (500 nm film-thickness) coupled to 25 m *Chirasil-Nickel-OC₃* column at 90 °C and 110 kPa helium as inert carrier gas.

Both results obtained from normal or reverse column coupling show characteristic regions of peak-fronting and “retracing” (*cf.* Figure 31). None of these regions are detected twice, resp. in odd numbers, and the peak areas can be considered equal in both cases. The explanation for the occurrence of these additional, abnormal-shaped peak areas is based on the interconversion process of the chalcogran isomers. In principle, the characteristic plateau formation observed during interconversion results from the interconversion between the epimers of chalcogran (epimerization). Since this process is time-dependent and since each epimer interacts differently with the CSP, the retention of the parts currently being interconverted into the opposite epimer will be different and unselective to a certain extent. Due to enhanced or reduced interactions with the CSP the elution of small amounts is

therefore retained or accelerated. In particular, two interconversion profiles, each featuring a plateau between the interconverting epimers will be observed.

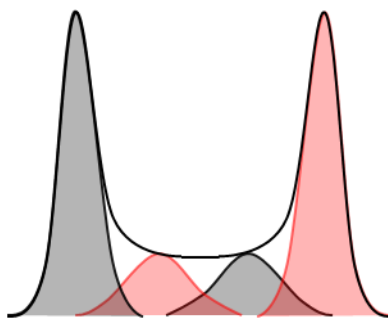


Figure 32 Schematic illustration of the basic components during interconversion process of two compounds A and B.

A and B represent interconverting species highlighted in different colors (non gaussian-shaped deconvolution).

The observed plateau is formed by an overlap between two parts of interconverting structures originating from each epimer. Therefore, a theoretical separation of the plateau into its basic components would result in four independent areas for two plateaus (two contributions for each plateau).

By coupling of *Chirasil-Nickel-OC₃* and *Chirasil-β-Dex* two stationary phases of different separation capabilities either featuring retention by complexation or retention by inclusion were combined. The interconversion process was divided into its basic contributions and a real physical separation of the plateau components was made observable. The detection of one pair of fronting/retracing peak areas shows the separation of one plateau, whereas the other plateau of epimerization stays intact without separation. A total reversal of the elution order of each part of the plateau, as observed for standard and reversal CSP-coupling, can only be detected, when the enantioselectivity of the chiral selector changes completely in favor of the opposite enantiomer during CSP-change! With a CSPs selecting the same enantiomers but exhibiting different enantioselectivity a step-wise plateau formation would be expected and the order of eluted enantiomers will be retained. A schematic representation of the interconversion process and its basic components is illustrated in Figure 32.

This novel approach provides a fast and efficient method for the assignment of enantiomer configurations and their distribution present in an unknown mixture of enantiomers. A typical, straightforward determination of compound purity utilizes gas chromatography, which combines selectivity, efficiency, high resolution and the need of only small sample quantities within a fast method. The standard analytical procedure for the gas chromatographic determination of the enantiomeric purity of an optional impure sample consists of three steps: (A) initial injection and analysis of a test-mixture, preferentially racemic, (B) single analysis of

each enantiomer and (C) analysis of the sample of interest followed by comparison of retention-times and elution-orders under equal separation conditions.

Generally, a transfer of results, regarding especially retention times, to the own results lacks due to sample preparation and composition, slightly differing separation conditions, column properties and varying technical equipment. Thus, without having both enantiopure compounds in hand or at least in their enantioenriched forms, a successful validation is not possible. Furthermore, the elution-order within the same class of compounds can change unexpectedly by passing its *iso*enantioselective temperature (T_{iso}),^[59, 167] which represents a potential source for errors and wrong conclusions. Therefore each enantiomer has to be isolated and analyzed independently for an exact validation. In case of the novel developed approach by CSP-coupling only the sample is analyzed and three chromatographic runs are sufficient enough for an efficient assignment of enantiomer configuration, determination of enantiomeric composition and enantiopurity. Furthermore, three independent methods can be used for the validation of the correct enantiomer assignment after one measurement on the coupled phase thus increasing the level of confidence.

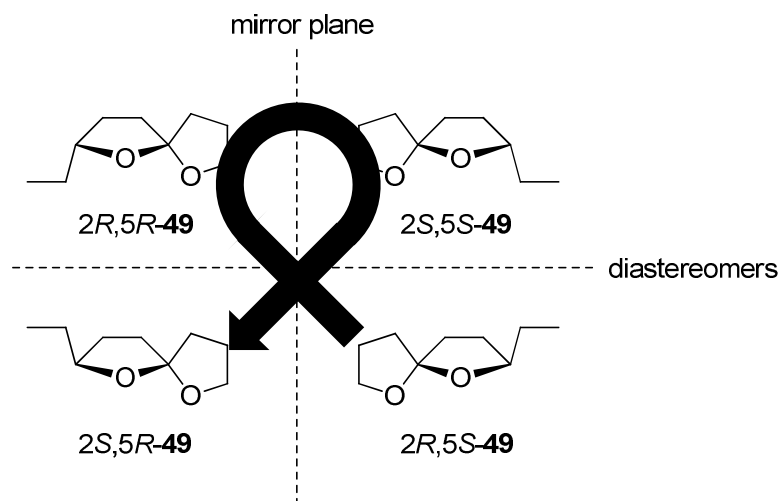
A) Total Retention Model – Additive/ Subtractive Separation Tendency [$t_{R1}(A)+t_{R2}(A)+\dots$]

B) α -Model – Decrease/ Increase of Separation-Factor α of the Analytes

C) Interconversion-Model – Generation of Dynamic Elution Profiles (in Case of Stereolabile Stereoisomers)

Assignment of Chalcogran Enantiomers via CSP-Coupling -- A Case Study

The prerequisite necessary for the application of this method is the existence of literature reports, dealing with the enantiomer configuration and the elution order of its enantiomers, as given for chalcogran.^[154] The assignment of all chalcogran stereoisomers on a CSP of unknown properties represents a challenging task without having the isolated isomers in hands and is not possible by standard state-of-the-art techniques. In the following section all three methods for validation will be demonstrated. The elution-order of chalcogran on *Chirasil- β -Dex* was reported^[154] to follow (*E*)-(2*R*, 5*S*)-2-ethyl-1,6-dioxaspiro[4.4]nonane; (2*R*, 5*S*)-**49** (bottom right), (*Z*)-(2*R*, 5*R*)-2-ethyl-1,6-dioxaspiro[4.4]nonane; (2*R*, 5*R*)-**49** (top left), (*Z*)-(2*S*, 5*S*)-2-ethyl-1,6-dioxaspiro[4.4]nonane; (2*S*, 5*SR*)-**49** (top right) and (*E*)-(2*S*, 5*R*)-2-ethyl-1,6-dioxaspiro[4.4]nonane; (2*S*, 5*R*)-**49** (bottom right) latest (*cf.* Scheme 16).



Scheme 16 Elution order (illustrated by arrow) of chalcogran stereoisomers on *Chirasil-β-Dex* as the chiral stationary phase.

By simple injection only into *Chirasil-β-Dex* and *Chirasil-Nickel-OC₃* columns no pronounced differences are observed and the elution-order on the novel, *Chirasil-Nickel-OC₃* phase remains unknown (*cf.* Figure 30, Figure 31). However, by injection on the coupled CSPs different retention times, varying α -values and the peculiarities, regarding the separation of the interconversion plateau-components, are observed. The observables directly point to the three models for validation of enantiomer assignment. Since the elution order on *Chirasil-β-Dex* is known, beside the fact that the overall retention time for all stereoisomers will be increased, the following considerations are accurate:

Total Retention Model:

- increased retention times for enantiomers are expected along with similar enantioselectivity on *Chirasil-Nickel-OC₃* and the distance between enantiomers will be lengthened (linear relationship!)
- a change of enantioselectivity on *Chirasil-Nickel-OC₃* will influence retention times of enantiomers
- a reversal of enantioselectivity on *Chirasil-Nickel-OC₃* will lead to accelerated elution of unfavored and prolonged retention of selector-favored analytes (enhanced complex formation)
- a reversal of enantioselectivity on *Chirasil-Nickel-OC₃* shortens the distance between enantiomers and might lead to a reverse elution order of enantiomers

α -Model:

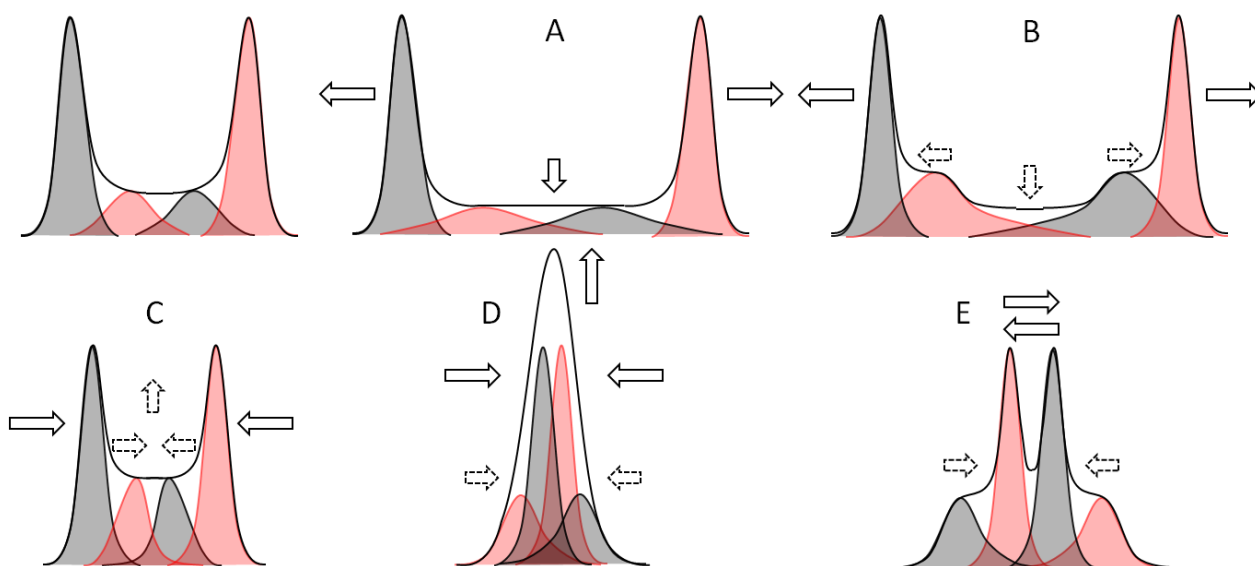
- increased α -values will be observed along with similar and increased enantioselectivity on *Chirasil-Nickel-OC₃* and the distance between enantiomers will be lengthened
- a change of enantioselectivity on *Chirasil-Nickel-OC₃* will influence the separation-factor α and the quality of resolution
- a reversal of enantioselectivity on *Chirasil-Nickel-OC₃* will lead to reduced α -values (pure time-dependency of α)
- a reversed elution order will lead to an increase in the α -value ($\alpha < 1$) after passing the peak coalescence on *Chirasil-Nickel-OC₃*. Resolution quality might be increased even though α -values < 1 are generated. For sake of definition, the order of division has to be changed from $t_{R(B)}/t_{R(A)}$ to $t_{R(A)}/t_{R(B)}$ and in this case α -values ($\alpha > 1$) will be obtained again for sufficient separation.

Interconversion Model:

- a stepwise plateau formation is expected along with similar enantioselectivity on *Chirasil-Nickel-OC₃*, the distance between enantiomers will be lengthened and the plateau will be stretched
- a change of enantioselectivity on *Chirasil-Nickel-OC₃* will influence the plateau formation, the shape and the positioning of the principal components of the interconversion plateau
- a reversal of enantioselectivity on *Chirasil-Nickel-OC₃* separates the principal components of interconversion plateaus
- a reversal of enantioselectivity on *Chirasil-Nickel-OC₃* shortens the distance between epimer pairs and might lead to a reverse elution order of enantiomers characterized by frontening and retracing peak areas

All the aspects elucidated are realized for the time-dependent resolution of chalcogran isomers on the coupled stationary phases! To interpret the novel peak-profiles some considerations and illustrations will briefly be discussed: By coupling of two CSPs of same length and identical enantioselectivity two enantiomers will be separated to equal extend and retention of will be doubled (linear relationship). Same is true for two interconverting enantiomers and thus the plateau will be elongated (case A). Changing only the selectivity of the selector (in favor of the opposite enantiomer) on one of the two CSPs a step-shaped plateau is expected (due to interconversion on both phases), but again the linear relationship

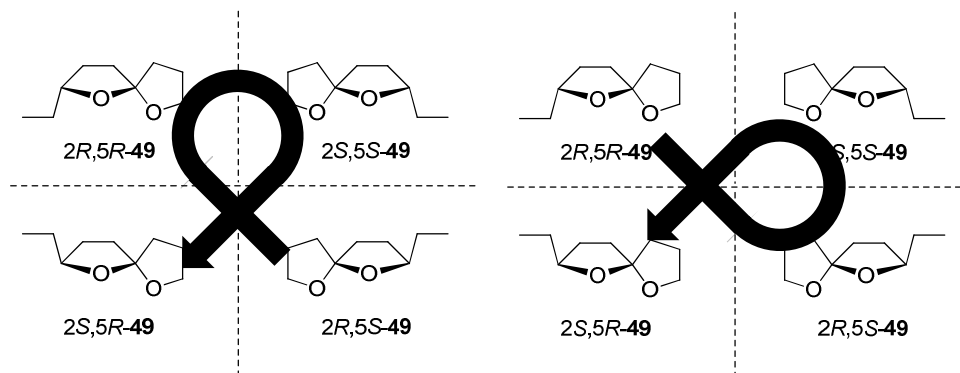
of retention will be retained (case B). Reversal of the enantioselectivity on one phase results in converging peaks and an increased plateau height is observed (case C). With increasing enantioselectivity of the selector present on the second CSP each enantiomer and its corresponding, interconverted enantiomer (as one part of the plateau) will first superpose the others (point of coalescence, case D) and pass them to generate a novel peak-profile, featuring additional fronting and retracing peak areas (case E, *cf.* Scheme 17).



Scheme 17 Peak-profiles observed for an interconversion process on coupled CSPs with different and enantioselectivity (case A – E, non gaussian-shaped deconvolution).

By comparison of the results a change in the elution order is observed for chalcogran on the coupled-CSPs. However, the complete and correct assignment of all peaks to this complex chromatographic pattern is challenging. As both CSPs exhibit the same polysiloxane-based backbone diastereoselectivity is retained and therefore no change in the elution order of both epimeric groups is possible! This is validated by an increase in the overall retention times for both epimeric pairs (29 and 32 min). The retention time has to be at least as long as the sum of the retention times observed on both separated phases (*Chirasil-β-Dex*: $t_{R\text{-range}} = 8 - 9$ min; *Chirasil-Nickel-OC₃*: $t_{R\text{-range}} = 8 - 10$ min, linear relationship of retention). The deviation from the theoretical expected retention range (16 – 19 min) to 29 – 32 min for chalcogran on the coupled-CSP is originated at the pressure decay observed along with increasing column length leading to prolonged retention times.

Highly pronounced is the change in enantioselectivity for the first epimeric pair (related to study case E) and evidenced by plateau separation between (2*R*, 5*R*)-**49** (top left), (2*R*, 5*S*)-**49** (bottom right, *cf.* Scheme 18). A change in the diastereoselectivity for both interconverting



Scheme 18 Different elution orders on *Chirasil-β-Dex* (left) and *Chirasil-Nickel-OC₃* (right) efficiently determined by the developed CSP-coupling method (elution order illustrated by black arrows in each case).

epimeric pairs is not likely to happen reconsidering the linear retention relationship (equal polysiloxane backbone equals similar diastereoselectivity). This is validated since the second plateau between (2*S*, 5*S*)-**49** (top right) and (2*S*, 5*R*)-**49** (bottom left) remained intact and therefore no change in diastereoselectivity is possible, nor by changing the order of coupled CSPs. The novel method allowed the determination of enantiomer configuration and peak assignment to all four chalcogran stereoisomers on the novel *Chirasil-Nickel-OC₃* stationary phase. The different elution orders on *Chirasil-β-Dex* and *Chirasil-Nickel-OC₃* are illustrated in Scheme 18.

The novel approach allows the transfer of existing or standardized elution-orders from reference columns to other columns. Furthermore, a comparative determination of the relative configuration and validation of the absolute configuration by a reference compound is possible. This is very important for the analysis of enantiomers, especially for the determination of the enantiomeric excess (% *e.e.*) in asymmetric catalysis as transfer of otherwise incomparable ligand-systems of unknown enantioselectivity becomes possible. The overall expenditure of measurement periods is reduced and the set-up is simple. The need for one chiral reference column for the comparison with literature reports is not necessarily a drawback of this approach as the columns can be used for standard separations as well. Plus, only a small number of chiral columns are commonly employed for separations and therefore excessive investment in different chiral CSP columns is limited. In fact, this approach opens the way for an additional application of already existing columns. Furthermore, and also likely to be the major advantage beside the straightforward approach and simple set-up is the injection of only the sample of interest, instead of having all isolated compounds (enantiomers) at hands. Since only small amounts of analytes are necessary for GC analysis any bench-upscale and purification procedures become less important. By installation of a set-up with increased separation-performance (resp. a better resolution quality), peaks can be

further separated from each other allowing the determination of very high as well as very low enantiomeric excess' at the detection limits – a challenging task even with state-of-the-art *Chirasil-β-Dex* phases. Elution-orders of related compounds and compound-classes can be validated and changes thereof can be detected, which is important for the pharmacologic spectrum of activity within compound libraries (related to QSAR, QSPR). The method allows also a qualitative comparison between different separation columns. The direct detection of the selectivity-profile allows the user a fast and efficient determination of the benefit of a separation column, which helps to decide whether a column may be suitable for a given resolution-problem or not. As today high pressures have already been realized within LC-systems the compatibility of *Chirasil-Metal-OC₃* phases to carbon dioxide even renders this application suitable for sub- and supercritical fluid chromatography (SFC). The usefulness of CSP-coupling is finally underlined by direct comparison of the experimental chromatogram with the theoretical expected chromatogram for the separation of enantiomers and stereoisomers of all chalcogran components while epimerization takes place (Figure 33).

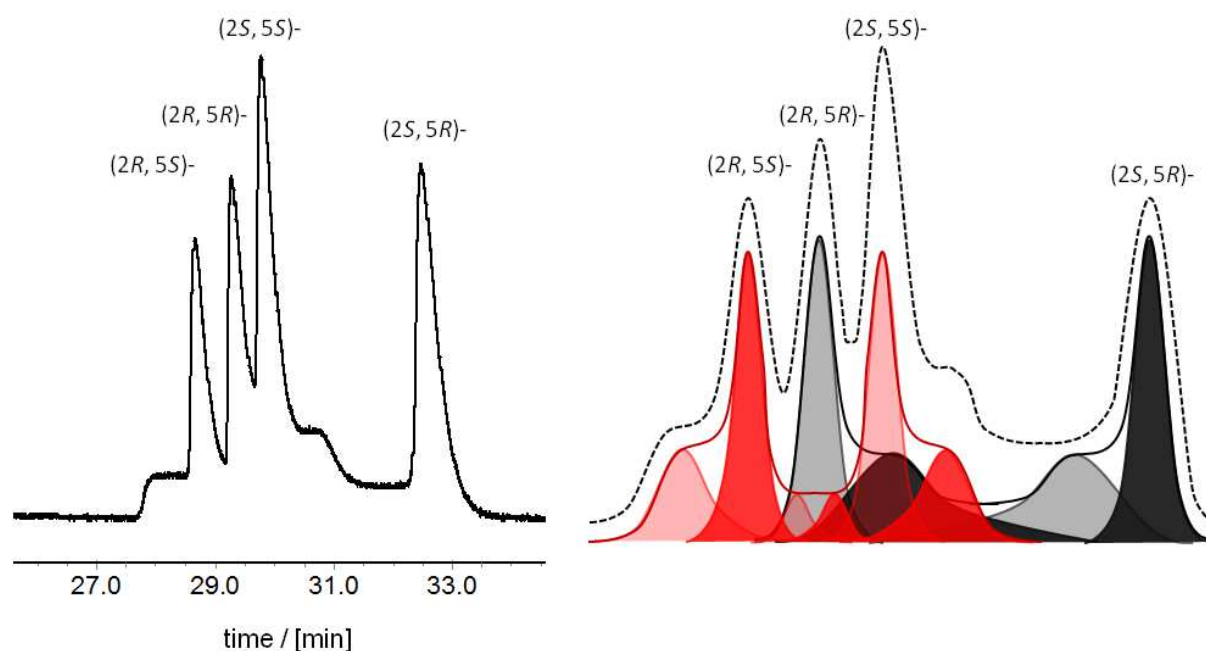
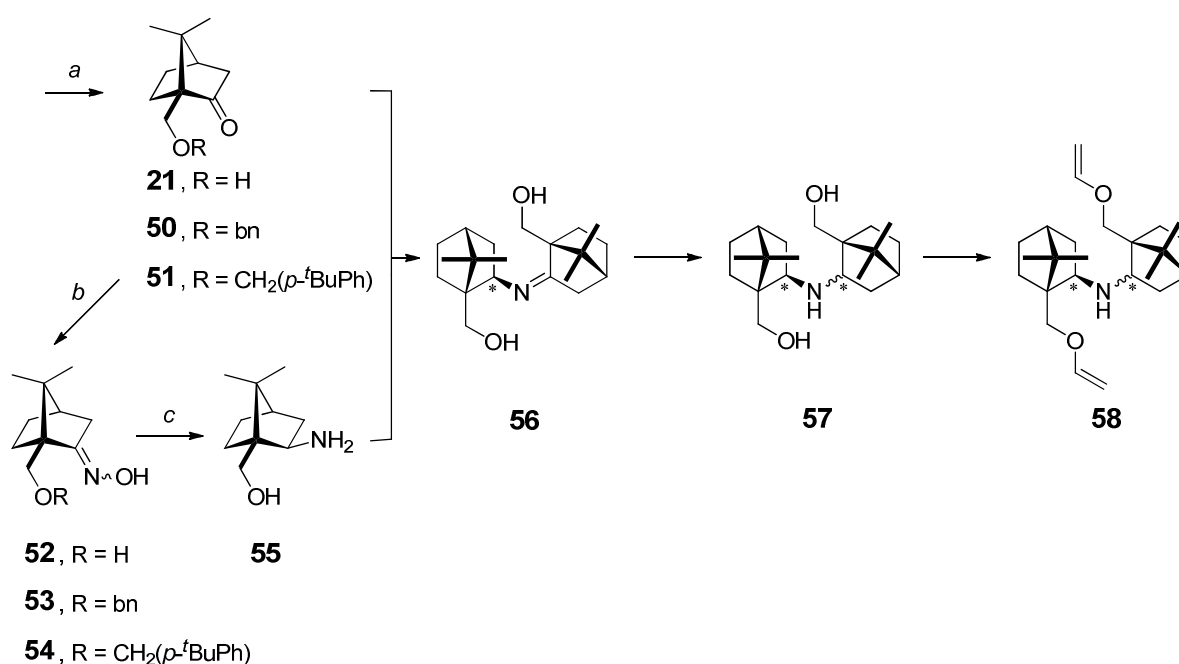


Figure 33 Experimental (left) and theoretical chromatogram splitted into its basic components (right) showing the chalcogran interconversion under CSP-coupling conditions.

Experimental chromatogram (left) as observed on coupled, fused silica capillary of 25 m *Chirasil-β-Dex* (500 nm film-thickness) and 25 m and *Chirasil-Nickel-OC₃* (**19**, 125 nm, 20% selector and 125 nm GE-SE 30) column with an overall column length of 50 m at 90 °C and 110 kPa helium. Schematic representation (right, non gaussian-shaped deconvolution): Epimeric pairs highlighted in red (resp. in black). The peak profiles for both interconversion processes and interconverting parts are displayed by a continuous line. The dotted line shows the overall expected chromatogram. Basic components corresponding to each other are of the same color and color-depth.

1.3.6 Camphordimers with Two Centers of Chirality – Towards New Acyclic, Metal-free Selectors for (CB)CSPs

During the endeavor towards the development of *Chirasil-Metal*-phases, the synthesis of acyclic, stationary phases for inclusion GC was envisaged. Natural *d*-(+)-camphor was chosen as the chiral building block. To increase the steric demand and enhance the chiral information present coupling of two camphor moieties was aimed. Following the developed procedure, 10-hydroxycamphor was used as starting material to allow allylether formation and immobilization by Pt-catalyzed hydrosilylation on the polysiloxane support in the late steps of synthesis. The synthetic pathway pursued is shown in Scheme 19.



Scheme 19 Synthetic approach towards acyclic selector **58** for (CB)CSPs.

Reaction conditions: a) **21**, NaH, THF, r.t., 3 h then arylbromide, THF, 67 °C, 2 h, r.t. 16 h, 96% for **50**, 98% for **51**. b) NH₂OH×HCl, pyridine, EtOH, 78 °C, 5 h, 84% for **52**, 88% for **53**, 96% for **54**. c) see Table 9.

The most challenging step in synthesis was the preparation of camphor-derived *sec*-amine **57** from commonly available or readily accessible starting materials. Corey et al.^[168] reported the formation of a related, unfunctionalized camphor *sec*-amine dimer by condensation of enantiopure *isobornylamine* with *d*-(+)-camphor in the presence of titanium tetrachloride followed by reduction in two steps. However, the need for pure 10-hydroxy *R*(-)-*isobornylamine* (**55**) as starting material made this method impossible. Even though unfunctionalized *R*(-)-*isobornylamine* can be obtained pure by reduction of readily available camphor oxime over Pd/C with hydrogen the preparation of pure 10-substituted *R*(-)-*isobornylamine* (**55**) proved to be challenging. Reduction of the corresponding 10-

hydroxycamphor oxime **52**, reduction of the corresponding benzyl- or *tert*-butylbenzyl protected oxime alcohols **53** and **54** did not furnish pure 10-hydroxy *isobornylamine* (**55**, cf. Table 9). 10-hydroxycamphor oxime **52** was prepared by reaction with hydroxylamine hydrochloride and pyridine in ethanol and obtained in 82% yield. The protected ketoalcohols **50** and **51** were prepared by Williamson ether synthesis with sodium hydride and arylbromides^[169] in tetrahydrofuran at reflux temperature and isolated in 96%, respectively 98% yield. The corresponding oximes were prepared using standard methods and obtained as colorless liquids (**53**, 88% and **54**, 96%).

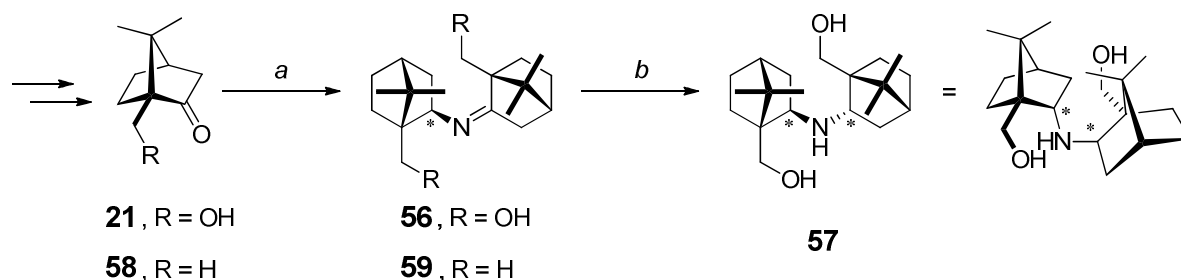
Table 9 Conditions intended to furnish pure *R*(-)-10-hydroxy *isobornylamine* **55**.

#	Substrate	Reagent	Reaction conditions	Product ratio _(exo-/endo) ^[b]
1	52	LiAlH ₄	Et ₂ O, 5 d, 35 °C	2.9 : 1 (48% <i>d.e.</i>)
2	52	Raney-Ni [®] , H ₂	MeOH, H ₂ , 48 h, r.t.	1.1 : 1 (5% <i>d.e.</i>)
3	52	<i>L</i> -Selectride [®]	THF, r.t., 15 h up to 3 d, 67 °C	no rct.
4	52	<i>K</i> -Selectride [®]	THF, r.t., 15 h up to 3 d, 67 °C	no rct.
5	52	DIBAL	THF, r.t., 15 h up to 3 d, 67 °C	complex mixture
6	52	9-BBN	THF, r.t., 15 h up to 3 d, 67 °C	side products, 1 : 1
7	53	LiAlH ₄	Et ₂ O, 35 °C, 1 – 6 d	mixture (>3 products)
8	54	LiAlH ₄	Et ₂ O, 35 °C, 1 – 6 d	mixture (>4 products)
9	ethyl acetate	Ti(O- <i>i</i> Pr) ₄ , NH ₃	EtOH, r.t., 24 h then NaBH ₄ , 3 h, 0 °C to 12 h, r.t.	100% acetamide
10	50	Ti(O- <i>i</i> Pr) ₄ , NH ₃	EtOH, r.t., 24 h then NaBH ₄ , 3 h, 0 °C to 12 h, r.t.	11.5 : 1 (84% <i>d.e.</i>) ^[c]
11	51	Ti(O- <i>i</i> Pr) ₄ , NH ₃	EtOH, r.t., 24 h then NaBH ₄ , 3 h, 0 °C to 12 h, r.t.	7.3 : 1 (76% <i>d.e.</i>) ^[c]

Conditions 0.3 mmol substrate, 1 – 2 eq. reagent, conditions as reported; ^[b] as determined by NMR spectroscopic measurements and chiral, gas chromatography on a 25 m *Chirasil-β-Dex* (500 nm film-thickness) column using a temperature gradient (80 °C, 2 min hold and 5 °C to 180 °C@120 kPa helium); ^[c] The corresponding alcohols were obtained.

Even though, *in-situ* conversion of ethyl acetate to acetamide was possible in a promising clean and high yielding reaction with ammonia in the presence of titanium tetra-*isopropoxide* and subsequent reduction with sodium borohydride, the reaction failed to work with camphor-ketones **50** and **51** even under hydrogenation conditions.^[170, 171] After an extensive screening

it was possible to directly couple two camphor building blocks via one central nitrogen atom in two steps. The corresponding imine **56** was first generated over Raney-Ni[®] *in situ* and reduced to the target amine **57** with lithium aluminiumhydride over a period of three days (*cf.* Scheme 20). The camphor-derived *sec*-amine **57** was isolated in 74% yield and its structure was unequivocally determined by X-ray crystallographic analysis of its carbonate salt (*cf.* Figure 34). Unexpectedly, the structure proofed to be 100% diastereopure. To validate these results the isolation of the imine intermediate was pursued. As no crystals from the hydroxyimine derivative **56** were obtained and to investigate the reaction mechanism more deeply the corresponding unfunctionalized natural camphor derived *sec*-imine dimer (*N*-*isobornyl*camphor imine, **59**) was synthesized, isolated and crystallized over a period of four month. The structure of **59** was determined by X-ray crystallographic analysis and showed the expected, target imine intermediate to be 100% diastereopure (*R*-configuration, *cf.* Figure 35)! Noteworthy, the configurations reported by Corey et al.^[168] [(*R*-, *R*-)-*diisobornyl*amine] differs from the one obtained by this novel approach and a more complex proton NMR spectrum, resulting from (*R*-) and (*S*-) configured camphor substructures is obtained for (*S*-)-*bornyl*-(*R*-)-*isobornyl*amine **57**.



Scheme 20 Synthesis of target, functionalized camphor *sec*-amine dimer **57**.

Reaction conditions: a) **21**, Raney-Ni[®], H₂, EtOH, r.t., 24 h then 50 °C, 4 d for **56** or **58**, Pd/C, NH₄OAc, MeOH, r.t., 5 d, 6% for **59**. b) LiAlH₄, THF, 0 °C to 67 °C, 60 h, 74% for **57**.

In conclusion, it was shown that both reactions were diastereoselective to furnish 100% pure *bornylisobornyl* **57**. The configuration was determined to be (*R*) for the imine derivative and the second stereocenter is installed selectively (*S*-configuration), while the camphor chirality is preserved. The obtained products give evidence for a reaction mechanism, in which one camphor monomer approaches the nickel surface from the less hindered *endo*-face followed by condensation with a second camphor molecule via desamination. In this particular case, the resulting imine dimers **56** and **59** are unreactive even under hydrogenation conditions over Raney-Ni[®] and can therefore be isolated, whereas Corey et al. used platinum on charcoal for hydrogenation of an imine to a *sec*-amine.

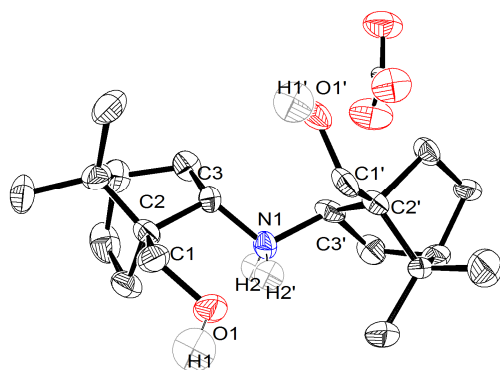


Figure 34 Molecular structure of target, 10-hydroxycamphor-derived *N*-bornylisobornylcamphor **57** (diastereopure with preserved chirality).

Thermal ellipsoids are plotted at 50% probability level and hydrogen atoms are omitted for clarity.

Selected bond lengths and angles for **57**: C3–N1 153.6(10) pm, N1–C3' 149.8(9) pm, C1–O1 142.5(1) pm, C1'–O1' 143.8(9) pm, C2–C3–N1 115.0°, C2'–C3'–N1 115.5°, C3–N1–C3' 115.5°.

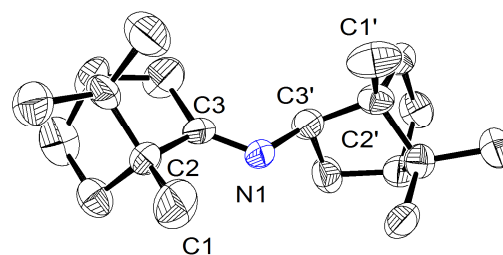
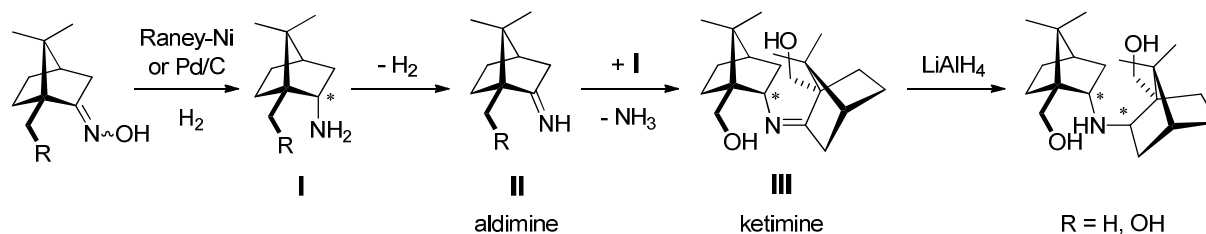


Figure 35 Structure of camphor-derived ketimine dimer **59** (diastereopure with preserved chirality) as determined by X-ray crystallographic analysis.

Thermal ellipsoids are plotted at 50% probability level and hydrogen atoms are omitted for clarity.

Selected bond lengths and angles for **59**: C3–N1 122.3(9) pm, N1–C3' 133.1(10) pm, C2–C3–N1 123.8°, C3–N1–C3' 117.6°.

The reductive coupling of *d*-(+)-camphor to **56** was reported to take place either on ruthenium and palladium with ammonium chloride as additive under hydrogenation conditions at 200 °C and pressures of 8 MPa!^[172] Literature proposed a reaction mechanism running via four steps^[173-175] consisting of a reduction to the amine, followed by aldimine formation (due to loss of molecular hydrogen) and condensation to the imine dimer under loss of ammonia. Finally, the ketimine is reduced to furnish the corresponding sec-amine (*cf.* Scheme 21).



Scheme 21 Proposed mechanism for the formation of targeted, camphor-derived *N*-(*S*)-bornyl-(*R*)-isobornylamine **57**.

Interestingly, the reaction might be considered autocatalytic, since the reaction consumes the hydrogen generated through aldimine formation and thus works without an external hydrogen source. The mechanism was further supported by the observation that aniline and *tert*-butyl

amine are completely unreactive as aldimine formation is not possible in these cases. The results obtained within this study validates the mechanism running via imin-amin formation in two steps with 100% diastereoselective introduction of chirality.

The central (*sec*-)amine is chemically inert, even under harsh conditions (methylolithium–HMPA, *n*-butyllithium-TMEDA at 60 °C) and methylation is not observed for diisobornylamine as reported from Corey et al.^[172] A related behavior is expected for the novel, camphor-derived hydroxyl substituted bornylisobornylamine **57** thus allowing synthesis of the corresponding allyl ether derivatives under classical conditions. By following, the synthetic strategy and immobilization steps as outlined in chapter 1.1.2 for *Chirasil-Metal-OC₃* the study and the successful preparation of the enantiopure key-fragment **56** and **59** are supposed to contribute to the development of novel, chemically-bound, acyclic, chiral stationary phases (CB)ACSPs for gas chromatographic applications.

1.4 Conclusion

In summary, the total synthesis and an improved synthetic access to novel camphor-derived and chemically bound (CB), chiral, stationary phases (CSPs) for gas chromatography were presented. The strategy involved the synthesis of the chiral-selector with an extraordinary improvement of the trifluoroacylation-step. The selector was chemically bonded onto a polysiloxane support. The immobilization step and metal incorporation of nickel(II), oxovanadium(IV), europium(III) and lanthanum(III) was studied in detail by ^1H , ^{19}F and ^{13}C NMR and IR spectroscopic measurements and verified for ligand, resp. metal-selector loadings of 3.5%, 10.2% and 20.0%. This allowed the user to validate immobilization and conversions >99% to the desired *Chirasil*-phases. The novel, so called *Chirasil-Metal-OC₃* phases were coated on the inner surface of fused silica capillaries (I.D. 250 nm) and their performance in complexation gas chromatography regarding the nature of the metal, selector-content, column length, polymer film-thickness and composition on the quality of separation of various racemic compounds was investigated. Besides findings that a selector-content as high as 20% is still beneficial for separation quality, it was shown that *Chirasil-Nickel*-phases exhibit the highest separation performance. An extraordinary, large retention difference between the enantiomers of chalcogran ($\Delta t_{\text{R}@Eu(hfpc)_3@PS} = 30$ min, ($\Delta t_{\text{R}@La(hfpc)_3@PS} = 25$ min) was observed for *Chirasil-Europium*-and *Lanthanum-OC₃* phases. An enhanced thermostability up to >160 °C was achieved with the novel *Chirasil-Nickel-OC₃* CSP – a major drawback for the applicability of the *Chirasil-Metal* phases in the past. Furthermore, the resolution of overall 29 racemic compounds extending the scope of complexation GC to different substitution patterns and group functionalities was presented. Throughout high separation factors as high as $\alpha = 1.66$ were obtained and all compounds were baseline separated. The development of thioether-linked *Chirasil-Metal-OC₃* phases was addressed as well. All four stereoisomers of chalcogran, the principle component of the aggregation pheromone of the bark beetle *pityogenes chalcographus*, were successfully separated using the novel *Chirasil-Nickel-OC₃* phases. The interconversion barrier for the epimerization process was determined to ΔG^\ddagger (289.15 K, 85 kPa) = 107.7 kJ/mol, $\Delta H^\ddagger = 66.7 \pm 7.9$ kJ/mol, $\Delta S^\ddagger = 137.4 \pm 52.2$ kJ/mol by temperature-dependent measurements using dynamic, complexation gas chromatography (DCGC). By comparison with results from dynamic GC on *Chirasil- β -Dex* a reasonable explanation for the different parameters was given. In particular, it proofed the influence of the stationary phases on the chalcogran interconversion process either via a coordination(complexation)-driven interconversion process or via an uncatalyzed (pressure independent) interconversion process through highly ordered electrostatic intermediates. The thermodynamic data obtained allowed for the first time the validation of the fundamental principle of enthalpy–entropy compensation in the liquid phase of polymer bound selectors in dynamic gas chromatography. Furthermore, a unique, novel approach to an

efficient assignment of enantiomer configurations via on column gas chromatography was developed. The generation of *dynamic elution profiles by CSP-coupling* allows the easy determination of enantiomeric excess, sample composition and enantiomer assignment within only three injections without the need of isolated enantiomers (only the a sample mix has to be injected). Combined with the need for only small quantities and the innecessity of having the isolated enantiomers in hand this approach was proven for the stereoresolution and assignment of all four stereoisomers of chalcogran. This method represents also an useful tool for the determination of the “direction” of enantioselectivity of chiral, stationary or catalytically active phase of known handedness but unknown selectivity! The individual peak-profiles obtained indicate changes in the enantioselectivity and the “direction” of enantiomer selection as well as diastereoselectivity. The effects observed by coupling of different CSPs were discussed in detail and compared to theory. By this novel approach it was possible to physically separate the principal components of an interconversion plateau into two parts of fronting and retracing peak areas! The development of an acyclic CSP using linked-camphor building blocks, featuring two centers of chirality by successive enantioselective synthesis, was addressed as well. The overall great versatility and potential of metal-coordinated (CB)CSPs, their capability of enantioseparation of smallest classes of chiral compounds (e.g. epoxides) in complexation gas chromatography (CGC) and the development of *dynamic elution profiles by CSP-coupling* was highlighted. The studies are also intended to re-envision their great potential^[176-178] and imply future applications for asymmetric reactions^[89, 93, 94, 179] and moreover to point to their compatibility to carbon dioxide used for supercritical liquid chromatography (SFC).^[59, 82, 155]

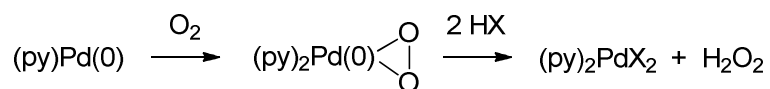
Chapter 2

Bi- and Tetradentate Pd-Bicamphorpyrazole Heterocycles (bcpz) – Synthesis, Characterization and Their Application in Catalysis

2.1 Introduction – Wacker Oxidation and Isomerization of Olefins

Recent Developments in the Wacker Oxidation of Olefins – Overview and Motivation

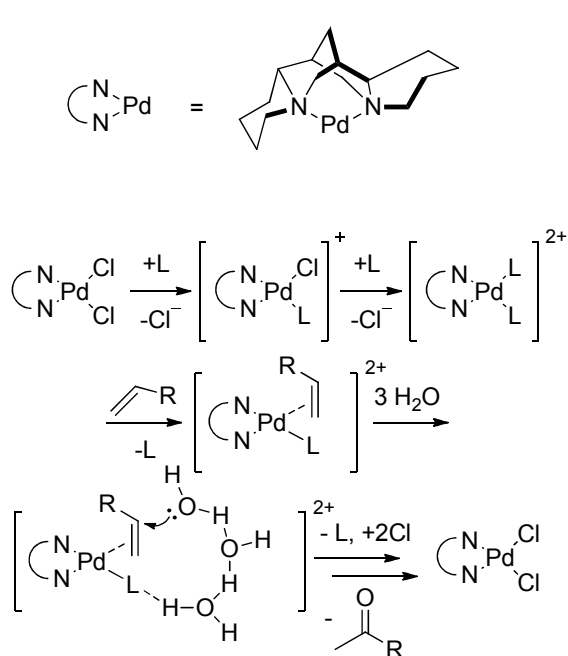
The Wacker process^[180] for the production of acetaldehyde from ethylene and oxygen is well known and represents an industrial process of multi thousands metric tons capacity per year.^[181] The industrial process proceeds by homogeneous catalysis on palladium(II) dichloride or heterogeneous on molten, eutectic copper(II) dichloride/potassium chloride catalyst-containing silica phases or $[\text{Pd}^{\text{II}}][\text{Cu}^{\text{II}}]$ -zeolites in the presence of water.^[132] *In situ* re-oxidation of the palladium is achieved via catalytic copper(II)/copper(I) reduction-oxidation cycles with oxygen. Even though, known since the 1959,^[182] the reaction still receives a lot of interest and has been studied in detail in the presence of chloride.^[183-187] However, for a laboratory scale version for the oxidation of terminal alkenes Wacker-Tsuji conditions^[184] are commonly employed utilizing water-miscible solvents like dimethylacetamide (DMA), dimethylformamide (DMF) or dimethyl sulfoxide (DMSO) as additives.^[188] DMSO and DMA were stated to stabilize the *in situ* generated Pd(0) species plus promoting the direct oxidation of Pd(0) to Pd(II) in the presence of oxygen.^[186, 188, 189] Several inorganic compounds, like manganese dioxide, sulfuric acid or other copper(II)salts and also organic peroxides or benzoquinone can be used. Alkyl nitrate/nitrite-systems^[190] are occasionally used even in industrial processes. More importantly, Pd(OAc)₂-pyridine (1 : 2) was found to be a simple and effective catalytic system for direct oxidation with oxygen without employing other co-catalysts.^[191] The proposed mechanism was likely to run via a Pd(0)(py)₂ complex being peroxidized to a peroxopalladium(II) bispyridine complex followed by conversion to a Pd(II) complex and hydrogen peroxide by protonolysis (*cf.* Scheme 22).^[192, 193]



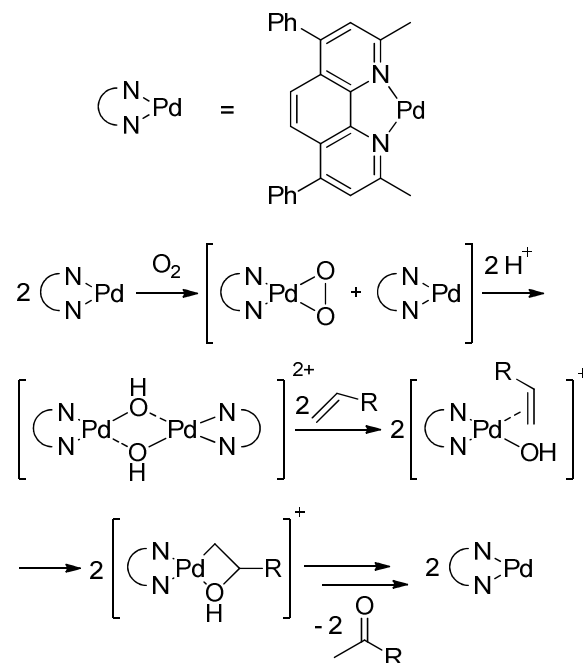
Scheme 22 Pd(OAc)₂-pyridine system for oxidation reactions using molecular oxygen as the sole oxidant.

Takas et al. reported the copper and chloride free Wacker oxidation using phenanthren as the *N*-heterocyclic ligand and envisaged an peroxopalladium(II) species, which is then converted by protonation. In this case, a disproportionation reaction between the oxopalladium(II)(phen) species and the initially present Pd(0)(phen) via protonolysis was considered. The resulting hydroxylated, dimer complex was assumed to be the active catalyst, which is then cleaved upon nucleophilic attacked by the incoming olefin. Therefore, the re-oxidizing step with

molecular oxygen will ingeniously proceed via formation/disproportionation reactions between peroxopalladium(II) and Pd(0) species (*cf.* Scheme 24). For sparteine, as the *N*-heterocyclic ligand, Anderson et al. reported a third-order dependency on water and proposed a catalytic system without formation of dimeric catalyst-species.^[186] Starting with a palladium(II) chloride sparteine complex, the mechanism was likely to run via positively charged, monomeric species. The oxidation step is explained by a nucleophilic attack of a water molecule and believed to run via an outersphere mechanism due to the third-order dependency on water. However, they noted that the controversy surrounding the mode of attack is challenging to determine, as the reaction is sensitive to the conditions employed. But by using relatively strong coordinating ligands, like DMA or bidentate, *N*-heterocyclic ligands the outersphere mechanism might be favored (*cf.* Scheme 23).^[194]



Scheme 23 Outersphere mechanism as proposed by Anderson et al.¹⁸⁸

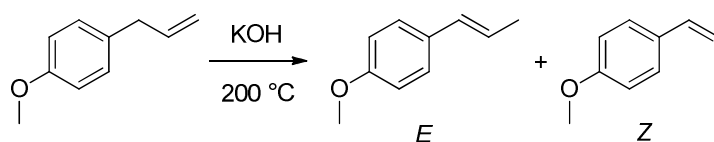


Scheme 24 Co-catalyst and chloride-free, innersphere Wacker oxidation mechanism reported by Takas et al.¹⁹⁵

These reports combined with the number of increasing, recent publications dealing with related Pd-catalyst complexes for oxidation reactions with *N*-heterocyclic ligands^[193, 195-202] triggered the development of camphor-derived bidentate, *N*-heterocycles and their investigation in the state-of-the-art co-catalyst free Wacker oxidation reaction. Since the Pd-sparteine system was also used in asymmetric, aerobic cyclization reactions^[198] and for separation of racemic alcohols^[197, 198] by enantioselective oxidation, the use of camphor as a sterically bulky, readily available and chiral compound as building block for the development of a well defined and modular, bidentate *N*-heterocyclic ligand was appealing.

Isomerization of Olefins with Palladium Catalysts – Overview and Motivation

The catalytic isomerization of olefins is an important and widely established process in industry and broadly employed in petrochemical refining processes (mostly in combination with heterogeneous catalysts).^[132, 181, 203] There is a large variety of existing synthetic methods for the construction of carbon-carbon double bonds or the introduction of an unsaturated functionality of which many deal with mixtures of (*E*)- and (*Z*)-isomers. The controlled migration of a pre-existing unsaturated functionality is a very elegant, alternative route of transformation.^[204] In particular, the isomerization of carbon-carbon double bonds obeys the sustainability criteria in that it is a 100% atom efficient reaction with widespread application, either for interconversion of (*E*)- and (*Z*)-alkenes^[205-207] or for stereo-controlled rearrangement of functionality along the carbon chain. This reaction is extensively deployed in the preparation of commodities for polymer synthesis, pharmaceuticals and fine chemicals, such as fragrances.^[208-211] The selective isomerization of terminal allylbenzenes into their internal counterpart represents a benchmark reaction for this kind of transformation, since the latter are common starting materials in the flavor and fragrance industry. Since (*Z*)-isomers are mostly characterized by an unpleasant odor and taste and are even toxic in some cases, processes with high yields, as well as high (*E*)-selectivity, are an attractive goal, but still remain a challenge. Nowadays, procedures range from heterogeneous catalysts on suitable supports at high temperatures to simple base catalyzed isomerizations, used for the conversion of estragol to *E*-anethol in KOH at 200 °C (*cf.* Scheme 25). The low yields of below 60% and only moderate *E/Z* selectivities (82:18, 64% *d.e.*) of this process requires additional separation steps and therefore many fragrances such as eugenol, estragol and safrol, as well as their internal alkenes, are still obtained by classical extraction techniques from natural sources with several million metric tons capacity per year.^[210, 212]



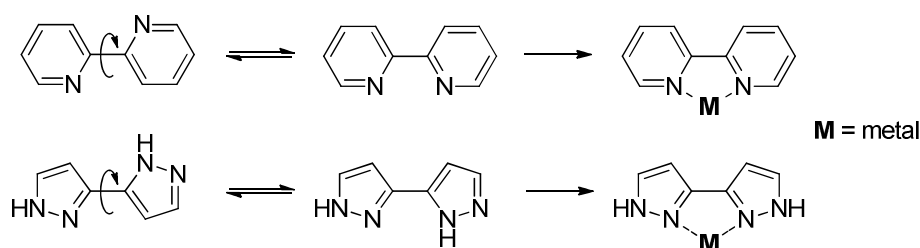
Scheme 25 Base-catalyzed, industrial process for the preparation of fragrances.

Despite the popularity of heterogeneous catalysts, which are known to be critically affected by the presence of water at high temperatures,^[132, 181] the use of homogeneous catalysts presents an attractive alternative.^[208] The isomerization of terminal alkenes can be accomplished by employing various transition metals, e.g. Pd,^[213-217] Pt,^[218-220] Ru,^[221-224] Rh,^[215, 225, 226] Ir^[227-229] or Ni,^[203, 230] which generally afford significant amounts of the thermodynamically more stable (*E*)-isomers. Since olefin isomerization is a kinetic

phenomenon, the thermodynamic driving forces, in particular the steric and electronic factors that control the β -H elimination process, can be investigated by following the kinetic distribution of *cis* and *trans* isomers early in the reaction process for various catalysts. The thermodynamic equilibrium ratio between (*E*) and (*Z*) may be tuned, especially by running the reactions at higher temperatures and using catalysts with long lifetimes.^[231, 232] Unfortunately, when transition metals catalyze the isomerization process, side-reactions with the carbon-carbon double bond occur, the kinetics and the product distribution is affected and hence the selectivity of the reaction changes. Examples, for which such side-reactions occur, include Grubbs-type hydride complexes, which can be modified in alcoholic solutions, with hydrogen, inorganic hydrides or alkoxides. They afford very active isomerization catalysts, which are usually accompanied by olefin self-dimerization, cross-metathesis and hydrogenation of the terminal alkene functionality.^[233-235] Transition metals in combination with additives, such as trialkylsilanes,^[222] boro- or aluminium-hydrides are used as well.^[206, 233, 234, 236] Besides isomerization, these reactions also lead to significant amounts of undesired hydrogenated side-products. To date there is no direct pathway for isomerization reactions, owing to the large variety of different catalysts, metals and ligands available for this kind of transformation.^[214] This being said, Pd²⁺ catalysis, is an area worth pursuing, since upon complexation with the appropriate ligands Pd²⁺ compounds are generally air and moisture stable.

Why Bipyrazoles as Ligands? – Structural and Electronic Properties

2,2'-Bipyridines are well-known and established ligands and upon one of the most explored chelate systems in coordination chemistry^[237] and due to its redox stability and ease of functionalization commonly used as catalysts,^[238] i.e. for allylic oxidations,^[239, 240] substitutions,^[241-243] cyclopropanations^[244, 245] and transfer hydrogenations.^[246] Surprisingly, 3,3'-bipyrazoles have been less used and investigated as potential ligands.^[247-249]



Scheme 26 2,2'-Bipyridines (top) and 3,3'-bipyrazoles (bottom) as structural motif.

Intrigued by the converse electronic nature of the π -excessive 3,3'-bipyrazoles^[250, 251] compared to 2,2'-bipyridines, which are π -acceptors, a more deeply investigation of this ligand class was envisaged (*cf.* Scheme 26).

The 3,3'-bipyrazole pattern was selected due to several advantages regarding structural and electronical properties.^[252] Besides the steric bulk, enhanced within the 3,3'-bipyrazole core compared to 2,2'-bipyridines, a complete, rigid ligand structure was not considered as retention of a certain degree of flexibility^[253] might be beneficial for later applications and transfer of the ligand system to other areas of interest. The protic structure is synthetically valuable as modifications might be more, readily achieved compared to transformations at the pyridine core. Furthermore, the protons are in close proximity to the metal-center and transformations, like the installation of flanking substituents, are expected to enhance steric congestion around the metal center thus influencing catalysis more efficiently. Generally, *N,N*-bidentate ligand pattern are of good thermal stability compared to ordinary *N*-monodentate ligands, like simple nitrile or amine coordination. This is especially interesting, since sparteine represents a pure σ -donor and stabilizing effects due to any π -bonding/backbonding interactions are impossible. The π -excessive nature of the 3,3'-bipyrazoles pattern, compared to bipyridines, phenanthrens, indoles and indazoles is supposed to increase the electrophilicity of the metal-center thus enhancing catalytic performance (*cf.* Figure 36).

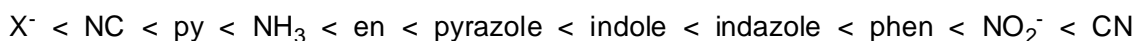
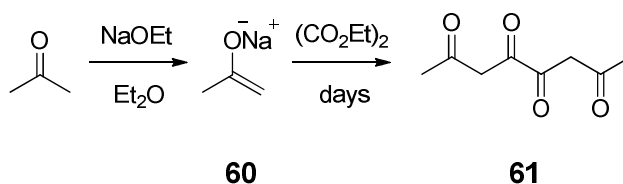


Figure 36 Electronic properties of 3,3'-bipyrazoles (spectrochemical series).

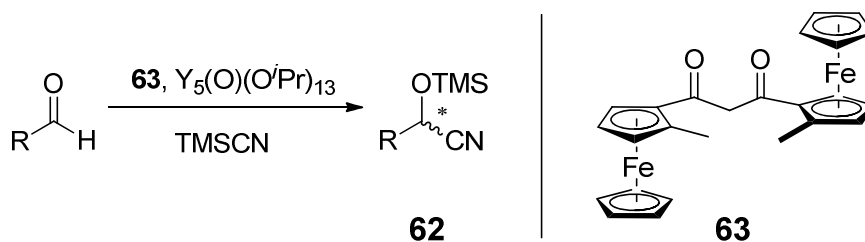
Tetraketones – Preparation, Scope, Structure Properties and Catalytic Activity

The most simple tetraketone can be derived from acetone and was reported already in 1888 by Claisen et al.^[254] using sodium methanolate to condensate the obtained acetone enolate **60** with diethyl oxalate. Acidic workup with acetic acid furnished 1,3,4,6-tetraketone **61** (*cf.* Scheme 27). In general, side products due to successive polymerization or monosubstitution are observed, which strongly depend on the reaction conditions, the procedure and the work-up process.



Scheme 27 1,3,4,6-acetone tetraketone first reported by Clasién et al.²⁵⁶

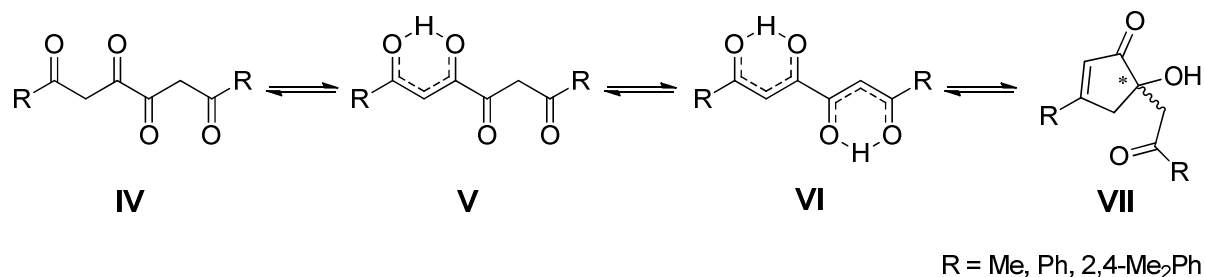
Even though, the catalytic activity of β -diketonate complexes in asymmetric transformations and their use as CSPs for GC and SFC was reported on a continuous basis since the early 1960s (*cf.* Chapter 1), literature reports on catalytically active 1,3,4,6-tetraketone metal complexes is extremely rare. With the chiral, ferrocenyl derived tetraketone **63** the yttrium-catalyzed, asymmetric silylcyanation of benzaldehyde showed promising results (95% yield, 90% e.e.). However, a decrease in the enantiomeric excess was observed with electron-deficient benzaldehyde derivatives (*cf.* Scheme 28).^[255, 256]



Scheme 28 Yttrium-catalyzed asymmetric silylcyanation of benzaldehyde using ferrocenyl-tetraketone **63** and TMSCN.^{257, 258}

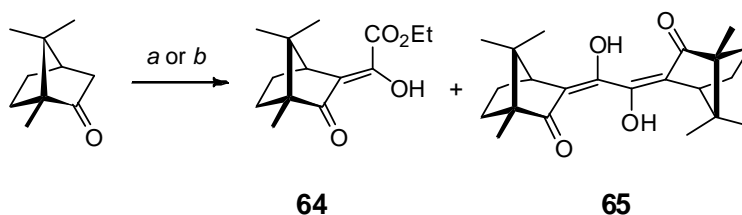
Reaction conditions: $\text{Y}_5(\text{O})(\text{O}^i\text{Pr})_{13}$, DCM, r.t., 1 h. DCM, r.t., 3 min. TMSCN, DCM, -78 °C to r.t.

The difluoroborane incorporated 1,3,4,6-tetraketone derived from acetophenone was successfully used for the preparation of semi-conductors^[257] and in environmental geochemistry 1,3,4,6-dimethyltetraketone was reported to be a sensor for iron and used for the determination of iron concentrations in water and soil.^[258, 259] The structures of 1,3,4,6-tetraketones were issued several times and different conformations and tautomeric isomers (keto-enol-tautomerism) were observed in the solid and liquid state. It was stated that 1,3,4,6-diphenyltetraketone, which exhibits a pure bisenolic form in chloroform (**VI**), tautomerizes in dimethyl sulfoxide to its keto-form (**IV**, $\text{ratio}_{\text{keto-enol}} = 1:1$).^[260] However, the fully enolized structure is present in the solid state.^[261] Semi-acetal structures (**VII**) were observed as well to a certain extent.^[262-264] On the other hand it was shown that 1,3,4,6-dimethyltetraketone does adopt a bisenolic form in chloroform (**VI**, 96%) and in dimethyl sulfoxide a mixture of the semi-acetalic (**VII**, 59%), the bisenolic (**VI**, 36%), the mono-enolic (**v**, 45%) and the pure tetraketone from (**IV**, 1%) exists. Semi-acetal formation (**VII**) was even increased to 90% in case of the corresponding 2,4-dimethylphenyl derivative.^[265] The dynamic, structural behavior and the challenges arising due to isolation of the compounds may account for the limited research reported in this field (*cf.* Scheme 30).



Scheme 30 Structure dynamics of 1,3,4,6-tetraketones.

Camphortetraketone **65** was first reported as an unwanted side product during preparation of ethylcamphor oxalate **64** at elevated temperatures (*cf.* Scheme 29). In addition to the described structural behavior two diastereomeric forms were detected by NMR-spectroscopic measurements and were assigned from the authors to *Z* and *E*-isomers (ratio_{E/Z} = 1.0 : 3.4).^[266] Hart et al. postulated the existence of overall six different isomers of 1,3,4,6-camphortetraketone **65**, in particular *cisoid* and *transoid* structures, enol-tautomers and rotamers due to the large bulk of the camphor moiety. Semi-acetal structures were not considered by the authors but have to be taken into account as well (*cf.* Figure 37).^[267]

Scheme 29 First report on 1,3,4,6-camphortetraketone **65** by Noe et al.²⁶⁸

Reaction conditions: a) NaH, (CO₂Et)₂, xylene, 50 °C, 95% for **64**. b) NaH, (CO₂Et)₂, xylene, 90 °C, 59% for **65**.

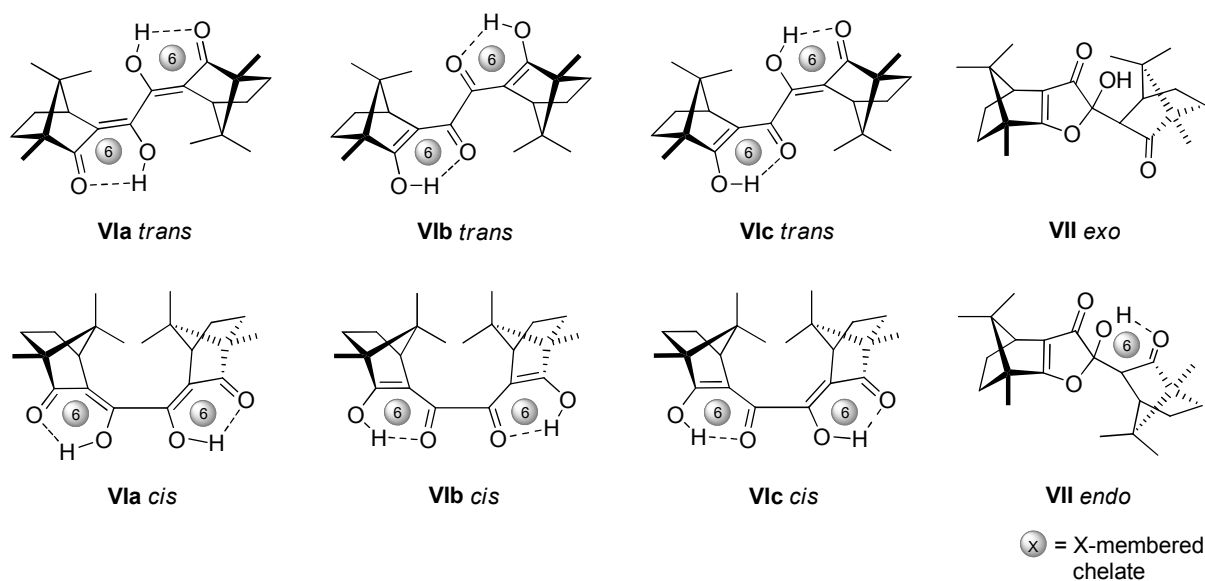
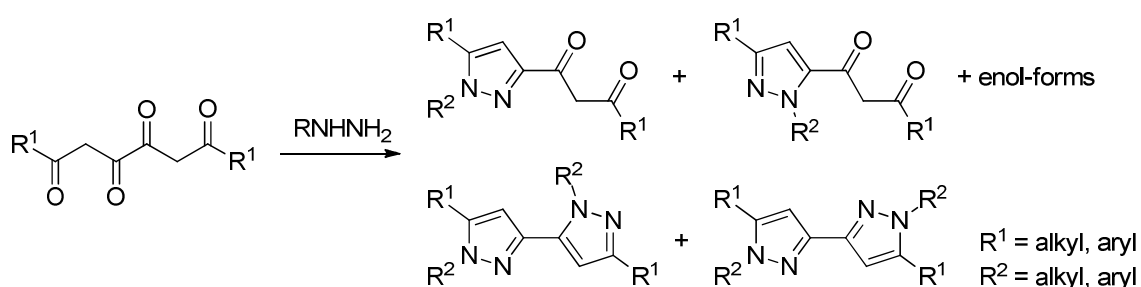


Figure 37 1,3,4,6-Camphortetraketone isomers as postulated by Hart (including semi-acetals).

From Tetraketones to Bipyrazoles – Preparation and Structure Properties

Doubtless the most employed and straightforward method for the preparation of the pyrazole heterocycle is the condensation of 1,3-diketones with hydrazine derivatives.^[268] The same strategy can be applied for the preparation of bipyrazoles from tetraketones. However, for the preparation of 3,3'-bipyrazoles from 1,3,4,6-tetraketones regioselectivity has to be considered. Despite a few examples, the use of substituted hydrazine derivatives in this case is of low synthetic value as a mixture of several condensation products are generally obtained (*cf.* Scheme 31).^[265, 269] Therefore, a two-step process featuring hydrazine hydrate condensation with 1,3,4,6-tetraketones followed by selective functionalization was envisaged.



Scheme 31 3,3'-bipyrazoles and isomers obtained by condensation with hydrazine derivatives.²⁶⁷

2.2 Objectives

The second part of the present thesis focuses on the development of a novel, bidentate *N*-heterocyclic ligand pattern derived from camphor (3,3-bicamphorpyrazole, bcpz), its coordination properties towards palladium(II), cobalt(II) and copper(II) and its catalytic activity considering the influence of steric as well as electronic effects. Therefore, a new ligand pattern was envisaged fulfilling the following criteria: (i) short synthesis from readily available starting materials, (ii) steric bulkiness with the possibility of introducing different moieties, (iii) a modular ligand system with a sterically and electronically diverse substitution pattern. Furthermore, this ligand system should be preliminarily screened for catalytic activity, so enabling further insights for development of stereoselective transformations (*cf.* Figure 38). Noteworthy, there is no literature about backbone fused 3,3'-bipyrazoles and their use as potential ligands in metal mediated catalysis so far.

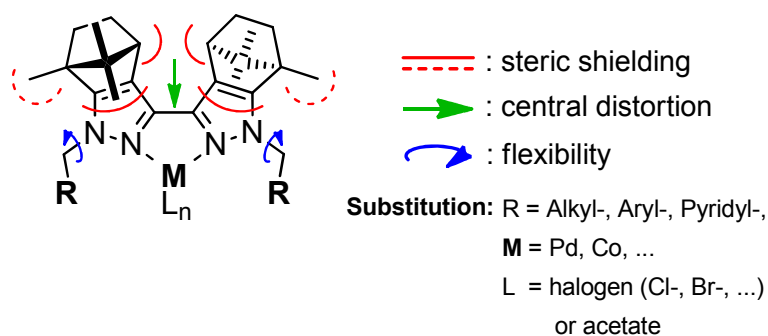


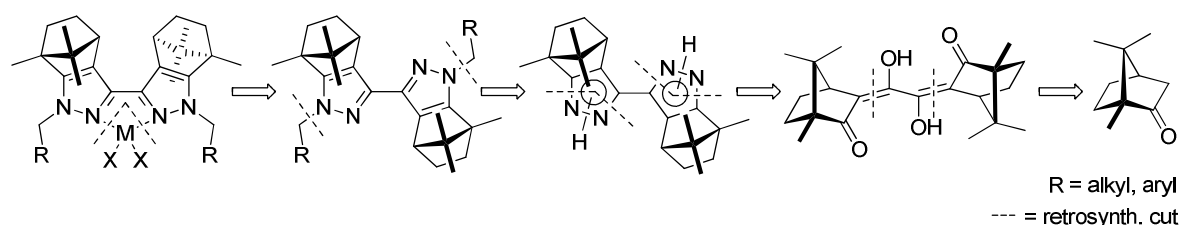
Figure 38 Target, camphor derived, bidentate 3,3'-bipyrazole complex pattern.

Furthermore, the synthetic approach includes the formation of chiral camphortetraketones in the first step, which were of considerable interest for the development of chiral, Lewis-acid catalysts (CLAs).^[176-178] In general, their synthesis is reported to be challenging, regarding yields, isolation and especially characterization of the obtained products. Therefore, an improved synthetic access to and the unequivocal determination of the tetraketone structure and reaction products was pursued. The identification and isolation of pure camphortetraketone is the prerequisite for any further synthetic steps to the bicamphorpyrazole ligand pattern as well as for preparation and any catalytic application of camphor-derived CLA catalysts. The structure dynamics of chiral tetraketones will be discussed and defined rhodium(I) and iridium(I) CLA-catalysts prepared. Afterwards, the synthesis, characterization and structural analysis of the chiral, bicamphorpyrazol (bcpz) ligands and metal complexes will be refocused. The catalytic activity of a series of bcpz-palladium catalysts in the copper-free Wacker oxidation and in the selective isomerization of terminal alkenes, regarding influence of electronic and steric properties, the role of the solvent

and starting materials will be investigated. The nature of active catalyst and insights into the isomerization mechanism deploying the novel catalysts were of main interest.

2.3 Results and Discussion

Natural *d*-(+)-camphor proved to be the building block of choice in the design of the new bicamphorpyrzole (bcpz) ligand class, since *d*-(+)-camphor fulfills all the above mentioned criteria and furthermore enables the user to extend this strategy to the majority of bicyclic monoterpenes commonly found in catalyst designs.^[122, 238, 245, 270-272] The retrosynthetic approach towards the newly, camphor-derived ligand pattern is depicted in Scheme 32.



Scheme 32 Retrosynthetic analysis of target, backbone-fused camphor 3,3'-bipyrazole ligand pattern.

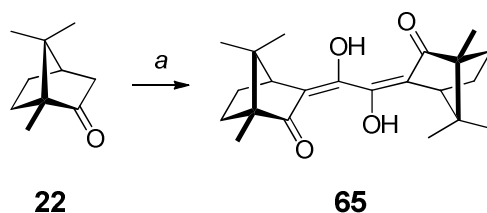
The synthetic route features the formation of 1,3,4,6-camphortetraketone in the first step, followed by tandem condensation to the *N*-heterocyclic bipyrazole core, which is then subjected to conditions intended to furnish wing-tip substitution, and finally metal incorporation to the desired catalysts.

2.3.1 Synthesis and Structural Dynamics of Chiral Tetraketones and Their Metal Complexes

Tetraketone Formation – Preparation, Isolation and Structure Determination

The first step towards 3,3'-bicamphorpyrazoles, as shown in Scheme 32, is the preparation of the 1,3,4,6-camphortetraketone **65**. This compound was prepared using a slightly modified procedure of Noe et al.^[266] As outlined in chapter 2.1 the reaction is sensitive to reaction conditions, reactant quantities, the synthetic protocol and work-up procedure. However, sodium hydride in boiling tetrahydrofuran was found to furnish complete camphorenolate formation over a period of three days prior to addition of diethyl oxalate and after several recrystallization steps 1,3,4,6-camphortetraketone **65** was isolated in 93% yield (*cf.* Scheme

33). NMR-spectroscopic measurements in deuterated chloroform showed the formation of only two independent isomers as indicated by two characteristic singlets at 11.6 ppm and 14.6 ppm (enolate-protons) and two signals at 2.9 ppm (respectively 3.2 ppm) for the isolated, tertiary CH-proton of the camphor backbone. This led to the assumption that in deed at least two diastereomeric forms are present in solution. To identify the true nature of the isomers all six structure isomers postulated by Hart^[267] plus two possible semi-acetal structures were taken into account. Whereas acetalization isomers were not observed, a differentiation between the six isomers remained challenging until X-ray crystal structure analysis revealed the existence of an unprecedented, isomeric 1,3,4,6-tetraketone structure (*cf.* Figure 39). Overall two independent enolate-structures, either chelating the enol-proton via a 6-membered or a 7-membered chelate structure, were found. The 6-membered *E*-diastereomer as postulated by Hart^[267] was verified by X-ray analysis and represents one of the isomers. The result is in line with the *transiod* structure observed for 1,3,4,6-diphenyltetraketone,^[261] regarding the orientation of the 1,3- β -diketonate substructures. The 7-membered, chelate-type tetraketone isomer instead has not been postulated before.



Scheme 33 Preparation of 1,3,4,6-camphortetraketone **65**.

Reaction conditions: a) NaH, THF, 67 °C, 3 d then (CO₂Et)₂, THF, 67 °C, 1 d, 93%.

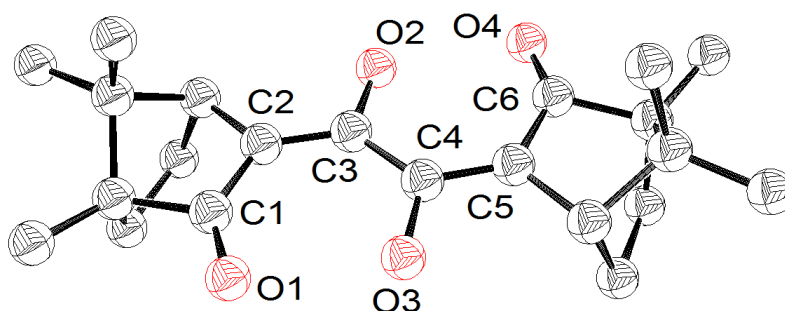


Figure 39 Solid state structure of camphortetraketone **65** showing the unprecedented, 7-membered, proton chelate structure.

X-Ray crystal structure of 1,3,4,6-camphortetraketone **65**, thermal ellipsoids are plotted at 50% probability level and hydrogens are omitted for clarity. Selected bond lengths for **65**: C1–O1 123.1(4) pm, C1–C2 145.4(4) pm, C2–C3 134.9(4) pm, C3–C4 147.4(4) pm, C4–O3 135.3(4) pm, C4–C5 135.7(4) pm, C5–C6 146.0(5) pm, C6–O4 146.0(5) pm.

A correct classification of this isomer was possible, but several aspects have to be elucidated: (i) by application of the same stereodescriptor rules for both isomers an *E*-configuration has to be assigned to the 7-membered chelate structure as well (since it's a *transoid* structure), therefore the structures are no *cis-trans*-isomers, (ii) by superposition of both structures all three characteristic methylsubstituents of the camphor-backbone (general a useful indicator to differentiate between isomers) point to the same direction, (iii) the positioning of all oxygen atoms of the 1,3- β -diketonate substructure in the overlay is (almost) similar, (iv) the isomers are no constitutional (structural) isomers as the *d*-(+)-configuration of enantiopure camphor is retained, (v) the structures are stereoisomeric to each other but no enantiomers, (vi) due to "fixation" of the structures via chelation they represent no rotamers of each other, (vii) the Newman-projection commonly used for the determination of conformer configuration (*gauche*, *anti*, *eclipsed*) is not valid, since both isomers are in plane and thus the isomers are no simple conformers, (viii) stereodescriptors, like *D*-, *L*- (carbohydrates, anomers), α -, β - (steroid/ terpene nomenclature), *P*-, *M*- (helicity) are not suitable and the isomers can not be differentiated by the coordinated proton (equal mode of coordination, e.g. κ -, η -, μ -, ...), (ix) the structures are no protomers and the isomers are obviously not a mesomeric representation of each other, (x) in conclusion the structures represent keto-enol type diastereomeric isomers.

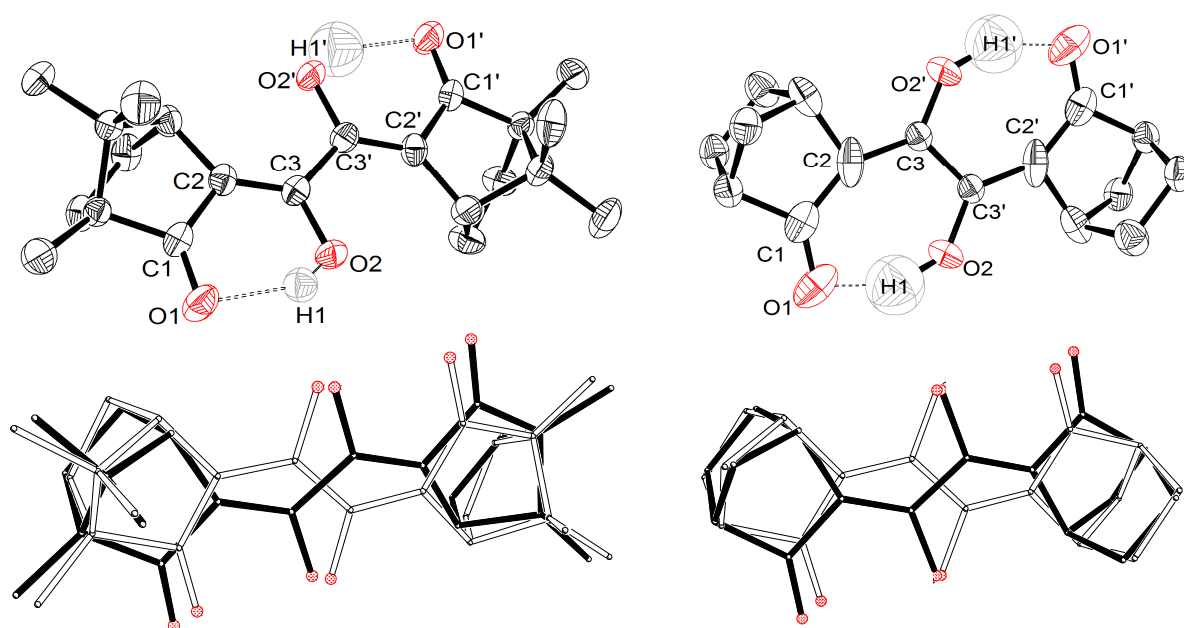
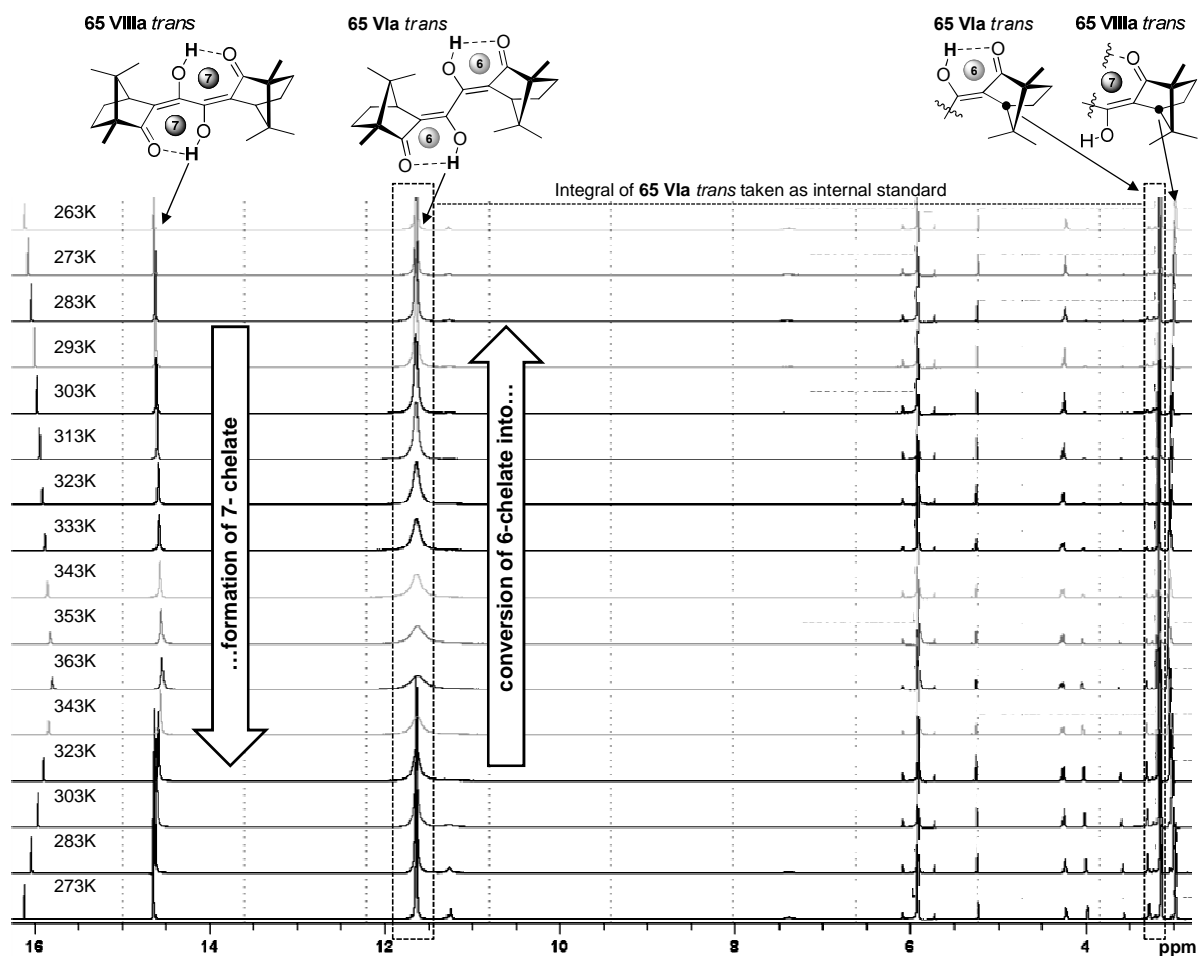


Figure 40 Solid-state structures shown for 6-membered 1,3,4,6-camphor- (left) and 7-membered 1,3,4,6-norcamphortetraketone (right) and superposition thereof. X-Ray crystal structure of camphortetraketone **65** (left), thermal ellipsoids are plotted at 50% probability level and hydrogens are omitted for clarity (except chelate-protons): 6-membered proto-chelate isomer (top left) and superposition of both isomers (bottom left). X-Ray crystal structure of 1,3,4,6-norcamphortetraketone (right), thermal ellipsoids are plotted at 50% probability level and hydrogens are omitted for clarity (except chelate-protons): 7-membered proto-chelate isomer (top right) and superposition of both isomers (bottom right)

To proof the formation of 6- and 7-membered chelates as a general property of sterical hindered, backbone-fused 1,3,4,6-tetraketones, the corresponding norcamphor-derived 1,3,4,6-tetraketone was prepared.^[273] Crystal structure analysis of this compound showed the same structural properties as seen with camphor (*cf.* Figure 40).

Considering the isomers as simple tautomers is somewhat inaccurate as by IUPAC definition tautomers represent “*readily interconvertible (frequently very rapid)*” isomers (keto-enol-, lactam-lactim-, amine-imine- and amide-imidic acid-tautomerism, for instance).^[274] Isolation of one tautomer is generally hampered without stabilizing effects, like aromatization. Prototropy is observed for both structures of 1,3,4,6-(nor)camphortetraketones, but a clear assignment to a known phenomenon, like annular tautomerism (e.g., 1*H*-, 2*H*-pyrazole) or ring-chain tautomerism (e.g., pyran/ furan structures of glucose/ fructose) is not possible. In particular, the present isomers may represent a unknown type of chelate-prototropy tautomerism accompanied by tandem-keto-enol rearrangements and rotation of two carbon-carbon bonds. Interconvertability is a necessary prerequisite for tautomers and therefore the influence of temperature on the distribution of isomers was investigated using VT proton NMR spectroscopy. 1,1,2,2-tetrachlorethane-*d*₂ (bp. 146 °C) was chosen as solvent and the results obtained from consecutive, temperature-dependent measurements (-10 °C → 90 °C, $\Delta T = 10$ °C and 90 °C → 0 °C, $\Delta T = 20$ °C) showed the selective conversion of the 6-membered proto-chelate to the 7-membered isomer (temperature driven). For comparison reasons, regarding signal-broadening and integration values, the sample was heated, then cooled again and spectra of the same temperature were analyzed and compared. The isolated CH-proton at the camphor backbone (2.9 ppm, 3.2 ppm), each corresponding to one chelate-isomer, was found to be an ideal internal standard. This approach allowed the observation of any small changes in isomer-distribution and allowed cross-validation by integration of two sets of signals for each isomer. A increase of 40% in favor of the 7-membered isomer upon heating was detected by freezing of the hydroxyl-integral for the 6-membered isomer. Cross-validation using the backbone as internal standard showed an increase of 42% again in favor of the 7-membered isomer. The results are in good agreement (cross validated) and account for a temperature driven conversion of the 6-membered 1,3,4,6-camphortetraketone isomer into its thermodynamically more stable 7-membered isomer. No change in this distribution ratio was obtained over a period of four weeks under standard conditions (*cf.* Scheme 34). To evaluate, whether the camphor- and norcamphortetraketones are suitable ligands for any application in transition-metal catalysis, the corresponding dirhodium(I) and diiridium(I) metal complexes were prepared in 54%, resp. 94% yield (*cf.* Scheme 35).

Unexpectedly, by metal incorporation the complex signal pattern of the mixed isomers observed via NMR spectroscopy were significantly reduced giving evidence for a selective

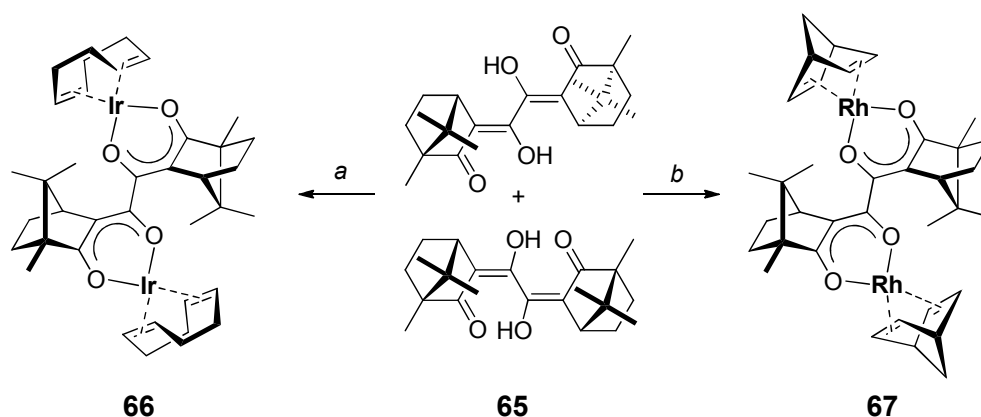


Scheme 34 VT proton NMR showing the conversion of 6-membered chelate isomer **65 Via** to 7-membered chelate isomer **65 VIIIa**.^[a]

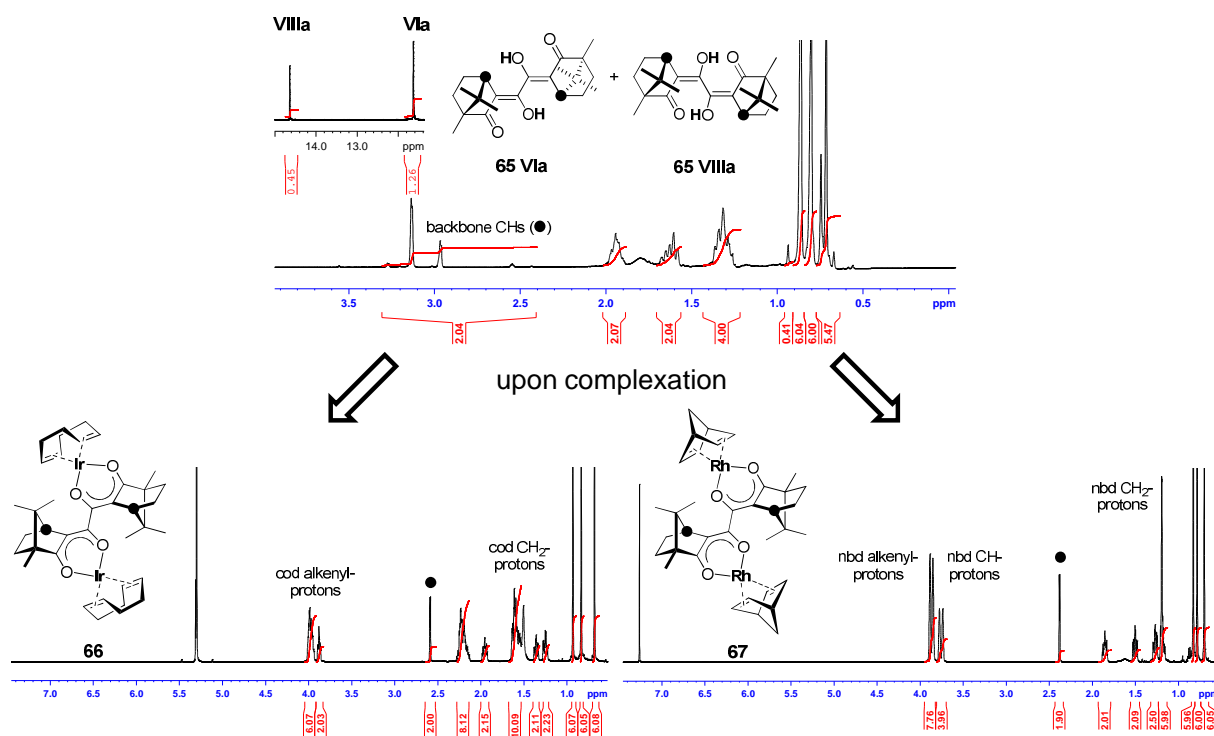
^[a] Recorded in 1,1,2,2-tetrachlorethane-*d*₂ between 263 K and 353 K

formation of only one transition-metal complex from the ligand mixture. This behavior was found for both metal complexes of camphor and norcamphor. Whereas all camphor-derived dirhodium(I) and diiridium(I) transition-metal complexes were obtained as yellow microcrystalline, air and moisture stable solids, the corresponding diiridium-norcamphor^[273] complex decomposed in anhydrous dichloromethane-*d*₂ and benzene-*d*₆ within 30 min or over prolonged exposure to air. However, ¹H NMR measurements showed selective formation of only one transition-complex species for all chiral 1,3,4,6-tetraketones from the diastereomeric mixtures (*cf.* Scheme 35 and Scheme 36)!

After numerous attempts crystals of bis(norbornadiene) dirhodium(I)-1,3,4,6-dicamphortetraketone **67** suitable for X-ray crystallographic analysis using synchrotron radiation were obtained. Noteworthy, the structure analysis confirmed the selective formation of one transition-metal complex diastereomer and showed the selective formation of the 6-membered rhodium(I)-chelate isomer from the diastereomeric ligand mixture. The rhodium(I)



Scheme 35 Metal-mediated, selective formation of 6-membered bis(*cyclooctadiene*) and bis(*norbornadiene*) metal(I)-1,3,4,6-dicamphortetraketonate complexes **66** and **67**. Reaction conditions for complex preparation: a) [Ir(cod)Cl]₂, KO^tBu, THF, r.t., 16 h, 94%. b) [Rh(nbd)Cl]₂, KO^tBu, THF, r.t., 16 h, 54%.



Scheme 36 Selective formation of **66** and **67** from the diastereomeric ligand mixture.

As observed by ¹H NMR spectroscopy and recorded in chloroform-*d*₃ (top, bottom right) and dichloromethane-*d*₂ (bottom left) at r.t.

β -diketonates are distorted to each other due to rotation of the central C3–C3' bond with a O2–C3–C3'–O2' torsion angle of 127.3° forming a *transoid* structure (52.7° deviation from planarity). An almost planar conformation for each rhodium(I) β -diketonate substructure is observed with a maximum out-of-plane deviation of 5°. Noteworthy, the distorted *transoid* structure is indicative for the steric demand of the camphor backbones and chirality might be

transferred to the metal center via two ways: (i) from the adjacent, fused camphor-backbone of the rhodium(I) β -diketonate substructure itself and (ii) from each neighboring camphor-backbone group being in close proximity to the metal center (in fact the neighboring camphor-backbone is 30 pm closer to the rhodium center in the solid state than the adjacent, fused one). Therefore, both rhodium(I) β -diketonate substructures are expected to “support” each other, regarding chiral induction, blocking of octants and approaching vectors for incoming substrates and thus enhancing asymmetric induction (*cf.* Figure 41).

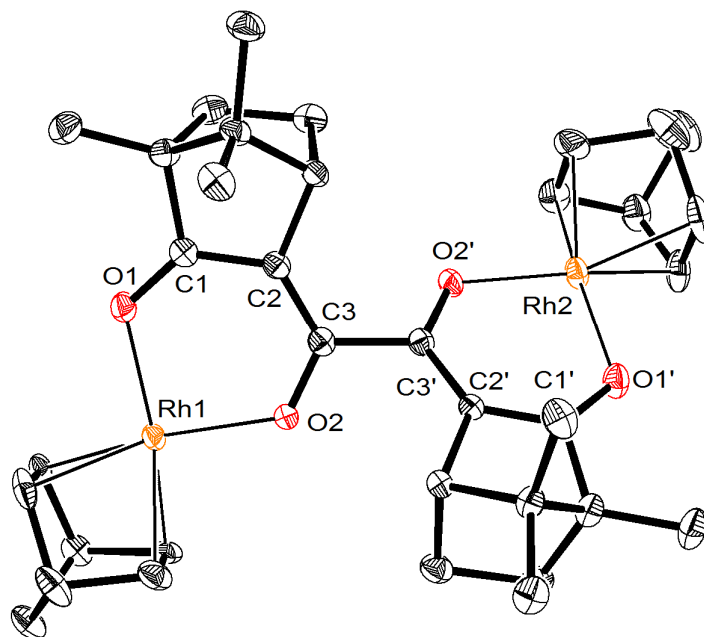


Figure 41 Solid state structure of bis(norbornadiene) dirhodium(I)-1,3,4,6-dicamphortetraketonate **67**.

Thermal ellipsoids are plotted at 50% probability level and hydrogen atoms are omitted for clarity. Selected bond lengths: Rh1–O1 204.5(19) pm, Rh1–O2 205.8(2) pm, O1–C1 126.7(4) pm, C1–C2 140.9(4) pm, C2–C3 137.6(5) pm, C3–O2 129.2(4) pm, C3–C3' 150.9(4) pm, Rh2–O1' 204.9(2) pm, Rh2–O2' 205.7(19) pm, O1'–C1' 127.0(4) pm, C1'–C2' 141.5(4) pm, C2'–C3' 138.0(4) pm, C3'–O2' 129.1(4) pm.

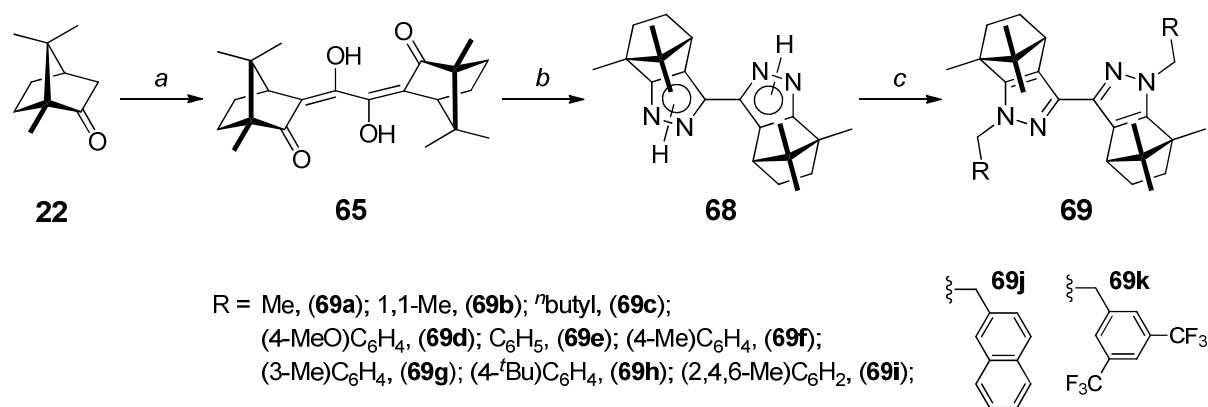
For preliminary catalytic tests, the iridium(I) and rhodium(I) complexes **66** and **67** were embedded in GE-SE 30 (polydimethylsiloxane) and coated onto the inner surface of fused-silica capillaries (0.25 mm I.D.) using the static method described by Grob^[139] resulting in a defined polymer film-thickness' of 250 nm. The column-capillaries were conditioned (for conditioning of columns *cf.* *Experimental Section*), installed into the GC and tested in the asymmetric hydrogenation of monoterpenes. (*S*)-(+)-Carvon was partially hydrogenated on the rhodium(I)-1,3,4,6-dicamphortetraketonate **67** containing column but a clear differentiation between hydrogenation of terminal, internal double bond or carbonyl functionality was not possible due to substantial loss of catalytic activity as determined by chiral GC-MS on a standard 25 m *Chirasil- β -Dex* column (50 °C to 120 °C, 4K@85 kPa

helium). By injection of (*S*)-(+)-carvon products exhibiting a characteristic camphor fragmentation pattern were detected and evaluation of the GC-MS data obtained suggests decomposition of the complex under reaction conditions. Competitive coordination in the catalyst between chelating tetraketone and carvon exhibiting a keto- and two olefinic positions may account for the observation. However, the successful preparation of chiral, defined dirhodium(I) and diiridium(I) catalysts via selective metal-incorporation and the unequivocally determination of the complex structures and isomers is remarkably as identification of the true nature of catalyst is fundamental for application in catalysis. Continuous research is going on to extend the scope of chiral 1,3,4,6-tetraketones, their metal-complex preparation and application in asymmetric rhodium(I)- and iridium(I)-mediated catalysis.

2.3.2 Palladium-bipyrazoles derived from Camphortetraketones

2.3.2.1 Synthesis and Characterization

The bipyrazole ligands **69a–k** were readily synthesized in a three step procedure starting from enantiopure *d*-(+)-camphor (*cf.* Scheme 37).



Scheme 37 Synthetic pathway to novel, camphor-derived 3,3'-bipyrazole ligands.

Reaction conditions for the preparation of 3,3'-bipyrazoles **69a–69k**. a) NaH, THF, 65°C, 3 d then (CO₂Et)₂, 65°C, 1 d, 93%; b) N₂H₅OH, EtOH, 78°C, 2 d, 91%; c) NaH, THF, 65°C, 2h then RCH₂X, 65°C, 4h (16h for **69c** and **69i**), 79 – 98%.

1,3,4,6-tetraketone **65** was obtained in two tautomeric enol forms (*cf.* Chapter 2.3.1) by double Claisen condensation with diethyl oxalate in 93% yield. A second tandem condensation with hydrazine hydrate^[265, 269] furnished the key intermediate 3,3'-bicycamphorpyrazole (bcpz) **68** as an insoluble powder in 91% yield. After several attempts to

solubilize **68** it was found that prolonged heating under basic conditions resulted in complete solvation of the 3,3'-bipyrazolate, which in turn provides a useful indicator of the reaction progress. Furthermore, dialkylation was achieved exclusively at the *N*-1,1'-pyrazole positions without formation of regioisomeric mixtures, which often hampers synthesis and requires additional separation steps (*cf.* Chapter 2.1).^[275-277] This was attributed to steric congestion and metal (sodium) complexation with the *N*-2,2'-atoms in the center of the ligand under the experimental conditions. It should be emphasized that, due to the here developed and optimized synthetic protocol and crystallizability of the intermediates, the synthesis of the ligands **69a** – **i** was achieved in only three steps in excellent overall yields between 67 and 82% and without the need for tedious work-up procedures or chromatographic separations. Single crystals of the free ligands were obtained by slow evaporation of saturated solutions in ethanol and revealed a C_2 -symmetric *transoid* structure state with respect to the pyrazole nitrogen atoms, which were obtained for all ligand structures reported here (solid states of **69e** – **j**). The crystal structures of the sterically most demanding ligands mesitylen-3,3'-bicamphorpyrazole **69i** and naphthalene-3,3'-bicamphorpyrazole **69j** are depicted in Figure 42 with an N-C-C-N torsion angle of 172.8° (**69i**) and 165.0° (**69j**), respectively.

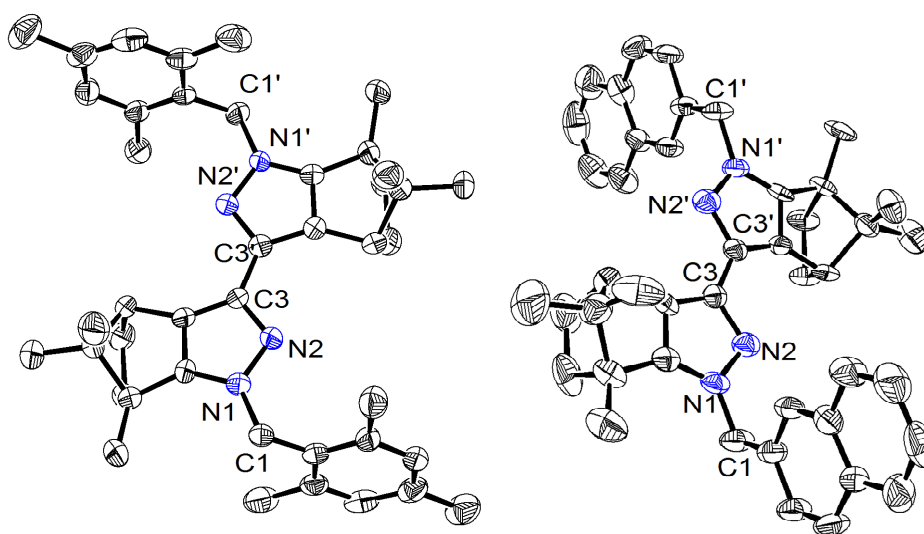
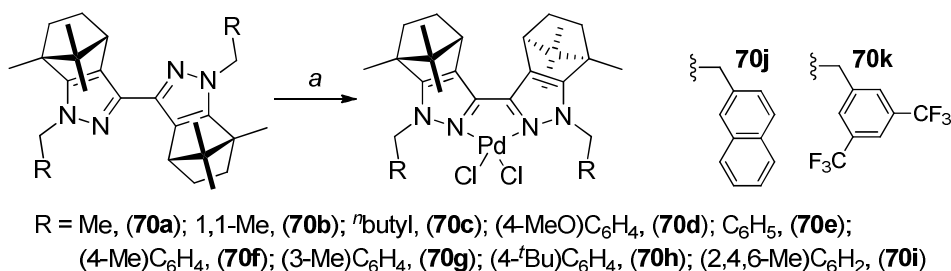


Figure 42 X-Ray crystal structures of ligand **69i** (left) and **69j** (right) showing the *transoid* structure.

Thermal ellipsoids are plotted at 50% probability level and hydrogen atoms are omitted for clarity. Selected bond lengths for **69i**: N1–N2 136.6(4) pm, N1'–N2' 135.8(4) pm, N2–C3 134.3(5) pm, N2'–C3' 134.8(5) pm; **69j**: N1–N2 139.0(10) pm, N1'–N2' 135.6(10) pm, N2–C3 136.5(11) pm, N2'–C3' 136.7(10) pm.

The monomeric palladium complexes of all eleven new ligands **70a** – **k** were obtained by ligand exchange with bis(acetonitrile)palladium(II) dichloride in acetonitrile at room



Scheme 38 Preparation of palladium(bcpz) complexes **70a – k**.

Reaction conditions: Pd(MeCN)₂Cl₂, MeCN, r.t., 12 – 16 h, 91 – 98%.

temperature in good yields (*cf.* Scheme 38). To confirm the ability of complex formation of the novel ligands, the monomeric bidentate copper(II) and cobalt(II) complexes of ligands **69h** and **69j** were prepared and **69h**^(Cu) crystallized from ethanol containing solutions. The copper(II) complex of **69h** shows a distorted structure between tetrahedral and square planar conformation, with an N-Cu-N plane twisted about 51.7° to the Cl-Cu-Cl plane, which is a known phenomena for κ^2 -LCuCl₂ complexes, but less pronounced in related κ^2 -N₂,N₂'-copper(II) compounds^[278] and hardly visible in κ^2 -N₂,N₂'-bipyridine copper(II) complexes^[279, 280] (*cf.* Figure 43). The two crystal structures represent, beside d⁶ complexes of Ru, the first examples for d⁸ (Pd) and d⁹ (Cu) 3,3'-bipyrazole complexes coordinating the N₂,N₂'-nitrogens through κ^2 .^[247, 281] All complexes were characterized by elemental analysis, NMR (except paramagnetic Cu, Co complexes), IR and MS.

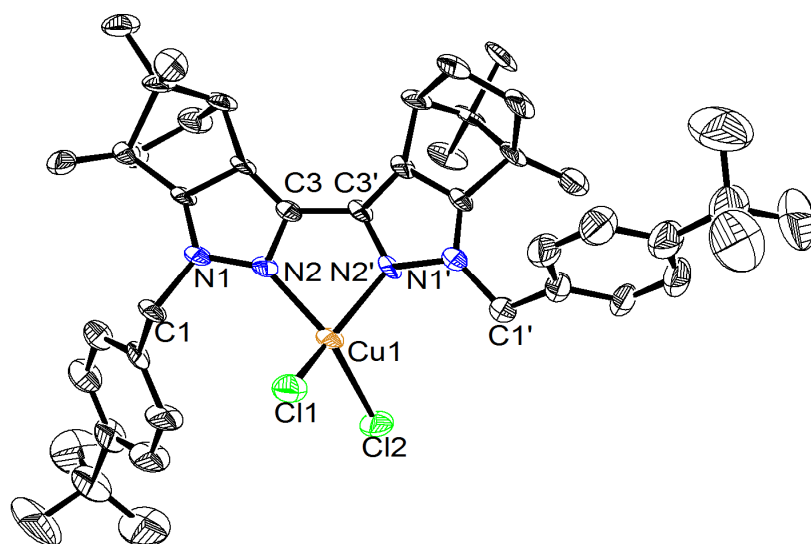


Figure 43 Distorted geometry observed in copper(II)-complex of **69h**.

Thermal ellipsoids are plotted at 50% probability level and hydrogen atoms are omitted for clarity.

Selected bond lengths for **69h**^(Cu): Cu–Cl1 220.3(4) pm, Cu–Cl2 221.3(4) pm, Cu–N2 200.2(12) pm, Cu–N2' 201.5(12) pm, N1–N2 138.5(16) pm, N1'–N2' 134.7(16) pm, N2–C3 139.9(19) pm, N2'–C3' 133.0(18) pm, C3–C3' 141.0(2) pm, Cu–Cl1 135.6(10) pm.

In contrast to the free ligands, the palladium complexes scarcely crystallized. However, small single crystals of **70h** suitable for X-ray analysis using synchrotron radiation were obtained by slow diffusion of pentane into a saturated diethyl ether solution. As shown in Figure 44, two molecules of the complex Pd[(bcpz)1,1'-(p-^tBuC₆H₄)₂] adopt a cage like structure with its benzyl wingtips encapsulating one single diethyl ether molecule (*cf.* Figure 44).

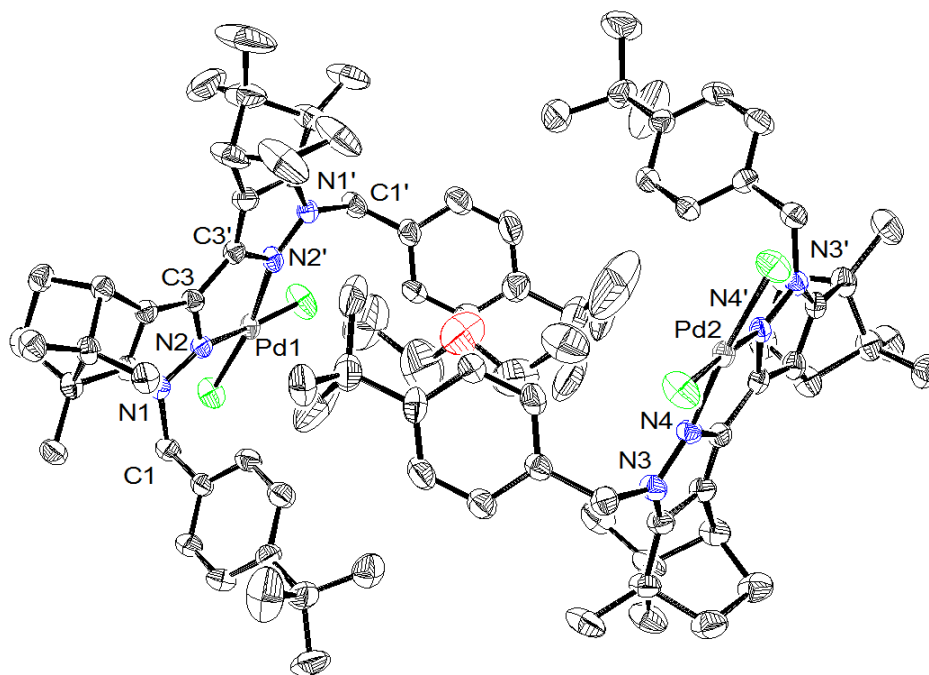
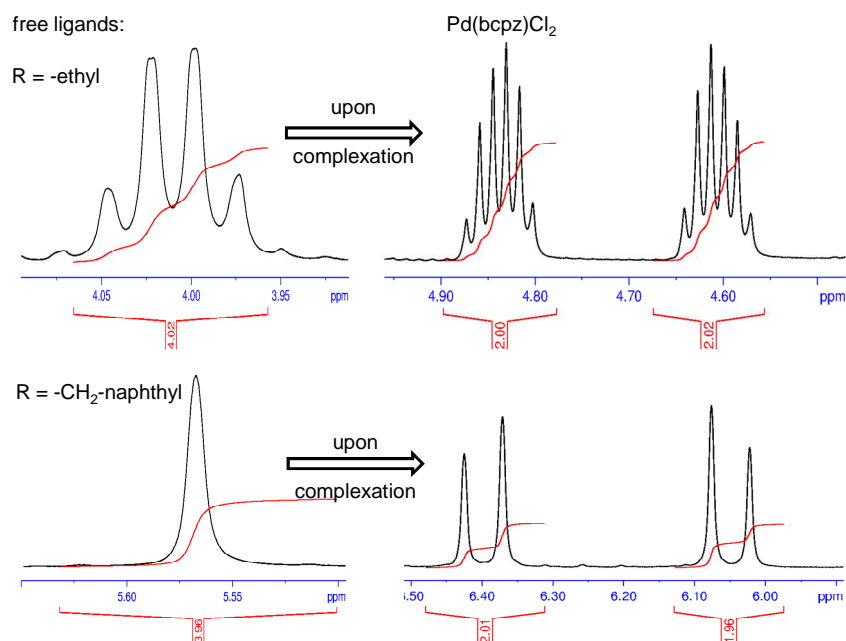


Figure 44 X-ray crystal structure of palladium 3,3'-bipyrazole complex **70h** showing the *cisoid* structure.

Thermal ellipsoids are plotted at 50% probability level and hydrogen atoms are omitted for clarity.

Selected bond lengths: Pd1–N2 206.4(3) pm, Pd1–N2' 207.5(3) pm, N1–N2 136.5(4) pm, N1'–N2' 137.3(4) pm, N2–C3 133.6(5) pm, N2'–C3' 136.8(5) pm.

The Pd1 atom lies 49.8 pm above the mean bipyrazole plane (Pd1 coordination plane 20.5° out of bipyrazole plane; for Pd2 41.7 pm and 16.5°, respectively) and the bite angle N–Pd–N is 78.3° for Pd1 and 78.9° for Pd2. The complex stability in solution, integrity of the *cisoid* structure and the feasibility to rotate the wingtips are the prerequisite for any application as a catalytic system in homogeneous catalysis. Therefore solutions of the palladium(II) complexes **70d** – **k** were studied by temperature dependent ¹H NMR spectroscopy. The two protons of each wingtip methylene group at C1 and C1' of the free ligands show a characteristic singlet between 5.0 and 5.6 ppm for arylated structures, as expected for two sets of enantiotopic protons, whereas complexation with Pd(II) results in a distinct pattern for the *cisoid* structure. Splitting of the methylene signals with a downfield shift to 5.8 and 6.3 ppm is generally observed for the two sets of diastereotopic protons of arylated bcpz compounds including geminal ²J_{CH} couplings (13.8 – 14.1 ppm for alkyl-; 15.6 – 16.7 ppm for benzylic protons).



Scheme 39 Distinctive ^1H NMR pattern of **69a** and **69j** showing splitting of wingtip methylene signals into a set of two diastereotopic protons upon complexation to afford **70a** and **70j** (recorded after 16h).

This is observed for the proton spectra of *N,N'*-alkylated ligands **69a** – **c** as well, which undergo downfield shifts between 4.3 ppm and 6.0 ppm combined with more complex splitting patterns (*cf.* Scheme 39). The geminal coupling of the dibromide complex of **69h**^[282] ($^2J_{\text{CH}} = 15.9$ Hz) and a downfield shift to 5.8 and 6.2 ppm is in agreement with the range and shift observed for the chloride complexes.

VT proton NMR spectra of **70h** – **j** in 1,1,2,2-tetrachloroethane- d_2 between 243 K and 363 K did not indicate the presence of further conformations in solution. The starting spectra remained unchanged, hence proving complex stability in a broad temperature range. To investigate the influence of solvent, the CD-spectra of Pd-complex **70h** were recorded in various solvents. The CD-spectra show two strong absorptions with a maximum positive Cotton effect at 266 – 271 nm and a negative Cotton effect at 225 – 227 nm in both tetrahydrofuran and dichloromethane solutions, which are larger than in the free ligand. The zero crossings in the CD-spectra are in satisfactory agreement with the maximum absorptions of the complexes, as can be seen in the UV-spectra (*cf. Experimental Section, Figure 65*). In contrast, in acetonitrile a more disordered random conformation seems to dominate. Surprisingly, evaluation of the CD-spectra of the Pd(II)-complexes revealed a reverse solution behavior exclusively for the 3,5-trifluorobenzyl substituted complex **70k**, with a pronounced broad positive Cotton effect between 275 – 283 nm (*cf. Figure 45*).

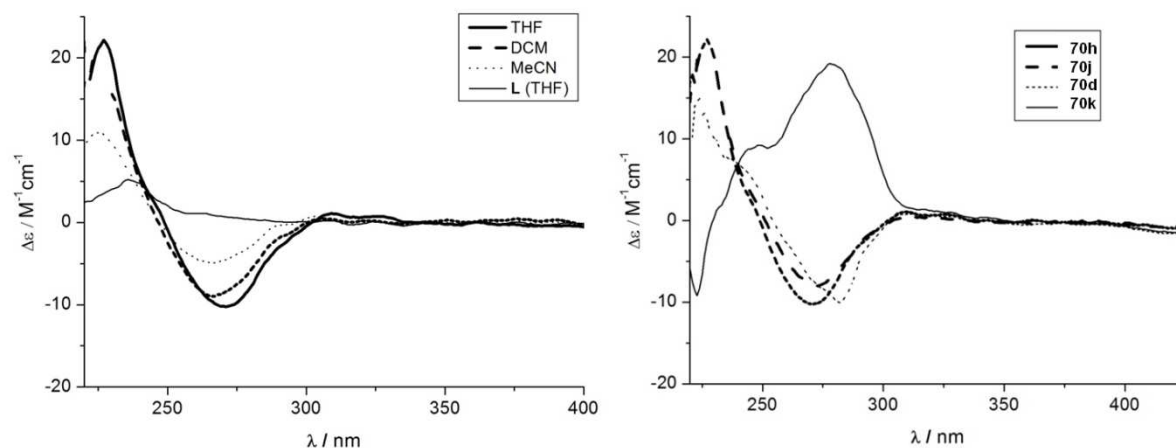


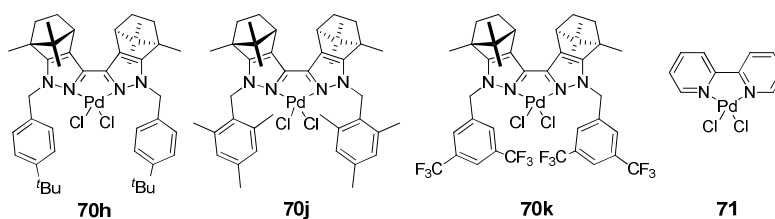
Figure 45 CD-spectra of free ligand **69h** and Pd-complex **70h** in different solvents (left) and Pd-complexes **70h – j** in THF (right, recorded at room temperature in different solvents).

2.3.2.2 Wacker-Oxidation of Terminal Olefins

With these ligands and complexes in hand their catalytic potential was screened^[283] in the copper-free catalytic oxidation of terminal alkenes.^[188, 201, 284] **70h** was arbitrarily chosen as the model complex for preliminary catalytic screening.^[285] For comparison, Pd(3,3'-bpy)Cl₂^[286] was synthesized and tested in parallel as a benchmark under the same reaction conditions. After optimizing reaction conditions, the oxidations of alkenes with molecular oxygen showed overall good conversions to the corresponding ketones (72 – 87%, *cf.* Table 10). These results are noteworthy, even though prolonged reaction times were required, since no or very low conversions were observed using molecular oxygen combined with Pd(3,3'-bpy)Cl₂ (**71**) as catalyst. Much shorter reaction times of 17 h were obtained with benzoquinone (BQ) as the internal oxidant with overall conversions of 89 – 99%. In order to evaluate the performance of the catalysts with respect to their substitution pattern a test set of three catalysts (**70h–k**) as representatives for *N,N'*-arylated Pd(bcpz)-compounds was chosen. The most electron deficient 3,5-bis(trifluoromethyl) substituted complex **70k** showed only low conversions of 1-octene and vinylcyclohexane, whereas catalysts **70h** (*p*-^tbutylbenzyl substituted) and **70i** (mesitylene substituted) were much more active. With **70i** yields of 83 – 99% of the corresponding ketones were obtained. We explain this by the higher redox potential of the 3,3-bipyrazoles, which are beside electronic effects also strongly influenced by sterics, which may be enforced by the ligand backbone. While still maintaining the structure, framework and coordination cavity higher reactivities and conversions with increasing electronic donating properties of arylsubstituted bcpz-type catalysts in the range of: *mesitylene* > *p*-^tButylbenzyl >> *3,5-bis(trifluoromethyl) benzyl* are observed. No conversion

was achieved using the corresponding palladium(II) acetates of **70h** and **71** as catalysts.^[287] Secondary alcohols as starting materials were not oxidized.^[200, 202] The formation of Pd black was not observed and all catalysts showed activity even after two cycles, which underlines the stability and recyclability of the here investigated catalysts.

Table 10 Summarized results of the copper-free Wacker oxidation of alkenes using Pd-complexes **70h**, **70i**, **70k** and **71**.²⁸³



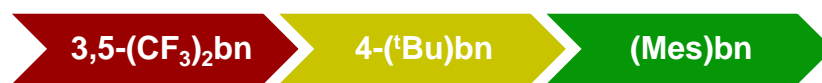
#	Substrate	Catalyst	Oxidant	Yield [%] ^[b]		Conversion [%] ^[b]
				aldehyde	ketone	
1	1-octene	71	O ₂	-	35	36
		70h	O ₂	-	80	94 ^[c]
2	4-methylstyrene	71	O ₂	25	1	34
		70h	O ₂	33	27	87
3	vinylcyclohexane	71	O ₂	-	3	5
		70h	O ₂	-	67	72
4	1-octene	71	benzoquinone	-	2	2
		70k	benzoquinone	-	19	19
		70h	benzoquinone	<1	99	>99
		70i	benzoquinone	2	97	>99
5	vinylcyclohexane	71	benzoquinone	-	3	3
		70k	benzoquinone	-	6	6
		70h	benzoquinone	-	61	62
6	1-octene	71	O ₂	-	35	36

Reaction conditions: catalyst (5 mol%), alkene (0.90 mM), O₂ (1 atm) or benzoquinone (3.00 equiv.) and *n*-undecane (10.0 μL) as internal standard in a DMA-water mixture (6:1) at 70 °C stirred for 17 h in a cap sealed vial (3d with O₂). Pd(bpy)Cl₂ **71** was prepared by S. Stockinger.^[283] ^[b] Reactions were monitored and yields determined by GC- and GC-MS analysis using a 25 m HP-5MS column and He as the inert carrier gas.^[283]

^[c] 11% of 1-octene isomers detected.

To this point it was shown that these palladium complexes showed higher activities with increasing electron donating properties induced by appropriate wingtip substitution (-CH₂R:

Mes > *p*-^tBuBn >> 3,5-(CF₃)₂Bn in the copper-free Wacker oxidation of terminal alkenes (*cf.* Scheme 40).



Scheme 40 Influence of flanking substituents on the reactivity in the Cu-free Wacker Oxidation of terminal alkenes

Color scheme: red to green (increasing reactivity).

2.3.2.3 Isomerization of Allylbenzenes – Insights into Catalyst Design and Activity, Role of Solvent, pH Effects and Mechanistic Considerations

In the following, the results in the Pd(II)-catalyzed isomerization of alkenes for the synthesis of fragrances under very mild conditions, employing media that did not need to be purified or dried, and using low catalyst loadings is described. In addition, the role of the solvent in terms of electronic and steric factors, as well as the influence of the halide concentration and the pH-value on the reaction progress when using bases and acids as additives was investigated and a possible reaction mechanism based on the observations and the results of deuterium labeling studies is discussed.

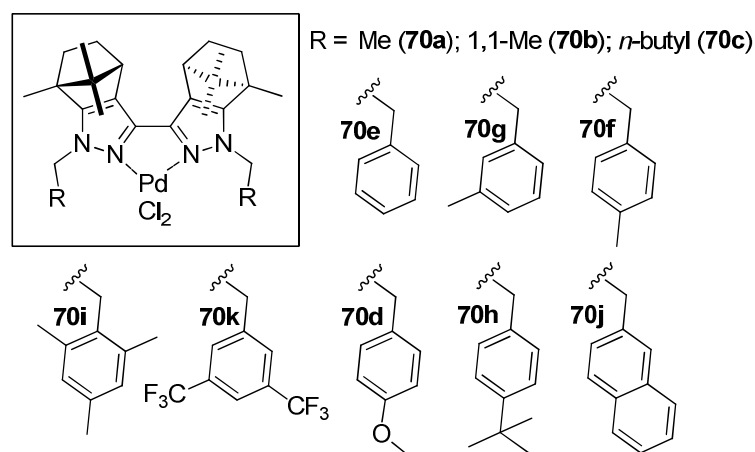
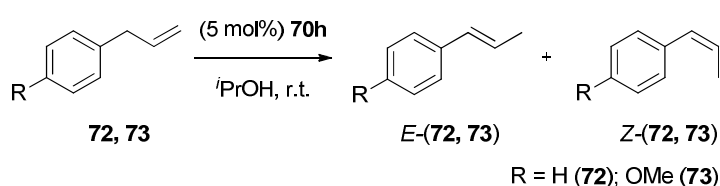


Figure 46 Catalysts for investigations of the Pd(II)-catalyzed isomerization of terminal allylic compounds.

As shown in Figure 46 all catalysts are mononuclear, neutral Pd(II) soft Lewis acids, with the *N2,N2'*-nitrogen atoms of the 3,3'-bipyrazole unit coordinated via κ^2 . The catalysts can be divided into two distinctive groups depending on the nature of wingtip substitution, either alkyl or benzylic residues. The ligands were chosen in order to be able to investigate and compare catalytic performance with steric factors and electronic properties within the group,

while maintaining the same ligand geometry and metal-coordination cavity. Overall eleven ligands of this family were tested in the isomerization reactions of allylpropenoids. In order to evaluate the performance of the catalysts in the Pd(II)-mediated selective isomerization of terminal alkenes a set of two arylpropenes (allylbenzene, entry 1; estragol, entry 2) were chosen as starting materials. Initially, the reactions were carried out using 5 mol% of Pd-catalyst **70h**, substrate (0.09 M) in *iso*-propanol and undecane (10 μ L) as internal standard. The reactions were monitored and yields determined by GC, GC-MS and ^1H NMR spectroscopy of isolated products. All starting materials were readily isomerized under very mild conditions in air at room temperature giving the (*E*)-isomers in high yields with high *E/Z*-selectivities of 97 : 3 for *trans*-allylbenzene and *trans*-anethol (94 % *d.e.*). Reactions were complete after 26 h at the latest by raising the temperature to 70 $^\circ\text{C}$. All reactions were carried out in unpurified solvent. Allylbenzene was isomerized in three hours in 98 % yield with an *E/Z* ratio remaining almost constant at 96:4 (92 % *d.e.*), which is noteworthy since isomerizations are known to be critically affected by water and impurities (*cf.* Table 11, Figure 47).

Table 11 Pd(II)-catalyzed selective isomerization of allylbenzene and estragol.



#	Substrate (R =)	time [h]	Yield of <i>E</i> -Isomer ^[b]	Product ratio (<i>E/Z</i>) ^[b]
1	H	5	80	97 : 3
		26	96	97 : 3
2	OMe	5	57	95 : 5
		26	93	97 : 3
3 ^[c]	H	3	98	96 : 4

Reaction conditions: catalyst **70h** (5 mol%), substrates (89 mM), undecane (10.0 μ L) as internal standard in a cap sealed vial at r.t. Average outcome of two repetitions. ^[b] Reactions were monitored and yields determined by GC analysis on a 25 m HP-5MS column. Product assignment determined by GC-MS and ^1H NMR analysis of isolated products. ^[c] Reaction at 70 $^\circ\text{C}$.

Promising conversions were even observed on lowering the catalytic amount of palladium to 1 mol%. After the encouraging results the role of the solvent was investigated more deeply. Interestingly, under the chosen reaction conditions almost no conversions were obtained in non-polar solvents (diethyl ether, toluene) as well as in aprotic polar solvents (acetonitrile, tetrahydrofuran, acetone, chloroform). Therefore the influence of the alcohol in terms of steric as well as electronic factors was considered. Metal-hydrides are known to be generated

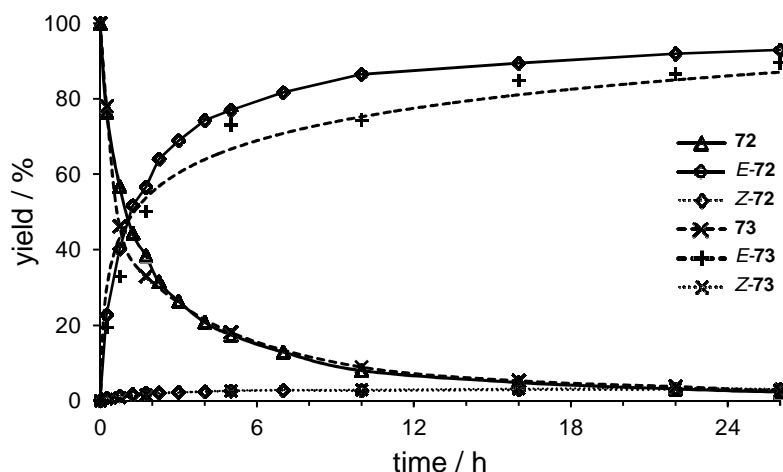


Figure 47 Isomerization of allylbenzene (x) and estragol (□) in *iso*-propanol at room temperature.

in situ by the use of additives, such as inorganic hydrides or, more recently, by weak acids, in particular alcohols, as is the case in the present study.^[221] Only absolute solvents of high purity were used for these tests and no conversions were observed without the addition of Pd(II)-catalysts, as proven by blank samples. Besides linear, monofunctional alcohols, such as methanol, ethanol and *n*-propanol, and secondary alcohols, such as *iso*-propanol, *cyclo*-hexanol as well as *tert*-butanol, 1,5-pentanediol, 1-propanthiol and 1-aminoheptane and glycerol, as a trifunctional alcohol, were employed. To complete the set also fluorinated alcohols were used, because remarkable effects have been reported for these substances.^[288-290] The results are depicted in Figure 48. Besides the need for a protic solvent, the electronic character is highly important as there is clear evidence for rate acceleration in the range of: *methanol* > *ethanol* > *n-propanol* > *iso-propanol* > *tert-butanol*. This result is in line with the pK_a -values of the alcohols (*cf.* Table 12).^[291, 292]

Table 12 pK_a -values of selected solvents.

solvent	H ₂ O	MeOH	EtOH	<i>i</i> PrOH	<i>t</i> BuOH	glycerol	ⁿ PrSH	TFE	HFB
pK_a ^[a]	15.7	15.5	15.9	16.5	17.0	4.4	13.2	12.4 ^[b]	11.4 ^[c]

As determined in H₂O, compiled and listed as reported by R. Williams,^[291, 292] significant digits left uncorrected.

^[b] 2,2,2-trifluoroethanol (TFE), pK_a of 11.3 in 50% aq. EtOH.^[292] ^[c] 2,2,3,3,4,4,4-heptafluorobutanol (HFB), measured in 50% aq. MeOH.^[292]

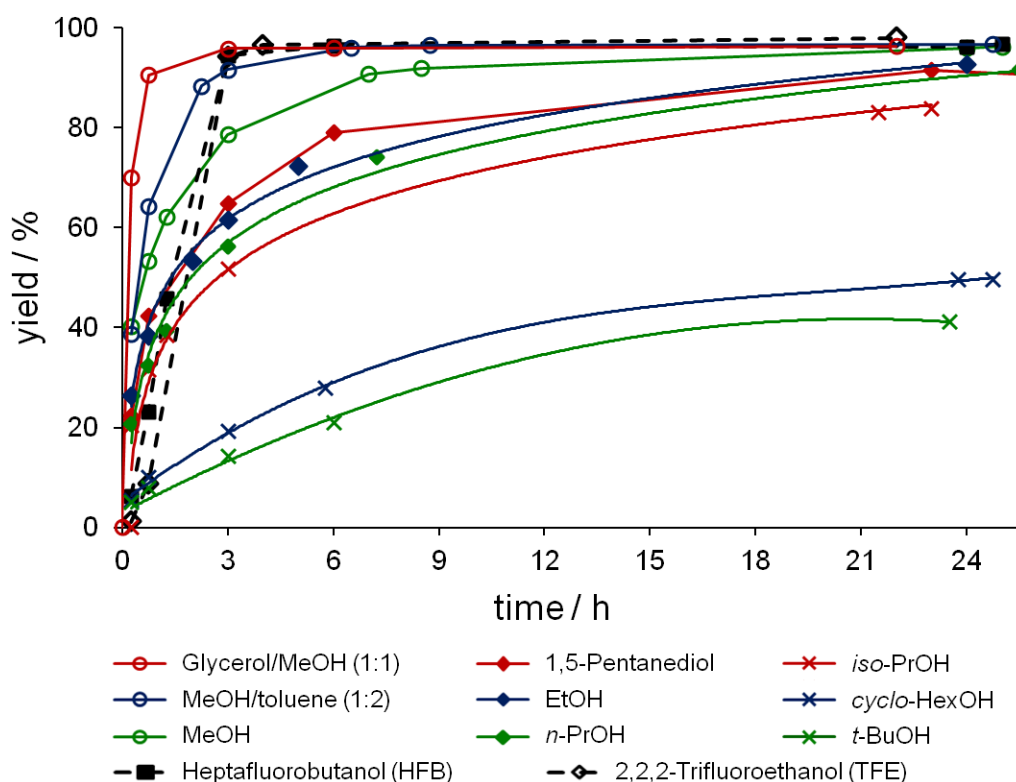
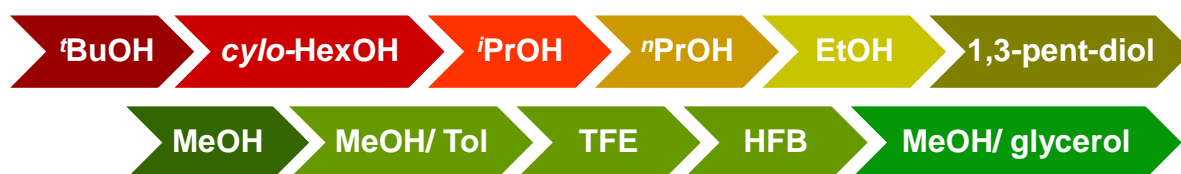


Figure 48 Solvent influence on the Pd(II)-catalyzed isomerization of allylbenzene.

Time-resolved formation of *trans*-methyl styrene over time as determined by GC and GC-MS.²⁸³ Reaction conditions: 1 mol% catalyst **70h**, substrate (98 mM) under air at r.t. (*t*-BuOH at 70 °C).

Nevertheless, besides inductive effects, steric bulk doubtless also has a significant influence on the pK_a values (due to disturbance of solvation and *H*-bonding). A drop of about 45% yield when comparing *iso*-propanol and *cyclo*-hexanol underlines these aspects, although the electronic properties of these two compounds tend to be quite similar. Whereas all other solvents and solvent mixtures led to almost equal conversions over time, a reaction progress analysis revealed a significant retardation of the reaction rate as the reaction proceeded (50% conversion after 24 h in *cyclo*-hexanol and 27% conversion after 23 h in *tert*-butanol, both at room temperature). Although decomposition of the catalyst provides an inadequate explanation, since only the type of alcohol for the given reaction conditions was changed, unknown inhibition effects of the catalyst cannot be ruled out. Surprisingly, no conversions were observed in more acidic 1-propanthiol (pK_a 13) and, as expected, no reaction occurred when using the more basic 1-aminoheptane as a solvent. Although, no isomerization occurred in pure acetonitrile due to its coordination capability, no inhibition was observed in methanol when adding 0.5 – 10 mol% acetonitrile, showing that low concentrations are still tolerated by the catalyst system. Two hydroxyl functionalities, as present in 1,5-pentanediol, had no significant effect and rates similar to those for ethanol were obtained. Even an increased acceleration compared to methanol was observed when 2,2,2-trifluoroethanol (TFE) and 2,2,3,3,4,4,4-heptafluorobutanol (HFB) were used as solvents, which is consistent with the

higher pK_a -values of fluorinated alcohols. By a closer look at the time-resolved conversion, a slightly different ascending slope bisecting the alcohol-mediated isomerization rate after an average of three hours, depending on the alcohol, can be detected for the fluorinated solvents. However, very high conversions and consistent diastereoselectivities are still maintained. It is worth mentioning, that by further optimization of the reaction conditions, fast conversions, similar to the results in fluorinated solvents, can be achieved using a 1:2 mixture of methanol and toluene. Since all catalysts are easily soluble in alcohols as well as in most aliphatic solvents, this observation is attributed to matching effects between solvent, starting materials (allylbenzene) and catalyst shape (bipyrazole-core and wingtip-arylation). Operating with this solvent mixture, allylbenzene conversion to the internal *E*-isomer was still very effective with catalyst loadings as low as 0.5 mol% Pd (92% yield, 92% *d.e.* after 6 h at r.t.) and even 0.1 mol% Pd (35% yield, 92% *d.e.* at r.t.; 70% yield, 90% *d.e.* at 60 °C; both measured after 6 h) with almost no decrease in diastereoselectivity. Remarkably, by using a solvent mixture (1:1) of glycerol and methanol at room temperature and catalyst loadings of 1 mol% the isomerization rate was even further accelerated (91% yield, 91% *d.e.* after 45 min) compared to the reaction in the toluene-methanol (2:1) solvent mixture (64% yield, 93% *d.e.* after 45 min). This is again in agreement with the low pK_a -value of glycerol, but may also be affected by the pronounced mesomeric stabilization capability within glyceric aldehyde. In summary, rate acceleration was obtained in the range of: *glycerol/methanol (1:1)* > *2,2,3,3,4,4,4-heptafluorobutanol* \approx *2,2,2-trifluoroethanol* \approx *methanol/toluene (1:2)* > *methanol* > *1,3,-pentanediol* > *ethanol* > *n-propanol* > *iso-propanol* > *cyclo-hexanol* > *tert-butanol* (cf. Scheme 41).



Scheme 41 Solvent influence on the Pd(II)-catalyzed isomerization of allylbenzene in the order of increased efficiency

Color scheme: red to green (increasing efficiency).

Substrate Screening

With the optimized conditions in hand we focused on the scope of the isomerization reaction deploying different starting materials, as well as the previously developed catalysts.

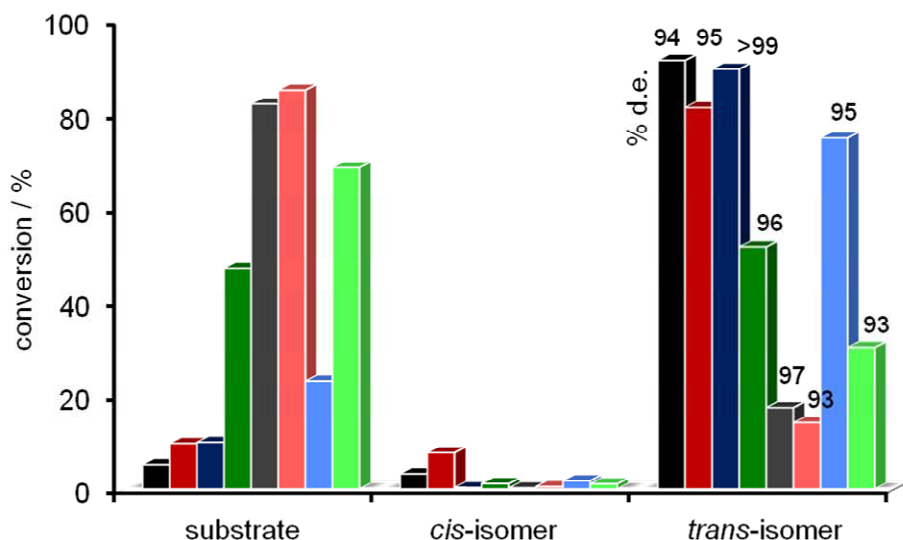


Figure 49 Conversion of allylbenzenes to internal alkenes after 3 h using catalyst **70h**.

Reaction conditions: 1 mol% catalyst **70h**, substrate (98 mM) in MeOH/ toluene (1:2) at r.t. under air.

Conversions monitored and product assignment determined by GC and GC-MS.²⁸³ Average outcome of three runs. Substrate order (left to right): 4-allylbenzene, 2-allylanisol, 2-allylphenol, estragol, 4-(trifluoromethyl) allylbenzene, eugenol, eugenyl acetate, 4-allyl-1,2,-dimethoxybenzene.

In order to get reliable results before varying the catalyst, the previous set of tests was extended to allylbenzenes with different functional groups at the aryl terminus (-CF₃, -OH, -OAc, -OMe). Applying the optimized reaction conditions (1 mol% Pd, 1:2 mixture methanol/toluene, air, room temperature) samples were taken and analyzed after 3 h. It has to be pointed out that the reactions were not allowed to run to completion in order to be able to evaluate the catalyst performance on the substrates regarding electronic properties and functional group tolerance. Several functionalities proved compatible to the catalytic conditions and after three hours 90% of allylbenzene and 4-hydroxy allylbenzene were converted to their corresponding *E*-isomers, followed by 2-allylanisol (80%), eugenyl acetate (75%), estragol (50%). 4-(trifluoromethyl) allylbenzene (20%) and eugenol (15%, *cf.* Figure 49). Low conversions of challenging, electron deficient starting materials, e.g. for fluorinated compounds, is a common phenomenon.^[217] As evidenced by the substrates the catalyst is compatible with donor heteroatoms, such as phenols and acetates and the overall high selectivities of 93 – 98% *d.e.* are among the highest ratios comparable to other well-studied systems.^[213, 217, 221, 223, 226, 231, 293] The excellent selectivity for *trans*-4-hydroxy allylbenzene (exclusively, >99%) is particularly remarkable and represents the highest diastereoselectivity reported so far.^[213, 231]

This effect may be attributed to the 2-hydroxyl functionality being in close proximity to the reaction center. A similar effect was observed recently and led to increased product formation and high selectivities in the Pd(II)-catalyzed double bond isomerization of 2-(but-3-enyl)phenols over two carbon-atoms.^[216]

Catalyst Screening

On the basis of the results obtained from the substrates, the influence of the electronic and steric properties of the catalysts on the isomerization reaction was of interest. With *N*-1,1'-alkylated bipyrazole catalysts **70a** – **70c** and their arylated counterparts **70d** – **70k** in hand, two types of Pd(II)-catalysts characterized by different steric demand (alkylated/ arylated) and with different electronic properties within each group were deployed.

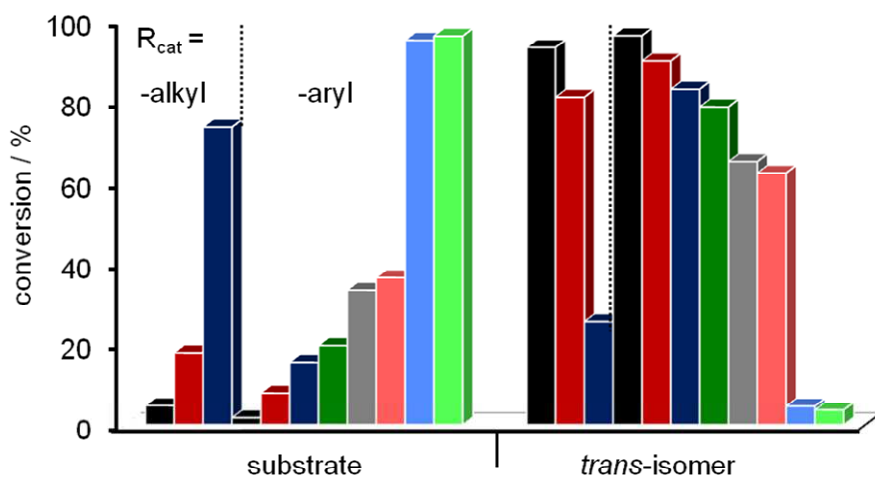


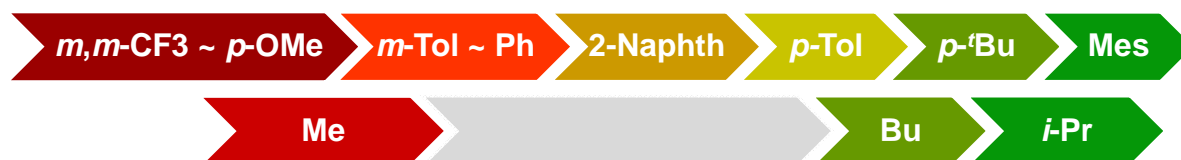
Figure 50 Catalyst performance evaluated in the selective isomerization of less reactive eugenyl acetate.

Reaction conditions: 1 mol% catalyst, eugenyl acetate (98 mm) in methanol/ toluene (1:2) at r.t. under air. Conversions monitored and product assignment determined by GC and GC-MS.²⁸² Average outcome of two repetitions. Catalyst order (left to right):

70b, 70c, 70a, 70i, 70h, 70f, 70j, 70e, 70g, 70k, 70d.

To obtain meaningful data for evaluation of the catalyst performance less reactive eugenyl acetate was chosen as a benchmark. The reactions were performed under the optimized reaction conditions (0.09 M, 1:2 mixture methanol/ toluene, 1 mol% Pd, room temperature) and samples were taken after three and six hours. For the *N*-1,1'-alkylated catalysts (**70a** – **70c**) increased activity was observed for **70b** (R = *iso*-propyl), followed by **70c** (R = *n*-pentyl) and the lowest conversions to the *E*-isomer was obtained by using catalyst **70a** (R = methyl). The results are indicative of a trend correlating higher electron-donating properties and

catalyst activity, since oxidative addition of substrates should be enhanced by higher electron density located at the metal center.^[184] For further evaluation, catalysts **70d** – **70k** were tested under equal conditions and showed a similar trend towards higher activity with increased electronic-density at the 3,3'-bipyrazole core. After six hours Pd(II)-catalyst **70i** (R = mesityl) showed the overall highest conversion of eugenyl acetate (96%), followed by **70h** (R = *para*-(*tert*-butylphenyl), 90%), **70f** (R = *para*-tolyl, 87%), **70j** (R = 2-naphthyl, 79%), **70e** (R = phenyl, 65%), **70g** (R = *m*-tol-, 62%) and **70k** (R = 3,5-di(trifluoromethyl)phenyl, 4%). This is in good agreement with the electron-donor capability of aryl substituents and verifies the results obtained for the *N*-1,1'-alkylated Pd(II)-catalysts. Surprisingly, catalyst **70d** (R = methoxy), with the most activating substituent pattern, did not fit into the trend (5% yield), but it represents the only catalyst exhibiting a heteroatom functionality at the wingtip-position. However, the reason is still unclear. Within the given ligand pattern a significant steric influence on the isomerization reaction was not observed and the high *E/Z*-selectivities (94 – 97% *d.e.*) achieved for eugenyl acetate were comparatively similar and remained almost constant during the reaction progress, as shown by variation of the catalysts. In summary, increased catalyst activity was obtained for Pd(II)(bcpz)-catalysts exhibiting a higher electron-density within the 3,3'-bipyrazole core induced by the substituents in the range of (R_{wingtip} =): *iso-propyl* > *n-pentyl* > *methyl* and *mesityl* > *para*-(*tert*-butylphenyl) > *para*-tolyl > 2-naphthyl > phenyl > *meta*-tolyl >> 3,5-di(trifluoromethyl)phenyl (*cf.* Figure 50 and Scheme 42).

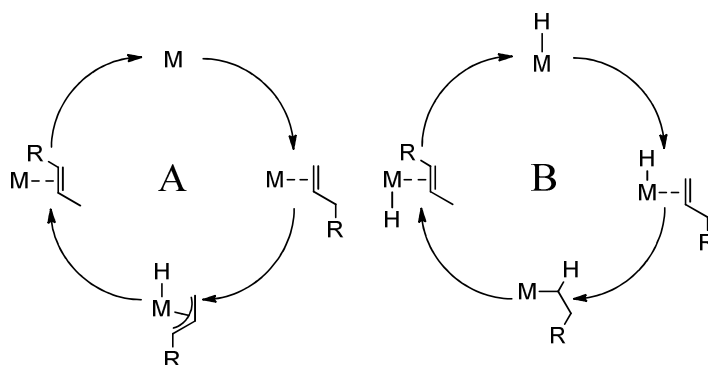


Scheme 42 Influence of flanking substituents on the reactivity in the Pd(II)-catalyzed isomerization of eugenyl acetate.

Color scheme: red to green (increasing efficiency).

Mechanistic Studies

Generally, two main reaction pathways for the isomerization of alkenes can be envisaged. The transition-metal catalyst can operate via a π -allyl mechanism (A) or a hydride addition-elimination mechanism (B) (*cf.* Scheme 43).



Scheme 43 Isomerization of terminal alkenes via π -allyl intermediate (A) and hydride addition elimination (B) reaction mechanism.

The metal-hydride complex can be initially present as catalyst or generated *in situ*, whereas the other mechanism features a rearrangement through a transitory π -allyl intermediate upon alkene coordination, which is followed by a reversible hydride transfer to form the π -allyl metal-hydride species. Overall olefin isomerization follows the thermodynamic driving forces, reaching an equilibrium distribution, with the thermodynamic more stable *E*-isomer being favored.^[206, 215, 233, 294] In particular, the kinetic distribution of the isomers depends on the electronic and steric factors controlling the β -elimination process. Moreover the kinetics and product distribution, and thus the selectivity of the reaction, is affected, when the transition metal catalyzes the isomerization as well as reaction at the double bond. Generally, the π -allyl intermediate mechanism has a dramatic effect on the distribution of isomers giving rise to high *E/Z*-selectivities, and *E/Z* ratios greater 4:1 will be generally observed.^[203] An interesting class of catalysts capable of this type of terminal olefin isomerization was derived from [(allyl)PdCl]₂, a triarylphosphine and silver triflate. Although the transformation was successfully achieved with the substrates employed, the *E:Z* ratio of the newly formed olefins were only moderate.^[215] Recently, ruthenium-hydride species, derived from thermally modified Grubbs 2nd generation metathesis catalysts have been developed and successfully applied in the isomerization of terminal olefins.^[221] However, the reactions are commonly accompanied by unwanted side reactions, such as reduction or self-dimerization.^[232, 235] Palladium(II)-hydride complexes are known to be generated *in-situ* by addition of alcohols, which undergo oxidation upon β -H-elimination.^[184, 295] Some peculiarities regarding the metal-hydride formation should be noted. Alcohols bearing no β -H atom, such as methanol or

phenol, are dehydrated (α -H atom) to their corresponding carbonyl derivatives, suggesting that β -elimination of water is not involved, whereas the reaction in *tert*-butanol is likely to proceed via β -H atom- and hydroxyl group-elimination forming a water molecule.^[295] Since the solvent screening revealed the necessity of alcoholic additives for the catalytic cycle to operate and the fact that Pd-assisted proton migration via a π -allyl mechanism is favored in non-polar aprotic media, as shown for PdCl₂(PhCN)₂,^[296] a hydride addition-elimination mechanism seems to be most conceivable for the here investigated catalyst system. The robustness of the catalysts is also in agreement with this mechanism, because π -allyl type based Pd-isomerization reactions usually require purified, anhydrous aprotic solvents^[297-302] and this catalyst system performed very well even in unpurified, non-anhydrous solvents under air. A complete lack of methoxylated and acetylated side products, which may arise from nucleophilic attack of the solvent at the carbon double bond is a further indication for a mechanism involving a hydride addition-elimination mechanism, instead of a π -allylic pathway.^[303, 304]

To get further insight into the reaction mechanism, isotopic labeling studies were performed. Even though both the metal-hydride addition-elimination- and the π -allyl hydride mechanism result in the same product, the two mechanistic pathways can be distinguished by looking at the hydrogen shift of deuterium labeled starting materials upon isomerization and at incorporation of deuterium into the substrates when the reactions are run in deuterated solvents. The π -allyl mediated mechanism initially involves a “*hydride-free*” metal precursor featuring two empty coordination sites. Coordination of the free olefin followed by oxidative addition of the allylic carbon-hydrogen bond would form the π -allyl metal-hydride catalyst, which transfers the hydride to the terminal position by reductive elimination yielding the isomerized alkene. Therefore, a formal [1,3-H] shift within the substrates should be observed for a π -allyl mechanism. If one considers the hydride which originates from the approaching olefin, the active catalyst is thus generated by an *intramolecular* reaction. The metal-hydride mechanism on the other hand involves a distinct metal-hydride complex being initially present before entering the catalytic cycle and can therefore be called *intermolecular*, because hydrides are successively displaced between catalyst and new incoming substrates during catalysis. In this case, the olefin coordinates to form a hydrido π -alkene complex, followed by β -addition, generating a σ -alkyl intermediate (hydropalladation) and finally β -H-elimination furnishes the isomerized olefin. The Markovnikov and *anti*-Markovnikov hydropalladation step across the double bond are both reversible and only Markovnikov addition leads to the isomerized product. This process results in a characteristic [1,2-H] shift when the metal-hydride mechanism is active. Although both reaction pathways proceed along different hydrogen-shifts, only the observation of a [1,2-H] shift is sufficient proof of the hydride

addition-elimination mechanism, because deuterium scrambling between the alkene-hydrogens and subsequent isomerization thereof by a hydride addition-elimination reaction results in a formal [1,3-H] shift as well, and thus preventing distinction. For this investigation α,α - d_2 -allylbenzene was prepared^[282] by Wittig-reaction of d_3 -methyl iodide and phenylethanal. Applying the standard reaction conditions using 1 mol% catalyst **70h** in a 0.9 M solution of deuterium labeled allylbenzene in methanol afforded the isomerized *E*-isomer as the major-product. By constant, careful monitoring of the starting materials, the reaction progress and the products by GC-MS measurements, a characteristic key fragment of the deuterated starting material and the products could be identified (*cf.* Figure 51).

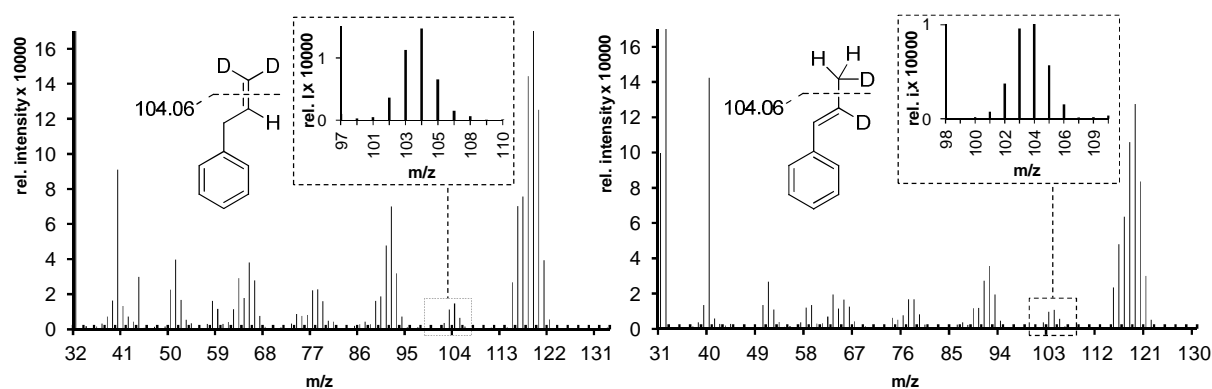


Figure 51 Mass spectra showing the characteristic fragments of α,α - d_2 -allylbenzene (left) and β - d_1 -(*E*)-propenyl benzene (right).

This allowed a clear differentiation, as to whether deuterium incorporation at C-2 took place or not. Even though starting materials and products exhibit the same molecular ion in the higher, and benzyl fragmentation in the lower mass region, the initial fragmentation of α,α - d_2 -allylbenzene generates fragment m/z 104.1 by loss of the d_2 -methylene group whereas m/z 103.1 is expected for the product, regardless of isomer-configuration. This fragment originates from α -methyl cleavage of the terminal methyl group within the product. Contrary to this a m/z 104.1 for the initial fragment of the *E*- and the *Z*-product was detected, which clearly demonstrates deuterium incorporation at the C-2 position of propenyl benzene. It has to be pointed out that during fragmentation of allyl systems in the gas phase, metastable ions induce carbon skeleton rearrangements and hydrogen migrations, which lead to complex mixtures of interconverting structures prior to further decomposition. Consequently, the identification of characteristic fragments and isomer assignment is quite challenging, as shown for the molecular ions of linear octene isomers. However, it has been previously demonstrated that scrambling of terminal hydrogens does not occur over the entire time range.^[305] Furthermore, it is important to check, whether the catalyst employed is capable of *trans*-isomerization. During multiple addition-reaction cycles a constant amount of *cis*-isomer was produced (kinetic distribution). On the account of this, the observed initial fragment (m/z

104.1) of *trans*-propenylbenzene originates from a [1,2-H] shift thus proving that only the hydride addition-elimination mechanism is active (*cf.* Scheme 43). Fragmentation patterns of undeuterated starting material and isolated products were cross validated in methanol and methanol- d_4 . Deuterium scrambling between starting materials and substrates was not observed and at low catalyst loadings in methanol- d_4 , no deuterated *E*-/*Z*-propenylbenzenes arising from initial deuterium transfer from the solvent to the catalyst, were detected.

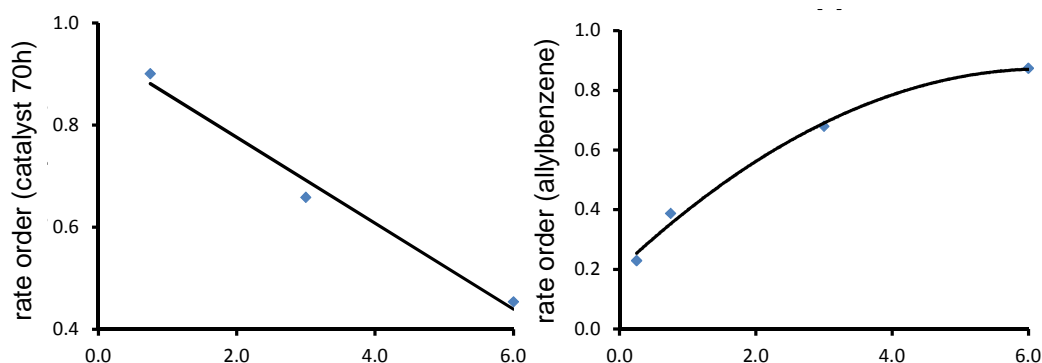


Figure 52 Effect of the concentration of catalyst **70h** (left) and allylbenzene (right) on the rate of isomerization.

Conditions: [sub]₀ 89 mM, resp. [cat]₀ 0.089 mM (1 mol%) in MeOH/toluene mixture (1:2) at room temperature. Reaction rate orders were determined by correlation of catalyst, resp. substrate concentration and product formation over time (not shown).²⁸²

To gain further insight into the catalytic cycle, the kinetics and the reaction-order of the isomerization was investigated using catalyst **70h**. Performing the reactions at catalyst loadings of 0.1 mol%, 0.5 mol% and 1 mol% and correlating catalyst concentration with product formation over time showed a first-order dependence on the initial catalyst concentration (*cf.* Figure 52, left). With constant catalyst loadings of 1 mol% a sub-first-order dependence on the initial (high) substrate concentration of about 0.20 was observed. During reaction progress the sub-first-order dependence on the initial substrate concentration changes and approximates 1.0 at very low substrate concentration, which indicates substrate inhibition (*cf.* Figure 52, right). For the solvent combination methanol/toluene, employing concentrations of 1:2, 1:1 and 1:0, a negative sub-first order dependence of -0.51 was obtained, leading to the following rate expression:

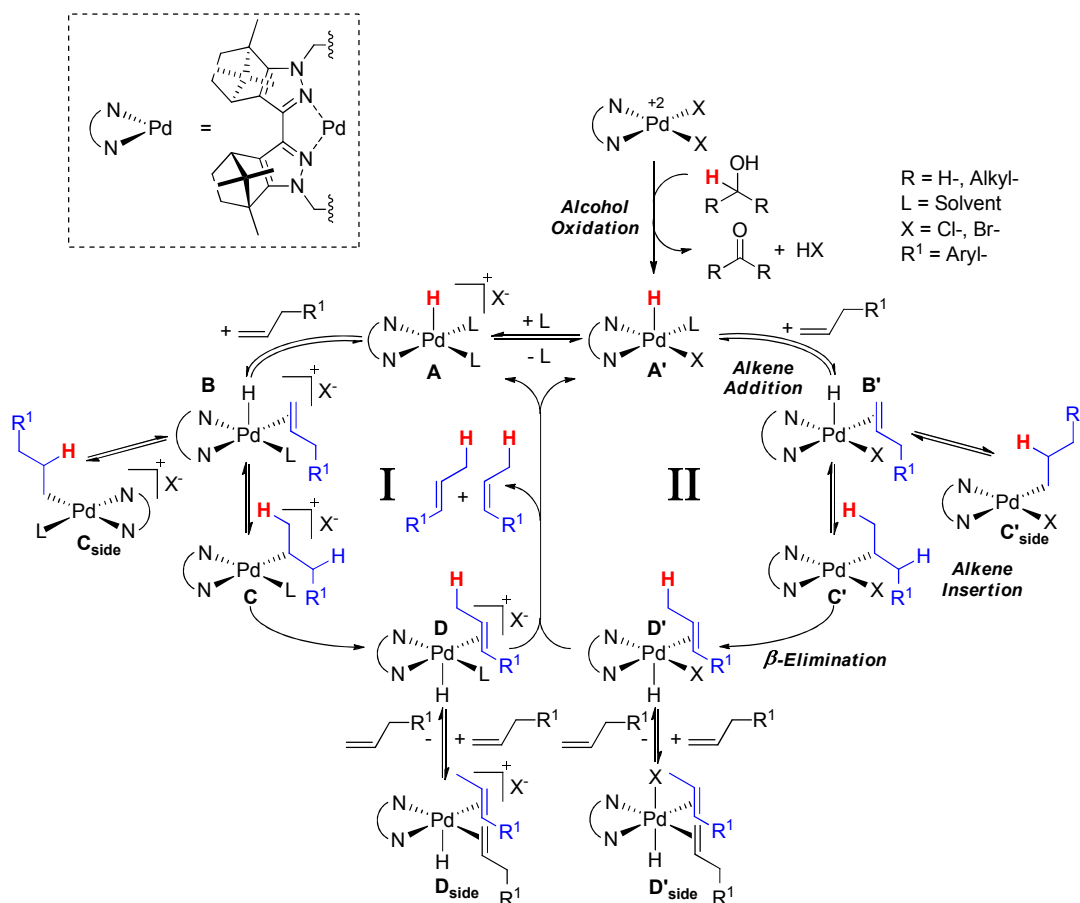
$$rate = k(T) \frac{[Pd]^{1.0} [substrate]^{0.2 \rightarrow 1.0 (t \rightarrow \infty)}}{[MeOH]^{0.51}}$$

The results are indicative of an inhibition effect of the starting materials and methanol at higher concentrations, or at least point towards a decelerating effect. The reaction order on the products was not assigned, but no rate deceleration or inhibiting effects were observed by the external addition of pure *trans*- nor *cis*-propenylbenzene to the reaction. Increased product concentration over time by performing the reaction over multiple substrate addition-reaction cycles had no effect on the conversion rates. The catalyst activity remained constant, thus proving catalyst stability and the inhibitive effect of the starting material (allylbenzene) concentration. No kinetic isotope effect was detected with undeuterated allylbenzene in methanol and methanol- d_4 leading to comparable reaction rates, yields and selectivities. Thus, generation of the metal-hydride complex is not the rate-limiting step, if one assumes that the formation of only small amounts of active hydride-species is insufficient for catalysis. In contrast, using α,α - d_2 -allylbenzene as starting material in methanol and methanol- d_4 resulted in a large kinetic isotope effect. No H/D-exchange was observed between starting materials and solvent at low catalyst loadings suggesting that the isomerization mechanism is an inner sphere interconversion after initial metal-hydride formation.^[295] With catalyst **70h** and allylbenzene or allylanisol the ^1H NMR spectra did not show the presence of any Pd-H species up to -100 ppm, which is usually observed at high-field resonances ($\delta < 0$ ppm). The same was true under substrate inhibition conditions. Indeed, many hydride catalysts are too reactive to be observed by spectroscopic measurements.

Scheme 44 suggests a possible reaction pathway that is in accordance with the spectrometric and kinetic evidence given above. Initially the alcohol present in the reaction media is oxidized and thus generates the active palladium-hydride species **A'**, which then enters the catalytic cycle. Upon oxidation of the alcohol, a vacant coordination site is exposed at the electron-deficient palladium center owing to liberation of HX, which may be occupied by solvent molecules. The hydride then moves to the axial position of the metal complex to furnish a *cis*-coordination-site for the incoming olefin, a necessary prerequisite for the hydropalladation step.

Whereas in **II** the catalytic cycle begins with the entering and coordination of the electron-rich olefin, complex **A'** is thought to be capable of losing its second halide in a reversible process, forming the cationic Pd(II)-hydride complex **A**, which may be stabilized under protic polar conditions.^[183, 306] This intermediate offers a second vacant coordination site for incoming substrates. Considering cycle **I**, olefin-addition to hydrido- π -alkene complex **B** occurs. β -Addition, either in a Markovnikov or *anti*-Markovnikov fashion, results in the hydropalladated σ -alkyl intermediates **C** and **C_{side}**, which are reversible steps and the reason for the [1,2-H] shift as previously described. The M- η^1 -C(β)-intermediate undergoes *syn*- β -hydride elimination and the palladium-hydride species **D** is regenerated, which liberates the

E-, and *Z*-isomers, respectively. Apart from retention of one halide coordinated to the metal center in cycle **II**, both mechanisms are equal and all catalytic species reported run through alternating 18 and 16VE complexes. The transition states for both hydride-transfers involve a *syn*-coplanar arrangement of the two carbon atoms, the metal center and the hydrogen participating and reductive elimination requires coordinative unsaturation of the Pd-complex (16VE, Scheme 44).^[184]



Scheme 44 Proposed mechanism for the isomerization reaction of terminal allylaryls to *E*- and *Z*-propenylaryls in alcoholic media using (bcpz)-type PdCl₂-catalysts.

Although rhodium-^[307, 308] and iridium-dihydride^[309] complexes have been reported for isomerization reactions, a palladium-dihydride species^[310, 311] is improbable under the reaction conditions, since dihydride species are prone to decomposition and capable of hydrogenation reactions, which were not detected. To rule out the presence of Pd(0) species within the catalytic cycle, Pd₂(dba)₃ was tested as precursor, which is not a catalyst under the reaction conditions reported here. Furthermore, the catalyst system was still active after multiple addition-reaction cycles (10×) without any loss of activity, conversion or selectivity. Palladium-black was not formed over prolonged reaction times, even at elevated temperatures (343 K). This was verified by careful monitoring of the reaction progress and fine-filtration of

the solution after each reaction cycle. When bis(acetonitrile)palladium(II) dichloride was employed as catalyst, fast isomerization was also observed under the reaction conditions, but a substantial loss of activity was observed, as early as after seven cycles (53% *E*-Isomer, 90% *d.e.*) and almost no conversions were detected after 21 cycles (11% *E*-Isomer, 88% *d.e.*, *cf. Experimental Section*). Liberation of HX from metal-hydride complex **A** to form a Pd(0) complex can be ruled out, since reductive elimination is likely to occur from a *trans*-configuration, which is not favored for our neutral bidentate *N*-ligand as it is coordinated at the equatorial positions. This together with the chelating properties and the π -back-bonding character of the bipyrazole ligands may account for the observed integrity of the bcpz-alcohol-catalyst system and explain the observed precipitation of palladium black by using bis(acetonitrile)palladium(II) dichloride as catalyst (*trans*-coordinated acetonitrile and chloride). Since no kinetic isotope effect was observed in deuterated solvents the rate-limiting step is thought to be the β -H-elimination reaction and not the initial formation of the metal-hydride complex, nor regeneration thereof. If the sub-first order on substrate and methanol concentration is taken into account, inhibition of the catalytic cycle may take place by trapping of a catalytic species. As found, decomposition to Pd(0) does not occur and therefore cannot account for this observation. Poisoning of the catalyst by impurities within substrates or methanol can also be ruled out, since the catalyst maintained its activity through multiple substrate addition-reaction cycles and with the use of absolute solvents. Reasons for the observed rate-deceleration may either originate from formation of inactive complexes, which would result in removal of catalytic species from the catalytic pool, or be caused by a competitive reaction, because simple saturation in allylaryls would not account for the prolonged reaction times. Deactivation of a certain amount of catalyst is improbable, since the catalyst recovers its previous activity after a certain time. More conceivable, seems to be another reversible pathway, which becomes competitive at higher substrate and methanol concentrations. This may operate by occupation of a secondary vacant coordination site offered by the metal center leading to **D_{side}** (*cf.* Scheme 44, route **I**, bottom). Related mechanisms, involving positively charged complex species due to loss of a secondary halide prior to olefin complexation, were recently proposed by Sigman et al. under Wacker oxidation conditions,^[186] and for the Pd-catalyzed reductive cross-coupling of styrenes in *iso*-propanol, also involving Pd-hydride π -alkene intermediates.^[312] However, ¹H-NOESY, ¹³C- and ¹⁵N-HMBC NMR measurements did not show additional complex species present in solution, giving no evidence for a competitive pathway.

pH-Influence on the Reaction Progress and Role of the Halide

The results show a strong solvent effect on the isomerization, regarding first of all the pK_a and the steric encumbrance as well as electronic effects originating from ligand design. Bearing the envisaged reaction mechanism (route **I**) in mind, the role of the pH value and the halide on the catalyst was investigated. Clearly, a hydride-driven reaction mechanism would be influenced by the external addition of acid and base (*cf.* Figure 53).^[313, 314]

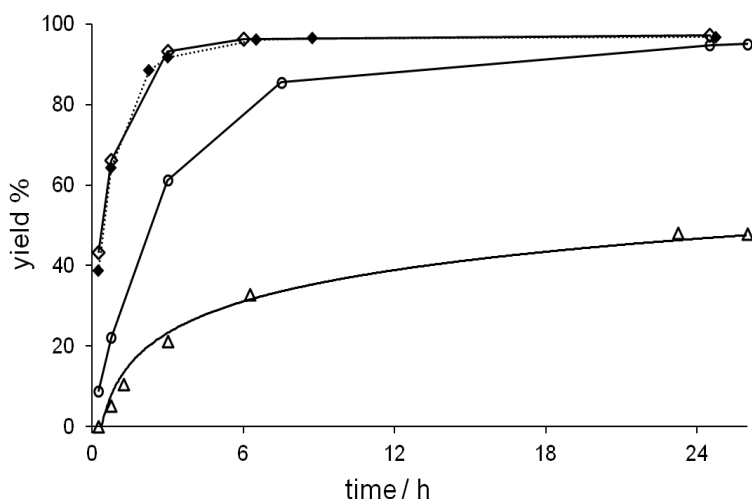


Figure 53 Influence of additives in the isomerization of allylbenzene catalyzed by **70h**. Reaction conditions: 1 mol% catalyst, 10 mol% additive [blank (◆), NaOMe (○), *p*-toluenesulfonic acid (Δ), acetic acid (◇)], allylbenzene (98 mM) in methanol/ toluene (1:2) at r.t. under air. Conversions monitored and product assignment determined by GC and GC-MS.²⁸⁵ Data points represent the mean of two repetitive experiments.

Therefore the standard reaction with 1 mol% **70h**, allylbenzene (89 mM) in a mixture of MeOH/toluene (1:2) at room temperature, combined with 10 mol% of an additive, was performed. As expected, the addition of sodium methanolate significantly slowed down the reaction rate, leading to lower conversions (48% *E*-isomer after 24 h, 93% *d.e.*) and with caesium carbonate no reaction was observed. Pd(II)-diacetate and the corresponding Pd(II)-diacetate of bcpz ligand **70h** did not promote the reaction either, regardless of ligand substitution, owing to the lack of metal-hydride formation. The addition of toluene sulfonic acid monohydrate did not accelerate the reaction and after prolonged reaction times (days) equal conversions as without additive were obtained. Interestingly, the observed reaction progress was almost identical with the results obtained for catalyst loadings between 0.5 mol% and 0.1 mol%. This is indicative of partial catalyst poisoning, which is generally attributed to sulfur containing substances,^[132, 315-317] and may account for no isomerization in *l*-propanethiol (pK_a 13.24) as well. Noteworthy, 10 mol% acetic acid did not have a positive influence on the outcome of the reaction and similar reaction rates, conversions and

selectivities were observed as without additive. This brings to mind the facile, mild and effective catalyst preparation, which occurs without the formation of typical by-products arising from acid-catalyzed dehydration reactions (alkenes, ethers).

For evaluation of the influence of the halide coordinated to the metal center on the isomerization, the dibromide palladium complex of **70h** was prepared and tested under standard conditions (1 mol% catalyst, 89 mM substrate, 2:1 toluene/methanol at room temperature). In order to effectively compare the catalyst performance, less reactive eugenyl acetate was chosen as the model substrate. Only small differences in the yield of *trans*-products were observed (77% for **70h** and 70% for the dibromide complex after 3 h; 92%, resp. 86% after 6 h). Selectivity was not affected, as expected, and finally almost equal conversions were obtained with both catalysts (99% for **70h**, resp. 96% after 24 h). The decreased isomerization rate can be understood in terms of the lower π -donation ability of bromide compared to chloride. Although less pronounced, the effect is in agreement with the results obtained for the iridium-hydride driven isomerization of allylbenzene, whereby higher reaction rates were observed by stabilization of unsaturation at the metal center originating from more effective π -donation of the halide in the order: I < Br < Cl < OH < F.^[309] Even further increased isomerization rates may therefore be realized with this novel catalyst system by fluoride substitution, an aspect that is still underestimated as a tunable parameter.

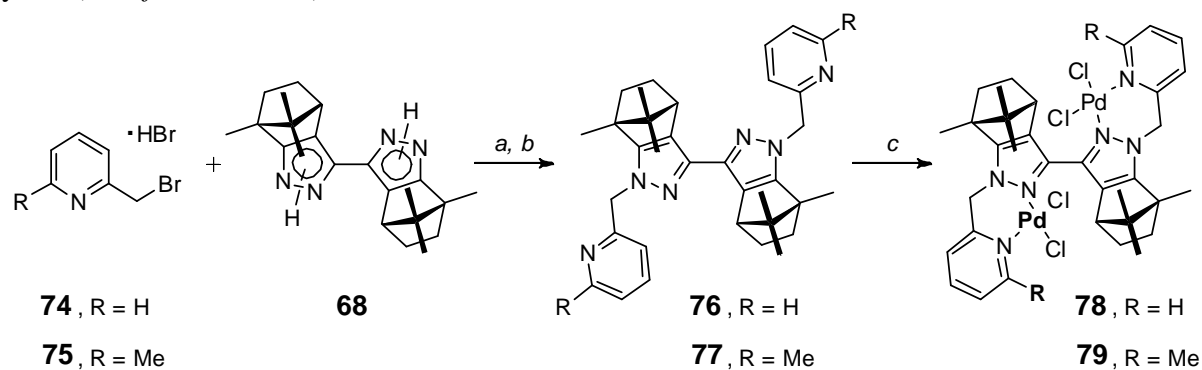
2.3.2.4 2nd-Generation (Tetradentate) Camphorbipyrazole Ligands and Their Palladium Complexes

The modular synthetic approach of the bcpz-ligand allowed further modifications on the flanking substituents and an extension of the coordination number to four was envisaged. Pyridine was found to be an ideal substituent for varying the coordination number plus changing the electronic properties. The (pyridine-2-ylmethyl)pyrazole structure represents an ambiguous, bidentate ligand pattern featuring a pyrazolyl (π -donor) and a pyridyl (π -acceptor)^[251] subunit for metal coordination. Complexes of palladium(II/ 0),^[318-323] platinum(II),^[324] ruthenium(II),^[247, 325-327] nickel(II)^[328, 329] and copper(II/ I)^[329, 330] are known for related pyrazole-pyridine motifs. Nickel(II)^[328] and palladium(II)^[318, 321, 323] complexes are reported to be active catalysts for ethylene oligo- and polymerization reactions. Successive metal alkylation-dehalogenation steps are necessary for activation of the catalyst, which is either employed in a preactivated form (as methylchloride complex, e.g.)^[318] followed by *in situ* dehalogenation (with silver(I) triflate, e.g.) or a dihalide complex combined with methylaluminoxane (MAO)^[321] or ethylaluminium dichloride^[328] for direct *in situ* activation can be used. However, cationic Pd(II)- η^3 -allyl complexes of (pyrazol-1-ylmethyl)pyridine

were also reported to be active catalysts in asymmetric allylic alkylations of arylated acetoxypropanes with dimethylmalonate (25 – 84% *e.e.*).^[320]

Preparation of Tetradentate 3,3'-bicamphorpyrazole Ligands and Pd-Complex Formation

The 3,3'-bicamphorpyrazole core was prepared following the standard procedure (*cf.* Chapter 2.2.3.1). For introduction of pyridine-2-ylmethyl wingtips under basic conditions the 2-(bromomethyl)pyridine (**74**) and 2-(bromomethyl)-6-methyl-pyridine (**75**) hydrobromide salts were first converted to the free bromopyridines with triethylamine over a period of 18 h and added to the sodium 3,3'-bipyrazolate. The pyridine and 6-methylpyridine derived bcpz ligands were obtained in moderate yields between 43 – 89% for **76** and 48 – 70% for **77**, depending on the reaction scale. In the solid state both ligands exhibit a C_2 -symmetric *transoid* structure (not shown) with respect to the pyrazole nitrogens similar to the structures observed for bcpz-ligands **69d** – **69k** (*cf.* Chapter 2.3.2.1). The bihomometallic palladium(II) dichloride complexes of both ligands were prepared by ligand exchange reaction with bis(acetonitrile)palladium(II) dichloride and were obtained in 97% (**78**), respectively 94% yield (**79**, *cf.* Scheme 45).

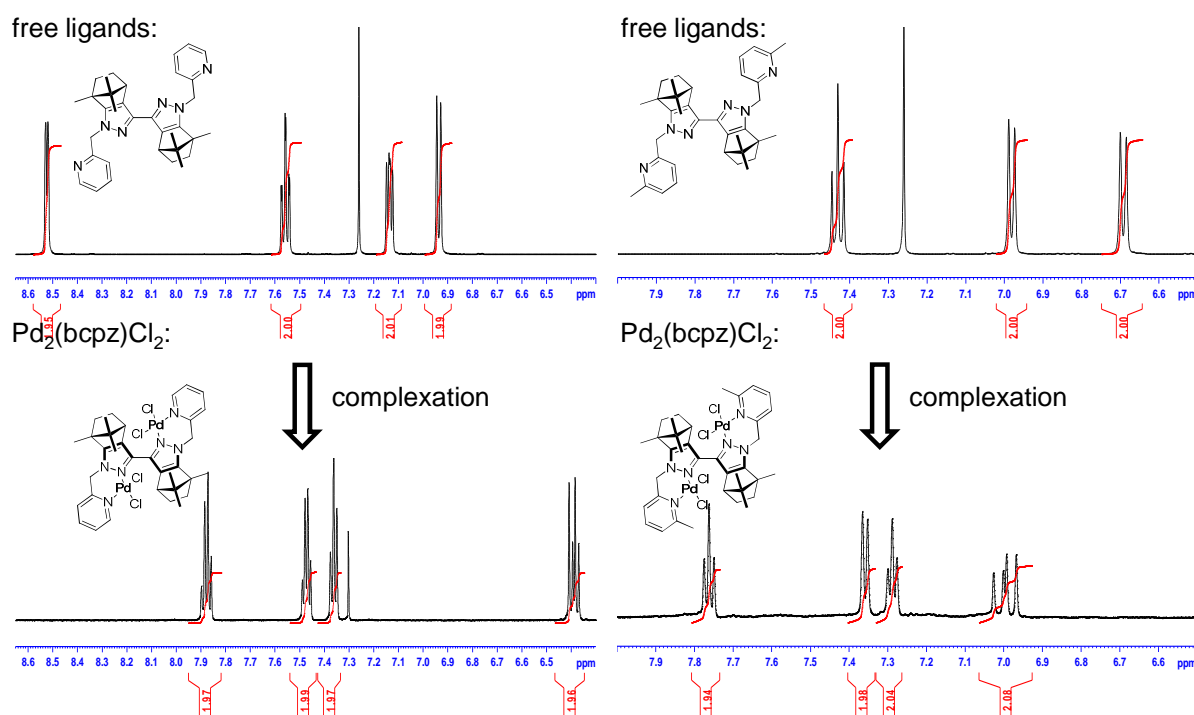


Scheme 45 Synthesis of tetradentate 3,3'-bicamphorpyrazole ligands **76**, **77** and their palladium complexes **78** and **79**.

Reaction conditions. a) **74** or **75**, NEt₃, THF, molecular sieve 3Å, slow stirring, r.t., 18 h. b) **68**, NaH, THF, 65°C, 2h then addition of free bromomethylpyridines at r.t., 1 h, then 65°C for 5h, then r.t., 12 h, 89% for **76** (70% for **77**). c) Pd(MeCN)₂Cl₂, DCM, r.t., 24 h, 97% for **78** (94% for **79**).

The free ligands show a characteristic doublet for the protons at the wingtip methylene group with germinal couplings of $^2J_{CH}$ of 16.7 Hz for both ligands indicative for a decrease in rotational freedom of the flanking substituents in the liquid state (diastereotopic protons). Complexation with Pd(II) results in a distinct pattern and an upfield shift of the methylene signals from 5.52 – 5.43 ppm to 5.28 – 5.38 ppm. A more complex signal pattern is observed

after complexation due to formation of two atropisomers (*cf.* Scheme 46). The proton signal attached to C1 of the pyridine substructure proved to be an excellent indicator for



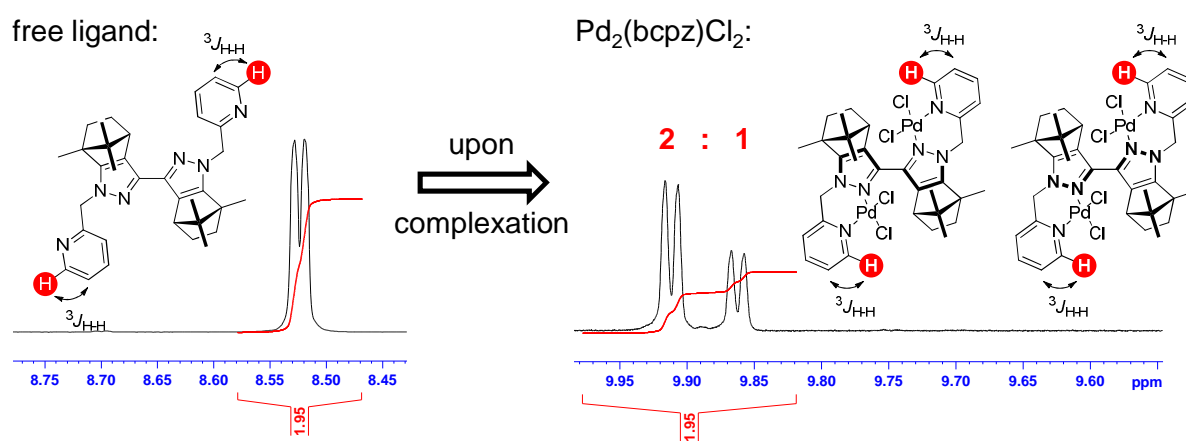
Scheme 46 Observed proton shifts in the aromatic region upon complexation with Pd.

¹H NMR proton shifts in the aromatic region of ligands (in CDCl₃) and Pd complexes (in CD₂Cl₂) recorded at room temperature.

determination of the atropisomeric ratio. By bisecting both 3,3-camphorbipyrazole atropisomers into their (pyridine-2-ylmethyl)pyrazole substructures overall two sets of resonance shifts are expected. Therefore, the observed signal intensities of the pyridine protons of 1.0 : 2.0 account for one atropisomer being favored under the reaction conditions, which was attributed to the bulkiness of the camphor backbone (*cf.* Scheme 47). No significant change in distribution was observed during and after product isolation of reaction at -80 °C to room temperature nor at 96 °C in boiling acetonitrile and account for the formation of stable atropisomers.

For determination of the atropisomeric ratio of the C1-methylated bihomometallic palladium(II) complex mixture, the neighboring proton signals, splitted into two independent doublets at 7.0 ppm and 6.9 ppm, was selected. Due to partial overlap of the signals a intensity ratio of approximately 1.0 : 1.2 was found indicating an almost similar distribution of atropisomers and might be caused by the installation of an additional methyl group at the pyridine substituent. The molecular structures of both complexes were determined by X-ray crystallographic analysis. Crystals of **78** were obtained by slow diffusion of hexane into a saturated diethyl ether/ dichloromethane solution (1:1) of **78**. Unexpectedly, with the sterical

less demanding pyridine substituted in palladium complex **78** a conformation, related to the *cisoid* structure of the monometallic Pd(bcpz) complexes **70e** – **70j** with a N-C-C-N torsion angle of 51.6 for atropisomer **78A** (38.1° for **78B**) was found. Note, that in the free complex of the sterical more demanding 6-methylpyridine ligand a quasiplanar *transoid* structure with



Scheme 47 Determination of the atropisomeric ratio of Pd complex **78**.

¹H NMR proton shifts of ligand **76** recorded in chloroform-*d*₃ and Pd complex **78** in dichloromethane-*d*₂ at r.t. Splitting into a set of two independent signals shown for the selected pyridine proton (highlighted in red).

a N2-C3-C3'- N2' torsion angle of 176.7° is realized. The methylene linker of the (pyridine-2-ylmethyl)pyrazole structure is distorted and adopts a boat-conformation to furnish a quadratic planar coordination sphere of palladium ($N_{\text{pyrazole}}\text{-CH}_2\text{-C}_{\text{Ar}} = 111.2^\circ$ and 112.6° for **78A**, 110.0° and 113.0° for **78B**). Both complex-substructures are in plane to each other with the chloride substituents and *N*-substituents being staggered and a Pd-Pd distance of 340.6 pm in **78A** and 331.3 pm in **78B** (*cf.* Figure 54). Single crystals suitable for X-ray analysis of the sterical more demanding bihomometallic palladium(II) 6-methylpyridine derived complex **79** were obtained by slow evaporation of a saturated chloroform solution. Interestingly and contrary to **78**, the solid state of **79** revealed a *transoid* structure. Moreover, only one atropisomer proved to be present in the crystal, which accounts for a stereoselective crystallization of one atropisomer, which is a fundamental prerequisite for any application of the complexes for asymmetric catalysis. In the *transoid* structure both metal centers are coordinated quadratic planar with the (pyridine-2-ylmethyl)pyrazole adopting a boat configuration ($N_{\text{pyrazole}}\text{-CH}_2\text{-C}_{\text{Ar}} = 111.2^\circ$ and 110.2° , Figure 55). Preliminary tests on the activity of both complexes for ethylene polymerization with MAO revealed less reactivity and only small amounts of products were obtained. However, these results might be in accordance to the sterical demand of the complexes as illustrated by the solid state structures. Nevertheless, the first results regarding selective crystallization from the atropisomeric mixture of **78** as well as the approach of combining chirality and atropisomerism within one chiral ligand pattern are promising (*cf.* Figure 56). The possibility of introducing different

metals to generate bihomometallic complexes, the preparation of heterobimetallic complexes (with cooperative metal-metal centers) or incorporation of preactivated complexes, like palladium allylic species is expected to be particularly useful for (asymmetric) catalytic transformations.

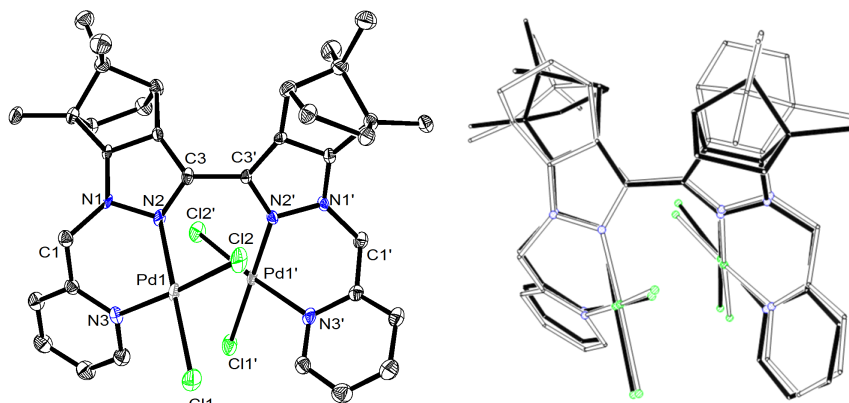


Figure 54 Solid state structure and overlay structure of atropisomeric palladium complexes **78A** (left) and **78B** (shown in overlay as unfilled structure).

Thermal ellipsoids are plotted at 50% probability level and hydrogen atoms are omitted for clarity. Selected bond lengths for **78A**: Pd1–N2 202.8(14) pm, Pd1'–N2' 197.4(14) pm, Pd1–N3 208.0(14) pm, Pd1–N3' 208.3(14) pm, Pd1–C11 227.6(5) pm, Pd1'–C11' 228.1(5) pm, Pd1–C12 228.1(5) pm, Pd1'–C12' 227.1(4) pm, N1–N2 139.9(8) pm, N1'–N2' 137.0(9) pm, N2–C3 130.0(2) pm, N2'–C3' 138.0(2) pm, C3–C3' 150.0(2) pm.

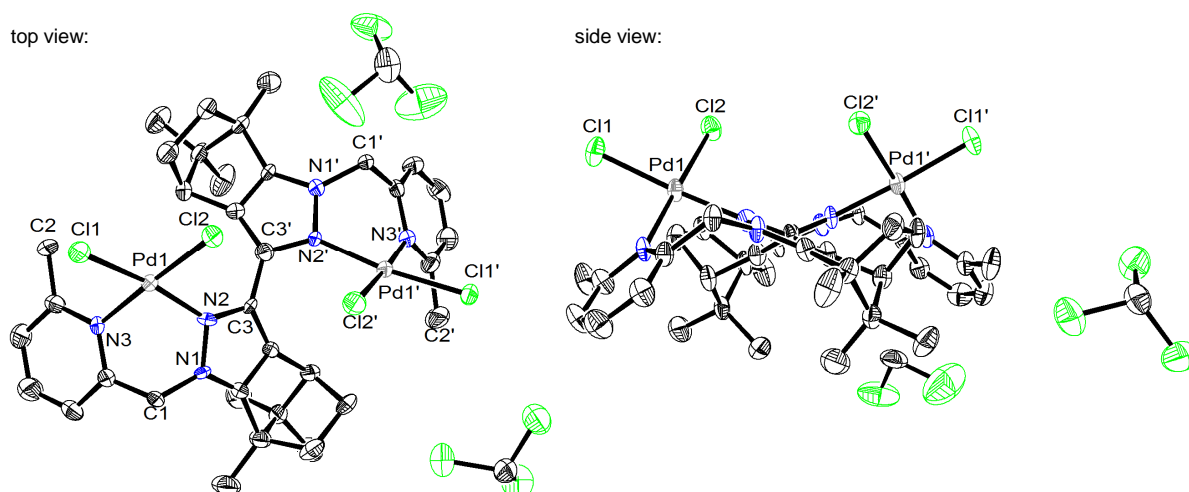


Figure 55 Solid state structure of palladium complex **79** after selective crystallization.

Thermal ellipsoids are plotted at 50% probability level and hydrogen atoms are omitted for clarity. Selected bond lengths for **79**: Pd1–N2 201.8(5) pm, Pd1'–N2' 202.8(6) pm, Pd1–N3 207.1(6) pm, Pd1–N3' 205.9(6) pm, Pd1–C11 229.0(17) pm, Pd1'–C11' 228.7(18) pm, Pd1–C12 228.8(18) pm, Pd1'–C12' 228.1(19) pm, N1–N2 137.2(8) pm, N1'–N2' 136.8(7) pm, N2–C3 135.1(8) pm, N2'–C3' 136.1(9) pm, C3–C3' 146.9(10) pm.

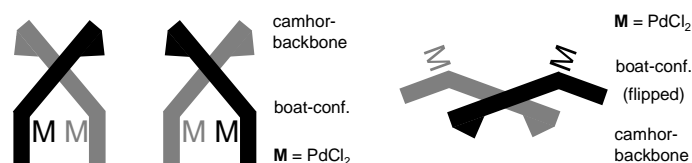


Figure 56 Schematic representation of the conformations in **78A**, **78B** and **79**.

2.4 Conclusion

In summary, a novel class (bcpz) of a sterically bulky ligand system was described, which features a rigid, bulky backbone, while still maintaining flexibility and diversity through different substitution patterns (wingtips), thus allowing electronic and steric tuning of the ligands. Since redox potentials of transition metal complexes are strongly influenced by steric effects, which may be enforced by the ligand backbone, the constant ligand sphere combined with variable and tunable substituents and the smaller cavity of 3,3'-bipyrazoles compared to the widely used 2,2'-bipyridines may help developing new catalysts. The ligands are accessible in a three step procedure by condensation with diethyl oxalate followed by tandem condensation with hydrazine hydrate and finally by aryl- or alkylation exclusively at the *N*-1,1'-pyrazole positions. X-ray crystallographic analysis of the synthesized camphortetraketone precursors revealed an unprecedented 7-membered proto-chelate tetraketone structure and combined with the proposed (and within this study validated) mixture of isomeric structures their dynamic behavior was studied giving evidence for a new proto-chelate type, keto-enol tautomerism. The chiral dirhodium(I) and diiridium(I)-tetraketone complexes were prepared, the structure unequivocally determined by X-ray crystallographic analysis (Rh-complex) showing the selective formation of the 6-membered-metal chelate structure and preliminary experiments using the chiral dirhodium(I) complex in on-column gas hydrogenation chromatography of olefins was addressed.

By condensation of camphortetraketone with hydrazine hydrate and selective *N*-1,1'-pyrazole wingtip substitution overall eleven new ligands with different electronic properties were obtained. The corresponding Cu(II)-, Co(II)- and a series of Pd(II) complexes were prepared and their conformational behavior was studied with regard to substitution in the solid, as well as in solution state using X-ray, CD- and VT proton NMR analyses. These complexes of **70h** represent the first examples of d^8 (Pd) and d^9 (Cu) 3,3'-bipyrazole complexes coordinating through κ^2 . Initial catalytic investigations revealed that these palladium complexes showed higher activities with increasing electron donating properties induced by appropriate wingtip substitution ($-\text{CH}_2\text{R}$: Mes > *p*-^tBuBn >> 3,5-(CF₃)₂Bn) in the copper-free Wacker oxidation of terminal alkenes.

In the second part of this chapter a detailed experimental investigation into the activity of these novel backbone-fused bipyrazole (bcpz) derived palladium catalysts, which are highly effective in the selective isomerization of arylpropenoids in alcoholic media was presented. Catalyst screening revealed that the donor-capability of the wingtip substituents of the bidentate ligand has a strong influence on the activity. Catalyst integrity, a prerequisite for any application in homogeneous catalysis, was shown to be maintained, even at elevated

temperatures (363 K) and over multiple addition-reaction cycles, with neither loss of activity nor degradation or decomposition to metallic palladium. Deuterium labeled mechanistic investigations revealed the formation of palladium-hydride species under the reaction conditions, as evidenced by a characteristic [1,2-D] shift detected by MS fragmentation experiments, and indicated that these species are the active catalysts. Taking the observed reaction orders into account, a catalytic cycle, which proceeds via a metal-hydride addition-elimination mechanism, is proposed ($\kappa_{\text{obs}}[\text{cat.}] \approx 1$ (0.94), $\kappa_{\text{obs}}[\text{substrate}] = 0.27$ and $\kappa_{\text{obs}}[\text{MeOH}] = -0.51$, for allylbenzene isomerization). Solvent screening revealed that the pK_{a} has a strong influence on the reaction rate. The impact of acid and base additives was also addressed. The absence of side-reactions, such as reduction or dimerizations and no precipitation of palladium-metal, compared to reported catalyst systems employing acids or metal-hydrides as co-reactants, highlights the mildness and effectiveness of the catalyst system, which operates in various alcoholic media at low catalyst loadings of 1 mol%. The investigation also show how the bcpz class of ligands can be used for catalyst design. The effect of substitution pattern, combined with substrate and solvent screening, and a discussion of electronic and steric factors, as well a solvent polarity, pK_{a} -value, the coordinated halide and additives, provide valuable information for future developments and improvements of related catalytic systems.

Finally, the 3,3-bipyrazole ligand pattern was extended to furnish two novel tetradentate ligands featuring either pyridine or methylpyridine as flanking substituents. Coordination to palladium(II) yielded the corresponding bihomometallic complexes. For both ligands two atropisomeric complexes were obtained, their distribution was determined and studied using VT proton NMR and their solid state structures were unequivocally determined using X-ray crystallographic analysis. The structures revealed a highly crowded system sensitive to methyl substitution at the pyridine (evidence by structural change: *cisoid* \rightarrow *transoid* conformation) and selective crystallization of one atropisomer was achieved.

At this point the general features of the new, optional chiral bcpz ligand class are briefly outlined:

- They exhibit a modular ligand pattern, which can be easily modified by wingtip substitution providing catalysts with different electronic and steric (e.g. alkyl vs. aryl substitution) properties, together with *cis*-coordination.^[217]
- The central coordination cavity and ligand pattern of the 3,3'-bipyrazole core structure is maintained, avoiding direct interference between ligand shape and catalyst performance.^[224]

- The *N,N*-bidentate ligand pattern exhibits good thermal stability and integrity up to 363 K compared to ordinary *N*-monodentate ligands (e.g. simple nitrile coordination).
- The bulkiness of the ligand (backbone and wingtips) is able to suppress single-side *N*-decoordination and out-of-plane rotation of the ligand, as well as avoiding any catalyst dimerization processes, whether as the catalytically active species or as causing the catalyst termination step.^[217, 295]
- Flexible wingtip substituents and extended backbone facilitate excellent solubility in most solvents including ethers, alcohols, nitriles, ketones and hydrocarbons (e.g. compared to 2,2'-bipyridines).
- The high electron donor capability and π -excessive nature of 3,3'-bipyrazoles, combined with a straightforward, high yielding preparation of catalysts and facile ligand synthesis provides an entirely new approach.

Therefore, it can be envisaged that the short and high yielding synthetic protocol, combined with the versatility of the system, allowing a systematic screening of steric as well as electronic effects, will give rise to a number of new types of fused and even optional chiral 3,3'-bipyrazoles in the near future.

Chapter 3

Chiral, *N*-heterocyclic Carbene (NHC) Pincer

Ligands using Camphoric Acid

as Chiral Building Block

3.1 Introduction – *N*-heterocyclic Carbene (NHC) Pincer Ligands

N-heterocyclic carbene (NHC) ligands have been studied extensively during the last decades and are still of considerable interest due to their unique electronic properties and the ability to form shell-shaped ligands by appropriate *N*-substituents, which renders them useful alternatives to tertiary phosphine ligands.^[230, 306] Their metal complexes are generally air and moisture stable and they can be employed as catalysts for a variety of coupling reactions.^[304, 331] With a second ancillary NHC ligand present in the complex thermal stability and reactivity of the catalysts, as observed under classical Suzuki-Miyaura and Mizoroki-Heck coupling reactions.^[332-337] More recently, NHC-pincer complexes have attracted much attention, as it was found that steric hindrance is an important factor for chemo- and stereoselectivity.^[338] In particular, throughout higher reactivities were observed for the palladium(II)-catalyzed hydroarylation of alkynes using pincer catalyst **83**, for instance.^[338] The authors stated, that increased steric demand aids the reductive elimination step during catalysis and complexes of higher steric encumbrance may allow the synthesis and stabilization of low coordination complexes to facilitate oxidative addition. However, the preparation of defined, pincer-chelate complexes proved to be more challenging than anticipated during the last years. Besides the change of substituents the structure of the C_{NHC}-C_{NHC} bridge has a pronounced influence on the complex formation, either leading to the desired pincer complexes, dimeric structures, 2:1 (metal/ ligand) complexes or to no complex formation at all. The formation of kinetically stable di- or multinuclear complexes in which the ligand itself behaves solely as the C_{NHC}-C_{NHC} bridge is a common phenomenon. Figure 57 represents state-of-the-art Pd-pincer complexes, in which the NHCs can be bridged via one methylene group (**80**) for Pd^[338] or higher homologues, like a butylene linker, as shown for the corresponding Rh-complexes.^[339-341] Introduction of a 1,3-benzyl bridge (**81**) or 2,6-dimethylpyridine (**82**)^[342] is also possible. Imidazolannulation,^[332] in particular a change to more electron donating benzimidazole was found to be beneficial for catalyst integrity and reactivity, as observed for the palladium(II)-catalyzed hydroarylation of alkynes (**83**).^[338] The C3-bridged palladium(II) dibenzimidazole complex (**84**) was also reported.^[343] Most recently, chiral Pd-chelating pincer NHCs (**85**) featuring an optically active binaphthyl-2,2'-diamine (BINAM) bridge and their use in asymmetric catalysis is emerging.^[344-346] However, the choice of the chiral bridge motif has significant impact on complex formation and will determine whether a certain geometry is feasible or not. In case of 1,2-diaminocyclohexane (DACH) only the dimeric complex was observed, since both benzimidazoles are positioned *trans* to each other making the formation of a monometallic pincer complex impossible (*cf.* Figure 57).^[347]

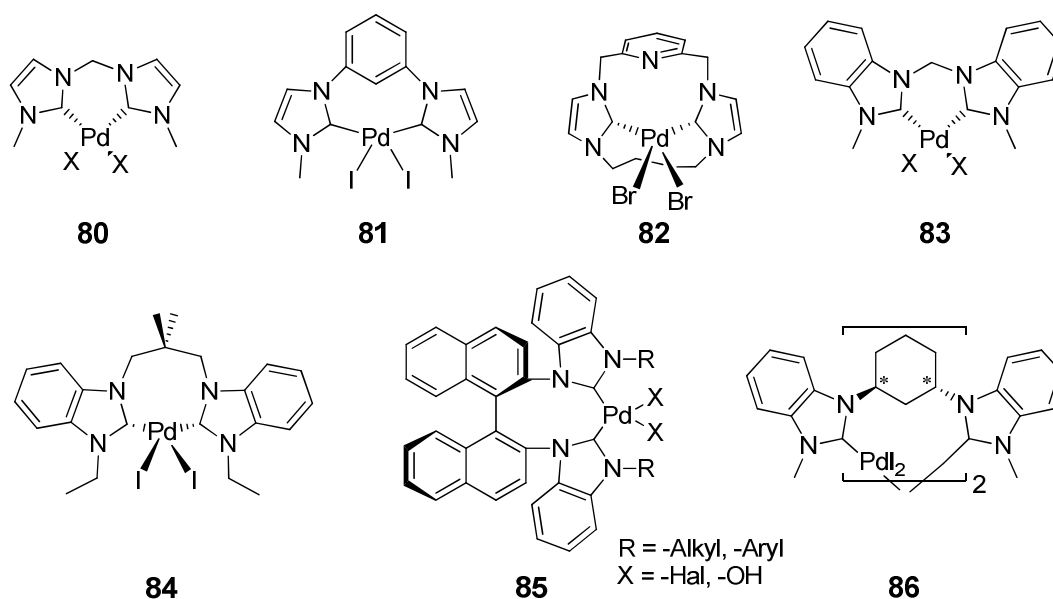


Figure 57 State-of-the-art pincer complexes of Pd deployed in homogeneous catalysis.

In short terms, sterically demanding (regarding substituents and backbone) benzimidazole based dicarbenes with short bridge lengths seem to be favorable for the preparation of effective palladium(II)-NHC catalysts. Furthermore an introduction of chirality by appropriate choice of substituents and a chiral bridge is most promising.

3.2 Objectives

The third section of this thesis is intended to demonstrate the versatility of camphor, in particular by using (1*R*, 3*S*)-camphoric acid as a chiral-building block. The synthesis of a chiral, camphor derived NHC pincer ligand pattern for incorporation of different metals and investigations in asymmetric catalysis is aimed. Reconsidering the results in homogeneous catalysis of modern palladium-pincer complexes (*cf.* Chapter 3.1) the use of a camphor pattern as the chiral C_{NHC}-C_{NHC} bridge was reasonable (*cf.* Figure 58).

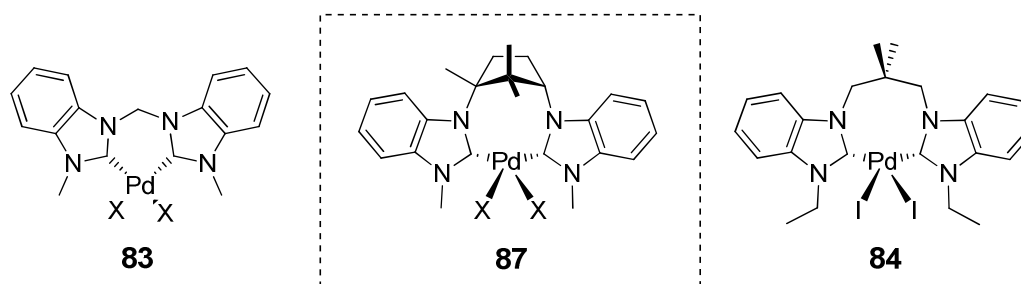
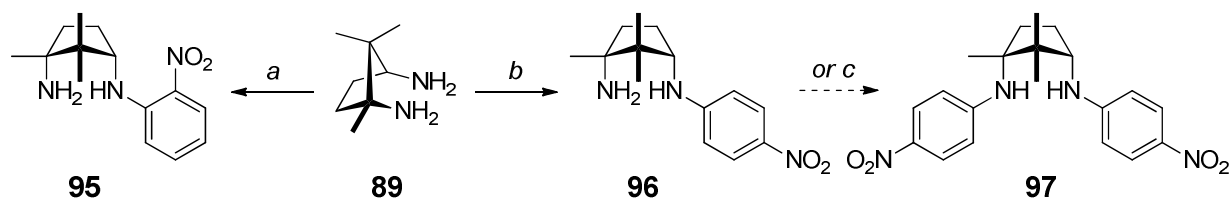


Figure 58 Target, chiral pincer NHC Pd(II)-complex **87** in structural relationship to complexes **83** and **84**.

analytically pure diamine building block in 94% yield (literature 57%).^[350] The obtained diamine, stable for month at -20 °C under argon, was subjected to arylation reaction with 1-fluoro-2-nitrobenzene. It was found that only harsh conditions furnish double aminoarylation to **90** at both nitrogen atoms of *R,S*-tmcp (**89**). Therefore, fresh powdered potassium carbonate and reactants suspended in anhydrous dimethyl sulfoxide were vigorously stirred in a small vessel at 110 °C for 4 days (yield 38 – 72% depending on the reaction scale). The corresponding *para*-nitrobenzene derivative **97**, obtained from *R,S*-tmcp (**89**) and 1-fluoro-4-nitrobenzene was also prepared, but in this case caesium carbonate proved to be more effective and improved the yield of **97** from 19% to 79%. Interestingly, both reactions were found to yield the mono arylated compounds **95** and **96** initially during the reaction progress or by employing insufficient reactant (1 equiv. fluoronitrobenzene) and the mono aminoarylated compound is formed selectively and in high yields (92% for **95** and 78% for **96**, *cf.* Scheme 49).



Scheme 49 Regioselective aminoarylation of *R,S*-tmcp (**89**).

Reaction conditions: a) 1-fluoro-2-nitrobenzene, K₂CO₃, DMSO, r.t., 30 min then 90 °C, 4 h then 110 °C, 2 d, 92%. b) 1-fluoro-4-nitrobenzene, K₂CO₃, DMSO, r.t., 30 min then 90 °C, 4 h then 110 °C, 2 d, 78%. c) 1-fluoro-4-nitrobenzene, K₂CO₃, DMSO, r.t., 30 min then 90 °C, 4 h then 110 °C, 4 d, 19% (79% by using Cs₂CO₃).

The crystal structure of the mono aminoarylated *para*-nitrobenzene derivative **96** is displayed in Figure 59 and validates the regioselective monoarylation at the sterically less hindered nitrogen atom at C1 under the here reported experimental conditions. The solid state structure revealed a straightened up motif (envelope conformation) related to the conformation of the camphor bicycle with a pronounced hydrogen bonding between both nitrogen atoms. Noteworthy, the envelop points upwards (not in plane with the *N*-substituents) resulting in a positive out of plane distortion of 39.0° to be capable of hydrogen bonding. In analogy to the reported NHC derived from *R,S*-tmcp,^[348] in which the C1 building block was successfully introduced fusing both nitrogens to a 7-membered carbene, the crystal structure of **95** (Figure 59) shows that the *cyclo*-pentene-structure is easily tightened up even by attracting forces forming a N1H1-NO₂ hydrogen bond pattern deviating 6.7° from planarity (hydrogen bonding length, H1-NO₂ = 234.4 pm). Noteworthy, isolation and crystallization of a side product revealed that even incorporation of carbon monoxide into *R,S*-tmcp (**89**) to form a 7-membered bornylurea derivative is possible under the reaction conditions (*cf.* Figure 59). The

results are important indicators for bringing both benzimidazole units together in the final palladium complex.

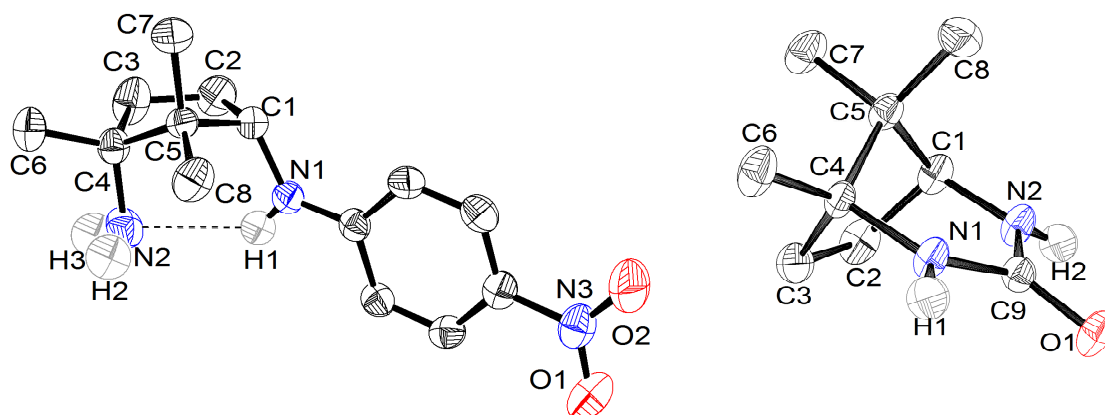


Figure 59 Molecular structures of regioselective, monoaminoarylated *R,S*-tmcp to **96** and incorporation of carbon monoxide to *R,S*-tmcp derived bornylurea derivative **97**.

Hydrogen bond indicated (dashed bond). Thermal ellipsoids are plotted at 50% probability level and hydrogen atoms are omitted for clarity, except for NH protons. Selected bond lengths for **96** (left): N2–C4 147.7(3) pm, C1–N1 145.4(3) pm, C4–C5 155.4(3) pm, C5–C1 155.6(3) pm, N2–H1 234.4(9) pm. Selected bond lengths for **97** (right): N1–C9 135.9(4) pm, N2–C9 135.1(3) pm, N1–H1 88.0(3) pm, N2–H2 85.0(3) pm, C9–O1 125.1(2) pm, C4–C5 154.8(4) pm, C5–C1 154.0(4) pm.

The regioselective monoarylation of *R,S*-tmcp is of particular interest, since the selective transformation of the diamine allows someone to enhance the chiral motif by introduction of a nitroaryl group first, followed by successive transformations at the C2 amino group to secondary diamines, which may be useful for the preparation of unsymmetrical NHCs as well. In contrast, the *ortho*-dinitrocompound **90** showed a more stretched structure in the solid state, regarding the central bornyl moiety. This can be explained by effective hydrogen bonding between the secondary amine and the adjacent *ortho*-nitro functionalities (bond lengths, H1-

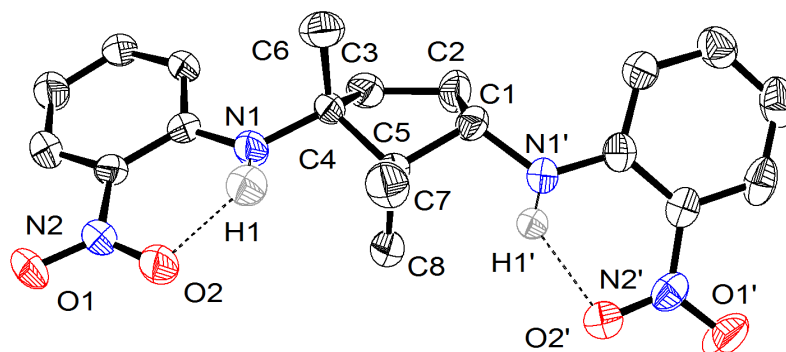
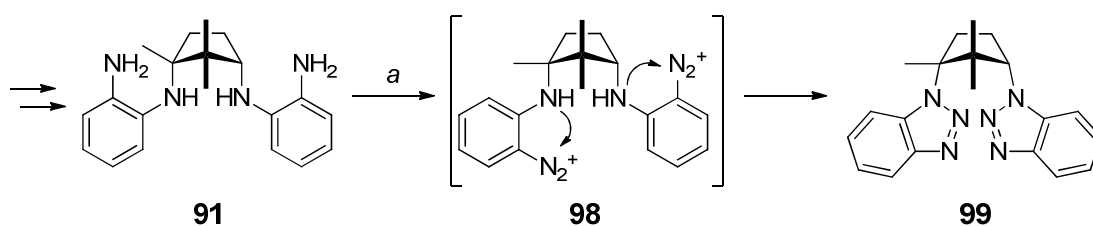


Figure 60 X-Ray crystallographic structure of diaminoarylated *R,S*-tmcp **90**.

Hydrogen bonds indicated (dashed bonds). Thermal ellipsoids are plotted at 50% probability level and hydrogen atoms are omitted for clarity, except for NH protons. Selected bond lengths for **90**: N1–C4 146.4(5) pm, C1–N1' 145.4(5) pm, N1–H1 87.0(5) pm, N1'–H1' 82.0(4) pm, C4–C5 155.0(6) pm, C5–C1 155.0(6) pm

O2 = 194.7 pm and H1'-O2' = 199.3 pm, *cf.* Figure 60). Instead of a positive out of plane distortion of the dimethyl *cyclo*-pentane bridgehead (envelope conformation), present in the solid states structures of **96** and **97** (Figure 59), a negative distortion of -39.9° is observed, resulting in a more planarized structure with an increased distance of 484.8 pm between the adjacent bornyl nitrogens (compared to 289.0 pm in **96**, caused by effective hydrogen-bonding, *cf.* Figure 59 and Figure 60).

By following the synthetic pathway, the dinitro compound **90** was reduced with molecular hydrogen on Pd/C in anhydrous methanol to yield the free tetramine **91** in 97% yield. This compound proved to be instable and was readily oxidized in minutes upon isolation. However, for sake of completeness and to validate the structure a complete characterization was carried out with small samples freshly prepared. Contrarily, small amounts of the compound are stable over hours in solution under argon and therefore synthesis was continued using the purified solution of tetramine **91**. However, the corresponding reduced *para*-aniline derivative of **97** proved to be too instable for isolation and characterization and decomposition was already observed under the experimental conditions and thus further investigation on this particular compound was abandoned. However, at this point two different approaches towards a chiral, pincer NHC were pursued. The successful preparation of the tetramine compound **91** allowed the incorporation of a C1 or N1 building block. *Tert*-butyl nitrite in degassed tetrahydrofuran at 40 °C over four days furnished the chiral dibenzotriazole **99** as orange, needle-shaped crystals (60%). By combination of *tert*-butyl nitrite and aqueous hypophosphorous acid in degassed tetrahydrofuran the reaction was completed within 16 h and **99** isolated in 74% yield.^[351-353] A two-step mechanism is proposed involving initial didiazonium salt formation followed by intramolecular tandem electrophilic substitution by the secondary amine (*cf.* Scheme 50).



Scheme 50 Proposed mechanism for the formation of chiral, dibenzotriazole **99**.

Reaction conditions: a) *t*-BuONO, H₃PO₂, degassed THF, 40 °C, 16 h, 74% (60% without H₃PO₂).

After preparation of the camphor-derived dibenzotriazole **99**, C1 incorporation to furnish the desired chiral pincer NHC was aimed. Under classical acid catalyzed conditions employing triethyl orthoformate and catalytic amounts of formic acid, condensation to dibenzimidazole was achieved at reflux heating and the product was isolated as an off white powder in 49%

yield. Methylation of the imidazole was carried out in anhydrous acetonitrile using methyl iodide. One hour at reflux heating was sufficient for complete conversion and the target chiral pincer NHC ligand was obtained as the diiodide salt **93** in 93% yield. As the choice of counter ions may be a crucial factor for the formation of a the pincer complex the corresponding ditriflate salt **94** of the target ligand was prepared as well. Methylation with trifluoromethanesulfonate was achieved after three hours at room temperature and the ditriflate **94** was obtained in 89% yield as a white, hygroscopic salt and was therefore stored at -20 °C under argon (*cf.* Scheme 48). The use of *Meerwein's* reagent (trietyloxonium tetrafluoroborate) is not recommended for preparation of the ditetrafluoroborate salt due to its low solubility leading to product mixtures.

Crystal structures of both ligands (**93**, **99**) were obtained by slow diffusion of hexane into a saturated diethyl ether-dichloromethane solution of the ligands (*cf.* Figure 61).

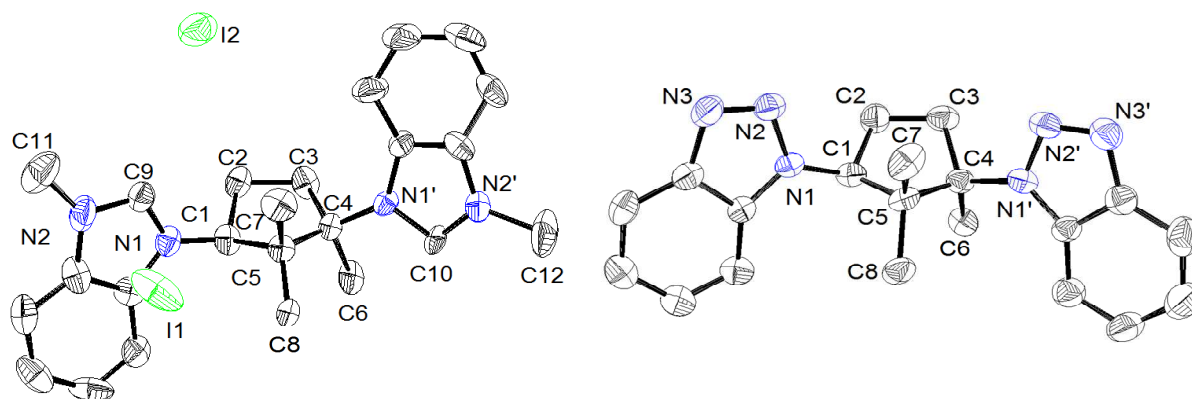


Figure 61 Molecular structure of target, chiral dibenzimidazole diiodide **93** (left) and dibenzotriazole **99** (right).

Thermal ellipsoids are plotted at 50% probability level and hydrogen atoms are omitted for clarity. Selected bond lengths for **93**: N2–C9 133.0(2) pm, N2'–C10 128.0(2) pm, N1–C9 130.0(2) pm, N1'–C10 140.0(2) pm, N1–C1 145.0(2) pm, N1'–C4 149.0(2) pm, N2–C11 146.0(2) pm, N2'–C12 144.0(3) pm. Selected bond lengths for **99**: N3–N2 130.9(6) pm, N3'–N2' 130.1(6) pm, N1–N2 137.0(4) pm, N1'–N2' 136.2(4) pm, N1–C1 145.5(5) pm, N1'–C4 147.6(5) pm.

In the solid state two benzotriazoles **99** are positioned pseudo symmetrical to each other in the unit cell and can be considered equal with only marginal structural variations. In contrast to the envelop-conformation pointing away from the *N*-substituents (positive out of plane distortion) observed for the monoarylated compound (*cf.* Figure 59), the central *cyclo*-pentane moiety of **99** adopts an envelop-conformation with the dimethyl bridgehead positioned in the center between the *N*-substituents, and are therefore competing for space necessary for metal-incorporation. The benzotriazole substituents are distorted out of plane (distortion angle for pseudo symmetric molecules in the unit cell: -19.7°/ -24.3° and -37.7°/ -30.6°) in respect to the *cyclo*-pentane moiety as expected and generally observed for the bridging unit in pincer-

type NHC complexes (*cf.* Figure 57).^[332, 339, 341-343, 354] The molecular structure of the chiral dibenzoimidazole diiodide salt **93** shows characteristics similar to the solid state structure of dibenzotriazole **99**. Two molecules are placed in the unit cell and the central bridgehead adopts an envelope-conformation with the methylene bridgehead being negatively distorted - 38.1°, resp. -40.1° out of the *cyclo*-pentane plane (same direction as *N*-substituents). In contrast, to the *cis* conformation observed for the benzotriazole ligand in **99**, a *trans* configuration of the benzimidazole substituents is realized in **93** (*cf.* Figure 61).

After successful preparation of the diiodide and ditriflate salt preliminary studies were undertaken to investigate their coordination properties towards palladium(II). The formation of a palladium pincer complex proved to be challenging and various conditions were applied,^[355-358] including standard conditions and metal precursors in combination with respect to the counter ions present at the ligand as well as transmetallation reactions with silver(I)^[359] and conditions intended to furnish, less sterical demanding carbon dioxide incorporation (*cf.* Table 13).

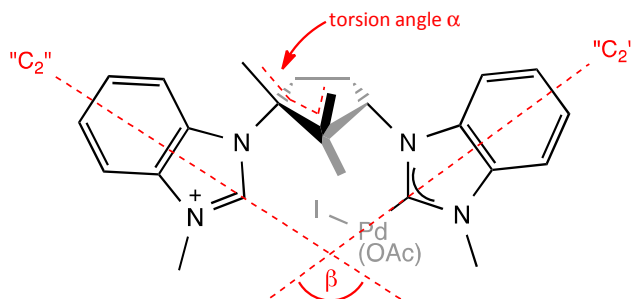
Table 13 Conditions intended to furnish palladium(II) pincer complexes of NHC ligand salts **93** and **94**.

#	Ligand	Metal-Precursor	Reaction Conditions ^[a]
1	93	Pd(OAc) ₂	MeCN, r.t. to 82 °C
2	93	Pd(OAc) ₂	THF, r.t. to 67 °C
3	93	Pd(OAc) ₂	DMSO, 50 °C/ 75 °C/ 105 °C/ 189 °C.
4	93	Ag ₂ CO ₃	THF, r.t., in the dark
5	93	Ag ₂ CO ₃	MeCN, r.t., in the dark
6	93	Ag ₂ CO ₃	DCM, r.t., in the dark
7	93	Ag ₂ CO ₃	DMSO, r.t., in the dark ^[b]
7	93	Ag ₂ CO ₃	DMSO, 75 °C, in the dark ^[b]
8	93	Ag ₂ O	MeCN, r.t., in the dark
9	94	Pd(MeCN)Cl ₂	LiHMDS, THF, r.t.
10	94	CO ₂	NaH, THF, -35 °C to r.t.
11	94	CO ₂	NaH, MeCN, -20 °C to r.t.

Reactions (150 – 200 μmol scale) were monitored over a period of at least 48 h, no complex formation observed.^[360] ^[b] Target Pd-pincer complex of **93** identified by HRMS.

The palladium(II) diiodide complex of dibenzimidazole **93** was only detected by MS measurements. Certainly, geometric strain and steric demand of the ligands obtained from camphoric acid strongly influences complex formation. The geometric change, in particular the flip of the bridgehead dimethyl group of the central *cyclo*-pentane moiety and central positioning of the methylene bridgehead observed for the solid state structures of ligand **93**,

99 and for the dinitroprecursor **90** in contrast to the monoaminoarylated structure (*cf.* figure 59) may account for this observation. By having a closer look into the structural properties of the dibenzimidazole ligand it was found, that for the formation of a pincer ligand, a complete flip of the central dimethyl bridgehead through the *cyclo*-pentane plane is necessary.



Scheme 51 Schematic representation of the geometrical properties of dibenzimidazole ligand **93**.

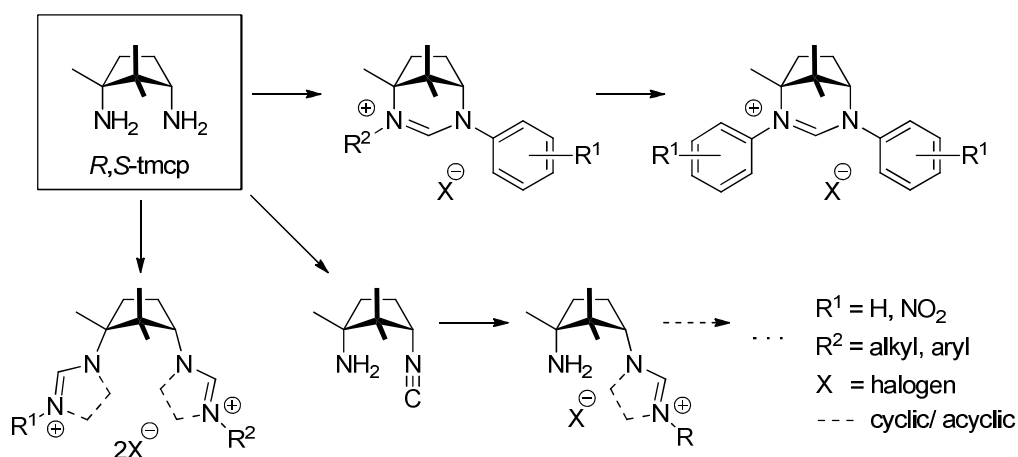
Cis-configuration of dibenzimidazole ligand **93** shown. Direction of flanking *N*-substituents for complex formation and impact of torsion angle highlighted.

Consequently, the torsion angle α between the *exo*-methyl group and the bridgehead methyl group of the 5-membered *cyclo*-pentane unit is changed with the methyl substituents approaching each other. They adopt first a staggered conformation, finally sweeping through the eclipsed positioning (*cf.* Scheme 51). Since a stepwise complex formation is likely to run through a monodentate NHC complex first, the distance between the Pd-NHC and the free NHC, considering the energetically more favored *trans*-configuration observed in the solid state of the free ligand **93**, might be improper as well.

3.4 Conclusion

In Summary, it was shown that (1*R*, 3*S*)-camphoric acid is a useful chiral starting material for the preparation of chiral *N*-heterocyclic ligands. Synthesis was accomplished in five steps to yield dibenzoimidazole diiodide salt **93** in good overall yield (30%). The corresponding ditriflate salt **94** was prepared in 29% yield. It was found, that aminoarylation of *R,S*-tmcp [(1*S*,3*R*)-1,3-diamino-1,2,2-trimethylcyclopentane] can be carried out regioselectively furnishing the monoarylated *para*- and *ortho*-nitro compounds. The regioselective formed product was unequivocally determined by X-ray crystal structure analysis and proofed substitution to occur at the sterically less hindered N2-position of the camphor motif. Furthermore, chiral dibenzotriazole **99** was prepared in four steps in 74% yield. Under the applied reaction conditions a two step mechanism was proposed, featuring didiazonium salt

formation followed by tandem intramolecular cyclization to form the benzotriazole core exclusively. Nitrodefunctionalization was not observed under the reaction conditions indicating the formation of benzotriazoles being favored. Investigations on the molecular structures of benzimidazole diiodide **93** and dibenzotriazole **99** revealed a configuration of the bridging unit believed to be disadvantageous for the formation of a pincer metal-chelate. In particular, the dimethyl bridgehead of the *cyclo*-pentane substructure is located in between, occupying space necessary for complex formation. Therefore, approaching of the benzimidazole substituents becomes difficult. Complex formation may be possible as the solid state structure of the regioselective monoarylated compound shows a pronounced hydrogen bonding pattern leading to a tightened up structure with the dimethyl bridgehead being flipped. However, the torsion angle and the close proximity of the *exo*-methyl group to the dimethyl group of the *cyclo*-pentane structure might be disadvantageous for an inversion (flip) of the camphor-related dimethyl bridgehead (*cf.* Scheme 51). Reconsidering the successful preparation of the ligands, the obtained solid state structures and the ability for regioselective transformations at *R,S*-tmcp, the development of chiral, pincer-type complexes is promising. An approach combining *R,S*-tmcp and regioselective *isonitrile* formation (*cf.* Chapter 4) for the preparation of chiral NHC-palladium(II)-complexes may be particularly interesting (*cf.* Scheme 52).



Scheme 52 *R,S*-tmcp and regioselective aminofunctionalized derivatives as versatile starting materials for the development of novel, chiral mono- and bidentate NHC ligands.

**Chapter 4 Six-Membered, Chiral Pd-NHCs
Derived from Camphor – Structure-Reactivity
Relationship in the Asymmetric Oxindole Synthesis**

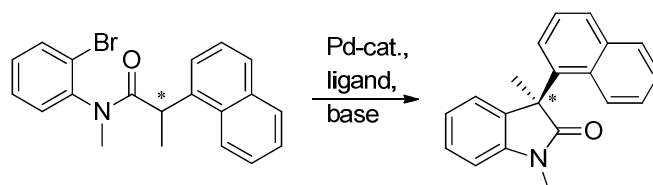
4.1 Introduction – NHC-Palladium Catalysts in Asymmetric Oxindole Synthesis

Known since the late 1960s,^[361-365] *N*-heterocyclic carbenes (NHCs) attracted little interest in the beginning, until Arduengo et al. reported the isolation of the first stable carbene in 1991.^[366] Due to their unique electronic and steric properties NHCs revolutionized today's organometallic chemistry and homogeneous transition-metal catalysis.^[367-370] NHCs are strong σ -donors with only weak π -acceptor capability^[371] and their structural properties are best described by the *buried volume* model developed by Nolan and Cavallo et al.^[371-373] In short terms, it gives a measure of the space occupied by an organometallic ligand in the metal NHC complex coordination sphere and is related to *Tolman's* cone angle θ ,^[374] which is used as descriptor for the steric demand of phosphine ligands. The sp^2 nature of the *N*-heterocyclic carbene donor is responsible for their unique steric properties, which are described by the *buried overlap volume* ($\%V_{\text{bur}}$). It represents a useful steric parameter indicative for the accessible metal surface, but noteworthy completely ignores ligand anisotropy (ligand rotation). The resulting complexes are typically characterized by a high stability^[375] of the NHC-metal bond, making them highly attractive for metal-complex formation and catalysis. Particularly, the preparation of chiral ligands and their potential in asymmetric catalysis are receiving growing attention.^[376-381] Various approaches towards the synthesis of chiral NHC-ligands were established.^[382-387] Besides the need for a short access to chiral ligand frameworks and evaluation of their coordination properties, focus on modular synthetic pathways, preferable convergent and high yielding, is emerging to investigate the impact of ligand design on catalysis. Besides electronic effects, steric demand of the ligand is an important factor for enhanced chirality transfer as well as for stabilization of low-coordinated metal complexes during catalysis. Latter are needed for challenging transformations, such as cross-coupling reactions of non-activated aryl chlorides.^[331, 388-390] Although increased steric encumbrance of the metal center in the complex is pursued for effective chirality transfer, the retention of certain flexibility within the catalyst seems to be a beneficial factor as well.^[253]

The intramolecular α -arylation of amides represents an ideal reaction for the investigation of ligand design in catalysis as both reactants are present within the substrate and concentration effects of reactants and the influence of the degree of dilution are significantly reduced. The reaction provides efficient and direct access to chiral 3,3-disubstituted oxindoles, a common structural motif present in many natural products. Currently, there are various routes towards enantiomerically enriched 3,3-disubstituted oxindoles with overall moderate success.^[391] In a pioneering work Hartwig et al.^[392] used chiral phosphines and NHCs for this type of transformation but it was shown that C_2 -symmetric NHC ligands gave better results with an enantiomeric excess (*e.e.*) up to 76% in

comparison to those obtained with potent chiral phosphines (BINAP, PHOX, DuPhos, Salen-Phosphines 2 – 53% *e.e.*). Glorius^[393], Dorta^[394] and more recently Kündig et al.^[395-397] managed this challenging type of α -amide arylation with moderate to high enantiomeric excess and yields. In 2011 Murakami^[398] reported a complete rigid chiral NHC ligand system for chirality transfer in the asymmetric oxindole synthesis. Commonly ligands based on 5-membered imidazoles,^[392, 395-397] imidazolines or oxazoles^[393, 399] are employed. Noteworthy, and this is true for all ligands employed for the asymmetric oxindole synthesis, the highest enantiomeric excess is obtained for 1-naphthyl derivatives as substrate. The privileged ligands, the reaction conditions employed as well as product yield and enantiopurity are summarized in chronological order in Table 14.

Table 14 Privileged ligands for the Pd-catalyzed asymmetric oxindole synthesis.



#	Ligand (and Year)	Synth. Steps	Conditions	Yield	e.e. [%]
1	2001 	3	Pd(dba) ₂ (10 mol%) NaOtBu (1.5 equiv.)	75	76
2	2002 	3	Pd(dba) ₂ (10 mol%) NaOtBu	95	43
3	2007 	4	Pd(OAc) ₂ (5 mol%) NaOtBu (1.5 equiv.)	72	79
4	2009 	7	[Pd(allyl)Cl] ₂ (2.5 mol%) NaOtBu (1.5 equiv.)	99	96
5	2011 	7 ^[a]	TMEDA, PdMe ₂ (5 mol%) NaOtBu (1.5 equiv.)	98	97

Synthesis requires optical resolution with tartaric acid.^[398]

All ligands employed for this type of transformation exclusively feature C_2 -symmetry, but the idea of chirality transfer is realized in different ways. Whereas the first ligand (*cf.* Table 14, entry 1) exhibits two bulky, chiral camphor building blocks each being attached as *N*-bornyl substituents to the imidazoline core, bisoxazolines were intended to benefit from complete rigidity of the tricyclic system thus enhancing enantioselectivity (*cf.* Table 14, entry 2). In fact, a lower enantioselectivity was observed with bisoxazolines thus indicating that the *tert*-butyl substituents induce chirality less effectively or implying that complete rigidity of the ligand is not a crucial factor. More recently, Glorius et al. enhanced the chiral information present at the bisoxazoline core by changing the *tert*-butyl groups into (-)-menthyl as chiral building block (*cf.* Table 14, entry 5). Contrary to this approach, Kündig et al.^[395-397] developed a flexible, chiral ligand pattern likely to combine aspects of chirality and restricted flexibility in the catalyst and reported conversions and enantioselectivities similar to the results with IBiox [(-)-menthyl]^[393] (*cf.* Table 14, entries 3, 4). Most recently in 2011, Murakami reported excellent enantioselectivities with a complete rigid, backbone-fused NHC (*cf.* Table 14, entry 5).^[398] However, still seven steps were needed for synthesis of the most efficient ligands employed for this type of transformation (*cf.* Table 14, entries 4, 5).

4.2 Objectives

Inspired by the work of Hartwig^[392] and Glorius^[393] a ligand pattern featuring two camphor chiral building blocks related to Hartwig's dibornylimidazoline ligand (*cf.* Table 14, entry 1) was envisaged. In regard to the recent proceedings in *N*-heterocyclic ligand design in the Hashmi group, a collaboration with Dominic Riedel focusing on the development of novel, expanded chiral camphor derived palladium(II) catalysts was launched. Expanded NHCs and furthermore unsymmetrical substituted chiral NHC-metal complexes have rarely been reported or investigated in the asymmetric α -arylation of amides. As rather different properties are reported for six-^[383, 400-405], seven-^[383, 406-409] and most recently 8-membered^[410] NHCs, in particular increased basicity (nucleophilicity),^[402, 403, 405] greater steric demand and higher congestion around the metal-center (larger N-C_{NHC}-N angle),^[403] the evaluation of a series of ligands featuring successive increasingly steric demand, while maintaining the same chiral substitution pattern (camphor), was aimed (*cf.* Figure 62).

With these catalysts the impact of substitution and steric hindrance on catalyst reactivity and selectivity in the asymmetric oxindole synthesis will be investigated. For observation of maximum effects of the catalyst substitution a catalyst pattern and substrates intended to yield moderate enantiomeric excess was envisaged. To get reliable insights natural *d*-(+)-camphor

(resp. bornylamine) was chosen as the chiral building block and arylbromides as well as arylchlorides with different substitution patterns were employed in the asymmetric α -arylation of amides.

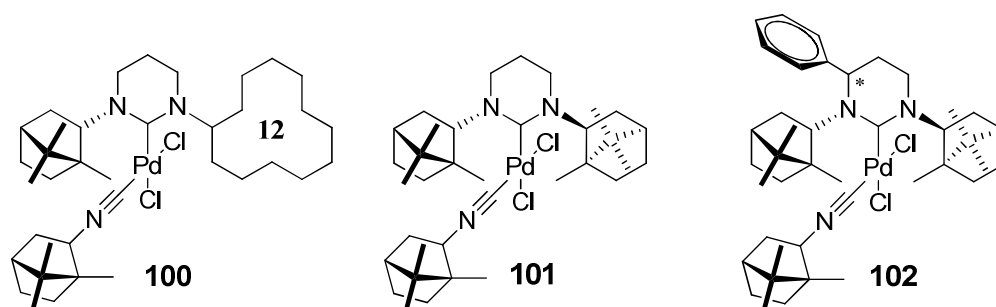


Figure 62 Target, chiral hexahydropyrimidine NHC Pd(II)-catalysts (**100** – **102**) with increasing steric demand for the asymmetric α -amide arylation.

4.3 Results and Discussion

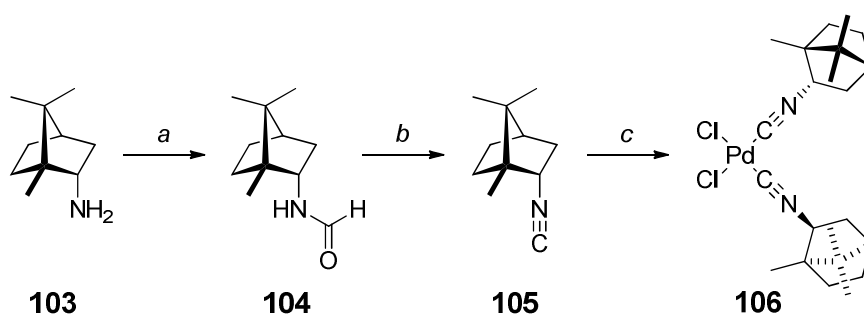
Note: The preparation and characterization of the three palladium catalysts (**100** – **102**) was accomplished by Dominic Riedel^[411] and will therefore be discussed in brief. Preparation of the substrates for the asymmetric oxindole synthesis, screening of the reaction conditions, evaluation of their catalytic performance of the novel catalysts and determination of the enantiomeric excess and the configuration was done by the author and is subject of this chapter.

4.3.1 Six-Membered, Chiral Pd-NHC-Camphorisonitrile Complexes

Overall a set of three chiral palladium catalysts featuring a 6-membered *N*-heterocyclic hexahydropyrimidine core was realized by modification of the flanking substituents and finally by installation an additional group at the NHC-backbone. The steric demand and the chiral information of the catalyst was successively increased. The synthesis of the 6-membered, chiral NHC-complexes was achieved utilizing a straightforward synthetic protocol developed in the Hashmi group.^[412-416] The modular and quite convergent pathway allowed the unprecedented short synthesis of three bornylamine-derived palladium-catalysts with varying types of backbone- and wingtip-substitution.

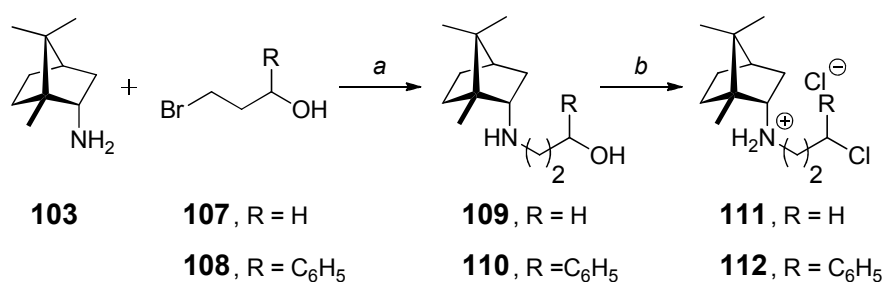
Bornylisonitrile **105** was prepared by neat reaction of ethyl formate and (1*R*,2*S*)-bornylamine **103** in an autoclave at 200 °C for 12 h and additional 5 h at 250 °C. This reaction furnished pure bornylformamide **104** as colorless crystals in 87% yield. Dehydration with

phosphorous trichloride and excess triethylamine gave bornylisonitrile **105** in 83% yield as an off white solid. The chiral palladium(II) isonitrile precursor **106** was obtained in 83% yield by ligand exchange reaction of bis(acetonitrile)palladium(II) dichloride and bornylisonitrile **3** (*cf.* Scheme 53). Aminoalkylchlorides were used as synthons for the installation of the NHC-backbone. Therefore, (1*R*,2*S*)-bornylamine (**103**) was reacted with 1-bromo-3-propanol **107** and **108** to furnish 3-hydroxypropylbornylamine (**109**) and 3-phenyl-3-hydroxypropylbornylamine (**110**) as colorless liquids. The chloride salts of **109** and **110** were prepared in very good yields using thionyl chloride. To ease purification and handling in further synthetic steps **111** and **112** were isolated as their corresponding chloride salts (94% for **111**, 88% for **112**). The *cyclo*-dodecanone derivative of **111** was prepared in a similar manner (*cf.* Scheme 54).



Scheme 53 Synthesis of chiral bornylisonitrile **105** and Pd-bis(isonitrile) complex **106**.

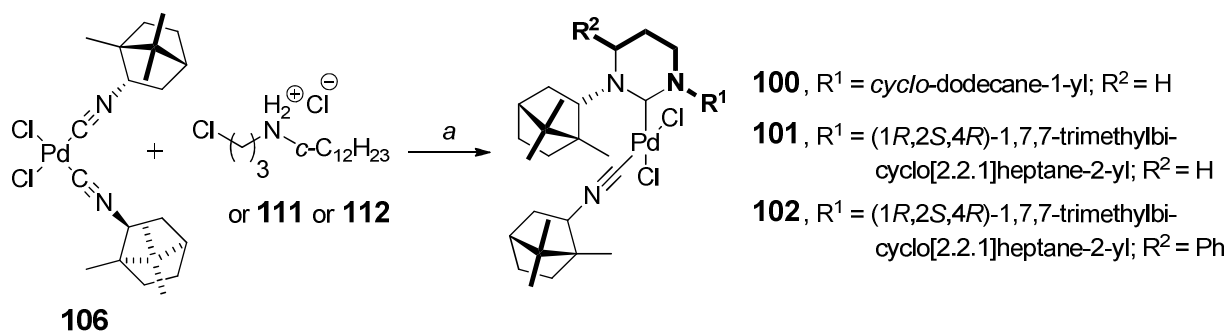
Reaction conditions: a) HCO_2Et , 200 – 250 °C, 12 h, 87%. b) POCl_3 , NEt_3 , DCM, -60 °C, 20 min, r.t., 18 h, 83%. c) $\text{Pd}(\text{MeCN})_2\text{Cl}_2$, toluene, r.t., 12 h, 83%.



Scheme 54 Preparation of NHC-backbone synthon **111** and **112**.

Reaction conditions: a) PhCN , 95 °C, 12 h, no yield reported. b) SOCl_2 , DCM, 40 °C, 12 h, 94% for **111** (88% for **112**).

The bornyl-derived Pd-isonitrile complexes **100** – **102** were prepared by *in situ* intramolecular cyclization with the appropriate aminoalkylchloride in presence of excess base and obtained in 67% (**100**), 64% (**101**) and 41% (**102**) yield (*cf.* Scheme 55).



Scheme 55 Formation of chiral Pd-isonitrile complexes **100** – **102** by intramolecular cyclization.

Reaction conditions: a) Pd(MeCN)₂Cl₂, NEt₃, DCM, r.t., 12 h, 67% for **100** (64% for **101**, 41% for **102**).

The molecular structures of palladium complexes **100** and **102** were determined by crystal structure analysis. In palladium-isonitrile complexes **100** the dihedral torsion angle between N(2)–C(1)–Pd–C(5) of -79.0° with 11° deviation from the orthogonality is indicative for steric congestion around the quadratic planar metal center and generally observed for NHC complexes exhibiting bulky substituents. The solid state structure of complex **101**, bearing two chiral bornylamine building blocks is in accordance to the structural features observed for complex **100**. Due to the higher steric demand due to the orientation of the *exo*-methyl groups at C25 and C27 of the bornyl substituents, a decrease of the dihedral torsion angle N(2)–C(1)–Pd–C(5) to -73.5° is observed. In relation to the NHC axis the isonitrile ligand points towards the sterically less crowded camphor backbone (C24, C23 and C19). The bornylisonitrile **3** is almost linearly coordinated to the palladium centers and a significant change of the Pd-carbene bonds and Pd-isonitrile distances is not observed (*cf.* Figure 63).

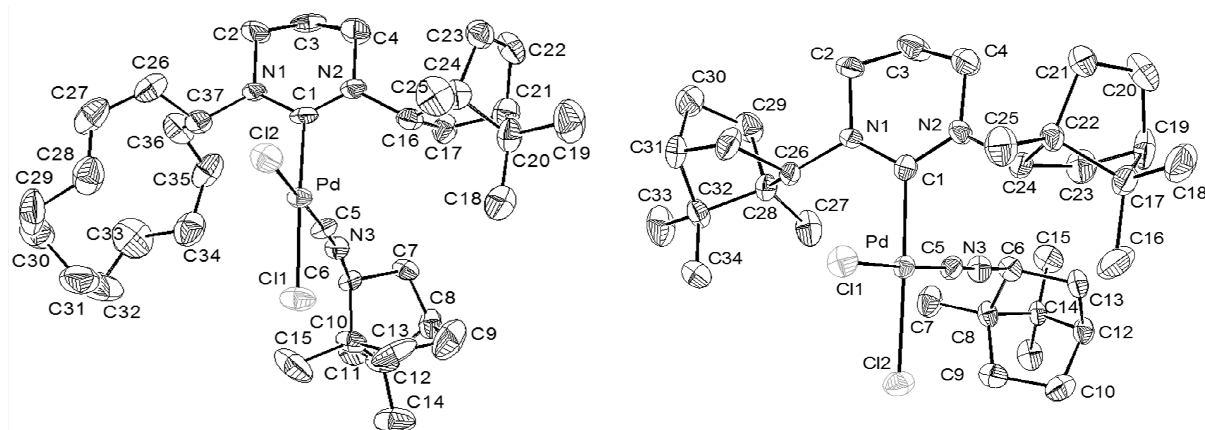
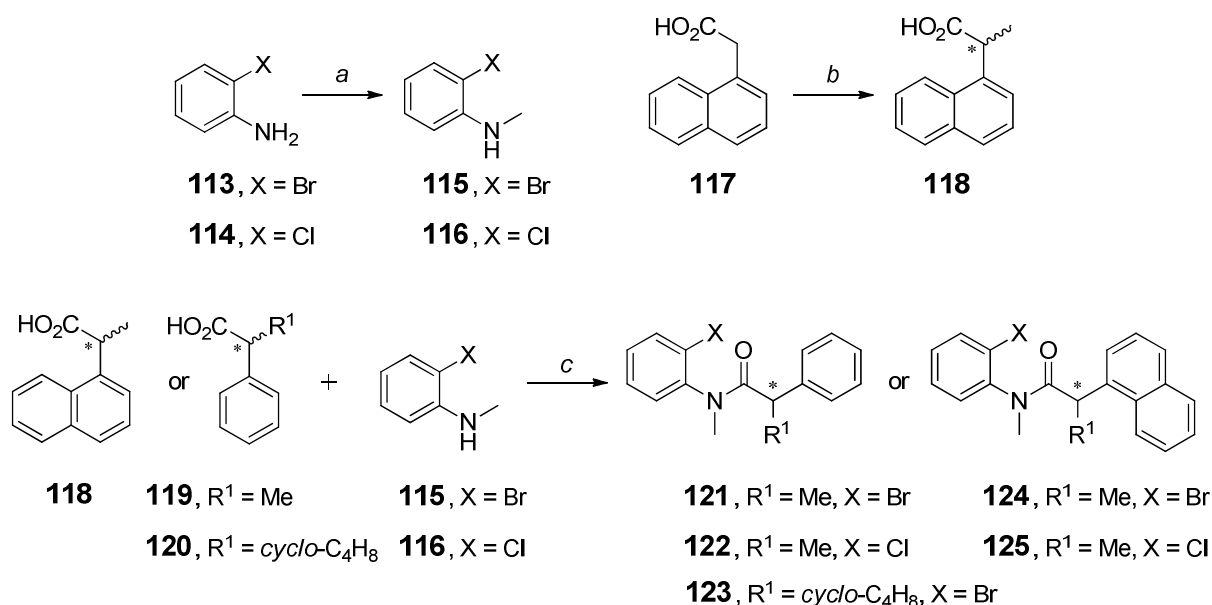


Figure 63 Solid state structures of Pd-NHC-complexes **100** (left) and **101** (right).

Selected bond lengths for **100**: C1–Pd 198.0(2) pm, Pd–C5 191.0(2) pm, C5–N3 115.0(3) pm, N3–C6 149.0(3) pm, C1–N1 132.0(2) pm, C1–N2 137.0(2) pm, N1–C37 150.0(2) pm, N2–C16 146.0(2) pm. Selected bond lengths for **101**: C1–Pd 201.4(4) pm, Pd–C5 191.7(5) pm, C5–N3 116.0(6) pm, N3–C6 143.6(6) pm, C1–N1 134.9(7) pm, C1–N2 133.2(7) pm, N1–C26 146.3(6) pm, N2–C24 148.6(6) pm.

4.3.2 Asymmetric Oxindole Synthesis

For a representative evaluation of the catalytic performance of the palladium-isonitrile complexes **100** – **102** overall 5 different substrates were synthesized according to literature.^[392, 417-420] Substrates bearing benzyl- and naphthyl-substituents and *N*-methylation were chosen to study the influence of the substitution pattern on selectivity. The corresponding bromide and chloride analogues and one *cyclo*-butylated substrate were prepared as well (*cf.* Scheme 56).



Scheme 56 Synthesis of substrates for the Pd-catalyzed asymmetric α -amide arylation.

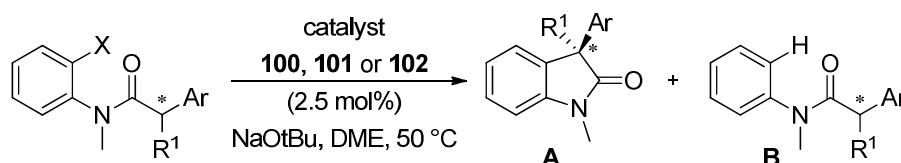
Reaction conditions: a) BuLi, THF, -50 °C, 1 h then MeI, -60 °C, 1 h then r.t., 16 h, 49% for **115** (50% for **116**). b) BuLi, LDA, THF, -78 °C, 1 h then MeI, 0 °C, 1 h then r.t., 18 h, 91%. c) SOCl₂, propanoic acid, 75 °C, 3 h then 2-halo-*N*-methylaniline, NEt₃, r.t., 16 – 24 h, 43% for **121** (41% for **122**, 72% for **123**, 89% for **124**, 93% for **125**)

Therefore the corresponding 2-haloanilines were first monomethylated using *n*-butyllithium and methyl iodide at -60 °C and the products were obtained after purification in 49% (**115**), respectively 50% yield (**116**). The arylpropanamides **121** – **125** were prepared by condensation of 2-phenylpropanoic (**119**) and naphthalenepropanoic acid chlorides (**118**) with 2-halo-*N*-methylanilines (**115**, **116**). The carboxylic acid chlorides were prepared by *in situ* by neat reaction with thionyl chloride. Monomethylated 2-(naphthalen-1-yl)propanoic acid **118** was synthesized by reaction with freshly prepared lithium diisopropylamide and methyl iodide at -78 °C and obtained as a colorless solid after purification (91%).

An initial solvent screening using tetrahydrofuran, ethanol, *iso*-propanol, diglyme, dioxane, dimethoxyethane and dimethyl sulfoxide revealed anhydrous dimethoxyethane combined with

sodium *tert*-butylate as base to be ideal. Catalyst loadings were successively decreased and loadings of 2.5 mol% were found to be sufficient for catalysis. Alcohols were not suitable solvents even though related Pd-isonitrile complexes were reported to be highly-active catalysts in alcoholic media for Suzuki cross-coupling of boronic acids.^[414] All reactions were performed at 50 °C to furnish complete conversions within a maximum of 18 h

Table 15 Asymmetric oxindole synthesis using Pd-isonitrile NHC-complexes **100** – **102**.



#	Catalyst	X	R ¹	Ar	A	B	Yield [%] ^[b]	ee [A; %] ^[c]
1	100	Br	Me	1-naphthyl	100	-	quant.	rac.
2	101	Br	<i>c</i> -C ₄ H ₈	Ph	100	-	95	55
3	101	Br	Me	Ph	100	-	90	58
4	101	Cl	Me	Ph	100	-	98	63
5	101	Br	Me	1-naphthyl	100	-	92	68
6	101	Cl	Me	1-naphthyl	100	-	95	72
7 ^[d]	102	Br	Me	Ph	36	64	89 ^[e]	8
8 ^[d]	102	Br	Me	1-naphthyl	-	100	91	-

Reaction conditions: 0.3 mmol scale, NaOtBu (0.45 mmol), catalyst (2.5 mol %) in DME (5 mL) at 50 °C, 14 – 18 h. ^[b] Isolated yields reported. ^[c] Determined by chiral HPLC (Chiralpak IA). Product configuration: (*R*-), determined by chiral HPLC (Chiralpak IB) of known compounds. ^[d] Reaction at 80 °C. ^[e] Isolated yield of **A** and **B**.

With chiral catalyst **100**, featuring a flexible *cyclo*-dodecanyl substituent at one *N*-terminus, the desired 3,3-disubstituted oxindole was obtained and isolated in quantitative yields (*cf.* Table 15, entry 1). After purification of the reaction mixture enantioselective HPLC-analysis of the product showed a racemic mixture of oxindole enantiomers and proved that no chiral induction takes place within a system bearing only one chiral substituent. Therefore, catalysis was continued using NHC-Pd-isonitrile complex **101** featuring two chiral bornyl substituents. With this catalyst all substrates were converted to their (*R*)-oxindole derivatives in very high

yields (*cf.* Table 15, entries 2 – 6, as determined by chiral HPLC). Benzyl-substituted substrates were obtained with an enantiomeric excess of 58% *e.e.* (bromide derivative, *cf.* Table 15, entry 3) and 63% *e.e.* (chloride derivative, *cf.* Table 15, entry 4). The corresponding naphthyl substrates showed higher enantioselectivities (68% *e.e.* and 72% *e.e.*, *cf.* Table 15, entries 5 and 6). The results are noteworthy, since temperature has a pronounced influence on the enantioselectivity. The related 5-membered NHC showed 70% *e.e.*, however only 58% *e.e.* at 0 °C with catalyst loadings of 10 mol% catalyst.^[392] The higher enantioselectivity of 72% *e.e.* (*cf.* Table 15, entry 6) at higher temperatures is attributed to the NHC-metal angle being enlarged within a 6-membered NHC, thus increasing steric congestion and chiral induction compared to the 5-membered derivative with the same chiral ligand pattern. A slight increase of 5% in enantioselectivity was observed for the chloro derivative in each case (*cf.* Table 15, entries 3, 4 and 5, 6). This data suggests that the halide is present on or at least in close proximity to the catalytic active species during the enantiodiscriminating step. Introduction of a *cyclo*-butyl substituent at the *N*-terminus of the substrate had no significant influence on enantioselectivity compared to the *N*-methylated substrate (*cf.* Table 15, entry 2 and 3).

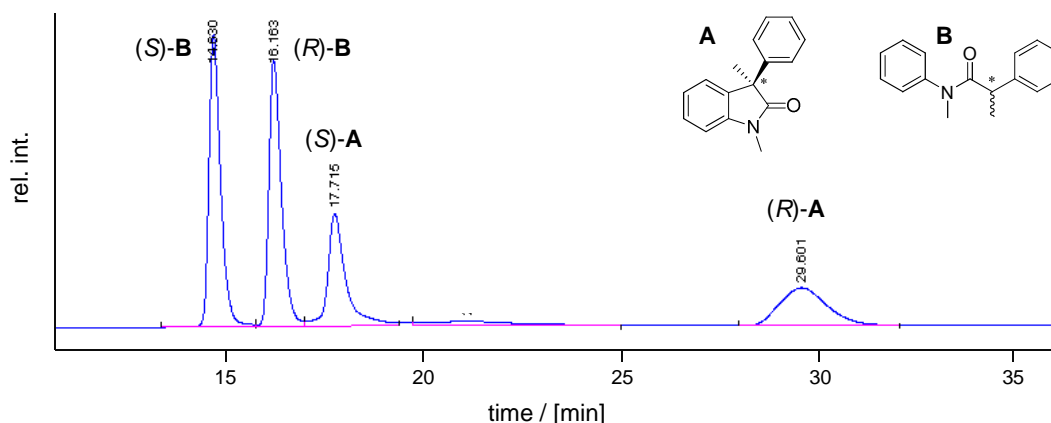


Figure 64 HPLC-chromatogramm showing the enantioselective oxindole and dehalogenation products using the sterically most demanding catalyst **102**.

Determined by chiral HPLC (Chiralpak IA). Elution order: racemic arylpropanamides (14.6 min and 16.2 min), (*S*)-oxindole (17.7 min), (*R*)-oxindole (29.6 min). Product configuration determined by reference measurements on chiral HPLC (Chiralpak IB) of known compounds.

Interestingly, palladium-isonitrile catalyst **102** bearing the same chiral bornyl-ligand pattern at the *N*-substituents but exhibiting an additional phenyl-substituent at the NHC-backbone in close proximity to the chiral-substituents showed a different reactivity. High conversions were observed by employing the bromo-phenyl derivative **121** (*cf.* Table 15, entry 7), but enantioselectivity dropped almost completely to 8%. Beside small amounts of 3,3-disubstituted oxindole product dehalogenation of the starting material was observed in 64%

yield leading to racemic arylpropanamides, as validated by NMR spectroscopic and chiral HPLC-MS measurements (*cf.* Figure 64). By changing the substrate to the even more sterically demanding bromo-naphthyl derivative only the racemic dehalogenation products were observed. The change in reactivity leading to dehalogenation of the substrates may be explained by the high sterical demand of catalyst **102** but moreover reasonable might be freezing of the C-N-rotation of one chiral bornylamine substituent to a certain extend. By increasing the sterical demand within the substrate dehalogenation via reductive elimination prior to insertion of the amide subunit becomes competitive and dominates the reaction profile of catalyst **102** by using bromo-naphthyl substrate **124** leading exclusively to dehalogenation.

4.4 Conclusion

In summary, the synthesis^[411] of three six-membered hexahydropyrimidine core based, camphor-derived NHC-Pd-isonitrile complexes and their application as catalysts in the asymmetric α -amide arylation was shown. The structure of two Pd-complexes was determined by X-ray crystallographic analysis. Taking advantage of a convergent, modular synthetic pathway the preparation of NHC ligands bearing different structural motifs present at the *N*-termini was accomplished. By successive increase of the chiral information and congestion within the catalyst pattern – while retaining the chiral motif (bornylamine) at the same time – their influence on enantioselectivity was demonstrated. All catalysts showed very good conversions of bromo- as well as chloro-substrates bearing aryl and naphthyl residues with catalysts loadings of 2.5 mol%. Whereas, catalyst **100** (exhibiting only one chiral bornylamine NHC- and one cyclododecyl substituent) showed no enantiodiscrimination in the oxindole synthesis, catalyst **101** bearing two bornylamine NHC substituents proved to be more effective. Higher enantioselectivities compared to the related, 5-membered bornylamine-derived imidazoline ligand was observed at even higher temperatures than the reported ones. With the sterically most demanding catalyst **102** exhibiting an additional phenylsubstituent at the NHC backbone in close proximity to the chiral *N*-bornyl substituent a reaction profile leading either to an arylation or dehalogenation product depending on the employed substrate was observed. Furthermore, the calculated buried overlap volume^[372, 373] of catalyst **101** ($\%V_{\text{bur}} = 40.9$) exceeds the value of 1,3-*di*-(1-adamantyl)-imidazol-2-ylidene (IAd, $\%V_{\text{bur}} = 36.1$)^[421] and represents the second highest volume reported so far for chiral *N,N*-heterocyclic carbene ligands (IBiox[(-)-menthyl], $\%V_{\text{bur}} = 47.7$ (Au-complex)).^[393] The results obtained show that higher hindrance of the metal by substituents is still beneficial for enantioselectivity but at a certain level of congestion or restriction of flexibility a further improvement of chiral induction within a given system is limited!

Experimental Section

General Methods and Materials

All reagents and solvents were obtained from Acros, ABCR, Alfa Aesar, Sigma-Aldrich or VWR and were used without further purification unless otherwise noted. Dichloromethane was freshly distilled from calcium hydride under argon atmosphere and tetrahydrofuran was freshly distilled from sodium under argon atmosphere. Deuterated solvents were purchased from Euriso-Top. Acetonitrile was dried by a MB SPS-800 with the aid of drying columns. Handling of air- and moisture-sensitive materials was carried out in flame dried flasks under an atmosphere of argon using Schlenk-techniques. Thin layer chromatography (TLC) was performed using Polygram[®] precoated plastic sheets SIL G/UV254 (SiO₂, 0.20 mm thickness) from Macherey-Nagel. NMR spectra were recorded on Bruker Avance 500, Bruker Avance 300 and Bruker ARX-250 spectrometers at RT. Chemical shifts (in ppm) were referenced to residual solvent protons.^[422] Signal multiplicity was determined as s (singlet), d (doublet), t (triplet), q (quartet) or m (multiplet). ¹³C assignment was achieved via DEPT135 spectra and HSQC experiments. GC- and GC-MS measurements were performed on a Thermo PolarisQ Trace GC-MS, equipped with split injector (250°C), flame-ionization detector (250°C) and a quadrupole ion-trap MS (Thermo, San Jose, CA). Fused silica capillaries (0.25 mm I.D.) were coated with polysiloxanes (GE SE 30, GE SE 52) and modified, stationary *Chirasil-Metal* phases and combinations thereof by the static method described by Grob.^[139] For on-column experiments and separations helium or nitrogen was used as carrier gas. Exact conditions for the measurements are reported in detail in the corresponding experimental sections. MS spectra were recorded on a Finnigan MAT TSQ 700 or JEOL JMS-700 spectrometer. IR spectra were recorded on a Bruker Vector 22 FT-IR. CD- and UV-Vis spectra were recorded on a JASCO J-810 spectropolarimeter. Crystal structure analysis was accomplished on Bruker Smart CCD and Bruker APEX diffractometers. Melting points were determined on a Büchi melting point apparatus and temperatures were uncorrected. Elemental analysis was performed on an Elementar Vario EL. Crystallographic data is available in electronic form on CD attached to this manuscript.

Experimental Section – Chapter 1

Potassium-(1*S*)-camphor-10-sulfonate (**17**):

(1*S*)-camphorsulfonic acid (350.0 g, 1.51 mol) was suspended in 150 mL water and neutralized by slow addition of a solution of potassium hydroxide (84.5 g, 1.51 mol) in 200 mL of water at 0 °C. The solvent was removed under reduced pressure and under high vacuum. The product was powdered and dried two times over phosphorus pentoxide for 48 h to yield sulfonate **17** (395 g, 1.46 mol, 97%) as a white salt. Mp. 320 – 328 °C. IR (KBr): ν 3454, 2954, 2232, 2082, 1740, 1728, 1469, 1414, 1374, 1284, 1217, 1186, 1166, 1103, 1040, 973, 934, 936, 851, 780, 710.

Phosphorus pentabromide:

To a dilution of phosphorus tribromide (499.5 g, 1.85 mol, 173.4 mL) in 220 mL carbon disulfide placed in a three-necked flask equipped with a mechanical stirrer was slowly added bromine (294.7 g, 1.84 mol, 94.5 mL) via a dropping funnel at 0 °C under an argon atmosphere under vigorous stirring. The solvent was distilled off under reduced pressure after three hours. After 48 h under high vacuum phosphorus pentabromide (796.3 g, 1.84 mol, quant.) was obtained as a bright yellow solid. The product was stored under an argon atmosphere.

(1*S*, 4*R*)-10-camphorsulfonic acid bromide and (1*S*, 4*R*)-10-bromocamphor (**18**):



(1*S*, 4*R*)-10-camphorsulfonic acid bromide was prepared according to literature.^[423] Potassium-(1*S*)-camphor-10-sulfonate (**17**, 200.0 g, 0.74 mol) was suspended in 1.1 L anhydrous diethyl ether in a three-necked flask equipped with a mechanical stirrer under an argon atmosphere. Phosphorus pentabromide (326.4 g, 0.76 mol) was added rapidly under vigorous stirring at 0 °C. The red solution was allowed to warm up to room temperature and stirring was continued for 30 min, followed by 30 min at 30 °C. For reasons of handling only $\frac{1}{3}$ of the reaction mixture was submitted to the work-up procedure at once. Therefore, $\frac{1}{3}$ of the solution was poured onto 1 kg ice and was immediately extracted with 3×250 mL diethyl ether, to minimize decomposition to (1*S*, 4*R*)-camphorsulfonic acid. Finally, the organic layers were combined, washed with 100 mL water and dried over magnesium sulfate. Evaporation of the solvent and drying under high vacuum yielded (1*S*, 4*R*)-10-camphorsulfonic acid bromide

(90.9 g, 0.31 mol, 41%) as microcrystalline, brown powder. ^1H NMR (300.13 MHz, CDCl_3): δ 0.93 (s, 3H, $-\text{CH}_3$), 1.14 (s, 3H, $-\text{CH}_3$), 1.43 – 1.52 (m, 1H), 1.74 – 1.83 (m, 1H), 1.99 (d, 1H, $J = 18.3$ Hz), 2.04 – 2.16 (m, 2H), 2.39 – 2.53 (m, 2H), 3.90 (d, 1H, $J = 14.7$ Hz, $-\text{CH}_2\text{SO}_2\text{Br}$), 4.50 (d, 1H, $J = 14.7$ Hz, $-\text{CH}_2\text{SO}_2\text{Br}$) ppm. ^{13}C NMR (75.46 MHz, CDCl_3): δ 19.7, 19.6, 25.4, 26.8, 42.2, 42.7, 48.0, 60.5, 69.1, 212.4 ppm. MS (EI): m/z (%) 41 (41), 81 (80), 109 (82), 151 (100) $[\text{M}-(\text{SO}_2\text{Br})]^+$, 187 (7), 229 (10). IR (KBr): ν 2954, 2891, 1739, 1456, 1414, 1392, 1376, 1279, 1182, 1127, 1094, 1038, 967, 933, 853, 794, 764, 710.

(1*S*, 4*R*)-10-Bromocamphor **18** was prepared according to literature.^[423] (1*S*)-10-camphorsulfonic acid bromide (45.0 g, 0.152 mol) was dissolved in 1.2 L of fresh distilled, anhydrous *o*-xylol in a three-necked flask equipped with an open, oil filled valve for the extrusion of gas. Then a small amount of calcium chloride was added and the mixture was stirred for 48 h under the exclusion of light. Afterwards calcium chloride was filtered off and the filtrate was heated to 144 °C under an argon atmosphere and the temperature was maintained, till the generation of sulfur dioxide ceased. The solvent was removed by rotary evaporation resulting in a dark brown oil, which was submitted to steam distillation (oilbath temperature 150 °C) over a period of four days to yield (1*S*, 4*R*)-10-bromocamphor (**18**, 12.30 g, 0.053 mol, 35%) as colorless, needle-shaped crystals. Mp. 66 – 69 °C. ^1H NMR (300.51 MHz, CDCl_3): δ 3.61 (d, 1H, $J = 11.2$ Hz, $-\text{CH}_2\text{Br}$), 3.40 (d, 1H, $J = 11.2$ Hz, $-\text{CH}_2\text{Br}$), 2.45 – 2.36 (m, 1H), 2.17 – 1.97 (m, 3H), 1.90 (d, 1H, $J = 18.3$ Hz), 1.59 – 1.51 (m, 1H), 1.44 – 1.36 (m, 1H), 1.10 (s, 3H, $-\text{CH}_3$), 0.94 (s, 3H, $-\text{CH}_3$) ppm. ^{13}C NMR (75.56 MHz, CDCl_3): δ 20.3, 20.4, 26.7, 27.7, 29.3, 43.0, 43.9, 48.2, 60.3, 215.5 ppm. MS (EI): m/z (%) 41 (37), 53 (18), 67 (41), 81 (72), 93 (20), 109 (74), 123 (38), 133 (7), 151 (100) $[\text{M}-\text{Br}]^+$, 173 (1), 230 (7) $[\text{M}]^+$. IR (KBr): ν 2967, 2935, 2884, 1744, 1465, 1451, 1421, 1382, 1328, 1287, 1234, 1215, 1195, 1167, 1071, 1043, 1018, 961, 934, 910, 873, 851, 809, 775, 745, 708.

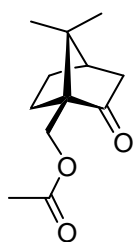
(1*S*, 4*R*)-10-iodocamphor (28):^[120, 121, 123, 169]



Synthesis of this compound was accomplished according to a procedure of Mulholland et al.^[120] Instead of column chromatography, purification by sublimation proved to be the method of choice. To a suspension of (1*S*)-10-camphorsulfonic acid (**16**, 65.0 g, 0.280 mol) in 500 mL toluene was added iodine (142.0 g, 0.560 mol) and triphenylphosphine (293.5 g, 1.120 mmol) and the mixture was heated at reflux for 16 h. Afterwards the solvent was removed under reduced pressure and ethyl acetate (500 mL) was added. The mixture was washed with saturated sodium thiosulfate solution (3×100 mL), water (3×50 mL) and brine (2×50 mL). The solvent was removed and the residue dried under high vacuum. Successive sublimation of small amounts of crude product yielded pure (1*S*, 4*R*)-10-iodocamphor (76.3 g, 0.274 mol,

98%) as colorless crystals. Mp. 79 – 82 °C. ^1H NMR (300.51 MHz, CDCl_3): δ 3.29 (d, 1H, $J = 10.6$ Hz, $-\text{CH}_2\text{I}$), 3.10 (d, 1H, $J = 10.6$ Hz, $-\text{CH}_2\text{I}$), 2.43 – 2.34 (m, 1H), 2.16 – 2.13 (m, 1H), 2.05 – 1.94 (m, 2H), 1.89 (d, 1H, $J = 18.3$ Hz), 1.63 – 1.56 (m, 1H), 1.41 – 1.35 (m, 1H), 1.06 (s, 3H, $-\text{CH}_3$), 0.89 (s, 3H, $-\text{CH}_3$) ppm. ^{13}C NMR (75.56 MHz, CDCl_3): δ 0.7, 20.1, 20.3, 26.7, 30.5, 42.9, 44.0, 28.3, 59.0, 215.0 ppm. IR (KBr): ν 2962, 2931, 1744, 1454, 1417, 1391, 1375, 1324, 1298, 1290, 1273, 1214, 1190, 1164, 1064, 1038, 766. Anal. calcd for $\text{C}_{10}\text{H}_{15}\text{IO}$, C: 43.18 H: 5.44. Found, C: 43.19 H: 5.47.

(1R, 4R)-10-acetatocamphor (19):



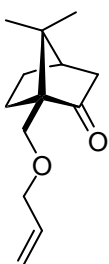
Method A: A mixture of (1S)-10-bromocamphor (**18**, 12.0 g, 0.052 mol), potassium acetate (35.7 g, 0.363 mol) and acetic acid (20.3 g, 0.338 mol, 19.3 mL) were stirred at reflux heating (175 °C) for 12 h. Afterwards the crude mixture was allowed to cool down (10 min) and was dissolved in 20 mL of water, while being hot. The solution was carefully neutralized with sodium carbonate and extracted with 4×50 mL diethyl ether. The organic layers were combined, washed with 50 mL brine and dried over magnesium sulfate. Evaporation of the solvent under reduced pressure followed by high vacuum yielded (1R, 4R)-10-acetatocamphor (10.2 g, 0.048 mol, 93%) as a colorless oil.

Method B: (1S)-10-iodocamphor (20.0 g, 0.072 mol) was used instead of (1S)-10-bromocamphor. Reaction conditions and work-up procedure is similar to method A. Pure (1R, 4R)-10-acetatocamphor (14.7 g, 0.070 mol) was obtained in 97% yield. ^1H NMR (500.13 MHz, CDCl_3): δ 0.98 (s, 3H, $-\text{CH}_3$), 1.05 (s, 3H, $-\text{CH}_3$), 1.37 – 1.41 (m, 2H), 1.88 (d, 2H, $J = 18.4$ Hz), 1.94 (dd, 1H, $J = 2.9$ Hz, $J = 12.8$ Hz, $-\text{CH}_2\text{CH}_2-$), 1.98 – 2.02 (m, 1H), 2.04 (s, 1H, $-\text{OCH}_3$), 2.07 – 2.09 (m, 1H), 2.40 – 2.45 (m, 1H), 4.23 (d, 1H, $^2J = 12.4$ Hz, $-\text{CH}_2\text{OCOH}$), 4.27 (d, 1H, $^2J = 12.4$ Hz, $-\text{CH}_2\text{OCOH}$) ppm. ^{13}C NMR (125.76 MHz, CDCl_3): δ 19.8, 20.7, 20.9, 25.5, 26.6, 43.3, 43.9, 47.0, 60.1, 60.5, 170.9, 216.1 ppm. MS (EI): m/z (%) 43 (100), 55 (14), 67 (18), 79 (43), 95 (49), 107 (55), 122 (16), 135 (11), 150 (78) $[\text{M}-(\text{CO}_2\text{CH}_3)]^+$, 167 (5) $[\text{M}-(\text{COCH}_3)]^+$, 192 (8), 210 (10) $[\text{M}]^+$. IR (KBr): ν 2964, 2887, 1746, 1454, 1417, 1392, 1366, 1322, 1242, 1200, 1034, 961, 857, 605.

(1*R*, 4*R*)-10-hydroxycamphor (20):

This is a known compound.^[424] (1*S*)-10-acetato-camphor (**19**, 10.2 g, 0.048 mol) was dissolved in a methanolic solution of potassium hydroxide (175 mL, 10wt%) and heated at reflux for 6 h. Afterwards the solution was allowed to cool down to room temperature and 200 mL of water was added.

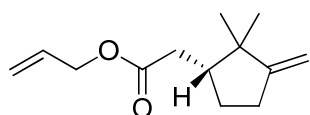
The solution was extracted with 3×100 mL diethyl ether. The organic layers were combined, washed with 50 mL brine, dried over magnesium sulfate and the solvent evaporated under reduced pressure. Recrystallization from pentane yielded 10-hydroxycamphor (**20**, 7.55 g, 0.045, 92%) as colorless crystals. Mp. 216 – 218 °C. ¹H NMR (300.51 MHz, CDCl₃): δ 3.87 (d, 1H, *J* = 11.8 Hz, -CH₂OH), 3.63 (d, 1H, *J* = 11.8 Hz, -CH₂OH), 2.54 (bs, 1H, -OH), 2.08 – 2.05 (m, 1H), 2.04 – 1.93 (m, 1H), 1.89 – 1.78 (m, 2H), 1.64 – 1.55 (m, 1H), 1.42 – 1.32 (m, 1H), 1.00 (s, 3H, -CH₃), 0.97 (s, 3H, -CH₃) ppm. ¹³C NMR (75.56 MHz, CDCl₃): δ 19.3, 20.8, 26.0, 26.6, 43.4, 43.9, 46.7, 60.6, 61.6, 221.0 ppm. MS (EI): *m/z* (%) 29 (20), 41 (48), 55 (28), 67 (33), 81 (40), 95 (95), 108 (100), 125 (13), 137(8) [M-(CH₃O)]⁺, 153 (39) [M-(CH₃)]⁺, 168 (18) [M]⁺. IR (KBr): ν 2955, 2876, 1729, 1610, 1457, 1417, 1390, 1370, 1323, 1300, 1288, 1272, 1217, 1201, 1178, 1162, 1143, 1107, 1060, 1028, 1009, 997, 950, 930, 919, 871, 852, 808, 769, 753, 710.

(1*R*, 4*R*)-10-allyloxycamphor (21):

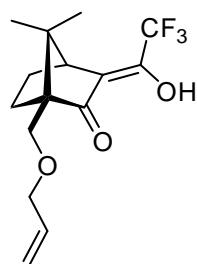
To a suspension of sodium hydride (1.20 g, 50 mmol) in 150 mL anhydrous tetrahydrofuran was slowly added a solution of 10-hydroxycamphor (**20**) (8.00 g, 48 mmol) in 30 mL anhydrous tetrahydrofuran at 0 °C. After 30 min the mixture was allowed to warm up to room temperature and was then heated at reflux for 30 min. Afterwards the reddish mixture was cooled to 0 °C and allylbromide (6.04 g, 50 mmol, 4.32 mL), dissolved in 30 mL anhydrous THF, was added dropwise. The reaction mixture was stirred for 30 min at room temperature and was then heated to 50 °C and maintained at this temperature for two hours. The mixture was cooled down to 0 °C, quenched with small amounts of ethanol (10 mL) and 200 mL of water was added. The solution was extracted with 4×50 mL pentane, the organic layers were combined, washed with 2×20 mL water and brine and dried over sodium sulfate. Evaporation of the solvent under reduced pressure, followed by high vacuum yielded analytical pure (1*R*, 4*R*)-10-allyloxycamphor (8.31 g, 40 mmol, 84%) as a colorless oil. ¹H NMR (500.13 MHz, CDCl₃): δ 5.92 – 5.85 (m, 1H, -OCH₂CH-), 5.26 (dd, 1H, *J* = 17.4 Hz, ²*J* = 1.6 Hz, methylene-CH₂*trans*), 5.14 (dd, 1H, *J* = 10.3 Hz, ²*J* = 1.6 Hz, methylene-CH₂*cis*), 3.98 (d, 2H, *J* = 5.3 Hz, -OCH₂CH-), 3.60 (d, 1H, ²*J* = 10.6 Hz, -CCH₂O),

3.56 (d, 1H, $^2J = 10.6$ Hz, $-CCH_2O-$), 2.60 – 2.64 (m, 1H, $-CHC(CH_3)_2$), 2.07 (d, 1H, $J = 18.0$ Hz), 2.42 – 2.37 (m, 1H), 2.12 – 1.96 (m, 3H), 1.84 (d, 1H, $J = 18.3$ Hz), 1.38 – 1.34 (m, 2H), 1.07 (s, 3H, $-CH_3$), 0.96 (s, 3H, $-CH_3$) ppm. ^{13}C NMR (125.76 MHz, $CDCl_3$): δ 20.3, 20.7, 25.2, 26.7, 43.5, 43.8, 47.0, 61.3, 66.4, 72.5, 116.3, 135.0, 217.6 ppm. MS (EI): m/z (%) 41 (52), 55 (17), 67 (24), 81 (25), 95 (38), 109 (100), 123 (20), 151 (52) $[M-(C_3H_5O)]^+$, 167 (6) $[M-(C_3H_5)]^+$, 208 (13) $[M]^+$. HR-MS (EI, m/z): calc. for $C_{13}H_{20}O_2$ $[M]$: 208.1463, found: 208.1451. ATR-FTIR: ν 2959, 2879, 1732, 1647, 1454, 1417, 1389, 1362, 1348, 1274, 1234, 1193, 1169, 1134, 1093, 1046, 1016, 988, 917, 857, 769, 723. Anal. calcd for $C_{13}H_{20}O_2$, C: 74.96 H: 9.68. Found, C: 75.10 H: 9.74.

(R)-allyl 2-(1,2,2-trimethyl-3-methylenecyclopentyl)acetate (31):

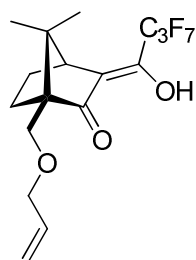


Sodium hydride (2.88 g, 120 mmol) was suspended in 20 mL anhydrous dimethylformamide in a three-necked flask under argon equipped with a reflux condenser and allylic alcohol (10.22 g, 176 mmol, 12.0 mL), dissolved in 20 mL anhydrous dimethylformamide, was added dropwise. The mixture was stirred at room temperature for two hours. To this mixture (1*S*, 4*R*)-10-iodocamphor **28** (33.38 g, 120 mmol) dissolved in 60 mL anhydrous dimethylformamide was added dropwise and stirred at 80 °C for 24 h. Afterwards water (100 mL) was added and the mixture was extracted with 3×100 mL diethyl ether. The organic layers were combined, dried over magnesium sulfate and the solvent carefully evaporated under reduced pressure (no high-vacuum!) to yield the title compound **31** as a colorless oil (14.4 g, 65 mmol, 54%). 1H NMR (300.13 MHz, $CDCl_3$): δ 6.01 – 5.88 (m, 1H, $-OCH_2CH-$), 5.34 (dt, 1H, $J = 17.3$ Hz, $^2J = 1.5$ Hz, methylene- CH_{2trans}), 5.26 (dt, 1H, $J = 10.3$ Hz, $^2J = 1.3$ Hz, methylene- CH_{2cis}), 3.80 (dt, 2H, $J = 6.4$ Hz, $^2J = 2.1$ Hz, $-CH_2CC(CH_3)-$), 4.60 (dt, 2H, $J = 5.8$, $J = 1.3$ Hz, $-CH_2O-$), 2.53 – 2.39 (m, 4H, $-CH_2CHCH_2-$), 2.21 – 2.12 (m, 1H, $-CH_2CHCH_2-$), 2.08 – 1.98 (m, 1H, $-(CO)CH_2CHCH_2-$), 1.44 – 1.34 (m, 1H, $-(CO)CH_2CHCH_2-$) 1.09 (s, 3H, $-CH_3$), 0.86 (s, 3H, $-CH_3$) ppm. ^{13}C NMR (75.47 MHz, $CDCl_3$): δ 23.4, 26.5, 28.3, 30.4, 35.2, 43.8, 46.5, 65.0, 103.6, 118.2, 132.2, 161.2, 173.3 ppm. LR-MS (EI, m/z): 41 (35), 55 (9), 67 (17), 79 (12), 93 (30), 108 (100), 121 (20), 133 (4), 150 (7), 167 (32) $[M-(C_3H_5)]^+$, 193 (10) $[M-(CH_3)]^+$, 208 (4) $[M]^+$. HR-MS (EI, m/z): calc. for $C_{13}H_{20}O_2$ $[M]$: 208.1463, found: 208.1462.

(1*R*, 4*S*)-3-trifluoromethanoyl-10-allyloxycamphor (32):

To a suspension of lithium hydride (160 mg, 20.1 mmol) in 50 mL anhydrous THF in a three-necked flask under argon equipped with a reflux condenser was dropwise added a solution of 10-allyloxycamphor **21** (2.000 g, 9.6 mmol) in 30 mL anhydrous tetrahydrofuran at 0 °C. The mixture was stirred for 15 min at this temperature, was then allowed to warm up to room temperature and stirred for further 15 min.

Afterwards the mixture was heated at reflux temperature for 8 h until the color of the solution turned to pale orange. The mixture was cooled to room temperature and trifluoromethyl ester (2.828 g, 22.1 mmol, 2.22 mL) dissolved in 40 mL anhydrous THF was added dropwise over a period of 30 min. After stirring for 20 min the mixture was heated at reflux temperature for 12 – 14 h. Progress of the reaction was monitored by gas-chromatography of pH neutral samples and if necessary additional trifluoromethyl ester (bp: 316 K) was added. After completion of the reaction 10 mL of conc. hydrochloric acid was added, followed by addition of water (500 mL) while stirring. The mixture was extracted with 3×100 mL diethyl ether, the organic layers were combined, washed with 2×200 mL water and brine. The organic phase was dried over sodium sulfate and the solvent was evaporated under reduced pressure. Drying *in vacuo* at elevated temperatures over a period of three days yielded analytical pure (1*R*, 4*S*)-3-trifluoromethanoyl-10-allyloxycamphor (**32**, 2.75 g, 9.0 mmol, 94%) as a colorless, viscous oil. ¹H NMR (500.13 MHz, CDCl₃): δ 11.4 (bs, 1H, OH), 5.93 – 5.86 (m, 1H, -OCH₂CH-), 5.28 (dd, 1H, *J* = 17.4 Hz, ²*J* = 1.6 Hz, methylene-CH₂*trans*), 5.18 (dd, 1H, *J* = 10.5 Hz, ²*J* = 1.5 Hz, methylene-CH₂*cis*), 4.00 (d, 2H, *J* = 5.4 Hz, -OCH₂CH-), 3.65 (d, 1H, ²*J* = 10.4 Hz, -CCH₂O-), 3.63 (d, 1H, ²*J* = 10.5 Hz, -CCH₂O-), 2.85 – 2.82 (m, 1H, -CHC(CH₃)₂), 2.16 – 2.08 (m, 2H), 1.50 – 1.39 (m, 2H), 1.07 (s, 3H, -CH₃), 0.97 (s, 3H, -CH₃) ppm. ¹³C NMR (125.76 MHz, CDCl₃): δ 19.4, 21.5, 25.7, 26.5, 47.9, 49.2, 61.6, 65.4, 72.6, 116.1, 116.7, 117.8 (q, *J* = 2.5 Hz, -CCCF₃), 119.4 (q, *J* = 276.6 Hz, -CF₃), 134.7, 148.5 (q, *J* = 37.2 Hz, -CCF₃), 212.2 ppm. ¹⁹F NMR (282.76 MHz, CDCl₃): δ -70.2 ppm. MS (EI): *m/z* (%) 177 (21), 191 (17), 205 (17), 233 (100) [M-(C₄H₇O)]⁺, 247 (15) [M-(C₃H₅O)]⁺, 263 (6) [M-(C₃H₅)]⁺, 304 (7) [M]⁺. HR-MS (EI, *m/z*): calc. for C₁₅H₁₉F₃O₃ [M]: 304.1286, found: 301.1288. ATR-FTIR: ν 2963, 2874, 1702, 1648, 1703, 1648, 1507, 1476, 1454, 1419, 1393, 1374, 1363, 1348, 1313, 1293, 1266, 1222, 1188, 1140, 1067, 1004, 989, 924, 891, 854, 816, 809, 753, 717. Anal. calcd for C₁₅H₁₉F₃O₃, C: 59.20 H: 6.29. Found, C: 59.24 H: 6.44.

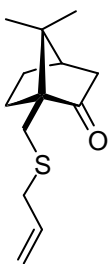
(1*R*, 4*S*)-3-heptafluorobutanoyl-10-allyloxycamphor (33):

To a suspension of lithium hydride (160 mg, 20.1 mmol) in 50 mL anhydrous tetrahydrofuran in a three-necked flask under argon equipped with a reflux condenser was dropwise added a solution of 10-allyloxycamphor **21** (2.000 g, 9.6 mmol) in 30 mL anhydrous tetrahydrofuran at 0 °C. The mixture was stirred for 15 min at this temperature, was then allowed to warm up to room temperature and stirred for further 15 min. Afterwards the mixture was heated at reflux temperature for 10 h until the color of the solution turned to pale orange. The mixture was cooled to room temperature and ethyl heptafluorobutyrate (5.346 g, 22.1 mmol, 3.83 mL) dissolved in 40 mL anhydrous tetrahydrofuran was added dropwise over a period of 30 min. After stirring for 20 min the mixture was heated at reflux temperature for 14 – 18 h. Progress of the reaction was monitored by gas-chromatography of pH neutral samples. After completion of the reaction 10 mL of conc. hydrochloric acid was added, followed by addition of water (500 mL) while stirring. The mixture was extracted with 3×100 mL diethyl ether, the organic layers were combined, washed with 2×200 mL water and brine. The organic phase was dried over sodium sulfate and the solvent was evaporated under reduced pressure. Drying *in vacuo* at elevated temperatures over a period of three days, followed by distillation at 120 °C under high vacuum (small-sized distillation apparatus equipped with a short connecting tube) yielded pure (1*R*, 4*S*)-3-heptafluorobutanoyl-10-allyloxycamphor (**33**, 2.898 g, 7.2 mmol, 75%) as a colorless, viscous oil. ¹H NMR (500.13 MHz, CDCl₃): δ 11.69 (bs, 1H, OH), 5.93 – 5.86 (m, 1H, -OCH₂CH), 5.28 (dd, 1H, *J* = 17.3 Hz, ²*J* = 1.5 Hz, methylene-CH_{2trans}), 5.18 (dd, 1H, *J* = 10.5 Hz, ²*J* = 1.5 Hz, methylene-CH_{2cis}), 4.00 (d, 2H, *J* = 5.2 Hz, -OCH₂CH), 3.66 (d, 1H, ²*J* = 10.7 Hz, -CCH₂O-), 3.63 (d, 1H, ²*J* = 10.7 Hz, -CCH₂O-), 2.82 – 2.79 (m, 1H, -CHC(CH₃)₂), 2.15 – 2.09 (m, 2H), 1.49 – 1.42 (m, 2H), 1.07 (s, 3H, -CH₃), 0.96 (s, 3H, -CH₃) ppm. ¹³C NMR (125.76 MHz, CDCl₃): δ 19.4, 21.4, 25.6, 26.4, 48.2, 49.3, 61.5, 65.4, 72.6, 116.7, 120.6, 134.7, 148.7 (dd, *J* = 29.5 Hz, *J* = 29.7 Hz, -CCF₂CF₂CF₃), 212.0 ppm. ¹⁹F NMR (282.76 MHz, CDCl₃): δ -127.3 – -127.4 (m, -CF₂CF₂CF₃), -119.4 (qdd, *J* = 8.8 Hz, *J* = 2.0 Hz, *J* = 283.4 Hz, -CF₂CF₂CF₃), -117.9 (qd, *J* = 8.8 Hz, *J* = 283.4 Hz, -CF₂CF₂CF₃), -119.4 (t, *J* = 8.8 Hz, -CF₂CF₂CF₃) ppm. MS (EI): *m/z* (%) 177 (7), 235 (5), 291 (9), 305 (10), 333 (100) [M-(C₄H₇O)]⁺, 347 (14) [M-(C₃H₅O)]⁺, 363 (4) [M-(C₃H₅)]⁺, 404 (16) [M]⁺. HR-MS (EI, *m/z*): calc. for C₁₇H₁₉F₇O₃ [M]: 404.1222, found: 404.1212. ATR-FTIR: ν 2963, 2874, 1699, 1642, 1479, 1454, 1422, 1393, 1374, 1345, 1315, 1292, 1215, 1185, 1165, 1118, 1097, 1067, 1023, 958, 920, 897, 886, 855, 813, 780, 743, 724. Anal. calcd for C₁₇H₁₉F₇O₃, C: 50.50 H: 4.74. Found, C: 51.05 H: 5.01.

(1S, 4R)-10-thiocamphor (29):

(1S)-10-camphorsulfonic acid (**16**, 50.0 g, 0.215 mol) and thionyl chloride (51.21 g, 0.430 mol, 31.3 mL) were placed in a three-necked flask equipped with a condenser under argon atmosphere and an exhaust line for direct gas-discharge into the fume hood. The reaction mixture was heated at 80 °C for 4 – 5 h until the evolution of hydrochloric acid and sulfur dioxide ceased.

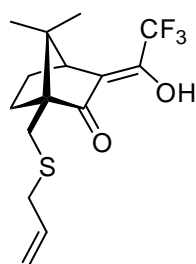
Afterwards thionyl chloride was removed under reduced pressure *in vacuo* at elevated temperature. To the crude 10-camphorsulfonic acid was added triphenylphosphine (169.2 g, 0.645 mol) together with a 1:4 mixture of water and dioxane and the suspension was stirred at reflux for 4 h. The suspension was allowed to cool down to room temperature, water (600 mL) was added and the mixture was extracted with 4×100 mL pentane. The organic layers were combined, washed several times with water (8×100 mL), followed by brine (2×25 mL) and dried over sodium sulfate. Evaporation of the solvent under reduced pressure and high vacuum yielded pure (1S, 4R)-10-thiocamphor (**29**, 42.1 g, 0.228, 94%) as colorless crystals. Mp. 55 – 57 °C. ¹H NMR (300.51 MHz, CDCl₃): δ 2.88 (d, 1H, *J* = 6.8 Hz, -CH₂SH), 2.83 (d, 1H, *J* = 6.8 Hz, -CH₂SH), 2.39 – 2.30 (m, 2H), 2.08 – 2.05 (m, 1H), 2.03 – 1.83 (m, 4H), 1.72 – 1.65 (m, 1H), 1.41 – 1.35 (m, 1H), 1.01 (s, 3H, -CH₃), 0.90 (s, 3H, -CH₃) ppm. ¹³C NMR (75.56 MHz, CDCl₃): δ 19.8, 20.3, 21.4, 26.6, 27.0, 43.2, 43.6, 47.8, 60.6, 217.8 ppm. MS (EI): *m/z* (%) 55 (18), 67 (30), 81 (47), 95 (42), 109 (50), 123 (37), 141 (34), 151(23) [M-(SH)]⁺, 169 (5) [M-(CH₃)]⁺, 184 (100) [M]⁺. Anal. calcd for C₁₀H₁₆OS, C: 65.17 H: 8.75. Found, C: 65.40 H: 8.76.

(1S, 4R)-10-allylmercaptocamphor (30):

To a suspension of sodium hydride (2.74 g, 114 mmol) in 250 mL anhydrous tetrahydrofuran was slowly added a solution of camphorthiol (**29**, 20.00 g, 109 mol) in 50 mL anhydrous tetrahydrofuran at 0 °C. After 30 min the mixture was allowed to warm up to room temperature and was then heated at reflux for 30 min. Afterwards the reddish mixture was cooled to 0 °C and allylbromide (13.39 g, 111 mmol, 9.58 mL), dissolved in 50 mL anhydrous tetrahydrofuran, was added dropwise. The reaction mixture was stirred for 30 min at room temperature and was then heated to 50 °C and maintained at this temperature for two hours. The mixture was cooled down to 0 °C, quenched with small amounts of ethanol (15 mL) and 400 mL of water was added. The solution was extracted with 4×100 mL pentane, the organic layers were combined, washed with 2×50 mL water and brine and dried over sodium sulfate. Evaporation of the solvent under reduced pressure, followed by high vacuum yielded analytical pure (1S, 4R)-10-allylmercaptocamphor (19.74 g, 88 mmol, 81%)

as a colorless oil. ^1H NMR (500.13 MHz, CDCl_3): δ 5.84 – 5.75 (m, 1H, $-\text{SCH}_2\text{CH}-$), 5.15 – 5.09 (m, 2H, methylene- CH_2), 3.20 – 3.12 (m, 2H), 2.74 (d, 1H, $^2J = 13.1$ Hz, $-\text{CCH}_2\text{S}-$), 2.47 (d, 1H, $^2J = 13.0$ Hz, $-\text{CCH}_2\text{S}-$), 2.39 – 2.34 (m, 1H), 2.08 – 1.96 (m, 3H), 1.86 (d, 1H, $J = 18.4$ Hz), 1.53 – 1.48 (m, 1H), 1.39 – 1.35 (m, 1H), 1.04 (s, 3H, $-\text{CH}_3$), 0.90 (s, 3H, $-\text{CH}_3$) ppm. ^{13}C NMR (125.76 MHz, CDCl_3): δ 20.20, 20.2, 26.8, 26.9, 27.7, 37.0, 43.1, 43.5, 47.8, 60.9, 117.1, 134.4, 217.5 ppm. MS (EI): m/z (%) 55 (28), 67 (30), 81 (39), 95 (14), 109 (39), 123 (20), 151 (16) $[\text{M}-(\text{C}_3\text{H}_5\text{S})]^+$, 168 (13), 183 (62) $[\text{M}-(\text{C}_3\text{H}_5)]^+$, 224 (100) $[\text{M}]^+$. HR-MS (EI, m/z): calc. for $\text{C}_{13}\text{H}_{20}\text{OS}$ $[\text{M}]$: 224.1325, found: 224.1237. ATR-FTIR: ν 3080, 2958, 2887, 1725, 1634, 1469, 1453, 1416, 1389, 1372, 1317, 1298, 1281, 1227, 1197, 1159, 1128, 1101, 1062, 1049, 1026, 989, 964, 914, 866, 851, 754. Anal. calcd for $\text{C}_{13}\text{H}_{20}\text{OS}$, C: 69.59 H: 8.97. Found, C: 69.54 H: 8.97.

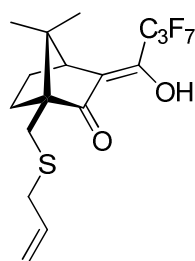
(1*S*, 4*S*)-3-trifluoromethanoyl-10-allylmercaptocamphor (34):



Lithium hydride (149 mg, 18.7 mmol) in 60 mL anhydrous tetrahydrofuran was placed in a three-necked flask under argon equipped with a reflux condenser and a solution of 10-allylmercaptocamphor **30** (2.000 g, 8.9 mmol) in 40 mL anhydrous tetrahydrofuran was added dropwise at 0 °C. After stirring for 15 min the suspension was allowed to warm up to room temperature and stirred for further 15 min. Afterwards the mixture was heated at reflux temperature for 24 h until the color of the solution turned to pale orange. The mixture was cooled to room temperature and trifluoromethyl ester (2.630 g, 20.5 mmol, 2.07 mL) dissolved in 30 mL anhydrous tetrahydrofuran was added dropwise over a period of 30 min. After stirring for 20 min the mixture was heated at reflux temperature for 12 – 14 h. Progress of the reaction was monitored by gas-chromatography of pH neutral samples and if necessary additional trifluoromethyl ester (bp: 316 K) was added. After completion of the reaction 10 mL of conc. hydrochloric acid was added, followed by addition of water (500 mL) while stirring. The mixture was extracted with 3×100 mL diethyl ether, the organic layers were combined, washed with 2×200 mL water and brine. The organic phase was dried over sodium sulfate and the solvent was evaporated under reduced pressure. Drying *in vacuo* at elevated temperatures over a period of three days yielded analytical pure (1*S*, 4*S*)-3-trifluoromethanoyl-10-allylmercaptocamphor (**34**, 2.693 g, 8.4 mmol, 94%) as a colorless oil. ^1H NMR (300.08 MHz, CDCl_3): δ 11.43 (bs, 1H, OH), 5.87 – 5.74 (m, 1H, $-\text{SCH}_2\text{CH}-$), 5.17 – 5.11 (m, 2H, methylene- CH_2), 3.26 – 3.13 (m, 2H), 2.87 – 2.83 (m, 1H), 2.80 (d, 1H, $^2J = 13.3$ Hz, $-\text{CCH}_2\text{S}-$), 2.51 (d, 1H, $^2J = 13.2$ Hz, $-\text{CCH}_2\text{S}-$), 2.17 – 2.03 (m, 2H), 1.67 – 1.58 (m, 1H), 1.50 – 1.44 (m, 1H), 1.04 (s, 3H, $-\text{CH}_3$), 0.91 (s, 3H, $-\text{CH}_3$) ppm. ^{13}C NMR

(75.46 MHz, CDCl_3): δ 19.3, 20.9, 26.5, 26.8, 27.4, 36.9, 47.6, 50.1, 61.3, 117.4, 121.1 ($-\text{CF}_3$), 134.2, 148.4 (m, $J = 37.0$ Hz, $-\text{CCF}_3$), 212.4 ppm. ^{19}F NMR (282.76 MHz, CDCl_3): δ -70.1 ppm. MS (EI): m/z (%) 191 (15), 219 (21), 233 (24) $[\text{M}-(\text{C}_4\text{H}_7\text{S})]^+$, 247 (34) $[\text{M}-(\text{C}_3\text{H}_5\text{S})]^+$, 261 (27), 279 (56) $[\text{M}-(\text{C}_3\text{H}_5)]^+$, 320 (100) $[\text{M}]^+$. HR-MS (EI, m/z): calc. for $\text{C}_{15}\text{H}_{19}\text{F}_3\text{O}_2\text{S}$ $[\text{M}]$: 320.1058, found: 320.1068. ATR-FTIR: ν 2962, 2915, 1702, 1652, 1479, 1453, 1428, 1405, 1393, 1975, 1316, 1267, 1224, 1187, 1123, 1112, 1055, 1021, 1004, 990, 973, 952, 916, 869, 888, 748, 710. Anal. calcd for $\text{C}_{15}\text{H}_{19}\text{F}_3\text{O}_2\text{S}$, C: 56.24 H: 5.98. Found, C: 56.28 H: 6.09.

(1*S*, 4*S*)-3-heptafluorobutanoyl-10-allylmercaptocamphor (35):

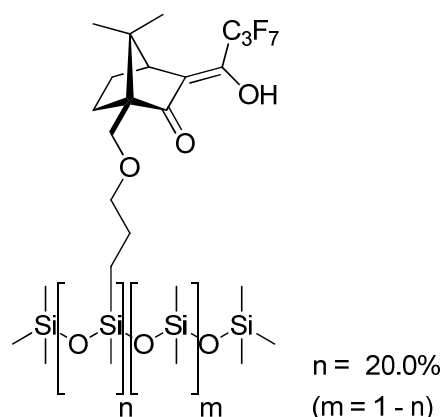


Lithium hydride (149 mg, 18.7 mmol) in 50 mL anhydrous tetrahydrofuran was placed in a three-necked flask under argon equipped with a reflux condenser and a solution of 10-allylmercaptocamphor **30** (2.000 g, 8.9 mmol) in 40 mL anhydrous tetrahydrofuran was added dropwise at 0 °C. After stirring for 15 min the suspension was allowed to warm up to room temperature and stirred for further 15 min. Afterwards the mixture was heated at reflux temperature for 24 h until the color of the solution turned to pale orange. The mixture was cooled to room temperature and ethyl heptafluorobutyrate (4.963 g, 20.5 mmol, 3.56 mL) dissolved in 30 mL anhydrous tetrahydrofuran was added dropwise over a period of 30 min. After stirring for 20 min the mixture was heated at reflux temperature for 14 – 18 h. Progress of the reaction was monitored by gas-chromatography of pH neutral samples. After completion of the reaction 10 mL of conc. hydrochloric acid was added, followed by addition of water (500 mL) while stirring. The mixture was extracted with 3×100 mL diethyl ether, the organic layers were combined, washed with 2×200 mL water and brine. The organic phase was dried over sodium sulfate and the solvent was evaporated under reduced pressure. Drying *in vacuo* at elevated temperatures over a period of three days, followed by distillation at 120 °C under high vacuum (small-sized distillation apparatus equipped with a short connecting tube) yielded pure (1*S*, 4*S*)-3-heptafluorobutanoyl-10-allylmercaptocamphor (**35**, 2.893 g, 6.9 mmol, 77%) as a colorless, viscous oil. ^1H NMR (500.13 MHz, CDCl_3): δ 11.68 (bs, 1H, OH), 5.84 – 5.76 (m, 1H, $-\text{SCH}_2\text{CH}-$), 5.16 – 5.12 (m, 2H, methylene- CH_2), 3.24 – 3.16 (m, 2H), 2.83 – 2.81 (m, 1H), 2.80 (d, 1H, $^2J = 13.2$ Hz, $-\text{CCH}_2\text{S}-$), 2.51 (d, 1H, $^2J = 13.2$ Hz, $-\text{CCH}_2\text{S}-$), 2.14 – 2.06 (m, 2H), 1.65 – 1.60 (m, 1H), 1.49 – 1.46 (m, 1H), 1.04 (s, 3H, $-\text{CH}_3$), 0.89 (s, 3H, $-\text{CH}_3$) ppm. ^{13}C NMR (125.76 MHz, CDCl_3): δ 19.3, 20.8, 26.5, 26.8, 27.4, 37.0, 43.3 (d, $J = 47.7$ Hz), 47.9, 50.1, 61.2, 117.4, 120.1 ($-\text{CF}_3$), 134.2, 148.8 (dd, $J = 29.4$ Hz, $J = 29.5$ Hz, $-\text{CCF}_2\text{CF}_2\text{CF}_3$), 212.2 ppm. ^{19}F NMR (282.46 MHz, CDCl_3): δ -

127.4 (s, $-\text{CF}_2\text{CF}_2\text{CF}_3$), -119.4 (qd, $J = 9.0 \text{ Hz}$, $J = 283.1 \text{ Hz}$, $-\text{CF}_2\text{CF}_2\text{CF}_3$), -117.9 (qd, $J = 9.0 \text{ Hz}$, $J = 283.5 \text{ Hz}$, $-\text{CF}_2\text{CF}_2\text{CF}_3$), -80.6 (t, $J = 8.8 \text{ Hz}$, $-\text{CF}_2\text{CF}_2\text{CF}_3$) ppm. MS (EI): m/z (%) 251 (7), 291 (12), 305 (9) 319 (16), 333 (19) $[\text{M}-(\text{C}_4\text{H}_7\text{S})]^+$, 347 (32) $[\text{M}-(\text{C}_3\text{H}_5\text{S})]^+$, 379 (53) $[\text{M}-(\text{C}_3\text{H}_5)]^+$, 420 (100) $[\text{M}]^+$. HR-MS (EI, m/z): calc. for $\text{C}_{17}\text{H}_{19}\text{F}_7\text{O}_2\text{S}$ $[\text{M}]$: 420.0994, found: 420.0999. ATR-FTIR: ν 2963, 2916, 1743, 1700, 1639, 1479, 1454, 1429, 1405, 1394, 1375, 1338, 1312, 1292, 1258, 1215, 1183, 1162, 1110, 1099, 1058, 1025, 1007, 991, 973, 946, 918, 881, 813, 742, 729. Anal. calcd for $\text{C}_{17}\text{H}_{19}\text{F}_7\text{O}_2\text{S}$, C: 48.57 H: 4.56. Found, C: 48.81 H: 4.86.

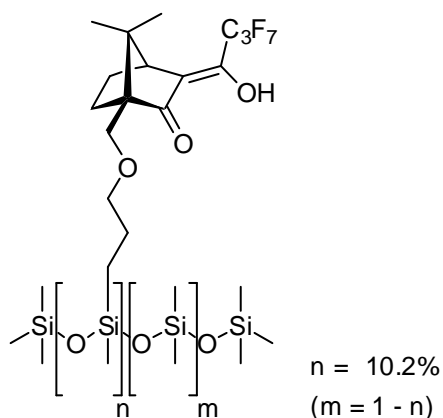
General procedure for the hydrosilylation of (1*R*, 4*S*)-3-heptafluorobutanoyl-10-allyloxycamphor on polysiloxanes: Hydridomethylpolysiloxane (HMPS, 0.17 – 0.36 mmol polymer, 3.5, 10.2 or 20.0% SiH content) was dissolved in 40 mL anhydrous toluene under an argon atmosphere. To the solution was added (1*R*, 4*S*)-3-heptafluorobutanoyl-10-allyloxycamphor (**33**) (for exact amounts *cf.* experimental details of each compound) and five drops (app. 50 mg, 0.1 mg “Pt”, 5.1×10^{-4} mmol “Pt”, 0.05 mol%) of platinum-1,1,3,3-tetramethyl-1,3-divinylidisiloxane (*Karstedt's* catalyst, 2%wt “Pt” in toluene). The solution was stirred for 5 h at room temperature under ultrasonic (control of temperature!) followed by 36 h starting at room temperature reaching 70 °C after 10 h. The reaction progress was monitored by ^1H NMR measurements and additional (1*R*, 4*S*)-3-heptafluorobutanoyl-10-allyloxycamphor (**33**) or HMPS was added until all SiH- and all allylic proton signals disappeared indicating full conversions of starting materials. After completion of the reaction the solvent was evaporated under reduced pressure. The crude product was dissolved in 25 mL of dichloromethane, filtered (pore size $\phi = 0.45 \mu\text{m}$) and 5 mL of methanol and active charcoal were added. The mixture was stirred for 24 h at reflux temperature, filtered (pore size $\phi = 0.45 \mu\text{m}$) and the solvents were evaporated under reduced pressure. Column chromatography (silica, height $\uparrow = 19.0 \text{ cm}$, diameter $\phi = 1.5 \text{ cm}$, dichloromethane/ethanol = 98:2) of the crude polymer yielded the analytical pure (1*R*, 4*S*)-3-heptafluorobutanoyl-10-allyloxycamphor immobilized on polysiloxane. For ease of reproduction the following amounts of starting materials proved to be necessary for complete immobilization and full consumption of starting material [23, 49 and 92 mg (1*R*, 4*S*)-3-heptafluorobutanoyl-10-allyloxycamphor (**33**) per 100 mg of HMPS (3.5%, 10.2%, 20.0% SiH content)].

[(1*R*, 4*S*)-3-heptafluorobutanoyl-10-propoxycamphor]_{20.0%}-polysiloxane (38**):**



The compound was prepared according to the general procedure for immobilization of (1*R*, 4*S*)-3-heptafluorobutanoyl-10-allyloxycamphor (**33**) on polysiloxane. Therefore, hydridomethylpolysiloxane (523 mg, 0.174 mmol polymer, 20.0% SiH content) and (480 mg, 0.129 mmol) (1*R*, 4*S*)-3-heptafluorobutanoyl-10-allyloxycamphor (**33**) were reacted and purified by the given procedure to yield 735 mg (73%) [(1*R*, 4*S*)-3-heptafluorobutanoyl-10-propoxycamphor]_{20.0%}-polysiloxane (**38**) as a colorless, viscous oil. ¹H NMR (500.13 MHz, CDCl₃): δ 11.70 (bs, 1H, OH), 3.63 (d, 1H, *J* = 10.5 Hz, -CCH₂O-), 3.61 (d, 1H, *J* = 10.5 Hz, -CCH₂O-), 3.40 (dt, 2H, *J* = 1.8 Hz, *J* = 6.6 Hz, -OCH₂CH₂-), 2.82 – 2.78 (m, 1H, -CHC(CH₃)₂), 2.15 – 2.08 (m, 2H, -OCH₂CH₂-), 1.61 – 1.54 (m, 2H, -CHCH₂-), 1.47 – 1.39 (m, 2H, -CHCH₂CH₂-), 1.06 (s, 3H, -CH₃), 0.95 (s, 3H, -CH₃), 0.91 (t, 2H, *J* = 7.4 Hz, -SiCH₂-), 0.56 – 0.46 (m, 0.4H, -Si(CH₃)_[1-n]), 0.12 – 0.04 (m, 19H, -O(CH₃)_[1-n]Si(CH₃)_[1-n](CH₃)_[n](hfc)_[n]) ppm. ¹³C NMR (125.76 MHz, CDCl₃): δ 0.8, 1.0, 1.8, 1.6, 19.4, 21.4, 22.8, 25.5, 26.4, 48.2, 49.3, 61.6, 65.9, 73.5, 111.0 (dd, *J* = 32.0 Hz, *J* = 29.8 Hz, -CF₂CF₂CF₃), 116.6 (d, *J* = 32.0 Hz, -CF₂CF₂CF₃), 118.6 (d, *J* = 32.0 Hz, -CF₂CF₂CF₃), 120.7, 148.6 (dd, *J* = 26.1 Hz, *J* = 26.2 Hz, -CCF₂CF₂CF₃), 212.0 ppm. ATR-FTIR: ν 2963, 2867, 1735, 1701, 1642, 1507, 1580, 1457, 1392, 1378, 1344, 1315, 1259, 1229, 1216, 1186, 1164, 1068, 1091, 1015, 979, 957, 920, 896, 886, 841, 795, 744, 723, 707.

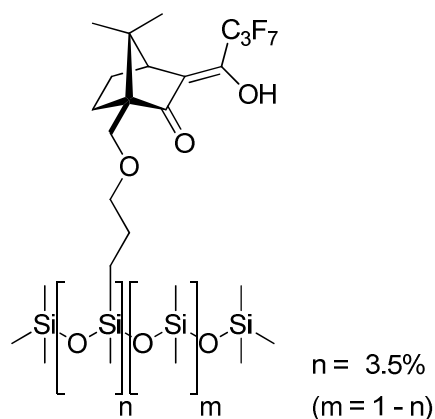
[(1*R*, 4*S*)-3-heptafluorobutanoyl-10-propoxycamphor]_{10.2%}-polysiloxane (37**):**



The compound was prepared according to the general procedure for immobilization of (1*R*, 4*S*)-3-heptafluorobutanoyl-10-allyloxycamphor (**33**) on polysiloxane. Therefore hydridomethylpolysiloxane (1092 mg, 0.364 mmol polymer, 10.2% SiH content) and (532 mg, 1.316 mmol) (1*R*, 4*S*)-3-heptafluorobutanoyl-10-allyloxycamphor (**33**) were reacted and purified by the given procedure to yield 605 mg (73%) [(1*R*, 4*S*)-3-heptafluorobutanoyl-10-propoxycamphor]_{10.2%}-polysiloxane (**37**) as a colorless oil. Analytical data is in agreement to polymer-bound [(1*R*, 4*S*)-3-heptafluorobutanoyl-10-propoxycamphor] on polysiloxane (hfc content 20.0%). ATR-FTIR: ν 2962, 2879, 1734, 1700, 1654, 1643, 1457, 1393, 1374, 1344, 1315, 1258, 1231, 1218, 1185,

1164, 1067, 1011, 959, 921, 897,793, 744, 724, 704.

[(1*R*, 4*S*)-3-heptafluorobutanoyl-10-propoxycamphor]_{3.5%}-polysiloxane (36):

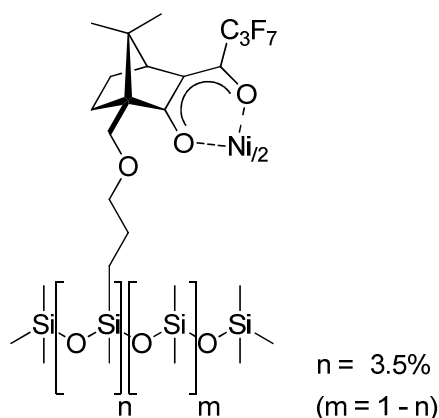


The compound was prepared according to the general procedure for immobilization of (1*R*, 4*S*)-3-heptafluorobutanoyl-10-allyloxycamphor (**33**) on polysiloxane. Therefore, hydridomethylpolysiloxane (560 mg, 0.187 mmol polymer, 3.5% SiH content) and (131 mg, 0.324 mmol) (1*R*, 4*S*)-3-heptafluorobutanoyl-10-allyloxycamphor (**33**) were reacted and purified by the given procedure to yield 605 mg (88%) [(1*R*, 4*S*)-3-heptafluorobutanoyl-10-propoxycamphor]_{3.5%}-polysiloxane (**36**) as a colorless oil. Analytical data is in agreement to polymer-bound [(1*R*, 4*S*)-3-heptafluorobutanoyl-10-propoxycamphor] on polysiloxane (hfc content 20.0%). ATR-FTIR: ν 2962, 2905, 1735, 1700, 1415, 1353, 1257, 1231, 1216, 1011, 833, 788, 699.

General procedure for the preparation of nickel(II)-bis[(1*R*, 4*S*)-3-heptafluorobutanoyl-10-propoxycamphorate]_{20.0%}-polysiloxane – *Chirasil Nickel-OC₃*: Metal incorporation was accomplished using a modified procedure of *M. Fluck*.^[83] A two phase solution of ligand polymer (100 – 390 mg, 3.5, 10.2 or 20.0% (1*R*, 4*S*)-3-heptafluorobutanoyl-10-propoxycamphor content) in a mixture of anhydrous *n*-heptane/methanol (3:2, 100 mL) was stirred for 1 h at room temperature and an additional hour at reflux temperature upon which the solvents became miscible. The ligand polymer dissolved and cooling back to room temperature resulted in separation of the two phases. This step is recommended to furnish clean polymer dissolution and polymer-purification prior to metal incorporation. To the solutions was added nickel(II) acetate tetrahydrate (for exact amounts cf. experimental details of each compound) and the mixture was stirred at room temperature for 1 h and an additional hour at reflux temperature. The solution was allowed to cool down to room temperature resulting in phase re-separation. Metal incorporation can be monitored by color change of the polymer-containing *n*-heptane phase from colorless to green as well as decolorization of the nickel-salt containing methanol phase. The *n*-heptane phase was decanted off and the methanol layer was extracted once with 30 mL *n*-heptane. The organic layers were combined, the solvent was evaporated under reduced pressure and the residue dissolved in 50 mL *n*-pentane. The organic phase was washed with 5×100 mL water and dried over small amounts of magnesium sulfate. Evaporation of the solvent and drying in vacuo for three days yielded

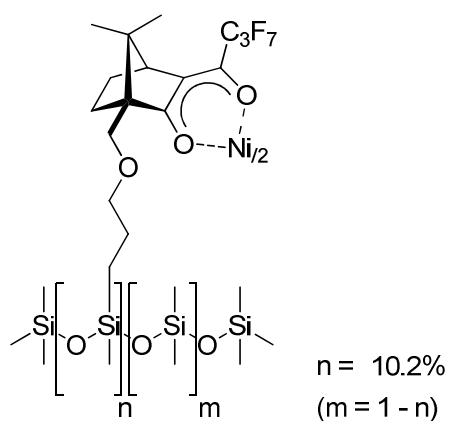
nickel(II)-bis[(1*R*, 4*S*)-3-heptafluorobutanoyl-10-propoxycamphorate]-polysiloxanes (*Chirasil Nickel-OC₃*) as green, viscous oils.

Nickel(II)-bis[(1*R*, 4*S*)-3-heptafluorobutanoyl-10-propoxycamphorate]_{3.5%}-polysiloxane – *Chirasil Nickel-OC₃* 3.5% (39):



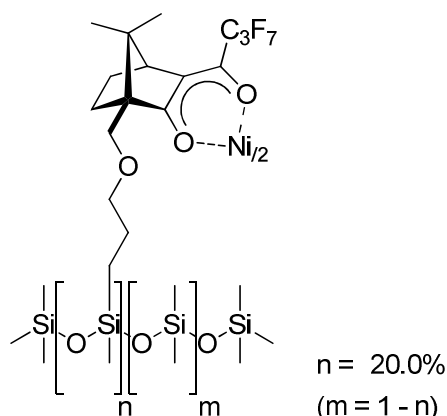
This compound was prepared according to the general procedure for the preparation of *Chirasil Nickel-OC₃*. Therefore, 298 mg ligand polymer and 15 mg (0.060 mmol) nickel(II) acetate tetrahydrate were reacted and purified by the given procedure to yield 277 mg (92%) nickel(II)-bis[(1*R*, 4*S*)-3-heptafluorobutanoyl-10-propoxycamphorate]_{3.5%}-polysiloxane as a pale green oil. ATR-FTIR: ν 2962, 2905, 1737, 1654, 1637, 1481, 1447, 1413, 1344, 1257, 1231, 1216, 1182, 1010, 835, 788, 700.

Nickel(II)-bis[(1*R*, 4*S*)-3-heptafluorobutanoyl-10-propoxycamphorate]_{10.2%}-polysiloxane – *Chirasil Nickel-OC₃* 10.2% (40):



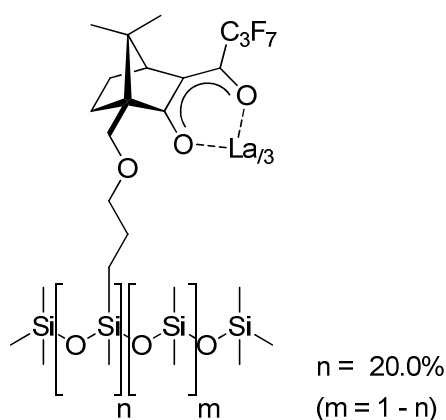
This compound was prepared according to the general procedure for the preparation of *Chirasil Nickel-OC₃*. Therefore, 390 mg ligand polymer and 56 mg (0.225 mmol) nickel(II) acetate tetrahydrate were reacted and purified by the given procedure to yield 360 mg (89%) nickel(II)-bis[(1*R*, 4*S*)-3-heptafluorobutanoyl-10-propoxycamphorate]_{10.2%}-polysiloxane as a pale green oil. ATR-FTIR: ν 2962, 2906, 1739, 1640, 1627, 1576, 1512, 1481, 1445, 1412, 1373, 1345, 1258, 1230, 1216, 1183, 1075, 1010, 828, 788, 751, 702.

Nickel(II)-bis[(1*R*, 4*S*)-3-heptafluorobutanoyl-10-propoxycamphorate]_{20.0%}-polysiloxane – *Chirasil Nickel-OC₃* y _{20.0%} (41**):**



This compound was prepared according to the general procedure for the preparation of *Chirasil Nickel-OC₃*. Therefore, 190 mg ligand polymer and 53 mg (0.060 mmol) nickel(II) acetate tetrahydrate were reacted and purified by the given procedure to yield 173 mg (85%) nickel(II)-bis[(1*R*, 4*S*)-3-heptafluorobutanoyl-10-propoxycamphorate]_{20.0%}-polysiloxane as a green oil. ATR-FTIR: ν 2962, 2878, 1739, 1641, 1627, 1481, 1457, 1413, 1388, 1373, 1344, 1258, 1229, 1215, 1183, 1163, 1075, 1015, 918, 833, 789, 750, 703.

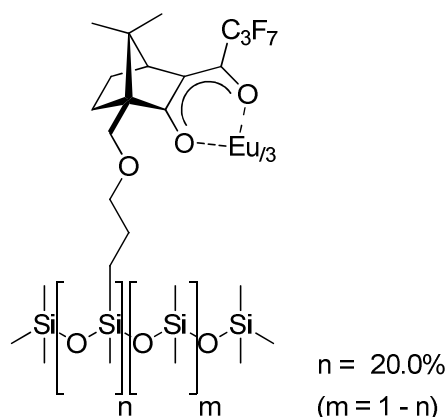
Lanthanum(III)-tris[(1*R*, 4*S*)-3-heptafluorobutanoyl-10-propoxycamphorate]_{20.0%}-polysiloxane – *Chirasil Lanthanum-OC₃* _{20.0%} (46**):**



Incorporation of lanthanum was accomplished following the standard procedure for *Chirasil Vanadyl-OC₃*. Vanadyl(IV) sulfate pentahydrate was replaced by lanthanum(III) acetate hydrate (87.6 mg, 0.226 mmol) and 200 mg ligand polymer and 0.50 mL (685 mg, 6.772 mmol) anhydrous, distilled triethylamine were used. Incorporation of lanthanum is indicated by colorchange of the *n*-heptane phase from colorless to an orange-red color. Work-up and purification including column chromatography as described for *Chirasil*

Vanadyl-OC₃ yielded 199 mg (86%) lanthanum(III)-tris[(1*R*, 4*S*)-3-heptafluorobutanoyl-10-propoxycamphorate]_{20.0%}-polysiloxane as an orange to red viscous oil. ATR-FTIR: ν 2962, 2879, 1687, 1684, 1645, 1525, 1480, 1455, 1413, 1387, 1372, 1344, 1258, 1229, 1214, 1197, 1184, 1161, 1074, 1014, 918, 838, 791, 748.

Europium(III)-tris[(1*R*, 4*S*)-3-heptafluorobutanoyl-10-propoxycamphorate]_{20.0%}-polysiloxane – *Chirasil Europium-OC₃* 20.0% (45):



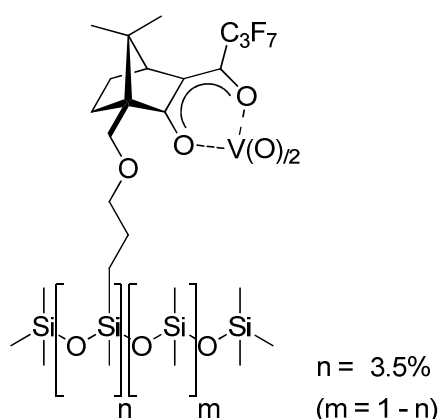
Europium was incorporated following the standard procedure for *Chirasil Vanadyl-OC₃*. Vanadyl(IV) sulfate pentahydrate was replaced by europium(III) acetate hydrate (78.8 mg, 0.196 mmol) and 212 mg ligand polymer and 0.50 mL (685 mg, 6.772 mmol) anhydrous, distilled triethylamine were used. Incorporation of lanthanum is indicated by color change of the *n*-heptane phase from colorless to a yellow color. Work-up and purification including column chromatography as described for *Chirasil Vanadyl-OC₃* yielded 193 mg

(80%) lanthanum(III)-tris[(1*R*, 4*S*)-3-heptafluorobutanoyl-10-propoxycamphorate]_{20.0%}-polysiloxane as an orange to yellow to pale orange viscous oil. ATR-FTIR: ν 2962, 2877, 1738, 1702, 1685, 16447, 1577, 1575, 1530, 1479, 1457, 1413, 1389, 1372, 1345, 1258, 1229, 1214, 1198, 1182, 1161, 1075, 7014, 917, 833, 791, 745, 703.

General procedure for the preparation of oxovanadium(IV)-bis[(1*R*, 4*S*)-3-heptafluorobutanoyl-10-propoxycamphorate]_{20.0%}-polysiloxane – *Chirasil Vanadyl-OC₃*:

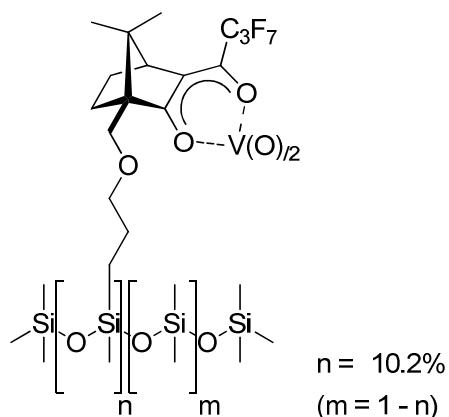
Incorporation of oxovanadium was accomplished using a modified procedure of *M. Fluck*.^[83] Ligand polymer (200 – 450 mg, 3.5, 10.2 or 20.0% (1*R*, 4*S*)-3-heptafluorobutanoyl-10-propoxycamphor content) was dissolved in a mixture of anhydrous *n*-heptane/methanol (3:2, 100 mL) and was stirred for 1 h at room temperature and one hour at reflux temperature upon which the solvents became miscible. This step is recommended to furnish clean polymer dissolution and polymer-purification prior to metal incorporation. Excess oxovanadium(IV) sulfate pentahydrate was added at room temperature and the mixture was stirred for 1 h (for exact amounts cf. experimental details of each compound). Afterwards the solution was heated at reflux temperature, anhydrous, distilled triethylamine was added and the solution was stirred for 3 – 4 h at this temperature. Reaction progress can be monitored by color change of the *n*-heptane phase from colorless to purple as well as decolorization of the vanadyl sulfate-salt containing methanol phase. Purification was accomplished following the work-up procedure including column chromatography as described for the preparation of *Chirasil Nickel-OC₃*. The oxovanadium(IV)-bis[(1*R*, 4*S*)-3-heptafluorobutanoyl-10-propoxycamphorate]-polysiloxanes (*Chirasil Vanadyl-OC₃*) were obtained as reddish-purple, viscous oils.

Oxovanadium(IV)-bis[(1*R*, 4*S*)-3-heptafluorobutanoyl-10-propoxycamphorate]_{3.5%}-poly-siloxane – *Chirasil Vanadyl-OC₃* 3.5% (42):



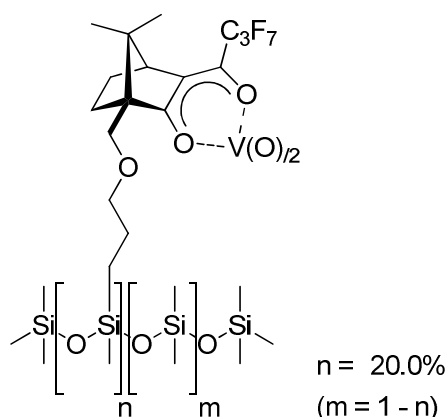
The compound was prepared according to the general procedure for the preparation of *Chirasil Vanadyl-OC₃*. Therefore, 200 mg ligand polymer, 270 mg (1.067 mmol, excess) vanadyl(IV) sulfate pentahydrate and 0.10 mL (138 mg, 1.364 mmol) triethylamine were reacted and purified by the given procedure to yield 157 mg (79%, corresponding to polymer starting material) oxovanadium(IV)-bis[(1*R*, 4*S*)-3-heptafluorobutanoyl-10-propoxycamphorate]_{3.5%}-poly-siloxane as a pale reddish-purple oil. ATR-FTIR: ν 2962, 2905, 1739, 1639, 1446, 1412, 1352, 1257, 1231, 1216, 1182, 1011, 834, 789, 701.

Oxovanadium(IV)-bis[(1*R*, 4*S*)-3-heptafluorobutanoyl-10-propoxycamphorate]_{10.2%}-poly-siloxane – *Chirasil Vanadyl-OC₃* 10.2% (43):



The compound was prepared according to the general procedure for the preparation of *Chirasil Vanadyl-OC₃*. Therefore, 450 mg ligand polymer, 1.750 g (6.917 mmol, excess) vanadyl(IV) sulfate pentahydrate and 0.33 mL (455 mg, 4.504 mmol) triethylamine were reacted and purified by the given procedure to yield 314 mg (70%, corresponding to polymer starting material) oxovanadium(IV)-bis[(1*R*, 4*S*)-3-heptafluorobutanoyl-10-propoxycamphorate]_{10.2%}-poly-siloxane as a reddish-purple oil. ATR-FTIR: ν 2962, 2905, 1739, 1685, 1638, 1576, 1560, 1517, 1446, 1413, 1373, 1346, 1258, 1231, 1217, 1184, 1197, 1011, 828, 789, 701.

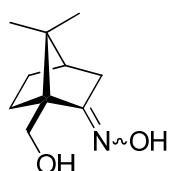
Oxovanadium(IV)-bis[(1*R*, 4*S*)-3-heptafluorobutanoyl-10-propoxycamphorate]_{20.0%}-poly-siloxane – *Chirasil Vanadyl-OC₃* 20.0% (44**):**



The compound was prepared according to the general procedure for the preparation of *Chirasil Vanadyl-OC₃*. Therefore, 230 mg ligand polymer, 1.760 g (6.957 mmol, excess) vanadyl(IV) sulfate pentahydrate and 0.33 mL (455 mg, 4.504 mmol) triethylamine were reacted and purified by the given procedure to yield 170 mg (74%, corresponding to polymer starting material) oxovanadium(IV)-bis[(1*R*, 4*S*)-3-heptafluorobutanoyl-10-propoxycamphorate]_{10.2%}-poly-siloxane as a reddish-purple, viscous oil. ATR-FTIR: ν 2962, 2875, 1737, 1702, 1700, 1686, 1635, 1521, 1479, 1457, 1414, 1389, 1373, 1346, 1258, 1230, 1217, 1197, 1185, 1165, 1013, 917, 829, 792.

General procedure for the preparation of oximes from ketones: To a solution of ketone (1.00 eq.) and pyridine (1.2 eq.) in ethanol was added hydroxylamine hydrochloride (1.75 eq.) and the mixture was stirred at reflux temperature for 4 – 5 h. The solvent was evaporated under reduced pressure, 10 mL of aqueous hydrochloric acid (1M) was added and the mixture was extracted with 3×50 – 100 mL dichloromethane. The combined organic layers were washed with 25 mL brine, the organic layer was separated and the aqueous layer was extracted with 2×50 – 100 mL dichloromethane. The combined organic layers were dried over sodium sulfate and the solvent was evaporated to yield the desired oximes.

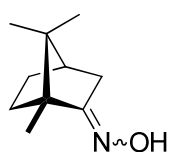
(1*S*, 4*R*)-10-hydroxycamphor oxime (52**):**



The title compound was synthesized using the general method for the preparation of oximes. (1*S*)-10-hydroxycamphor (**21**, 2.36 g, 14.0 mmol), hydroxylamine hydrochloride (1.70 g, 24.5 mmol) and pyridine (1.33 g, 16.8 mmol, 1.36 mL) were used and (1*S*, 4*R*)-10-hydroxycamphor oxime (**52**, 2.15 g, 11.7 mmol, 84%) was obtained as an off-white powder. Mp. 193 – 195 °C. ¹H NMR (300.51 MHz, CDCl₃): δ 0.91 (s, 3H, -CH₃), 0.95 (s, 3H, -CH₃), 1.31 – 1.08 (m, 1H, -CH₂CH₂-), 1.93 – 1.61 (m, 4H, -CH₂CH₂-, -CH₂CH₂-, CH₃CCH₂-), 2.05 (d, 1H, *J* = 17.8 Hz), 3.20 (bs, 0.6H, -OH), 3.65 (d, 1H, *J* = 11.6 Hz, -CH₂OH), 3.91 (d, 1H, *J* = 11.6 Hz, -CH₂OH), 8.01 (bs, 0.7H, NOH) ppm. ¹³C NMR (75.56 MHz, CDCl₃): δ 18.9,

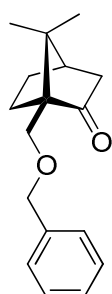
20.4, 26.9, 28.9, 33.0, 44.6, 48.1, 56.3, 61.8 ppm. MS (EI): m/z (%) 41 (31), 55 (16), 67 (22), 79 (13), 94 (19), 107 (9), 122 (15), 140 (100), 150 (8), 166 (32) $[M-OH]^+$, 183 (53) $[M]^+$. HR-MS (EI, m/z): calc. for $C_{10}H_{17}NO_2$ $[M]$: 183.1259, found: 183.1259. IR (KBr): ν 3278, 2959, 2873, 1745, 1685, 1604, 1443, 1384, 1370, 1322, 1299, 1281, 1259, 1239, 1221, 1199, 1181, 1165, 1098, 1076, 1054, 1040, 1017, 1002, 984, 973, 950, 924, 865, 854, 839, 809, 783, 765, 709.

(1*R*, 4*R*)-camphor oxime (**58**):



This is a known compound^[425] and was synthesized using the general method for the preparation of oximes. (1*R*)-camphor (**22**, 2.36 g, 14.0 mmol), hydroxylamine hydrochloride (1.70 g, 24.5 mmol) and pyridine (1.33 g, 16.8 mmol, 1.36 mL) were used and (1*R*, 4*R*)-camphor oxime (**58**, 2.15 g, 11.7 mmol, 84%) was obtained as an off-white powder. Mp. 110 – 114 °C. ¹H NMR (300.08 MHz, CDCl₃): δ 0.80 (s, 3H, -CH₃), 0.91 (s, 3H, -CH₃), 1.00 (s, 3H, CH₃CCH₂-), 1.19 – 1.28 (m, 1H, -CH₂CH₂-), 1.41 – 1.50 (m, 1H, -CH₂CH₂-), 1.70 (dt, 1H, $J = 4.2$ Hz, $J = 12.5$ Hz, CH₃CCH₂-), 1.78 – 1.88 (m, 1H, CH₃CCH₂-), 1.91 (t, 2H, $J = 4.2$ Hz), 2.05 (d, 3.91, $J = 18.0$ Hz), 2.55 (dt, 1H, $J = 4.0$ Hz, $J = 18.0$ Hz, -CCH), 7.76 (bs, 1H, NOH) ppm. ¹³C NMR (75.56 MHz, CDCl₃): δ 11.1, 18.5, 19.4, 27.2, 32.6, 33.1, 43.7, 48.3, 51.8, 170.0 ppm. MS (EI): m/z (%) 69 (29), 79 (25), 94 (28), 110 (41), 124 (81), 150 (34) $[M-OH]^+$, 151 (5), 167 (100) $[M]^+$. Anal. calcd for $C_{10}H_{17}NO$, C: 71.81 H: 10.25 N: 8.37. Found, C: 71.81 H: 10.35 N: 8.21. The analytical data are in accordance to the reported one.^[425]

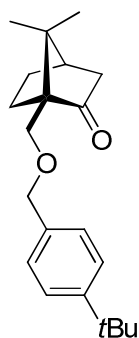
(1*R*, 4*R*)-10-benzyloxycamphor (**50**):



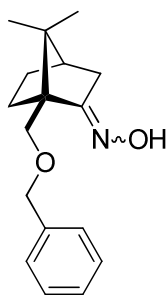
This compound was prepared by a method described by Chelucci et al.^[169] Sodium hydride (0.24 g, 10.00 mmol) suspended in 100 mL anhydrous tetrahydrofuran was placed in a three necked round bottom flask and (1*S*)-10-hydroxycamphor (**21**, 1.50 g, 8.92 mmol) dissolved in 50 mL anhydrous tetrahydrofuran was added dropwise and the mixture was stirred for 3 h at room temperature. A solution of benzyl bromide (1.60 g, 9.35 mmol) dissolved in 30 mL anhydrous tetrahydrofuran was slowly added to the mixture over a period of one hour. The mixture was stirred for two hours at reflux temperature and additional 16 h at room temperature. 300 mL water was added followed by extraction with 3×50 mL diethyl ether. The organic layers were combined, washed with brine and dried over sodium sulfate. Evaporation of the solvent under reduced

pressure yielded the title compound as a colorless liquid (2.22 g, 8.58 mmol, 96%). ^1H NMR (500.13 MHz, CDCl_3): δ 0.89 (s, 3H, $-\text{CH}_3$), 1.01 (s, 3H, $-\text{CH}_3$), 1.27 – 1.33 (m, 2H), 1.78 (d, 1H, $J = 17.7$ Hz), 1.91 – 2.00 (m, 2H), 2.02 – 2.07 (m, 1H), 2.33 (dt, 1H, $J = 18.3$ Hz, $J = 3.5$ Hz, $\text{CH}_3\text{CCH}-$), 3.54 (d, 1H, $^2J = 10.3$ Hz, $-\text{CH}_2\text{OBn}$), 3.58 (d, 1H, $^2J = 10.3$ Hz, $-\text{CH}_2\text{OBn}$), 4.47 (s, 2H, $-\text{CH}_2\text{Ar}$), 7.19 – 7.34 (m, 5H, ArH) ppm. ^{13}C NMR (125.75 MHz, CDCl_3): δ 20.3, 20.8, 25.3, 26.7, 33.5, 43.5, 43.8, 47.1, 61.3, 66.5, 73.5, 127.3, 128.2, 138.7, 217.5 ppm. MS (EI): m/z (%) 55 (17), 64 (23), 67 (19), 77 (20), 79 (19), 81 (17), 91 (100), 107 (7) $[\text{CH}_2\text{OBn}]^+$, 152 (26), 258 (4) $[\text{M}]^+$. HR-MS (EI, m/z): calc. for $\text{C}_{17}\text{H}_{22}\text{O}_2$ $[\text{M}]$: 258.1620, found: 258.1633. IR (KBr): ν 2961, 2879, 1743, 1496, 1470, 1453, 1416, 1389, 1365, 1274, 1199, 1169, 1104, 1047, 1027, 738, 700.

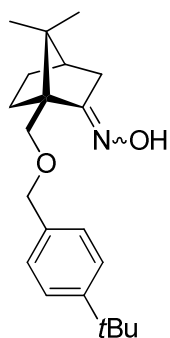
(1R, 4R)-10-(4-*tert*-butylbenzyl)oxycamphor (51):



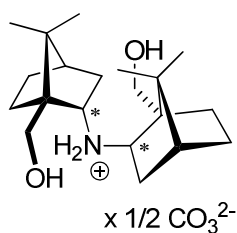
This compound was prepared by a method described by Chelucci et al.^[169] Sodium hydride (0.24 g, 10.00 mmol) suspended in 100 mL anhydrous tetrahydrofuran was placed in a three necked round bottom flask and (1*S*)-10-hydroxycamphor (**21**, 1.50 g, 8.92 mmol) dissolved in 50 mL anhydrous tetrahydrofuran was added dropwise and the mixture was stirred for 3 h at room temperature. A solution of 4-*tert*-butylbenzyl bromide (2.13 g, 9.40 mmol) dissolved in 30 mL anhydrous tetrahydrofuran was slowly added to the mixture over a period of one hour. The mixture was stirred for two hours at reflux temperature and additional 16 h at room temperature. 300 mL water was added followed by extraction with 3×50 mL diethyl ether. The organic layers were combined, washed with brine and dried over sodium sulfate. Evaporation of the solvent under reduced pressure yielded the title compound as a colorless liquid (2.75 g, 8.74 mmol, 98%). ^1H NMR (500.13 MHz, CDCl_3): δ 0.96 (s, 3H, $-\text{CH}_3$), 1.08 (s, 3H, $-\text{CH}_3$), 1.32 (s, 9H, $-(\text{CH}_3)_3$), 1.36 (d, $J = 9.0$ Hz), 1.84 (d, 1H, $J = 17.9$ Hz), 1.99 – 2.04 (m, 2H), 2.08 – 2.16 (m, 1H), 2.37 – 2.42 (m, 1H), 3.59 (d, 1H, $^2J = 10.4$ Hz, $-\text{CH}_2\text{OBn}$), 3.64 (d, 1H, $^2J = 10.4$ Hz, $-\text{CH}_2\text{OBn}$), 4.47 – 4.53 (m, 2H, $-\text{CH}_2\text{Ar}$), 7.25 – 7.37 (m, 4H, ArH) ppm. ^{13}C NMR (125.75 MHz, CDCl_3): δ 20.4, 20.8, 25.3, 26.8, 31.2, 31.4, 33.6, 34.5, 43.5, 43.8, 47.1, 61.4, 66.5, 73.4, 125.1, 125.8, 127.1, 128.8, 135.7, 150.2, 217.6 ppm. MS (EI): m/z (%) 69 (6), 81 (6), 109 (100), 117 (13), 132 (17), 147 (47), 152 (32), 163 (84) $[\text{O}^t\text{BuBn}]^+$, 257 (6) $[\text{M}-^t\text{Bu}]^+$, 314 (24) $[\text{M}]^+$. HR-MS (EI, m/z): calc. for $\text{C}_{21}\text{H}_{30}\text{O}_2$ $[\text{M}]$: 314.2246, found: 314.2265. IR (KBr): ν 3285, 3264, 3242, 2962, 2869, 1743, 1621, 1468, 1362, 1210, 1108, 1047, 818.

(1*S*, 4*R*)-10-benzyloxycamphor oxime (53):

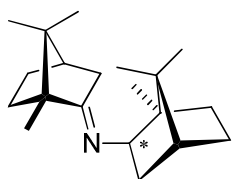
The title compound was synthesized using the general method for the preparation of oximes. (1*R*, 4*R*)-10-benzyloxycamphor (**50**, 730 mg, 2.83 mmol), hydroxylamine hydrochloride (236 mg, 3.40 mmol) and pyridine (268 mg, 3.39 mmol, 0.27 mL) were used and (1*S*, 4*R*)-10-benzyloxycamphor oxime (681 mg, 2.49 mmol, 88%) was obtained as a colorless liquid. ¹H NMR (500.13 MHz, CDCl₃): δ 0.89 (s, 3H, -CH₃), 1.02 (s, 3H, -CH₃), 1.25 – 1.30 (m, 2H), 1.45 – 1.20 (m, 1H), 1.85 – 1.91 (m, 2H), 2.06 (d, 1H, *J* = 17.8 Hz), 2.10 – 2.13 (m, 1H), 2.54 – 2.60 (m, 1H, CH₃CCH-), 3.61 (d, 1H, ²*J* = 10.0 Hz, -CH₂OBn), 3.70 (d, 1H, ²*J* = 10.0 Hz, -CH₂OBn), 4.51 (d, 1H, ²*J* = 12.2 Hz, -CH₂Ar), 4.55 (d, 1H, ²*J* = 12.2 Hz, -CH₂Ar), 7.24 – 7.35 (m, 5H, ArH), 7.82 (bs, 1H, NOH) ppm. ¹³C NMR (125.75 MHz, CDCl₃): δ 20.1, 20.2, 27.0, 28.3, 33.0, 44.5, 48.6, 55.3, 67.8, 73.5, 127.3, 127.4 (2×), 128.2 (2×), 138.8, 168.3 ppm. MS (EI): *m/z* (%) 79 (9), 91 (100), 111 (7), 124 (14), 150 (18), 167 (56) [M-CH₂OBn]⁺, 182 (27) [M-tolyl]⁺, 230 (5), 256 (5) [M-OH]⁺, 274 (1) [M]⁺. HR-MS (EI, *m/z*): calc. for C₁₇H₂₃NO₂ [M]: 273.1729, found: 273.1731. IR (KBr): ν 2950, 2878, 2802, 1723, 1610, 1495, 1452, 1388, 1366, 1201, 1111, 1096, 1073, 1027, 927, 836, 737, 700.

(1*S*, 4*R*)-10-(4-*tert*-butylbenzyl)oxycamphor oxime (54):

The title compound was synthesized using the general method for the preparation of oximes. (1*R*, 4*R*)-10-(4-*tert*-benzyl)oxycamphor (**51**, 1.00 g, 3.18 mmol), hydroxylamine hydrochloride (0.27 g, 3.81 mmol) and pyridine (0.30 g, 3.82 mmol, 0.31 mL) were used and (1*S*, 4*R*)-10-(4-*tert*-benzyl)oxycamphor oxime (1.01 mg, 3.05 mmol, 96%) was obtained as a colorless liquid. ¹H NMR (500.13 MHz, CDCl₃): δ 0.90 (s, 3H, -CH₃), 1.04 (s, 3H, -CH₃), 1.24 – 1.92 (m, 2H), 1.31 (s, 9H, -(CH₃)₃), 1.44 – 1.49 (m, 1H), 1.85 – 1.91 (m, 2H), 2.06 (d, 1H, *J* = 17.7 Hz), 2.09 – 2.15 (m, 1H), 2.54 – 2.60 (m, 1H, CH₃CCH-), 3.61 (d, 1H, ²*J* = 10.1 Hz, -CH₂OBn), 3.70 (d, 1H, ²*J* = 10.1 Hz, -CH₂OBn), 4.50 (d, 1H, ²*J* = 12.5 Hz, -CH₂Ar), 4.53 (d, 1H, ²*J* = 12.6 Hz, -CH₂Ar), 7.26 – 7.28 (m, 2H, ArH), 7.34 – 7.36 (m, 2H, ArH) ppm. ¹³C NMR (125.75 MHz, CDCl₃): δ 20.1, 20.2, 27.0, 28.2, 31.4 (3×), 33.0, 34.5, 44.5, 48.6, 55.4, 61.9, 67.8, 73.4, 125.1 (2×), 127.1 (2×), 135.8, 150.2, 168.6 ppm. MS (EI): *m/z* (%) 79 (5), 91 (130), 105 (12), 111 (20), 117 (20), 124 (38), 132 (23), 138 (13), 140 (12), 147 (77), 150 (64), 167 (100) [M-(4-*tert*-butylbenzyloxy)]⁺, 182 (7) [M-(4-*tert*-butyl)tolyl]⁺, 312 (45) [M-OH]⁺, 329 (2) [M]⁺. HR-MS (EI, *m/z*): calc. for C₂₁H₃₁NO₂ [M]: 329.2355, found: 329.2383. IR (KBr): ν 3162, 2960, 2869, 1451, 1391, 1363, 1268, 1109, 1094, 1074, 927, 844, 738.

***N*-Bornylisobornylcamphor amine (57):**

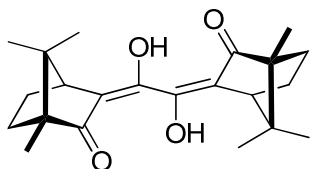
(1*S*, 4*R*)-10-hydroxycamphor oxime (**52**, 9.07 g, 0.050 mol) was dissolved in 100 mL anhydrous ethanol and Raney-Nickel[®], thoroughly washed several times with absolute ethanol, was added under nitrogen and hydrogenation was allowed to proceed at 50 °C over a period of three days. The mixture was filtered (pore size 0.45 μm), the solvent was evaporated and dried for one day under high vacuum to yield a yellow oil. Lithium aluminum hydride was suspended in 250 mL anhydrous tetrahydrofuran and filtered carefully. The solution was cooled to 0 °C and the obtained oil dissolved in 50 mL anhydrous tetrahydrofuran was added over a period of one hour. The mixture was allowed to warm up to room temperature and was stirred for 36 h at reflux temperature. The reaction was quenched at 0 °C with anhydrous methanol and the ¾ of the solvent was evaporated. The crude product was taken up in 300 mL dichloromethane, 200 mL of saturated, aqueous sodium/ potassium tartrate was added and the mixture was vigorously stirred for 24 h. The organic layer was separated, the pH was adjusted to one with 3M hydrochloric acid and extracted three times with 75 mL water. The aqueous layers were combined, basified with 3M sodium hydroxide and 10 ml of aqueous, saturated sodium carbonate and extracted three times with 50 mL dichloromethane. The combined organic layer was dried over sodium sulfate, the solvent was evaporated under reduced pressure and the crude product was purified by flash column chromatography (silica, chloroform/ methanol = 20:1 to 7:1). Evaporation of the solvent yielded the *N*-bornylisobornylcamphor amine carbonate salt **57** as colorless crystals (6.44 g, 0.0184 mol, 74%). ¹H NMR (500.13 MHz, MeOD-*d*₄): δ 0.89 – 0.92 (m, 1H), 0.93 (s, 3H, -CH₃), 0.94 (s, 3H, -CH₃), 0.95 – 1.02 (m, 4H, -CH₂CH₂-, -CH₃), 1.04 (s, 3H, -CH₃), 1.08 – 1.26 (m, 2H), 1.30 – 1.40 (m, 2H), 1.54 – 1.60 (m, 1H), 1.63 – 1.79 (m, 4H), 1.82 – 1.93 (m, 4H), 2.36 – 2.43 (m, 1H), 3.03 – 3.10 (m, 1H), 3.60 (d, 1H, ²*J* = 10.3 Hz, -CH₂OH), 3.65 (d, 1H, ²*J* = 11.2 Hz, -CH₂OH), 3.81 (d, 1H, ²*J* = 10.3 Hz, -CH₂OH), 3.83 – 3.91 (m, 1H, NH), 3.94 (d, 1H, ²*J* = 11.3 Hz, -CH₂OH) ppm. ¹³C NMR (125.75 MHz, MeOD-*d*₄): δ 19.6, 20.3, 21.1, 21.3, 25.2, 27.5, 28.9, 33.5, 47.2, 7.3, 48.1, 48.8, 52.8, 54.0, 62.1 (2×), 64.5 (2×), 65.7, 65.8 ppm. MS (CI, pos. mode, *iso*-butane): *m/z* (%) 322 (100) [M-H]⁺, 364 (11) [M+C₄H₉]⁺. MS (EI): *m/z* (%) 67 (30), 79 (30), 81 (26), 93 (41), 111 (35), 135 (27), 152 (22) [M-(*isobornylamin*)yl]⁺, 168 (37) [M-bornyl]⁺, 182 (32), 196 (23), 234 (74), 290 (25), 304 (100), 321 (100) [M]⁺. HR-MS (EI, *m/z*): calc. for C₂₀H₃₅NO₂ [M]: 321.2668, found: 321.2695. ATR-FTIR: ν 3385, 2986, 2934, 2876, 1653, 1448, 1384, 1273, 1299, 1273, 1225, 1211, 1183, 1128, 1100, 1088, 1053, 1022, 984, 967, 920, 894, 875, 860, 845, 788, 768, 741.

***N*-Isobornylcamphor imine (59):**

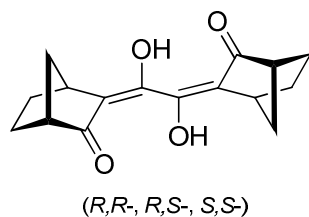
(1*R*)-camphor oxime (**58**, 5.07 g, 0.030 mol) was dissolved in 100 mL anhydrous methanol, palladium on charcoal and ammonium formate (5.66 g, 0.120 mmol) was added. The mixture was stirred for five days at room temperature, filtered (pore size 0.45 μm) and the solvent was evaporated under reduced pressure. The crude product was dissolved in 100 mL diethyl ether and washed twice with 25 mL aqueous 3M sodium hydroxide solution. The organic layer was acidified to pH 2 with 1M hydrochloric acid and washed two times with 25 mL diethyl ether to remove the starting material. The pH was adjusted to 7 with 1M sodium hydroxide solution and extracted three times with 50 mL diethyl ether. The combined organic layers were dried over sodium sulfate and the crude product was deposited on celite and purified by flash column chromatography (silica, hexane/ ethyl acetate = 15:1 to 1:1) to yield a small fraction of the desired bornyl ketimine condensation product. *N*-Isobornylcamphor imine **59** was obtained as a colorless oil (255 mg, 0.89 mmol, 6%). Crystals suitable for X-Ray diffraction were obtained over a period of 9 month from a saturated diethyl ether/ pentane solution. ^1H NMR (500.13 MHz, CDCl_3): δ 0.64 (s, 3H, - CH_3), 0.67 (s, 3H, - CH_3), 0.76 (s, 3H, - CH_3), 0.81 (s, 3H, - CH_3), 0.84 (s, 3H, - CH_3), 1.04 – 1.10 (m, 4H, - CH_2CH_2 -, - CH_3), 1.06 – 1.21 (m, 1H, - CH_2CH_2 -), 1.43 – 1.56 (m, 4H, var. - CH_2CH_2 -), 1.59 – 2.24 (m, 3H, var. - CH_2CH_2 -, - CCH_{amin} substructure), 1.69 – 1.77 (m, 1H), 1.80 (t, 1H, $^2J = 4.5$ Hz, $J = 7.5$ Hz, - CCH_{imin} substructure), 2.22 (dt, 1H, $J = 16.7$ Hz, $^2J = 3.9$ Hz, - $\text{N}=\text{CCH}_2$ -), 3.02 (dd, 1H, $^2J = 5.4$ Hz = $\text{N}-\text{CH}$ - 1H) ppm. ^{13}C NMR (125.75 MHz, CDCl_3): δ 11.4, 12.3, 19.1, 19.6, 2.4, 20.9, 27.6, 27.8, 32.3, 34.9, 36.4, 38.8, 44.1, 45.7, 46.2, 47.0, 49.2, 53.3, 68.4, 175.9 ppm. MS (EI): m/z (%) 67 (9), 81 (29), 95 (16), 137 (28) [$\text{M}-(\text{isobornylamin})\text{yl}]^+$, 152 (97) [$\text{M}-\text{bornyl}]^+$, 178 (20), 218 (11), 244 (6), 259 (31), 272 (14) [$\text{M}-\text{CH}_3$] $^+$, 287 (100) [$\text{M}]^+$. HR-MS (EI, m/z): calc. for $\text{C}_{20}\text{H}_{33}\text{N}$ [M]: 287.2613, found: 287.2610.

Experimental Section – Chapter 2

Bis((1*R*,4*S*)-7,7-dimethyl-3-oxobicyclo[2.2.1]heptan-2-ylidene)glyoxal, camphor tetraketone (**65**):

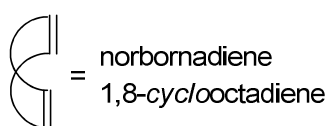
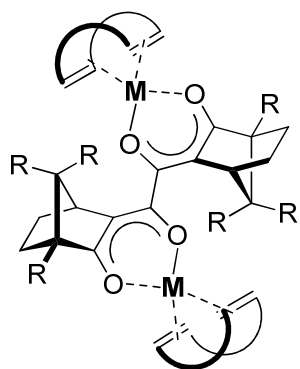


This compound was prepared using a modified procedure of the reported one.^[266] To a solution of (1*R*)-camphor (**22**, 5.00 g, 0.033 mol) in 150 mL anhydrous tetrahydrofuran was slowly added sodium hydride (0.87 g, 0.036 mol). The suspension was stirred at reflux temperature (75 °C) for 3 d until the mixture turned into a yellow, clear solution. The solution was allowed to cool down to room temperature and half of the volume of diethyl oxalate (2.4 g, 0.016 mol) dissolved in 100 mL of anhydrous tetrahydrofuran was added dropwise. After 2 h the remaining diethyl oxalate solution was added dropwise and the orange solution was stirred at reflux temperature for one day. The red solution was cooled down to room temperature and the solvent was evaporated under reduced pressure. 200 mL of dichloromethane was added and the suspension was extracted three times with 200 mL of water. The aqueous layer was acidified with aqueous 1N hydrochloric acid and extracted with diethyl ether until the aqueous layer remained almost colorless. The organic layers were combined, washed with brine, dried with sodium sulfate and the solvent removed under reduced pressure to obtain an orange powder. Purification by washings with a small amount of acetone and drying under high vacuum yielded 5.47g (0.015 mmol, 93%) of **65** as a bright yellow powder. Mp. 178 – 186 °C; ¹H NMR (500.13 MHz, CDCl₃, TMS): δ 0.84 (s, 6H, 2×(-CH₃)), 0.93 (s, 6H, 2×(-CH₃)), 0.99 (s, 6H, 2×(-CH₂CCH₃)), 1.40 – 1.51 (m, 4H, 2×(-CCH₂-)), 1.69 – 1.79 (m, 2H, 2×(-CHCH₂-)), 2.01 – 2.10 (m, 2H, 2×(-CHCH₂-)), 3.28 (d, *J* = 4.0 Hz, 2H, 2×(-CH)), 11.83 (bs, 2H, 2×(-OH)); ¹³C NMR (125.75 MHz, CDCl₃, TMS): δ 8.7, 18.6, 20.6, 27.1, 30.5, 48.5, 48.9, 57.9, 120.6, 155.3, 214.7 ppm. MS (EI): *m/z* (%) 151 (15), 179 (100) [C₁₁H₁₅O₂]⁺, 247 (94), 330 (54), 358 (34) [M]⁺. HRMS (EI): *m/z* calcd for C₂₂H₃₀O₄: 358.2144. Found: 358.2158. IR (KBr): ν 3442, 2960, 2871, 1661, 1579, 1456, 1390, 1376, 1337, 1269, 1225, 1179, 1155, 1146, 1106, 1069, 1027, 826, 815. Anal. calcd for C₂₂H₃₀O₄, C: 73.71 H: 8.44. Found, C: 73.22 H: 8.40.

Bis (3-oxobicyclo[2.2.1]heptan-2-ylidene)glyoxal, norcamphor tetraketone, mixture of three isomers (65b):

Synthesis was accomplished using racemic norcamphor as starting material and overall three diastereomers were obtained (*R,R*-, *R,S*- and *S,S*-diastereomer). The title compound was prepared by Golo Storch.^[273] To a suspension of 2.90 g (0.121 mol, 2.05 eq.) sodium hydride in anhydrous tetrahydrofuran (500 mL) was dropwise added norcamphor (13.00 g, 0.118 mol) dissolved in 50 mL tetrahydrofuran and stirred under reflux heating over night. Additional 0.28 g (11.8 mmol) sodium hydride was added to ensure complete deprotonation and stirring was continued for another 24 h. To the mixture 8.19 g (56.1 mmol) diethyl oxalate diluted in 60 mL tetrahydrofuran were added dropwise over a period of three hours at room temperature and stirring was continued for 6 h under reflux heating. After evaporation of the solvent under reduced pressure and high vacuum the crude product was dissolved in 800 mL of water and washed three times with diethyl ether (overall volume 1 L). The pH of the aqueous layer was adjusted to 3 with 3M hydrochloric acid and extracted two times with 300 mL dichloromethane. The organic layers were combined, dried over sodium sulfate and the solvent was evaporated under reduced pressure to yield the product as a dark, yellow oil. further purification was achieved by re-dissolution in a dichloromethane-water mixture (1:1), pH adjustment to 1 and extraction with dichloromethane. Drying over sodium sulfate and evaporating of the solvent yielded norcamphor tetraketone 5.07 g (29.9 mmol, 52%) as an yellow to orange oil. ¹H NMR and ¹³C-NMR data and a detailed discussion due to formation of diastereomers are reported elsewhere.^[273] MS (EI): *m/z* (%) 67 (26), 91 (25), 137 (31) [M₂]⁺, 145 (30), 174 (99), [M-CO-CO₂-C₂H₄]⁺, 201 (100), [M-2CO-OH]⁺, 202 (97) [M-CO-CO₂]⁺, 229 (79) [M-CO-OH]⁺, 246 (12) [M-CO]⁺, 274 (2) [M]⁺. HR-MS (EI, *m/z*): calc. for C₁₆H₁₈O₄ [M]: 274.1205, found: 274.1201. ATR-FTIR: ν 3400, 2954.4, 2874.4, 1785.8, 1716.3, 1656.6, 1450.2, 1299.8, 1243.9, 1197.6, 1184.1, 1148.4, 1088.6, 1071.3, 1024.98, 942.1.

General procedure for the preparation of Rh- and Ir tetraketone complexes derived from camphor- or norcamphor tetraketones:

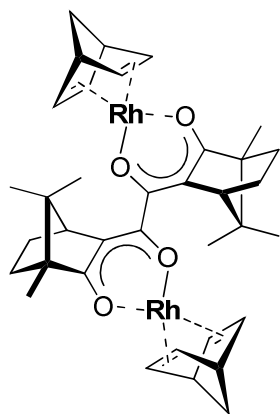


M = Rh(I), Ir(I)

R = CH₃ (for camphor-) and
H (for norcamphor-derivatives)

To a solution of enantiopure tetraketone **65** (camphor) or **65b** (norcamphor) (150 mg, 0.42 mmol, 1.00 eq.) in anhydrous tetrahydrofuran was added potassium *tert*-butylate (94 mg, 0.84 mmol, 2.00 eq.) in one portion at room temperature. After 20 min 0.42 mmol metal precursor (1.00 eq.) was added and the mixture stirred over night. The solvent was evaporated under reduced pressure, the residue is dissolved in a small quantity of dichloromethane and filtered through a short pad of celite. Evaporation of the solvent and recrystallization from a dichloromethane-petrolether mixture (1:20–100) by evaporation of the solvents followed by precipitation at low temperatures (-60 °C) yields the rhodium- and iridium chelate-complexes as bright, yellow powders.

Preparation of enantiopure dirhodium(I)-camphor tetraketone complex (**67**):

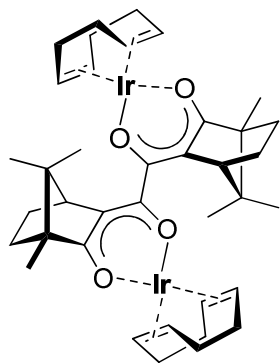


This compound was prepared according to the general method for tetraketone metal complex formation using enantiopure camphor tetraketone **65** (150 mg, 0.42 mmol), potassium *tert*-butylate (94 mg, 0.84 mmol) and dichloro-bis(norbornadiene)dirhodium(I) (193 mg, 0.42 mmol). Reaction was stirred at 50 °C for one day after metal precursor addition. Purification was accomplished following the general procedure to yield the title compound as a bright, yellow microcrystalline powder (294 mg, 0.39 mmol, 94%). Mp. >210 °C (decomp.); ¹H NMR (500.13 MHz, CDCl₃, TMS): δ 0.70 (s, 6H, 2×(-CH₃)),

0.78 (s, 6H, 2×(-CH₃)), 0.83 (s, 6H, 2×(-CH₃)), 1.17 – 1.21 (m, 6H, 2×(-CH₂)_{nb}, 2×(-CH₂-)), 1.25 – 1.30 (m, 2H, 2×(-CH₂-)), 1.48 – 1.53 (m, 2H, 2×(-CH₂-)), 1.83 – 1.88 (m, 2H, 2×(-CH₂-)), 2.38 (d, 2H, *J* = 3.4 Hz, 2×(-CCH-)), 3.76 (d, 2H, *J* = 19.0 Hz, 2×(-CCH-)_{nb}), 3.87 (d, 8H, *J* = 16.8 Hz, 4×(-CHCH-)_{nb}) ppm. ¹³C NMR (125.75 MHz, CDCl₃, TMS): δ 9.5, 19.3, 20.4, 27.5, 30.9, 49.1, 49.5, 51.4, 51.8, 51.9, 52.0, 52.1 (2×), 52.7 (2×), 57.9, 60.3, 60.4, 112.6, 172.4, 201.1 ppm. HR-MS (FAB): *m/z* (%) calcd for C₃₆H₄₄Rh₂O₄ [M]⁺: 746.1350, found: 746.1335. ATR-FTIR: ν 2991, 2948, 2906, 1602, 1580, 1437, 1397, 1389, 1382, 1373,

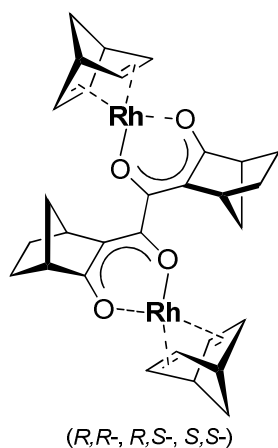
1319, 1364, 1304, 1301, 1278, 1242, 1217, 1192, 1178, 1164, 1152, 1104, 1073, 1054, 966, 938, 926, 916, 881, 848, 829, 808, 795, 776, 766, 743, 723.

Preparation of enantiopure diiridium(I)-camphor tetraketone complex (**66**):



This compound was prepared according to the general method for tetraketone metal complex formation using enantiopure camphor tetraketone **65** (150 mg, 0.42 mmol), potassium *tert*-butylate (94 mg, 0.84 mmol) and bis(1,5-cyclooctadiene)diiridium(I) dichloride (281 mg, 0.42 mmol) to yield the title compound as a bright, yellow microcrystalline powder (216 mg, 0.23 mmol, 54%). Mp. >225 °C (decomp.); ¹H NMR (500.13 MHz, CD₂Cl₂, TMS): δ 0.68 (s, 6H, 2×(-CH₃)), 0.84 (s, 6H, 2×(-CH₃)), 0.93 (s, 6H, 2×(-CH₃)), 1.23 – 1.28 (m, 2H, 2×(-CH₂-)), 1.33 – 1.38 (m, 2H, 2×(-CH₂-)), 1.52 – 1.64 (m, 10H, 8×(-CH₂-)_{cod}, 2×(-CH₂-)), 1.93 – 1.99 (m, 2H, 2×(-CH₂-)), 2.13 – 2.28 (m, 8H, 8×(-CH₂-)_{cod}), 2.59 (d, 2H, *J* = 3.6 Hz, 2×(-CCH-)), 3.86 – 3.90 (m, 2H, 2×CH_{cod}), 3.94 – 4.01 (m, 6H, 6×CH_{cod}) ppm. ¹³C NMR (125.75 MHz, CD₂Cl₂, TMS): δ 9.2, 19.0, 19.9, 27.5, 30.8 (2×), 30.9, 31.2, 31.3, 49.6, 51.7, 58.4 (2×), 59.0, 59.2 (2×), 116.2, 170.5, 202.6, 210.7 ppm. HR-MS (FAB): *m/z* (%) calcd for C₃₈H₅₂¹⁹¹Ir¹⁹³IrO₄ [M]⁺: 956.3102, found: 956.3069. ATR-FTIR: ν 2959, 2875, 2828, 1606, 1582, 1464, 1447, 1399, 1383, 1373, 1364, 1318, 1286, 1279, 1262, 1242, 1220, 1196, 1180, 1164, 1156, 1108, 1102, 1077, 1057, 1009, 999, 978, 938, 913, 891, 867, 845, 828, 813, 779, 748, 724.

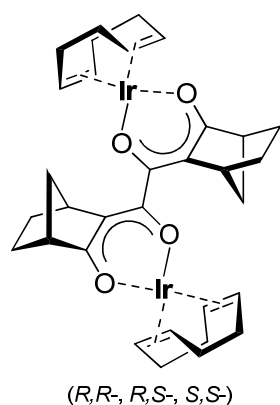
Preparation of dirhodium(I)-norcamphor tetraketone complex (**67b**):^[273]



This compound was prepared according to the general method for tetraketone metal complex formation using norcamphor (rac.) tetraketone (**65b**, 48 mg, 0.17 mmol), potassium *tert*-butylate (39 mg, 0.35 mmol) and dichlorobis(norbornadiene)dirhodium(I) (193 mg, 0.17 mmol). Purification was accomplished following the general procedure to yield the title compound as a bright, yellow powder (114 mg, 0.17 mmol, 98%). Mp. >200 °C (decomp.); ¹H NMR (300.51 MHz, CDCl₃, TMS): δ 1.21 (s, 4H, 2×(-CH₂)_{nb}), 1.21 – 1.35 (m, 6H, 2×(-CH₂-), 2×(-CH₂-), 2×(-CH₂-)), 1.55 – 1.56 (m, 2H, 2×(-CH₂-)), 1.65 – 1.80 (m, 4H, 2×(-CH₂-), 2×(-CH₂-)), 2.69 (s, 2H, 2×(-

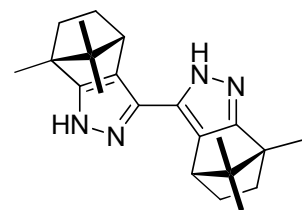
CCH-)), 2.98 (s, 2H, 2×(-CCH-)), 3.77 (d, 4H, $J = 45.1$ Hz, 4×(-CCH-)_{nb}d), 3.92 (d, 8H, $J = 86.7$ Hz, 4×(-CHCH-)_{nb}d) ppm. ^{13}C NMR (75.48 MHz, CDCl_3 , TMS): δ 24.4, 29.0, 40.5, 43.1, 49.5, 50.0 (4×), 52.1 (2×), 52.2, 52.3, 52.6, 52.7 (2×), 52.9, 60.5, 60.6, 113.1, 173.1, 200.6 ppm. HR-MS (FAB): m/z (%) calcd for $\text{C}_{30}\text{H}_{32}\text{Rh}_2\text{O}_4$ $[\text{M}]^+$: 662.0411, found: 662.0392. IR (KBr): ν 2947.7, 2915.8, 2866.7, 1578.5, 1435.7, 1382.7, 1219.8, 1097.3, 930.5.

Preparation of diiridium(I)-camphor tetraketone complex (**66b**):^[273]



This compound was prepared according to the general method for tetraketone metal complex formation using norcamphor (rac.) tetraketone (**65b**, 29 mg, 0.10 mmol), potassium *tert*-butylate (24 mg, 0.21 mmol) and bis(1,5-cyclooctadiene)diiridium(I) dichloride (70 mg, 0.10 mmol) to yield the title compound as a bright, yellow powder (38 mg, 0.04 mmol, 41%). The redissolved compound is not stable and decomposes within 60 min in solution (dichloromethane, chloroform and benzene). Mp. >200 °C (decomp.); ^1H NMR (300.51 MHz, CD_2Cl_2 , TMS): δ 1.25 – 1.40 (m, 6H, 2×(-CH₂-), 2×(-CH₂-), 2×(-CH₂-)), 1.56 – 1.69 (m, 10H, 2×(-CH₂-), 2×(-CH₂CH₂-)_{cod}, 2×(-CH₂CH₂-)_{cod}), 1.80 – 1.83 (m, 4H, 2×(-CH₂-), 2×(-CH₂-)), 2.21 – 2.25 (m, 8H, 2×(-CH₂CH₂-)_{cod}, 2×(-CH₂CH₂-)_{cod}), 2.86 (s, 2H, 2×(-CCH-)), 3.23 (s, 2H, 2×(-CCH-)), 4.00 (s, 8H, 4×(-CHCH-)_{nb}d) ppm. HR-MS (FAB): m/z (%) calcd for $\text{C}_{32}\text{H}_{39}^{191}\text{Ir}^{193}\text{IrO}_4$ $[\text{M}]^+$: 871.2085, found: 871.2110. IR (KBr): ν 2936.1, 2866.7, 2830.0, 1583.3, 1446.4, 1375.0, 1220.7, 1100.2, 975.8.

4,8,8'-trimethylbicyclo[2.2.1]-4,4',5,5',6,6',7,7'-octahydro-1H,1'H-3,3'-bipyrazole (**68**):

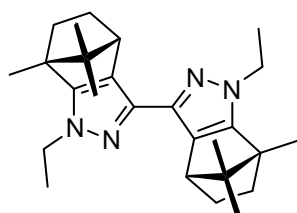


To a boiling solution of **65** (3.50 g, 9.76 mmol) in 200 mL absolute ethanol was added hydrazinium hydroxide 9.5 mL g (9.22 g, 0.184 mol) at once through a short reflux condenser. After heating for two days at this temperature the precipitate was collected by hot filtration. The filtrate was concentrated under reduced pressure at 70 °C and the formed precipitates were successively collected. Washings with ethyl acetate and drying under high vacuum yielded 3.13 g (8.93 mmol, 91%) of pure **68** as a fluffy, insoluble white powder. Mp. > 250 °C; MS (EI): m/z (%) 55 (15), 77 (16), 67 (22), 121 (23), 133 (31), 159 (35), 176 (20) $[\text{C}_{11}\text{H}_{16}\text{N}_2]^+$, 177 (69), 187 (19), 220 (19), 307 (32) $[\text{M}-(3\times\text{CH}_3)]^+$, 350 (17) $[\text{M}]^+$. HRMS (EI): m/z calcd for $\text{C}_{22}\text{H}_{30}\text{N}_4$: 350.2470, found: 350.2442. IR (KBr): ν 3428, 3262, 2957,

2871, 1632, 1473, 1453, 1418, 1388, 1375, 1367, 1270, 1237, 1180, 1170, 1129, 1083, 969, 950. Anal. calcd for C₂₂H₃₀N₄, C: 75.39 H: 8.63 N: 15.98. Found, C: 75.18 H: 8.88 N: 15.77.

General procedure for alkylation and arylation of (68): Compound **68** (1.00 eq.) and sodium hydride (2.30 eq.) were suspended in anhydrous tetrahydrofuran (10 – 50 mM, referred to **2**), stirred for 30 min at room temperature and heated at reflux temperature for 2 h until it turned into a clear colorless solution. The solution was then cooled to room temperature and the appropriate amount of arylhalogenide (2.05 eq.) was added. The solution was stirred at room temperature for 30 min and at reflux temperature for 4 – 16 h. The precipitate was filtered off and the solvent was evaporated under reduced pressure. The residue was taken up in dichloromethane, washed with H₂O and brine. The organic phase was separated, dried with sodium sulfate and the solvent was evaporated under reduced pressure to yield the corresponding arylated compounds as analytically pure solids. In case of alkylation 2.20 eq. of alkylhalogenides were added. Standard work-up procedure and drying at elevated temperatures under high vacuum yielded pure alkylated compounds. Whenever necessary the compounds were washed with small amounts of pentane.

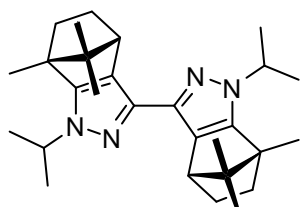
1,1'-diethyl-4,8,8'-trimethylbicyclo[2.2.1]-4,4',5,5',6,6',7,7'-octahydro-1H,1'H-3,3'-bipyrazole (69a):



Compound **69a** was prepared following the standard procedure using **68** (150 mg, 0.427 mmol), sodium hydride (25 mg, 1.024 mmol) and ethyl bromide (116 μ L, 0.938 mmol) in 80 mL anhydrous tetrahydrofuran. The solution was stirred at reflux temperature for 16 h. Extensive drying at elevated temperature under high vacuum yielded pure **69a** (229 mg, 0.542 mmol, 97%) as a yellowish powder. Mp. 132 – 148 °C; ¹H NMR (300.13 MHz, CD₃CN): δ 0.73 (s, 6H, 2 \times (-CH₃)), 0.93 (s, 6H, 2 \times (-CH₃)), 1.02 – 1.10 (m, 2H, 2 \times (-CCH₂-)), 1.16 – 1.20 (m, 2H, 2 \times (-CCH₂-)), 1.24 (t, 6H, J = 7.2 Hz, 2 \times (-CH₂CH₃)), 1.34 (s, 6H, 2 \times (-CH₂CCH₃)), 1.82 – 1.90 (m, 2H, 2 \times (-CHCH₂-)), 2.08 – 2.17 (m, 2H, 2 \times (-CHCH₂-)), 2.90 (d, 2H, J = 3.9 Hz, 2 \times (-CCH)), 4.01 (q, 4H, J = 7.2 Hz, 2 \times (-CH₂CH₃)) ppm. ¹³C NMR (75.46 MHz, CD₃CN): δ 11.9, 17.7, 20.2, 21.1, 28.7, 34.7, 46.1, 49.5, 53.7, 63.9, 127.3, 138.9, 155.4 ppm. MS (EI): m/z (%) 73 (26), 133 (14), 355 (13), 377 (75), 406 (14), 420 (33) [M-(*n*-pentyl)]⁺, 434 (11) [M-(*n*-butyl)]⁺, 447 (73) [M-(3 \times CH₃)]⁺, 420 (9) [M-(ethyl)]⁺, 475 (9) [M-(CH₃)]⁺, 490 (62) [M]⁺. HRMS (EI): m/z

calcd for $C_{32}H_{50}N_4$: 490.4035, found: 490.4018. IR (KBr): ν 3428, 2957, 2870, 1632, 1504, 1451, 1386, 1378, 1365, 1352, 1310, 1282, 1247, 1133, 1107, 1082, 1060, 1049, 1029.

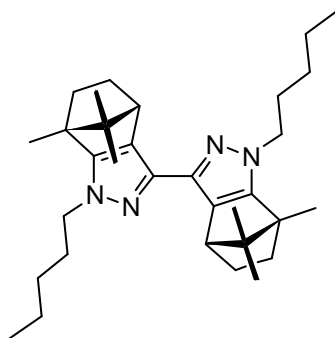
1,1'-diisopropyl-4,8,8'-trimethylbicyclo[2.2.1]-4,4',5,5',6,6',7,7'-octahydro-1H,1'H-3,3'-bipyrazole (69b):



Compound **69b** was prepared following the standard procedure using **68** (200 mg, 0.571 mmol), sodium hydride (33 mg, 1.376 mmol) and *iso*-propyl bromide (215 μ L, 2.29 mmol) in 90 mL anhydrous tetrahydrofuran. After 2 h at reflux temperature another 215 μ L *iso*-propyl bromide was added.

Extensive drying at elevated temperature under high vacuum yielded pure **69b** (236 mg, 0.542 mmol, 95%) as a yellowish powder. Mp. 155 – 162 $^{\circ}$ C; 1 H NMR (300.13 MHz, $CDCl_3$, TMS): δ 0.74 – 0.68 (m, 2H, $2\times(-CHCH_2-)$), 0.78 (s, 6H, $2\times(-CH_3)$), 0.91 (s, 6H, $2\times(-CH_3)$), 1.02 – 1.10 (m, 2H, $2\times(-CHCH_2-)$), 1.36 (s, 6H, $2\times(-CH_2CCH_3)$), 1.50 (d, 6H, $J = 6.9$ Hz, $2\times(-NCHCH_3)$), 1.53 (d, 6H, $J = 6.9$ Hz, $2\times(-NCHCH_3)$), 1.90 – 1.73 (m, 2H, $2\times(-CHCH_2-)$), 2.02 – 2.15 (m, 2H, $2\times(-CHCH_2-)$), 2.85 (d, 2H, $J = 5.0$ Hz, $2\times(-CCH)$), 4.47 (q, 2H, $J = 6.8$ Hz, $2\times(-CH_2CH_3)$) ppm. ^{13}C NMR (125.75 MHz, $CDCl_3$, TMS): δ 12.5, 19.9, 20.6, 23.2, 23.4, 27.6, 34.1, 48.4, 51.9, 52.8, 62.4, 126.5, 137.7, 152.7 ppm. MS (EI): m/z (%) 307 (11), 349 (60) $[M-(2\times i\text{-Pr})]^+$, 355 (9), 377 (8), 391 (55) $[M-(i\text{-Pr})]^+$, 405 (8), 419 (20) $[M-(CH_3)]^+$, 434 (58) $[M]^+$. HRMS (EI): m/z calcd for $C_{28}H_{42}N_4$: 434.3409, found: 434.3405. IR (KBr): ν 3394, 2954, 2869, 1627, 1474, 1452, 1386, 1373, 1366, 1269, 1250, 1234, 1082, 1058, 1020, 971, 954, 915.

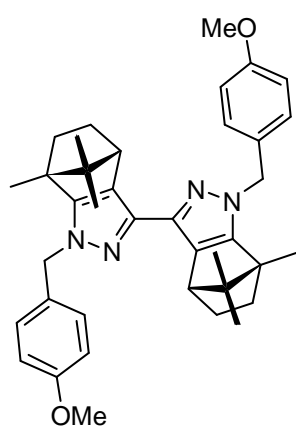
1,1'-dipentyl-4,8,8'-trimethylbicyclo[2.2.1]-4,4',5,5',6,6',7,7'-octahydro-1H,1'H-3,3'-bipyrazole (69c):



Compound **69c** was prepared following the standard procedure using **68** (150 mg, 0.427 mmol), sodium hydride (25 mg, 1.024 mmol) and *n*-pentyl bromide (116 μ L, 0.938 mmol) in 80 mL anhydrous tetrahydrofuran. The solution was stirred at reflux temperature for 16 h. Extensive drying at elevated temperature under high vacuum yielded pure **69c** (229 mg, 0.542 mmol, 97%) as a yellowish,

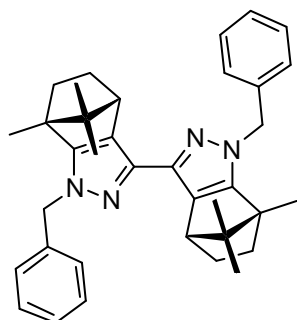
insoluble powder. Mp. > 250 °C; MS (EI): m/z (%) 73 (26), 133 (14), 355 (13%), 377 (75), 406 (14), 420 (33) [M-(*n*-pentyl)]⁺, 434 (11) [M-(*n*-butyl)]⁺, 447 (73) [M-(3×CH₃)]⁺, 420 (9) [M-(ethyl)]⁺, 475 (9) [M-(CH₃)]⁺, 490 (62) [M]⁺. HRMS (EI): m/z calcd for C₃₂H₅₀N₄: 490.4035, found: 490.4018. IR (KBr): ν 3431, 2956, 2871, 1627, 1511, 1454, 1387, 1375, 1366, 1286, 1277, 1260, 1135, 1109, 1084, 1058, 1043, 1015, 1000.

1,1'-di(4-methoxybenzyl)-4,8,8'-trimethylbicyclo[2.2.1]-4,4',5,5',6,6',7,7'-octahydro-1*H*,1'*H*-3,3'-bipyrazole (69d):



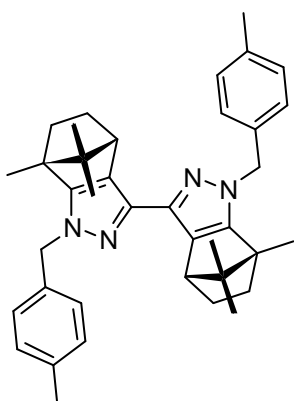
Compound **69d** was prepared following the standard procedure using **68** (300 mg, 0.856 mmol), sodium hydride (45 mg, 1.883 mmol) and 4-methoxybenzyl chloride (246 μ L, 1.75 mmol) in 100 mL anhydrous tetrahydrofuran. The solution was stirred at reflux temperature for 4 h. After crystallization from ethanol and washings with acetone **69d** (398 mg, 0.676 mmol, 79%) was obtained as a yellowish powder. Mp. 151 – 154 °C; ¹H NMR (500.13 MHz, CDCl₃, TMS): δ 0.78 (s, 6H, 2×(-CH₃)), 0.87 (s, 6H, 2×(-CH₃)), 1.07 – 1.09 (m, 2H, 2×(-CCH₂-)), 1.10 (s, 6H, 2×(-CH₂CCH₃)), 1.18 – 1.23 (m, 4H, 2×(-CCH₂-)), 1.65 – 1.70 (m, 2H, 2×(-CHCH₂-)), 2.06 – 2.08 (m, 2H, 2×(-CHCH₂-)), 2.92 (d, 2H, $J = 3.7$ Hz, 2×(-CCH)), 3.73 (s, 6H, 2×(-OCH₃)), 5.32 (d, 2H, ² $J_{H-H} = 15.9$ Hz, -NCH₂-), 5.36 (d, 2H, ² $J_{H-H} = 16.0$ Hz, -NCH₂-), 6.68 (s, 2H, 2×(ArH)), 6.73 – 6.77 (m, 4H, 2×2(ArH)), 7.17 – 7.20 (m, 2H, 2×(ArH)) ppm. ¹³C NMR (125.75 MHz, CDCl₃, TMS): δ 11.3, 19.6, 20.4, 27.3, 33.4, 48.4, 52.4, 54.0, 55.2, 62.6, 112.0, 13.0, 119.1, 127.2, 129.3, 138.2, 140.2, 154.0, 159.7 ppm. MS (EI): m/z (%) 121 (44) [C₈H₉O]⁺, 469 (94) [M-(methoxybenzyl)]⁺, 483 (17) [M-(C₈H₉O)]⁺, 547 (48), 575 (7) [M-(CH₃)]⁺, 590 (100) [M]⁺. HRMS (EI): m/z calcd for C₃₈H₄₆O₂N₄: 590.3621, found: 590.3585. IR (KBr): ν 3436, 2955, 2871, 1602, 1587, 1491, 1455, 1437, 1387, 1365, 1348, 1281, 1261, 1147, 1117, 1085, 1045, 999.

1,1'-dibenzyl-4,8,8'-trimethylbicyclo[2.2.1]-4,4',5,5',6,6',7,7'-octahydro-1H,1'H-3,3'-bipyrazole (69e):



Compound **69e** was prepared following the standard procedure using **68** (700 mg, 1.997 mmol), sodium hydride (115 mg, 4.792 mmol) and benzyl bromide (484 μ L, 4.093 mmol) in 110 mL anhydrous tetrahydrofuran. The solution was stirred at reflux temperature for 4 h. **69e** (1.002 g, 1.888 mmol, 94%) was obtained as a yellowish powder. Mp. 151 – 161 °C; ^1H NMR (500.13 MHz, CDCl_3 , TMS): δ 0.76 (s, 6H, $2\times(-\text{CH}_3)$), 0.86 (s, H, $2\times(-\text{CH}_3)$), 1.07 (s, 6H, $2\times(-\text{CH}_2\text{CCH}_3)$), 1.18 – 1.23 (m, 4H, $2\times(-\text{CCH}_2-)$), 1.63 – 1.68 (m, 2H, $2\times(-\text{CHCH}_2-)$), 2.02 – 2.07 (m, 2H, $2\times(-\text{CHCH}_2-)$), 2.91 (d, 2H, $J = 4.0$ Hz, $2\times(-\text{CCH})$), 5.35 (d, 2H, $^2J_{\text{H-H}} = 16.0$ Hz, $-\text{NCH}_2$), 5.39 (d, 2H, $^2J_{\text{H-H}} = 16.0$ Hz, $-\text{NCH}_2$), 7.13 – 7.22 (m, 10H, $2\times 5(\text{ArH})$) ppm. ^{13}C NMR (125.75 MHz, CDCl_3 , TMS): δ 11.4, 19.8, 20.6, 27.5, 33.6, 48.6, 52.6, 54.2, 62.8, 126.9, 127.4, 128.5, 138.3, 138.8, 154.2 ppm. MS (EI): m/z (%) 91 (95) $[\text{C}_7\text{H}_7]^+$, 439 (77) $[\text{M}-(\text{benzyl})]^+$, 453 (14) $[\text{M}-(\text{C}_6\text{H}_5)]^+$, 487 (86) $[\text{M}-(3\times\text{CH}_3)]^+$, 515 (8) $[\text{M}-(\text{CH}_3)]^+$, 530 (100) $[\text{M}]^+$. HRMS (EI): m/z calcd for $\text{C}_{36}\text{H}_{42}\text{N}_4$: 530.3409, found: 530.3420. IR (KBr): ν 3430, 2955, 2870, 1496, 1473, 1454, 1421, 1386, 1376, 1364, 1308, 1279, 1244, 1118, 1086, 1047, 1029, 999.

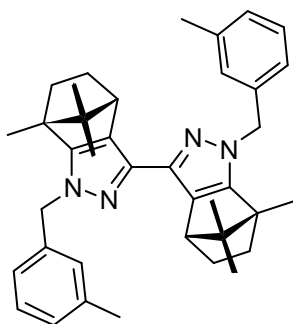
1,1'-di(4-methylbenzyl)-4,8,8'-trimethylbicyclo[2.2.1]-4,4',5,5',6,6',7,7'-octahydro-1H,1'H-3,3'-bipyrazole (69f):



Compound **69f** was prepared following the standard procedure using **68** (440 mg, 1.255 mmol), sodium hydride (72 mg, 3.014 mmol) and 4-methylbenzyl bromide (476 mg, 2.573 mmol) in 100 mL anhydrous tetrahydrofuran. The solution was stirred at reflux temperature for 4 h. **69f** (690 mg, 1.235 mmol, 98%) was obtained as a yellowish powder. Mp. 71 – 92 °C; ^1H NMR (300.13 MHz, CDCl_3 , TMS): δ 0.77 (s, 6H, $2\times(-\text{CH}_3)$), 0.86 (s, 6H, $2\times(-\text{CH}_3)$), 1.09 (s, 6H, $2\times(-\text{CH}_2\text{CCH}_3)$), 1.16 – 1.31 (m, 4H, $2\times(-\text{CCH}_2-)$), 1.61 – 1.70 (m, 2H, $2\times(-\text{CHCH}_2-)$), 2.00 – 2.10 (m, 2H, $2\times(-\text{CHCH}_2-)$), 2.30 (s, 6H, ArCH_3), 2.91 (d, $J = 3.6$ Hz, 2H, $2\times(-\text{CCH})$), 5.30 (d, 2H, $^2J_{\text{H-H}} = 15.7$ Hz, $-\text{NCH}_2-$), 5.36 (d, 2H, $^2J_{\text{H-H}} = 15.9$ Hz, $-\text{NCH}_2-$), 7.03 – 7.09 (m, 8H, $4\times 2(\text{ArH})$) ppm. ^{13}C NMR (75.46 MHz, CDCl_3 , TMS): δ 11.4, 19.8, 20.6, 21.2, 27.5, 33.5, 48.6, 52.5,

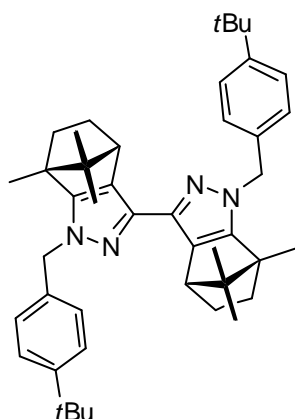
54.0, 62.7, 126.8, 127.3, 129.1, 135.7, 136.9, 138.2, 154.0 ppm. MS (EI): m/z (%) 105 (100) $[C_8H_9]^+$, 453 (90) $[M-(p\text{-xylynyl})]^+$, 467 (14) $[M-(C_7H_7)]^+$, 515 (18) $[M-(3\times CH_3)]^+$, 543 (3) $[M-(CH_3)]^+$, 558 (65) $[M]^+$. HRMS (EI): m/z calcd for $C_{38}H_{46}N_4$: 558.3722, found: 558.3704. IR (KBr): ν 3433, 2956, 2868 1515, 1472, 1453, 1422, 1386, 1375, 1364, 1352, 1309, 1298, 1280, 1118, 1085, 1046, 1020, 998.

1,1'-di(3-methylbenzyl)-4,8,8'-trimethylbicyclo[2.2.1]-4,4',5,5',6,6',7,7'-octahydro-1H,1'H-3,3'-bipyrazole (69g):



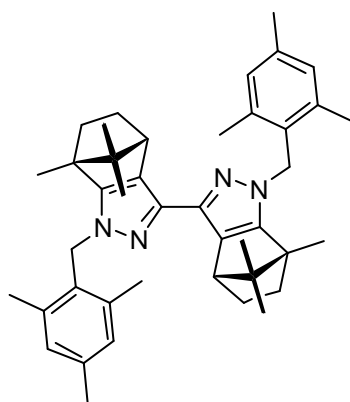
Compound **69g** was prepared following the standard procedure using **68** (500 mg, 1.427 mmol), sodium hydride (82 mg, 3.424 mmol) and 3-methylbenzyl bromide (541 mg, 2.923 mmol) in 100 mL anhydrous tetrahydrofuran. The solution was stirred at reflux temperature for 4 h. **69g** (730 g, 1.306 mmol, 92%) was obtained as a yellowish powder. Mp. 132 – 140 °C; 1H NMR (300.13 MHz, $CDCl_3$, TMS): δ 0.78 (s, 6H, $2\times(-CH_3)$), 0.87 (s, 6H, $2\times(-CH_3)$), 1.07 (s, 6H, $2\times(-CH_2CCH_3)$), 1.09 – 1.26 (m, 4H, $2\times(-CCH_2-)$), 1.63 – 1.71 (m, 2H, $2\times(-CHCH_2-)$), 2.01 – 2.11 (m, 2H, $2\times(-CHCH_2-)$), 2.28 (s, 6H, Ar CH_3), 2.92 (d, 2H $J = 3.6$ Hz, $2\times(-CCH)$), 5.34 (s, 4H, $2\times(-NCH_2-)$), 6.92 – 7.16 (m, 8H, $2\times 4(ArH)$) ppm. ^{13}C NMR (75.46 MHz, $CDCl_3$, TMS): δ 11.4, 19.8, 20.6, 21.5, 27.5, 33.6, 48.6, 52.6, 54.2, 62.8, 124.0, 127.4, 127.6, 128.1, 128.4, 138.1, 138.2, 138.6, 154.1 ppm. MS (EI): m/z (%) 105 (92) $[C_8H_9]^+$, 453 (100) $[M-(m\text{-xylynyl})]^+$, 467 (14) $[M-(C_7H_7)]^+$, 515 (19) $[M-(3\times CH_3)]^+$, 543 (4) $[M-(CH_3)]^+$, 558 (94) $[M]^+$. HRMS (EI): m/z calcd for $C_{38}H_{46}N_4$: 558.3722, found: 558.3690. IR (KBr): ν 3435, 2952, 2869, 1609, 1504, 1493, 1455, 1435, 1424, 1386, 1374, 1365, 1347, 1275, 1117, 1081, 1045.

1,1'-di(4-*tert*-butylbenzyl)-4,8,8'-trimethylbicyclo[2.2.1]-4,4',5,5',6,6',7,7'-octahydro-1*H*,1'*H*-3,3'-bipyrazole (69h):



Compound **69h** was prepared following the standard procedure using **68** (500 mg, 1.427 mmol), sodium hydride (82 mg, 3.424 mmol) and 4-*tert*-butylbenzyl bromide (534 μ L, 2.906 mmol) in 100 mL anhydrous tetrahydrofuran. The solution was stirred at reflux temperature for 4 h. **69h** (887 mg, 1.380 mmol, 97%) was obtained as a yellowish powder. Mp. 214 – 226 $^{\circ}$ C; ^1H NMR (300.13 MHz, CDCl_3 , TMS): δ 0.78 (s, 6H, 2 \times (-CH₃)), 0.87 (s, 6H, 2 \times (-CH₃)), 1.12 (s, 6H, 2 \times (-CH₂CCH₃)), 1.17 – 1.30 (m, 22H, 2 \times -*t*Bu, 2 \times (-CCH₂-)), 1.63 – 1.71 (m, 2H, 2 \times (-CHCH₂-)), 2.00 – 2.10 (m, 2H, 2 \times (-CHCH₂-)), 2.91 (d, J = 3.1 Hz, 2H, 2 \times (-CCH)), 5.28 (d, 2H, $^2J_{\text{H-H}}$ = 15.7 Hz, -NCH₂-), 5.36 (d, 2H, $^2J_{\text{H-H}}$ = 15.8 Hz, -NCH₂-), 7.08 – 7.11 (m, 4H, 2 \times 2(ArH)), 7.27 – 7.29 (m, 4H, 2 \times 2(ArH)) ppm. ^{13}C NMR (75.46 MHz, CDCl_3 , TMS): δ 11.5, 19.8, 20.6, 27.5, 31.5, 33.6, 34.6, 48.5, 52.6, 53.9, 62.7, 125.3, 126.7, 127.2, 135.6, 138.3, 150.2, 154.1 ppm. MS (EI): m/z (%) 147 (78) [$\text{C}_{11}\text{H}_{15}$]⁺, 495 (100) [M-($\text{C}_{11}\text{H}_{15}$)]⁺, 509 (13) [M-($\text{C}_{10}\text{H}_{13}$)]⁺, 599 (19) [M-(3 \times CH₃)]⁺, 627 (5) [M-(CH₃)]⁺, 643 (91) [M]⁺. HRMS (EI): m/z calcd for $\text{C}_{44}\text{H}_{58}\text{N}_4$: 642.4661, found: 642.4662. IR (KBr): ν 3455, 2952, 2869, 1609, 1504, 1493, 1455, 1435, 1424, 1386, 1374, 1365, 1347, 1275, 1117, 1081, 1045.

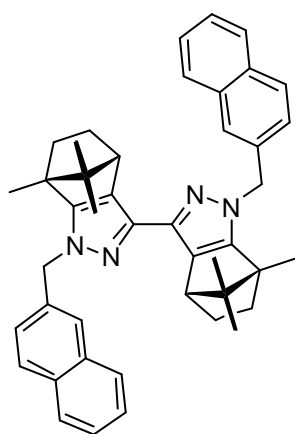
1,1'-di(2,4,6-trimethylbenzyl)-4,8,8'-trimethylbicyclo[2.2.1]-4,4',5,5',6,6',7,7'-octahydro-1*H*,1'*H*-3,3'-bipyrazole (69i):



Compound **69i** was prepared following the standard procedure using **68** (244 mg, 0.695 mmol), sodium hydride (40 mg, 1.667 mmol) and 2,4,6-trimethylbenzyl chloride (240 mg, 1.423 mmol) in 50 mL anhydrous tetrahydrofuran. The solution was stirred at reflux temperature for 16 h. **69i** (398 mg, 0.647 mmol, 93%) was obtained as a yellowish foam. Mp. 153 – 179 $^{\circ}$ C; ^1H NMR (500.13 MHz, CDCl_3 , TMS): δ 0.78 (s, 6H, 2 \times (-CH₃)), 0.85 (s, 6H, 2 \times (-CH₃)), 0.96 (s, 6H, 2 \times (-CH₂CCH₃)), 1.06 – 1.16 (m, 4H, 2 \times (-CCH₂-)), 1.60 – 1.65 (m, 2H, 2 \times (-CHCH₂-)), 1.98 – 2.03 (m, 2H, 2 \times (-CHCH₂-)), 2.27 (s, 6H, 2 \times (ArCH₃)), 2.29 (s, 12H, 4 \times (ArCH₃)), 2.88 (d, J = 3.5 Hz, 2H, 2 \times (-CCH)), 5.32 (s, 4H, 2 \times (-NCH₂-)), 6.85 (s, 4H,

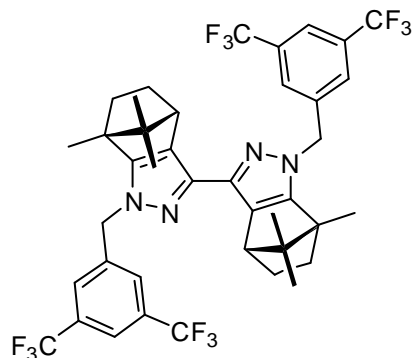
4×(ArH)) ppm. ^{13}C NMR (125.75 MHz, CDCl_3 , TMS): δ 11.5, 19.9, 20.6, 21.1, 27.4, 33.6, 48.2, 49.3, 53.3, 62.4, 127.1, 129.4, 130.6, 137.4, 138.1, 153.7 ppm. MS (EI): m/z (%) 133 (100) $[\text{C}_{10}\text{H}_{13}]^+$, 481 (86) $[\text{M}-(\text{C}_{10}\text{H}_{13})]^+$, 495 (22) $[\text{M}-(\text{mesityl})]^+$, 571 (24) $[\text{M}-(3\times\text{CH}_3)]^+$, 599 (5) $[\text{M}-(\text{CH}_3)]^+$, 614 (71) $[\text{M}]^+$. HRMS (EI): m/z calcd for $\text{C}_{42}\text{H}_{54}\text{N}_4$: 614.4348, found: 614.4359. IR (KBr): ν 3442, 2956, 2869, 1614, 1487, 1463, 1425, 1386, 1375, 1365, 1284, 1261, 1237, 1118, 1080, 1050, 1032, 997.

1,1'-di(naphthalene-2-ylmethyl)-4,8,8'-trimethylbicyclo[2.2.1]-4,4',5,5',6,6',7,7'-octahydro-1*H*,1'*H*-3,3'-bipyrazole (69j):



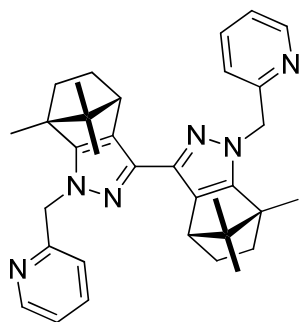
Compound **69j** was prepared following the standard procedure using **68** (300 mg, 0.856 mmol), sodium hydride (49 mg, 2.043 mmol) and 2-(bromomethyl)naphthalene (382 mg, 1.728 mmol) in 80 mL anhydrous tetrahydrofuran. The solution was stirred at reflux temperature for 4 h. **69j** (519 mg, 0.823 mmol, 96%) was obtained as a white powder. Mp. 200 – 223 °C; ^1H NMR (300.13 MHz, CDCl_3 , TMS): δ 0.81 (s, 6H, 2×(-CH₃)), 0.86 (s, 6H, 2×(-CH₃)), 1.08 (s, 6H, 2×(-CH₂CCH₃)), 1.10 – 1.30 (m, 4H, 2×(-CCH₂-)), 1.61 – 1.70 (m, 2H, 2×(-CHCH₂-)), 2.03 – 2.13 (m, 2H, 2×(-CHCH₂-)), 2.96 (d, J = 3.7 Hz, 2H, 2×(-CCH)), 5.57 (s, 4H, 2×(-NCH₂-)), 7.31 – 7.35 (m, 2H, 2×(ArH)), 7.42 – 7.47 (m, 4H, 2×2(ArH)), 7.59 (s, 2H, 2×(ArH)), 7.75 – 7.82 (m, 6H, 2×3(ArH)) ppm. ^{13}C NMR (75.46 MHz, CDCl_3 , TMS): δ 11.5, 19.8, 20.6, 27.5, 33.6, 48.6, 52.6, 54.4, 62.8, 125.1, 125.4, 125.9, 126.2, 127.6, 127.8, 128.0, 128.3, 132.9, 133.4, 136.3, 138.4, 154.3 ppm. MS (EI): m/z (%) 141 (100) $[\text{C}_{11}\text{H}_9]^+$, 489 (71) $[\text{M}-(\text{C}_{11}\text{H}_9)]^+$, 503 (8) $[\text{M}-(2\text{-naphthyl})]^+$, 587 (8) $[\text{M}-3\times(\text{CH}_3)]^+$, 615 (2) $[\text{M}-(\text{CH}_3)]^+$, 630 (44) $[\text{M}]^+$. HRMS (EI): m/z calcd for $\text{C}_{44}\text{H}_{46}\text{N}_4$: 630.3722, found: 630.3679. IR (KBr): ν 3425, 2956, 2870, 1509, 1453, 1438, 1419, 1387, 1376, 1366, 1278, 1261, 1117, 1085, 1046, 1019, 999, 810.

1,1'-bis(3,5-di(trifluoromethyl)benzyl)-4,8,8'-trimethylbicyclo[2.2.1]-4,4',5,5',6,6',7,7'-octahydro-1*H*,1'*H*-3,3'-bipyrazole (69k):



Compound **69k** was prepared following the standard procedure using **68** (300 mg, 0.856 mmol), sodium hydride (45 mg, 1.88 mmol) and 3,5-di(trifluoromethyl)benzyl chloride (322 μ L, 1.75 mmol) in 90 mL anhydrous tetrahydrofuran. The solution was stirred at reflux temperature for 4 h. After crystallization from diethyl ether and washings with pentane **69k** (289 mg, 0.360 mmol, 42%) was obtained as a white powder. Mp. 155 – 158 $^{\circ}$ C; 1 H NMR (500.13 MHz, CDCl_3 , TMS): δ 0.80 (s, 6H, $2\times(-\text{CH}_3)$), 0.90 (s, 6H, $2\times(-\text{CH}_3)$), 1.08 – 1.25 (m, 8H, $2\times-\text{CH}_2\text{CCH}_3$, $2\times(-\text{CCH}_2-)$), 1.19 – 1.25 (m, 2H, $2\times(-\text{CCH}_2-)$), 1.75 – 1.80 (m, 2H, $2\times(-\text{CHCH}_2-)$), 2.08 – 2.14 (m, 2H, $2\times(-\text{CHCH}_2-)$), 3.00 (bs, 2H, $2\times(-\text{CCH})$), 5.46 (d, 2H, $^2J_{\text{H-H}} = 16.5$ Hz, $-\text{NCH}_2-$), 5.52 (d, 2H, $^2J_{\text{H-H}} = 16.3$ Hz, $-\text{NCH}_2-$), 7.58 (s, 4H, $4\times(\text{ArH})$), 7.77 (s, 2H, $2\times(\text{ArH})$) ppm. ^{13}C NMR (125.75 MHz, CDCl_3 , TMS): δ 11.28, 19.5, 20.1, 27.1, 33.6, 48.4, 52.6, 53.0, 62.9, 121.5, 122.0, 124.2, 126.9, 128.1, 131.9, 140.9, 154.7 ppm. MS (EI): m/z (%) 227 (11) $[\text{C}_9\text{H}_5\text{F}_6]^+$, 575 (23) $[\text{M}-(3,5\text{-di(trifluoromethyl)benzyl})]^+$, 589 (4) $[\text{M}-(\text{C}_9\text{H}_5\text{F}_6)]^+$, 759 (100), 787 (7) $[\text{M}-(\text{CH}_3)]^+$, 803 (24) $[\text{M}]^+$. HRMS (EI): m/z calcd for $\text{C}_{40}\text{H}_{38}\text{F}_{12}\text{N}_4$: 802.2905, found: 802.2914. IR (KBr): ν 3447, 2964, 2874, 1624, 1505, 1464, 1437, 1381, 1348, 1323, 1277, 1245, 1178, 1134, 1084, 1045, 906, 888.

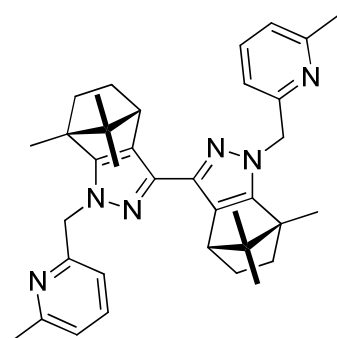
1,1'-di(pyridine-2-ylmethyl)-4,8,8'-trimethylbicyclo[2.2.1]-4,4',5,5',6,6',7,7'-octahydro-1*H*,1'*H*-3,3'-bipyrazole (76):



For the preparation of compound **76** 2-(bromomethyl)pyridine (444 mg, 1.755 mmol) was suspended in 20 mL anhydrous tetrahydrofuran, freshly distilled triethylamine (230 μ L, 1.799 mmol) and molecular sieve (3 \AA) was added. The mixture was stirred slowly for 18 h at room temperature. Triethylammonium bromide was filtered off and the solution was transferred to sodium 3,3'-bicyclo[2.2.1]octane-3,3'-dicarboxylate in anhydrous tetrahydrofuran, as prepared following the standard procedure (3,3'-bicyclo[2.2.1]octane-3,3'-dicarboxylic acid, 300 mg, 0.856 mmol and sodium hydride, 42 mg, 1.75 mmol). The

solution was stirred for one hour at room temperature, five hours at reflux temperature and additional 12 h at room temperature. Workup, purification and isolation of the compound was achieved following the standard procedure for bcpz-ligand preparation and washing with acetone once. Compound **76** (409 mg, 0.761 mmol, 89%) was obtained as white, needle-shaped crystals. Mp. 213 – 218 °C; ¹H NMR (500.13 MHz, CDCl₃, TMS): δ 0.78 (s, 6H, 2×(-CH₃)), 0.88 (s, 6H, 2×(-CH₃)), 1.11 (s, 6H, 2×(-CH₂CCH₃)), 1.12 – 1.16 (m, 2H, 2×(-CCH₂-)), 1.21 – 1.25 (m, 2H, 2×(-CCH₂-)), 1.69 – 1.74 (m, 2H, 2×(-CHCH₂-)), 2.06 – 2.12 (m, 2H, 2×(-CHCH₂-)), 2.94 (d, 2H, *J* = 3.7 Hz, 2×(-CCH)), 5.48 (d, 2H, ²*J*_{H-H} = 16.6 Hz, -NCH₂-), 5.52 (d, 2H, ²*J*_{H-H} = 16.7 Hz, -NCH₂-), 6.94 (d, 2H, *J* = 8.1 Hz, 2×ArH), 7.14 (dd, 2H, *J* = 5.1 Hz, *J* = 1.9 Hz, 2×ArH), 7.56 (dd, 2H, *J* = 7.7 Hz, *J* = 1.7 Hz, 2×ArH), 8.50 (d, 2H, *J* = 4.3 Hz, 2×ArH) ppm. ¹³C NMR (125.75 MHz, CDCl₃, TMS): δ 10.9, 19.6, 20.4, 27.3, 33.4, 48.5, 52.5, 55.8, 62.7, 121.3, 122.2, 127.4, 136.8, 138.5, 148.8, 154.7, 158.5 ppm. MS (EI): *m/z* (%) 398 (10), 412 (9), 440 (79) [M-(C₇H₆N)]⁺, 454 (17) [M-(C₆H₄N)]⁺, 489 (26), 503 (12), 517 (9) [M-(CH₃)]⁺, 532 (100) [M]⁺. HRMS (EI): *m/z* calcd for C₃₄H₄₀N₆: 532.3314, found: 532.3312. IR (KBr): ν 3439, 2954, 2870, 1591, 1572, 1507, 1474, 1437, 1387, 1376, 1365, 1348, 1279, 1245, 1117, 1083, 1046, 997, 839, 757.

1,1'-di[(6-methylpyridine-2-yl)methyl]-4,8,8'-trimethylbicyclo[2.2.1]-4,4',5,5',6,6',7,7'-octahydro-1*H*,1'*H*-3,3'-bipyrazole (77**):**



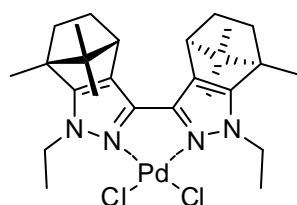
This compound was synthesized following the procedure for the preparation of 1,1'-bis(pyridine-2-ylmethyl)-3,3'-bicyclo[2.2.1]-4,4',5,5',6,6',7,7'-octahydro-1*H*,1'*H*-3,3'-bipyrazole (**77**). 2-(bromomethyl)-6-methylpyridine (319 mg, 1.715 mmol), triethylamine (230 μL, 1.799 mmol), 3,3-bicyclo[2.2.1]-4,4',5,5',6,6',7,7'-octahydro-1*H*,1'*H*-3,3'-bipyrazole (300 mg, 0.856 mmol) and sodium hydride (42 mg, 1.75 mmol). Workup, purification and isolation of the compound was achieved following the standard procedure for bcpz-ligand preparation and washing

with acetone once. Compound **77** (335 mg, 0.597 mmol, 70%) was obtained as white, needle-shaped crystals. Mp. 186 – 192 °C; ¹H NMR (500.13 MHz, CDCl₃, TMS): δ 0.78 (s, 6H, 2×(-CH₃)), 0.88 (s, 6H, 2×(-CH₃)), 1.12 (s, 6H, 2×(-CH₂CCH₃)), 1.14 – 1.25 (m, 4H, 4×(-CCH₂-)), 1.69 – 1.74 (m, 2H, 2×(-CCH₂-)), 1.69 – 1.74 (m, 2H, 2×(-CHCH₂-)), 2.05 – 2.12 (m, 2H, 2×(-CHCH₂-)), 2.52 (s, 6H, 2×ArCH₃), 2.93 (d, 2H, *J* = 3.6 Hz, 2×(-CCH)), 5.43 (d, 2H, ²*J*_{H-H} = 16.7 Hz, -NCH₂-), 5.48 (d, 2H, ²*J*_{H-H} = 16.7 Hz, -NCH₂-), 6.69 (d, 2H, *J* = 7.8 Hz, 2×ArH),

6.98 (d, 2H, $J = 7.3$ Hz, $2 \times \text{ArH}$), 7.43 (dd, 2H, $J = 7.8$ Hz, $J = 7.8$ Hz, $2 \times \text{ArH}$) ppm. ^{13}C NMR (125.75 MHz, CDCl_3 , TMS): δ 10.9, 19.6, 20.4, 24.3, 27.4, 33.4, 48.5, 52.5, 55.9, 62.7, 118.2, 121.6, 127.3, 136.9, 138.5, 154.6, 157.5, 157.8 ppm. MS (EI): m/z (%) 412 (8), 426 (8), 454 (75) $[\text{M}-(\text{C}_8\text{H}_8\text{N})]^+$, 468 (21) $[\text{M}-(\text{C}_7\text{H}_6\text{N})]^+$, 517 (27), 531 (12), 545 (9) $[\text{M}-(\text{CH}_3)]^+$, 560 (100) $[\text{M}]^+$. HRMS (EI): m/z calcd for $\text{C}_{36}\text{H}_{44}\text{N}_6$: 560.3627, found: 560.3642. IR (KBr): ν 3425, 2954, 2870, 1594, 1577, 1506, 1457, 1438, 1386, 1375, 1365, 1332, 1278, 1244, 1116, 1094, 1083, 1046, 1000, 776.

General procedure for the preparation of bcpz palladium(II) chloride complexes. To a solution of the appropriate bipyrazole ligand (1 eq.) in anhydrous acetonitrile was added Bis(acetonitrile)dichloropalladium(II) (1 eq.) and the solution was stirred for 16h at room temperature. The solvent was evaporated under reduced pressure; the product was taken up in a small amount of chloroform and filtered through a short plug of silica. Evaporation and drying under high vacuum yielded the corresponding biamphorpyrazole palladium complexes as deep orange to red microcrystalline solids.

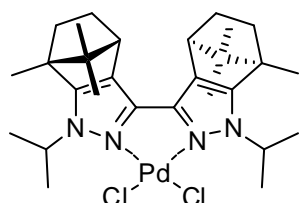
1,1'-diethyl-4,8,8'-trimethylbicyclo[2.2.1]-4,4',5,5',6,6',7,7'-octahydro-1H,1'H-3,3'-bipyrazole palladium(II) chloride (70a):



Compound **70a** was prepared following the standard procedure using **69a** (94 mg, 0.231 mmol) and bis(acetonitrile)dichloropalladium(II) (60 mg, 0.231 mmol) in 10 mL anhydrous acetonitrile to yield **70a** (132 mg, 0.226 mmol, 98%) as a ochre red powder. Mp. 147 – 158 °C; ^1H NMR (500.13 MHz, CDCl_3 , TMS): δ 4.84 (dddd, 2H, $J = 7.1$ Hz, $J = 7.0$ Hz, $J = 7.0$ Hz, $^2J_{\text{H-H}} = 14.1$ Hz, $2 \times (-\text{NCH}_2-)$), 4.61 (dddd, 2H, $J = 7.1$ Hz, $J = 7.0$ Hz, $J = 7.0$ Hz, $^2J_{\text{H-H}} = 14.1$ Hz, $2 \times (-\text{NCH}_2-)$), 2.86 (d, 2H, $J = 3.4$ Hz, $2 \times (-\text{CCH})$), 2.11 – 2.16 (m, 2H, $2 \times (-\text{CHCH}_2-)$), 1.87 – 1.92 (m, 2H, $2 \times (-\text{CHCH}_2-)$), 1.41 (dd, 6H, $J = 7.0$ Hz, $J = 7.0$ Hz, $2 \times (-\text{CH}_2\text{CCH}_3)$), 1.35 (s, 6H, $2 \times (-\text{CH}_2\text{CH}_3)$), 1.26 – 1.31 (m, 2H, $2 \times (-\text{CCH}_2-)$), 1.12 – 1.17 (m, 2H, $2 \times (-\text{CCH}_2-)$), 0.96 (s, 6H, $2 \times (-\text{CCH}_3)$), 0.76 (s, 6H, $2 \times (-\text{CCH}_3)$) ppm. ^{13}C NMR (125.75 MHz, CDCl_3 , TMS): δ 11.2, 17.5, 19.4, 20.4, 27.1, 33.6, 45.5, 47.9, 54.0, 63.2, 124.5, 138.6, 158.3 ppm. MS (FAB): m/z (%) 511 (100) $[\text{M}-(\text{HCl}), -(\text{Cl}^-)]^+$, 546 (8) $[\text{M}-(\text{Cl}^-)]^+$, 953 (51) $[\text{M}+(\text{L}), -(\text{Cl}^-)]^+$, 1129 (13) $[2 \times \text{M}-(\text{Cl}^-)]^+$. HRMS (FAB): m/z (%) calcd for $\text{C}_{26}\text{H}_{37}\text{N}_4^{106}\text{Pd}^+$ $[\text{M}-(\text{HCl}), -(\text{Cl}^-)]^+$: 511.2053, found: 511.2042. IR (KBr): ν 3443, 2964, 2872, 1635, 1559, 1508, 1466, 1390, 1380, 1306, 1287, 1276, 1247,

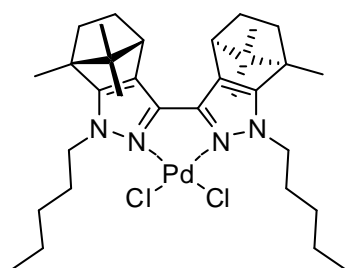
1206, 1182, 1137, 1100, 1082, 1063, 1015. Anal. calcd for $C_{26}H_{38}Cl_2N_4Pd \times 1/5 CHCl_3$, C: 51.37 H: 6.28 N: 9.13 Cl: 15.44 Pd: 17.38. Found, C: 51.25 H: 6.46 N: 9.28.

1,1'-diisopropyl-4,8,8'-trimethylbicyclo[2.2.1]-4,4',5,5',6,6',7,7'-octahydro-1H,1'H-3,3'-bipyrazole palladium(II) chloride (70b):



Compound **70b** was prepared following the standard procedure using **69b** (101 mg, 0.231 mmol) and bis(acetonitrile)di-chloropalladium(II) (60 mg, 0.231 mmol) in 10 mL anhydrous acetonitrile to yield **70b** (134 mg, 0.219 mmol, 95%) as a ochre red powder. Mp. 170 – 179 °C; 1H NMR (500.13 MHz, $CDCl_3$, TMS): δ 0.77 (s, 6H, $2 \times (-CCH_3)$), 0.96 (s, 6H, $2 \times (-CCH_3)$), 1.10 – 1.15 (m, 2H, $2 \times (-CCH_2-)$), 1.27 – 1.33 (m, 2H, $2 \times (-CCH_2-)$), 1.40 – 1.47 (m, 18H, $2 \times (-CH_2C(CH_3)_2)$, $2 \times (-CH_2CCH_3)$), 1.83 – 1.90 (m, 2H, $2 \times (-CHCH_2-)$), 2.11 – 2.16 (m, 2H, $2 \times (-CHCH_2-)$), 2.87 (d, 2H, $J = 3.7$ Hz, $2 \times (-CCH)$), 5.84 (q, 2H, $J = 6.9$ Hz, $2 \times (-NCH-)$) ppm. ^{13}C NMR (125.75 MHz, $CDCl_3$, TMS): δ 15.0, 19.8, 20.5, 22.5, 23.1, 27.0, 47.4, 54.4, 55.5, 62.9, 126.8, 137.8, 157.6 ppm. MS (FAB): m/z (%) 539 (25) $[M-(HCl), -(Cl)]^+$, 1010 (14) $[M+(L), -(Cl)]^+$. HRMS (FAB): m/z (%) calcd for $C_{28}H_{41}N_4^{106}Pd^+$ $[M-(HCl), -(Cl)]^+$: 539.2377, found: 539.2407. IR (KBr): ν 3444, 2966, 2872, 1628, 1559, 1438, 1389, 1369, 1331, 1288, 1277, 1259, 1207, 1181, 1136, 1104, 1083, 1049, 998. Anal. calcd for $C_{28}H_{42}Cl_2N_4Pd \times 1/3 CHCl_3$, C: 50.96 H: 6.38 N: 8.34. Found, C: 50.93 H: 6.47 N: 8.55.

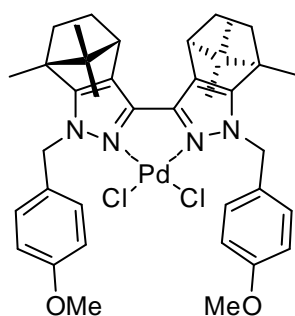
1,1'-dipentyl-4,8,8'-trimethylbicyclo[2.2.1]-4,4',5,5',6,6',7,7'-octahydro-1H,1'H-3,3'-bipyrazole palladium(II) chloride (70c):



Compound **70c** was prepared following the standard procedure using **69c** (114 mg, 0.231 mmol) and bis(acetonitrile)di-chloropalladium(II) (60 mg, 0.231 mmol) in 10 mL anhydrous acetonitrile to yield **70c** (134 mg, 0.211 mmol, 91%) as a ochre red powder. Mp. 149 – 154 °C; 1H NMR (500.13 MHz, $CDCl_3$, TMS): δ 0.76 (s, 6H, $2 \times (-CCH_3)$), 0.89 (t, 6H, $J = 7.4$ Hz, $2 \times (-CH_2CH_3)$), 0.96 (s, 6H, $2 \times (-CCH_3)$), 1.13 – 1.17 (m, 2H, $2 \times (-CHCH-)$), 1.26 – 1.37 (m, 16H, $2 \times (-CHCH_2CH_2-)$, $2 \times (-CHCH_2CH_2-)$, $2 \times (-CH_2CCH_3)$), 1.78 – 1.89 (m, 4H, $2 \times (-CH_2CH_2CH_3)$), 2.00 (s, 2H, $-CH_2CH_2-$), 2.11 – 2.16 (m, 2H, $2 \times (-$

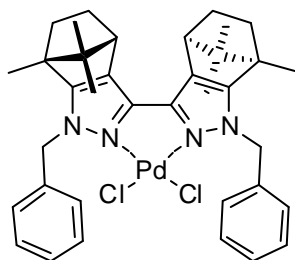
CH₂CH₂-), 2.85 (d, 2H, $J = 3.8$ Hz, 2×(-CCH)), 4.52 (ddd, 2H, , $J = 9.4$ Hz, $J = 6.0$ Hz, $^2J_{H-H} = 13.8$ Hz, -NCH₂-), 4.73 (ddd, 2H, , $J = 9.4$ Hz, $J = 6.3$ Hz, $^2J_{H-H} = 14.0$ Hz -NCH₂-) ppm. ¹³C NMR (125.75 MHz, CDCl₃, TMS): δ 11.3, 14.2, 19.4, 20.4, 22.5, 27.1, 28.8, 32.0, 33.6, 47.9, 50.4, 54.0, 63.2, 124.3, 138.6, 158.4 ppm. MS (FAB): m/z (%) 595 (84) [M-(HCl), -(Cl⁻)]⁺, 631 (4) [M-(Cl⁻)]⁺, 1121 (1) [M+(L), -(Cl⁻)]⁺, 1297 (7) [2×M-(Cl⁻)]⁺. HRMS (FAB): m/z (%) calcd for C₃₂H₄₉N₄¹⁰⁶Pd⁺ [M-(HCl), -(Cl⁻)]⁺: 595.2992, found: 595.2990. IR (KBr): ν 3445, 2959, 2931, 2871, 1627, 1465, 1390, 1378, 1307, 1287, 1276, 1247, 1206, 1184, 1137, 1105, 1086, 1067, 1015, 1000. Anal. calcd for C₃₂H₅₀Cl₂N₄Pd×5/6 CHCl₃, C: 51.38 H: 6.68 N: 7.63. Found, C: 51.42 H: 6.62 N: 7.72.

1,1'-di(4-methoxybenzyl)-4,8,8'-trimethylbicyclo[2.2.1]-4,4',5,5',6,6',7,7'-octahydro-1H,1'H-3,3'-bipyrazole palladium(II) chloride (70d):



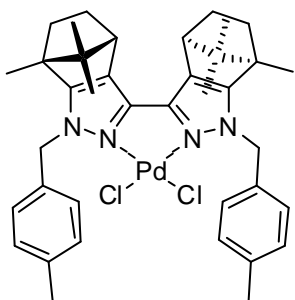
Compound **70d** was prepared following the standard procedure using **69d** (114 mg, 0.193 mmol) and bis(acetonitrile)dichloropalladium(II) (50 mg, 0.193 mmol) in 10 mL anhydrous acetonitrile to yield **70d** (145 mg, 0.189 mmol, 97%) as a deep orange powder. Mp. 218 – 222 °C; ¹H NMR (500.13 MHz, CDCl₃, TMS): δ 0.74 (s, 6H, 2×(-CCH₃)), 0.92 (s, 6H, 2×(-CCH₃)), 1.06 – 1.15 (m, 4H, 2×(-CH₂CH₂-), 2×(-CH₂CH₂-)), 1.23 (s, 6H, 2×(-CH₂CCH₃)), 1.72 – 1.76 (m, 2H, 2×(-CH₂CH₂-)), 2.08 – 2.13 (m, 2H, 2×(-CH₂CH₂-)), 2.87 (d, 2H, $J = 3.7$ Hz, 2×(-CCH)), 5.83 (d, 2H, $^2J_{H-H} = 15.9$ Hz, -NCH₂-), 6.18 (d, 2H, $^2J_{H-H} = 15.9$ Hz, -NCH₂-), 6.78 – 6.87 (m, 4H, 2×2(ArH)), 6.86 – 6.87 (m, 2H, 2×(ArH)), 7.20 – 7.23 (m, 2H, 2×(ArH)) ppm. ¹³C NMR (125.75 MHz, CDCl₃, TMS): δ 11.1, 19.2, 20.3, 26.8, 32.7, 47.7, 53.3, 54.0, 55.3, 63.2, 112.8, 113.3, 119.3, 125.5, 129.6, 138.3, 139.0, 159.5, 159.7 ppm. MS (FAB): m/z (%): 695 (96) [M-(HCl), -(Cl⁻)]⁺, 733 (24) [M-(Cl⁻)]⁺, 1323 (19) [M+(L), -(Cl⁻)]⁺. HRMS (FAB): m/z (%) calcd for C₃₈H₄₆³⁵ClN₄O₂¹⁰⁸Pd⁺ [M]⁺: 733.2347, found: 733.2348. IR (KBr): ν 3427, 2962, 2874, 1602, 1586, 1491, 1456, 1437, 1390, 1369, 1349, 1305, 1284, 1261, 1148, 1123, 1103, 1046, 1017. Anal. calcd for C₃₈H₄₆Cl₂N₄O₂Pd×1/11 CHCl₃, C: 57.93 H: 5.88 N: 7.07. Found, C: 57.43 H: 6.06 N: 6.84.

1,1'-dibenzyl-4,8,8'-trimethylbicyclo[2.2.1]-4,4',5,5',6,6',7,7'-octahydro-1*H*,1'*H*-3,3'-bipyrazole palladium(II) chloride (70e):



Compound **4e** was prepared following the standard procedure using **69e** (123 mg, 0.231 mmol) and bis(acetonitrile)dichloropalladium(II) (60 mg, 0.231 mmol) in 10 mL anhydrous acetonitrile to yield **70e** (158 mg, 0.223 mmol, 96%) as a deep orange powder. Mp. 164 – 170 °C; ¹H NMR (500.13 MHz, CDCl₃, TMS): δ 0.72 (s, 6H, 2×(-CCH₃)), 0.90 (s, 6H, 2×(-CCH₃)), 1.00 – 1.14 (m, 4H, 2×(-CH₂CH₂-), 2×(-CH₂CH₂-)), 1.19 (s, 6H, 2×(-CH₂CCH₃)), 1.68 – 1.73 (m, 2H, 2×(-CH₂CH₂-)), 2.06 – 2.12 (m, 2H, 2×(-CH₂CH₂-)), 2.86 (d, 2H, *J* = 3.6 Hz, 2×(-CCH)), 5.85 (d, 2H, ²*J*_{H-H} = 15.8 Hz, -NCH₂-), 6.23 (d, 2H, ²*J*_{H-H} = 15.9 Hz, -NCH₂-), 7.23 – 7.32 (m, 10H, 2×(ArH)) ppm. ¹³C NMR (125.75 MHz, CDCl₃, TMS): δ 11.2, 19.4, 20.4, 26.9, 32.8, 47.9, 53.6, 54.2, 63.4, 125.7, 127.3, 127.9, 128.7, 137.1, 139.1, 159.7 ppm. MS (FAB): *m/z* (%): 635 (82) [M-(HCl), -(Cl⁻)]⁺, 671 (26) [M-(Cl⁻)]⁺, 1203 (4) [M+(L), -(Cl⁻)]⁺, 1381 (6) [2×M-(Cl⁻)]⁺. HRMS (FAB): *m/z* (%) calcd for C₃₆H₄₂³⁵ClN₄¹⁰⁶Pd⁺ [M]⁺: 671.2143, found: 671.2164. IR (KBr): ν 3442, 2962, 2871, 1626, 1606, 1497, 1454, 1391, 1379, 1369, 1315, 1287, 1276, 1247, 1182, 1124, 1103. Anal. calcd for C₃₆H₄₂Cl₂N₄Pd×1/11 CHCl₃, C: 60.22 H: 5.89 N: 7.78. Found, C: 60.17 H: 6.06 N: 7.87.

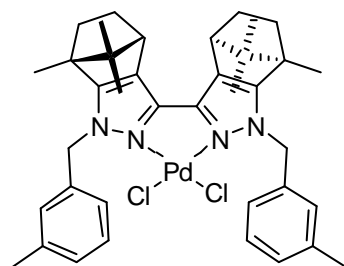
1,1'-di(4-methylbenzyl)-4,8,8'-trimethylbicyclo[2.2.1]-4,4',5,5',6,6',7,7'-octahydro-1*H*,1'*H*-3,3'-bipyrazole palladium(II) chloride (70f):



Compound **70f** was prepared following the standard procedure using **69f** (129 mg, 0.231 mmol) and bis(acetonitrile)dichloropalladium(II) (60 mg, 0.231 mmol) in 10 mL anhydrous acetonitrile to yield **70f** (166 mg, 0.226 mmol, 98%) as a deep orange powder. Mp. 151 – 160 °C; ¹H NMR (500.13 MHz, CDCl₃, TMS): δ 0.72 (s, 6H, 2×(-CCH₃)), 0.90 (s, 6H, 2×(-CCH₃)), 1.02 – 1.11 (m, 4H, 2×(-CH₂CH₂-)), 1.22 (s, 6H, 2×(-CH₂CCH₃)), 1.69 – 1.74 (m, 2H, 2×(-CH₂CH₂-)), 2.06 – 2.11 (m, 2H, 2×(-CH₂CH₂-)), 2.31 (s, 6H, 2×(ArCH₃)), 2.85 (d, 2H, *J* = 3.7 Hz, 2×(-CCH)), 5.77 (d, 2H, ²*J*_{H-H} = 15.6 Hz, -NCH₂-), 6.18 (d, 2H, ²*J*_{H-H} = 15.5 Hz, -NCH₂-), 7.11 (d, 4H, *J* = 8.0 Hz, 2×(ArH)), 7.18 (d, 4H, *J* = 8.0 Hz, 2×(ArH)) ppm. ¹³C NMR (125.75 MHz, CDCl₃, TMS): δ 11.3, 19.4, 20.4, 21.3, 26.9, 32.8, 47.9, 53.4, 54.1, 63.3, 125.6, 127.3, 129.4, 134.0, 137.6, 139.1, 159.5 ppm. MS

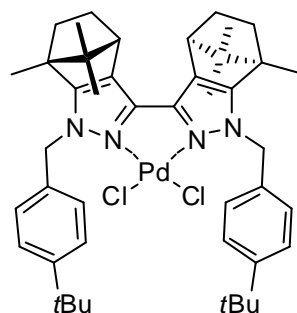
(FAB): m/z (%) 663 (91) $[M-(HCl), -(Cl^-)]^+$, 699 (30) $[M-(Cl^-)]^+$, 1258 (19) $[M+(L), -(Cl^-)]^+$, 1438 (6) $[2\times M-(Cl^-)]^+$. HRMS (FAB): m/z (%) calcd for $C_{38}H_{46}^{35}ClN_4^{106}Pd^+$ $[M]^+$: 699.2457, found: 699.2419. IR (KBr): ν 3432, 2963, 2872, 1617, 1516, 1457, 1390, 1369, 1316, 1287, 1276, 1248, 1205, 1184, 1124, 1103, 1072, 1050, 1018. Anal. calcd for $C_{38}H_{46}Cl_2N_4Pd \times 1/8 CHCl_3$, C: 60.83 H: 6.19 N: 7.44. Found, C: 60.89 H: 6.37 N: 7.30.

1,1'-di(3-methylbenzyl)-4,8,8'-trimethylbicyclo[2.2.1]-4,4',5,5',6,6',7,7'-octahydro-1H,1'H-3,3'-bipyrazole palladium(II) chloride (70g):



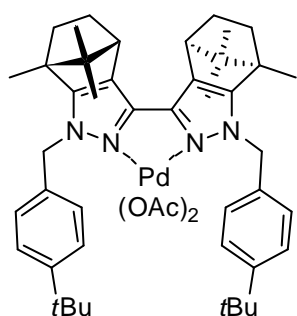
Compound **70g** was prepared following the standard procedure using **69g** (129 mg, 0.231 mmol) and bis(acetonitrile)di-chloropalladium(II) (60 mg, 0.231 mmol) in 10 mL anhydrous acetonitrile to yield **70g** (166 mg, 0.224 mmol, 97%) as a deep orange powder. Mp. 143 – 147 °C; 1H NMR (500.13 MHz, $CDCl_3$, TMS): δ 0.73 (s, 6H, $2\times(-CCH_3)$), 0.91 (s, 6H, $2\times(-CCH_3)$), 1.04 – 1.14 (m, 4H, $2\times(-CH_2CH_2-)$), 1.19 (s, 6H, $2\times(-CH_2CCH_3)$), 1.70 – 1.75 (m, 2H, $2\times(-CH_2CH_2-)$), 2.08 – 2.13 (m, 2H, $2\times(-CH_2CH_2-)$), 2.31 (s, 6H, $2\times(ArCH_3)$), 2.87 (d, 2H, $J = 3.7$ Hz, $2\times(-CCH)$), 5.84 (d, 2H, $^2J_{H-H} = 15.9$ Hz, $-NCH_2-$), 6.16 (d, 2H, $^2J_{H-H} = 15.9$ Hz, $-NCH_2-$), 7.01 – 7.06 (m, 6H, $2\times(3ArH)$), 7.17 – 7.20 (m, 2H, $2\times(ArH)$) ppm. ^{13}C NMR (125.75 MHz, $CDCl_3$, TMS): δ 11.2, 19.4, 20.4, 21.6, 26.9, 32.8, 47.9, 53.5, 54.1, 63.3, 124.2, 125.6, 127.8, 128.6, 128.7, 137.0, 138.3, 139.1, 159.6 ppm. MS (FAB): m/z (%) 663 (25) $[M-(HCl), -(Cl^-)]^+$, 699 (30) $[M-(Cl^-)]^+$, 1259 (2) $[M+(L),-(Cl^-)]^+$, 1439 (3) $[2\times M-(Cl^-)]^+$. HRMS (FAB): m/z (%) calcd for $C_{38}H_{46}^{35}ClN_4^{106}Pd^+$ $[M]^+$: 699.2457, found: 699.2478. IR (KBr): ν 3453, 2963, 2871, 1609, 1490, 1456, 1390, 1378, 1369, 1348, 1306, 1287, 1276, 1248, 1184, 1123, 1104, 1092. Anal. calcd for $C_{38}H_{46}Cl_2N_4Pd \times 1/8 CHCl_3$, C: 60.83 H: 6.18 N: 7.44. Found, C: 60.69 H: 6.36 N: 7.41.

1,1'-di(4-*tert*-butylbenzyl)-4,8,8'-trimethylbicyclo[2.2.1]-4,4',5,5',6,6',7,7'-octahydro-1H,1'H-3,3'-bipyrazole palladium(II) chloride (70h):



Compound **70h** was prepared following the standard procedure using **69h** (149 mg, 0.231 mmol) and bis(acetonitrile)dichloropalladium(II) (60 mg, 0.231 mmol) in 10 mL anhydrous acetonitrile to yield **70h** (187 mg, 0.224 mmol, 97%) as a deep orange powder. Mp. 203 – 205 °C; ^1H NMR (500.13 MHz, CDCl_3 , TMS): δ 0.74 (s, 6H, $2\times(-\text{CCH}_3)$), 0.92 (s, 6H, $2\times(-\text{CCH}_3)$), 1.05 – 1.14 (m, 4H, $2\times(-\text{CH}_2\text{CH}_2-)$), 1.24 (s, 6H, $2\times(-\text{CH}_2\text{CCH}_3)$), 1.29 (s, 18H, $2\times(-\text{C}(\text{CH}_3)_3)$), 1.72 – 1.76 (m, 2H, $2\times(-\text{CH}_2\text{CH}_2-)$), 2.08 – 2.13 (m, 2H, $2\times(-\text{CH}_2\text{CH}_2-)$), 2.87 (d, 2H, $J = 3.7$ Hz, $2\times(-\text{CCH})$), 5.81 (d, 2H, $^2J_{\text{H-H}} = 15.8$ Hz - NCH_2-), 6.18 (d, 2H, $^2J_{\text{H-H}} = 15.8$ Hz, $-\text{NCH}_2-$), 7.19 (d, 4H, $J = 8.3$ Hz, $2\times(\text{ArH})$), 7.32 (d, 4H, $J = 8.4$ Hz, $2\times(\text{ArH})$) ppm. ^{13}C NMR (125.75 MHz, CDCl_3 , TMS): δ 11.1, 19.2, 20.3, 26.8, 32.7, 34.5, 47.8, 53.0, 54.0, 63.2, 125.4, 126.9, 133.7, 139.0, 150.7, 159.4 ppm. MS (FAB): m/z (%) 747 (45) $[\text{M}-(\text{HCl}), -(\text{Cl})]^+$, 783 (19) $[\text{M}-(\text{Cl})]^+$, 1427 (3) $[\text{M}+(\text{L}),-(\text{Cl})]^+$. HRMS (FAB): m/z (%) calcd for $\text{C}_{44}\text{H}_{58}^{35}\text{ClN}_4^{106}\text{Pd}^+$ $[\text{M}]^+$: 783.3398, found: 783.3434. IR (KBr): ν 3445, 2961, 2871, 1622, 1514, 1458, 1415, 1391, 1367, 1316, 1276, 1247, 1205, 1193, 1125, 1050, 1019, 1001. Anal. calcd for $\text{C}_{44}\text{H}_{58}\text{Cl}_2\text{N}_4\text{Pd}\times 1/9 \text{CHCl}_3$, C: 63.45 H: 7.01 N: 6.71. Found, C: 63.47 H: 7.19 N: 6.82.

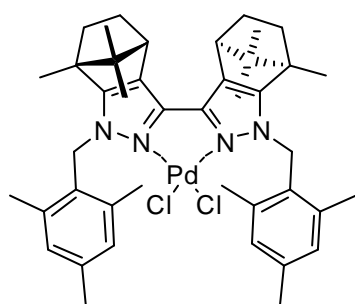
1,1'-di(4-*tert*-butylbenzyl)-4,8,8'-trimethylbicyclo[2.2.1]-4,4',5,5',6,6',7,7'-octahydro-1H,1'H-3,3'-bipyrazole palladium(II) acetate (70h^(OAc)):



Compound **70h^(OAc)** was prepared following the standard procedure using **69h** (100 mg, 0.156 mmol) and palladium(II) acetate (35 mg, 0.156 mmol) in 12 mL anhydrous dichloromethane to yield **70h^(OAc)** (129 mg, 0.149 mmol, 96%) as a white powder. Decomp. >170 °C; ^1H NMR (399.89 MHz, CD_2Cl_2): δ 0.75 (s, 6H, $2\times(-\text{CCH}_3)$), 0.90 (s, 6H, $2\times(-\text{CCH}_3)$), 1.08 (s, 6H, $2\times(-\text{CH}_2\text{CCH}_3)$), 1.12 – 1.20 (m, 4H, $2\times(-\text{CH}_2\text{CH}_2-)$), 1.30 (s, 18H, $2\times(-\text{C}(\text{CH}_3)_3)$), 1.49 (s, 6H, $2\times(-\text{OAc})$), 1.69 – 1.75 (m, 2H, $2\times(-\text{CH}_2\text{CH}_2-)$), 2.07 – 2.14 (m, 2H, $2\times(-\text{CH}_2\text{CH}_2-)$), 2.92 (d, 2H, $J = 3.6$ Hz, $2\times(-\text{CCH})$), 5.35 (d, 2H, $^2J_{\text{H-H}} = 16.1$ Hz - NCH_2-), 5.47 (d, 2H, $^2J_{\text{H-H}} = 16.2$ Hz, $-\text{NCH}_2-$), 7.06 (d, 4H, $J = 8.3$ Hz, $2\times(\text{ArH})$), 7.37 (d, 4H, $J = 8.3$ Hz, $2\times(\text{ArH})$) ppm. ^{13}C NMR (125.75 MHz, CDCl_3 , TMS):

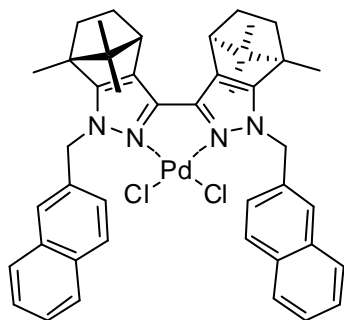
δ 11.0, 19.3, 20.4, 22.7, 27.0, 31.5, 32.9, 34.7, 47.9, 52.5, 53.9, 63.1, 125.7, 126.3, 133.4, 138.0, 150.8, 158.3, 179.1 ppm. MS (FAB): m/z (%) 747 (100) [M-(HOAc), -(OAc⁻)]⁺, 1391 (15) [M+(L), -2×(OAc⁻)]⁺. HRMS (FAB): m/z (%) calcd for C₄₄H₅₇N₄¹⁰⁶Pd⁺ [M]⁺: 747.3634, found: 747.3631. IR (KBr): ν 3432, 2961, 2871, 1638, 1581, 1515, 1458, 1414, 1391, 1367, 1288, 1262, 1206, 1184, 1128, 1108, 1017. Anal. calcd for C₄₈H₆₄N₄O₄Pd×1/9 CHCl₃, C: 66.46 H: 7.44 N: 6.46. Found, C: 65.41 H: 7.47 N: 6.39.

1,1'-di(2,4,6-trimethylbenzyl)-4,8,8'-trimethylbicyclo[2.2.1]-4,4',5,5',6,6',7,7'-octahydro-1H,1'H-3,3'-bipyrazole palladium(II) chloride (70i):



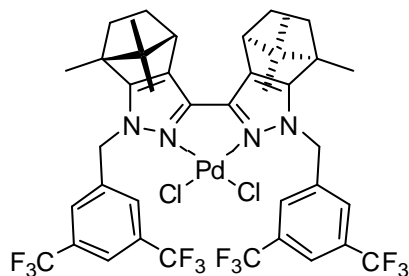
Compound **70i** was prepared following the standard procedure using **69i** (142 mg, 0.231 mmol) and bis(acetonitrile)di-chloropalladium(II) (60 mg, 0.231 mmol) in 10 mL anhydrous acetonitrile to yield **70i** (173 mg, 0.218 mmol, 95%) as a ochre red powder. Mp. 162 – 172 °C; ¹H NMR (500.13 MHz, CDCl₃, TMS): δ 0.60 (s, 6H, 2×(-CCH₃)), 0.68 (s, 6H, 2×(-CCH₃)), 0.81 (s, 6H, 2×(-CH₂CCH₃)), 0.85 – 0.91 (m, 2H, 2×(-CH₂CH₂-)), 1.05 – 1.10 (m, 2H, 2×(-CH₂CH₂-)), 1.47 – 1.52 (m, 2H, 2×(-CH₂CH₂-)), 2.02 – 2.07 (m, 2H, 2×(-CH₂CH₂-)), 2.10 (s, 12H, 2×(ArCH₃)), 2.24 (s, 6H, 2×(ArCH₃)), 2.81 (d, 2H, $J = 3.6$ Hz, 2×(-CCH)), 5.74 (d, 2H, $^2J_{H-H} = 16.6$ Hz, -NCH₂-), 6.35 (d, 2H, $^2J_{H-H} = 16.6$ Hz, -NCH₂-), 6.78 (s, 4H, 2×(ArH)) ppm. ¹³C NMR (125.75 MHz, CDCl₃, TMS): δ 10.5, 19.5, 20.4, 20.5, 21.0, 27.2, 32.2, 47.7, 51.8, 55.3, 63.1, 126.7, 130.0, 137.3, 137.7, 137.8, 159.0 ppm. MS (FAB): m/z (%) 719 (59) [M-(HCl), -(Cl⁻)]⁺, 754 (5) [M-(Cl⁻)]⁺, 1371 (6) [M+(L), -(Cl⁻)]⁺. HRMS (FAB): m/z (%) calcd for C₄₂H₅₄³⁵ClN₄¹⁰⁶Pd⁺ [M]⁺: 755.3084, found: 755.3137. IR (KBr): ν 3447, 2960, 2874, 1613, 1483, 1457, 1423, 1390, 1379, 1323, 1288, 1277, 1261, 1246, 1182, 1125, 1099, 1031, 1016, 850. Anal. calcd for C₄₂H₅₄Cl₂N₄Pd×1/4 CHCl₃, C: 61.11 H: 6.58 N: 6.73. Found, C: 61.01 H: 6.66 N: 6.85.

1,1'-di(naphthalene-2-ylmethyl)-4,8,8'-trimethylbicyclo[2.2.1]-4,4',5,5',6,6',7,7'-octahydro-1*H*,1'*H*-3,3'-bipyrazole palladium(II) chloride (70j):



Compound **70j** was prepared following the standard procedure using **69j** (150 mg, 0.238 mmol) and bis(acetonitrile)di-chloropalladium(II) (62 mg, 0.238 mmol) in 10 mL anhydrous acetonitrile to yield **70j** (173 mg, 0.225 mmol, 95%) as a deep orange powder. Mp. 158 – 170 °C; ¹H NMR (500.13 MHz, CD₂Cl₂, TMS): δ 0.78 (s, 6H, 2×(-CCH₃)), 0.91 (s, 6H, 2×(-CCH₃)), 1.03 – 1.19 (m, 4H, 2×(-CH₂CH₂-)), 1.21 (s, 6H, 2×(-CH₂CCH₃)), 1.69 – 1.77 (m, 2H, 2×(-CH₂CH₂-)), 2.07 – 2.17 (m, 2H, 2×(-CH₂CH₂-)), 2.96 (d, 2H, *J* = 3.7 Hz, 2×(-CCH)), 6.05 (d, 2H, ²*J*_{H-H} = 16.2 Hz, -NCH₂-), 6.40 (d, 2H, ²*J*_{H-H} = 16.2 Hz, -NCH₂-), 7.41 – 7.52 (m, 6H, 2×(ArH)), 7.62 (s, 2H, 2×(ArH)), 7.81 – 7.87 (m, 7H, 2×(ArH)) ppm. ¹³C NMR (125.75 MHz, CD₂Cl₂, TMS): δ 11.4, 19.5, 20.6, 27.2, 33.3, 48.5, 63.8, 125.3, 126.0, 126.4, 126.7, 126.9, 128.2, 128.4, 129.0, 133.4, 133.8, 135.4, 139.7, 160.4 ppm. MS (FAB): *m/z* (%) 735 (63) [M-(HCl), -(Cl)]⁺, 771 (8) [M-(Cl)]⁺, 1402 (4) [M+(L), -(Cl)]⁺. HRMS (FAB): *m/z* (%) calcd for C₄₄H₄₆³⁵ClN₄¹⁰⁶Pd⁺ [M]⁺: 771.2459, found: 771.2455. IR (KBr): ν 3446, 3115, 2963, 2872, 1654, 1634, 1602, 1509, 1457, 1424, 1390, 1378, 1370, 1329, 1286, 1275, 1248, 1124. Anal. calcd for C₂₈H₄₂Cl₂N₄Pd×1/8 CHCl₃, C: 64.25 H: 5.64 N: 6.79. Found, C: 64.06 H: 5.74 N: 6.87.

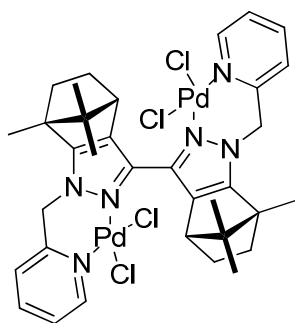
1,1'-di(3,5-di(trifluoromethyl)benzyl)-4,8,8'-trimethylbicyclo[2.2.1]-4,4',5,5',6,6',7,7'-octahydro-1*H*,1'*H*-3,3'-bipyrazole palladium(II) chloride (70k):



Compound **70k** was prepared following the standard procedure using **69k** (102 mg, 0.127 mmol) and bis-(acetonitrile)dichloropalladium(II) (33 mg, 0.127 mmol) in 10 mL anhydrous acetonitrile to yield **70k** (120 mg, 0.122 mmol, 96%) as a yellow powder. Mp. 145 – 148 °C; ¹H NMR (500.13 MHz, CDCl₃, TMS): δ 0.78 (s, 6H, 2×(-CCH₃)), 0.96 (s, 6H, 2×(-CCH₃)), 1.14 (s, 6H, 2×(-CH₂CCH₃)), 1.16 – 1.25 (m, 4H, 2×(-CH₂CH₂-), 2×(-CH₂CH₂-)), 1.84 – 1.89 (m, 2H, 2×(-CH₂CH₂-)), 2.17 – 2.23 (m, 2H, 2×(-CH₂CH₂-)), 2.97 (d, 2H, *J* = 3.7 Hz, 2×(-CCH)), 6.10 (d, 2H, ²*J*_{H-H} = 16.7 Hz, -NCH₂-), 6.32 (d, 2H, ²*J*_{H-H} = 16.7 Hz, -NCH₂-), 7.52 (s, 4H, 4×(ArH)), 7.80 (s, 2H, 2×(ArH)) ppm. ¹³C NMR

(125.75 MHz, CDCl₃, TMS): δ 10.9, 19.1, 20.0, 26.7, 33.0, 47.9, 52.5, 54.1, 63.6, 119.7, 121.7, 124.1, 126.3, 126.5, 132.1, 132.0, 139.3, 140.0, 159.9 ppm. MS (FAB): m/z (%): 907 (100) [M-(HCl), -(Cl)]⁺, 945 (26) [M-(Cl)]⁺. HRMS (FAB): m/z (%) calcd for C₄₀H₃₈³⁵ClF₁₂N₄¹⁰⁸Pd⁺ [M]⁺: 945.1632, found: 945.1594. IR (KBr): ν 3446, 2965, 2026, 1973, 1624, 1457, 1382, 1351, 1280, 1175, 1136, 1017, 907, 845. Anal. calcd for C₃₆H₄₂Cl₂N₄Pd \times 1/13 CHCl₃, C: 48.63 H: 3.88 N: 5.66. Found, C: 48.39 H: 4.02 N: 5.54.

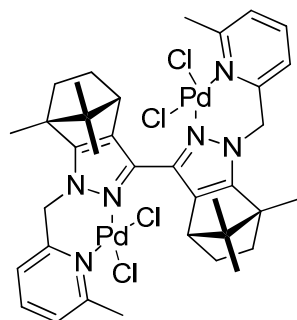
1,1'-di(pyridine-2-ylmethyl)-4,8,8'-trimethylbicyclo[2.2.1]-4,4',5,5',6,6',7,7'-octahydro-1H,1'H-3,3'-bipyrazole di(palladium(II) dichloride) (78):



To a solution of ligand **76** (28 mg, 0.053 mmol) in dichloromethane was added a solution of bis(acetonitrile)palladium(II) chloride (27 mg, 0.104 mmol) and stirred for 24 h at room temperature. The solution was concentrated under reduced pressure and the product allowed to crystallize. Washings with pentane furnished the title compound **78** as a dark, orange microcrystalline powder (45 mg,

0.051 mmol, 97%). Mp. 99 – 106 °C (decomp.); mixture of atropisomers: ¹H NMR (600.13 MHz, CD₂Cl₂, TMS): δ 0.76 – 0.79 (m, 0.7H), 0.87 – 0.96 (m, 8H), 1.07 – 1.11 (m, 0.7H), 1.30 – 1.56 (m, 13.7H), 1.72 – 1.82 (m, 1.4H), 1.96 – 2.01 (m, 1.4H), 2.15 – 2.20 (m, 1.3H), 2.65 – 2.71 (m, 2H), 5.28 – 5.34 (m, 4H), 6.37 – 6.39 (m, 2H, ArH), 7.35 – 7.38 (m, 2H, ArH), 7.46 – 7.49 (m, 2H, ArH), 7.86 – 7.90 (m, 2H, ArH), 9.86 – 9.92 (m, 2H, ArH) ppm. ¹³C NMR (150.90 MHz, CD₂Cl₂, TMS): δ 11.1, 11.2, 18.6, 19.1, 19.6, 19.9, 25.9, 27.4, 29.7, 33.0, 33.9, 47.3, 48.0, 54.3, 55.1, 55.2, 61.6, 65.1, 122.4, 122.8, 125.2, 125.3, 129.9, 130.4, 136.7, 138.1, 139.8, 139.9, 150.6, 150.5, 151., 155.4, 156.2, 157.9, 158.0 ppm. MS (FAB): m/z (%) 673 (77) [M-(PdCl₂), -(Cl)]⁺, 816 (10) [M-(HCl), -(Cl)]⁺, 851 (70) [M-(Cl)]⁺. HRMS (FAB): m/z (%) calcd for C₃₄H₄₀Cl₃N₆Pd₂⁺ [M]⁺: 851.0452, found: 851.0505. ATR-FTIR: ν 2953, 2884, 1602, 1479, 1445, 1410, 1392, 1379, 1371, 1310, 1287, 1270, 1210, 1183, 1151, 1120, 1104, 1098, 1047, 1022, 100, 948, 931, 841, 780, 761, 735, 701.

1,1'-di[(6-methylpyridine-2-yl)methyl]-4,8,8'-trimethylbicyclo[2.2.1]-4,4',5,5',6,6',7,7'-octahydro-1*H*,1'*H*-3,3'-bipyrazole di(palladium(II) dichloride) (79):

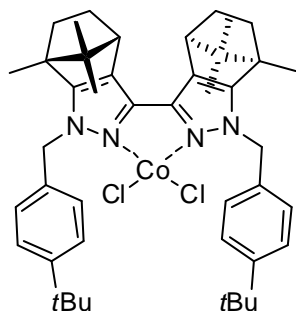


To a solution of ligand **77** (67 mg, 0.120 mmol) in dichloromethane was added a solution of bis(acetonitrile)palladium(II) chloride (62 mg, 0.239 mmol) and stirred for 24 h at room temperature. The solution was concentrated under reduced pressure and the product allowed to crystallize. Washings with pentane furnished the title compound **79** as a dark, orange microcrystalline powder (103 mg,

0.113 mmol, 94%). Mp. 161 – 168 °C (decomp.); mixture of atropisomers: ¹H NMR (600.13 MHz, CD₂Cl₂, TMS): δ 0.68 – 0.71 (m, 1.3H), 0.83 – 0.97 (m, 13H), 1.32 – 1.47 (m, 8H), 1.70 – 1.74 (m, 1H), 1.78 – 1.82 (m, 0.9H), 1.97 – 2.01 (m, 1.4H), 2.14 – 2.18 (m, 1H), 2.62 – 2.65 (m, 1.7H), 3.92 – 3.93 (m, 5H), 5.34 – 5.38 (m, 2H), 6.97 – 7.02 (m, 2H, ArH), 7.28 – 7.30 (m, 2H, ArH), 7.35 – 7.37 (m, 2H, ArH), 7.75 – 7.78 (m, 2H, ArH) ppm. ¹³C NMR (150.90 MHz, CD₂Cl₂, TMS): δ 10.8, 18.3, 18.7, 19.2, 19.8, 27.0, 29.3, 29.5, 29.6, 32.4, 33.5, 47.2, 48.0, 54.0, 55.8, 55.9, 61.2, 65.0, 119.8, 120.1, 126.7 (2×), 131.0, 136.6, 139.2, 151.4, 151.7, 155.8, 166.0 ppm. MS (EI): *m/z* (%) 703 (32) [M-(PdCl₂), -(Cl)]⁺, 843 (9) [M-(HCl), -(Cl)]⁺, 879 (23) [M-(Cl)]⁺. HRMS (FAB): *m/z* (%) calcd for C₃₄H₄₀Cl₃N₆Pd₂⁺ [M]⁺: 879.0766, found: 879.0652. ATR-FTIR: ν 2961, 1608, 1572, 1529, 1457, 1418, 1391, 1310, 1273, 1244, 1226, 1208, 1185, 1155, 1125, 1104, 1051, 1034, 1020, 1003, 947, 910, 844, 805, 762, 756, 716, 701.

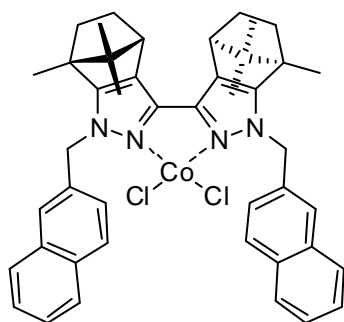
General procedure for the preparation of bcpz cobalt(II)- and copper(II) complexes. To a solution of the appropriate bipyrazole ligand (1 eq.) in absolute ethanol was added cobalt(II) chloride hexahydrate, respectively copper(II) chloride dihydrate (1 eq.). The solution lightens up and becomes cloudy. After 16 h at room temperature the solvent was evaporated, the residue was dissolved in a small amount of chloroform and filtered through a short plug of neutral aluminium oxide. The filtrate was evaporated and the product dried under high vacuum to yield the bipyrazole cobalt(II) complexes as fluffy, pale purple solids and the bipyrazole copper(II) complexes as red solids, respectively.

1,1'-di(4-*tert*-butylbenzyl)-4,8,8'-trimethylbicyclo[2.2.1]-4,4',5,5',6,6',7,7'-octahydro-1*H*,1'*H*-3,3'-bipyrazole cobalt(II) chloride (70h**^(Co)):**



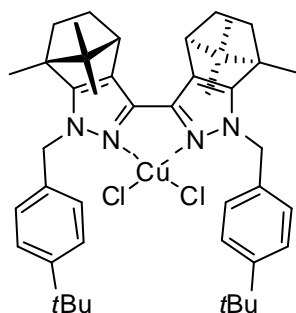
Compound **70h**^(Co) was prepared following the standard procedure using **69h** (49.9 mg, 0.078 mmol) and cobalt(II) chloride hexahydrate (18.5 mg, 0.078 mmol) in 3 mL absolute ethanol to yield **70h**^(Co) (54.2 mg, 0.070 mmol, 90%) as a fluffy, pale purple solid. Mp. 170 – 178 °C; MS (FAB): *m/z* (%) 700 (2) [M-(HCl), -(Cl)]⁺, 736 (100) [M-(Cl)]⁺, 1378 (11) [M+(L), -(Cl)]⁺. HRMS (FAB): *m/z* (%) calcd for C₄₄H₅₈³⁵ClN₄Co⁺ [M]⁺: 736.3682, found: 736.3704. IR (KBr): ν 3434, 2963, 2871, 1619, 1516, 1455, 1427, 1391, 1366, 1337, 1319, 1273, 1248, 1204, 1183, 1129, 1107, 1017. Anal. calcd for C₄₄H₅₈Cl₂CoN₄×1/15CHCl₃, C: 67.75 H: 7.49 N: 7.17. Found, C: 67.87 H: 7.59 N: 7.19.

1,1'-di(naphthalene-2-ylmethyl)-4,8,8'-trimethylbicyclo[2.2.1]-4,4',5,5',6,6',7,7'-octahydro-1*H*,1'*H*-3,3'-bipyrazole cobalt(II) chloride (70j**^(Co)):**



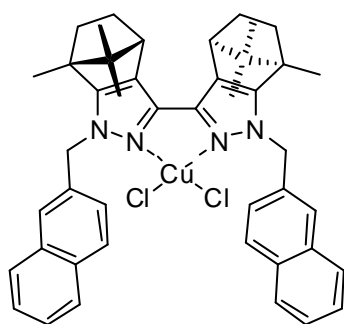
Compound **70j**^(Co) was prepared following the standard procedure using **69j** (47.8 mg, 0.076 mmol) and cobalt(II) chloride hexahydrate (18.0 mg, 0.076 mmol) in 3 mL absolute ethanol to yield **70j**^(Co) (53.7 mg, 0.071 mmol, 93%) as a fluffy, pale purple solid. Mp. 145 – 151 °C; MS (FAB): *m/z* (%) 688 (6) [M-(HCl), -(Cl)]⁺, 724 (93) [M-(Cl)]⁺, 1354 (1) [M+(L), -(Cl)]⁺. HRMS (FAB): *m/z* (%) calcd for C₄₄H₄₆³⁵ClN₄⁶³Co⁺ [M]⁺: 724.2743, found: 724.2808. IR (KBr): ν 3434, 3052, 2963, 1689, 1635, 1558, 1542, 1509, 1455, 1372, 1329, 1287, 1274, 1248, 1126, 1103. Anal. calcd for C₄₄H₄₆Cl₂CoN₄×1/5 CHCl₃, C: 67.66 H: 5.94 N: 7.14. Found, C: 67.52 H: 6.07 N: 7.11.

1,1'-di(4-*tert*-butylbenzyl)-4,8,8'-trimethylbicyclo[2.2.1]-4,4',5,5',6,6',7,7'-octahydro-1*H*,1'*H*-3,3'-bipyrazole copper(II) chloride (70h**^(Cu)):**



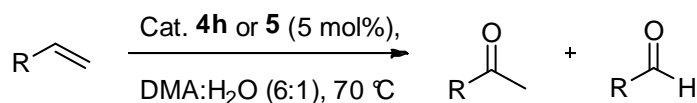
Compound **70h**^(Cu) was prepared following the standard procedure using **69h** (50.9 mg, 0.079 mmol) and copper(II) chloride dihydrate (13.5 mg, 0.079 mmol) in 3 mL absolute ethanol to yield **70h**^(Cu) (53.7 mg, 0.071 mmol, 89%) as a fine, red powder. Mp. 174 – 181 °C; MS (FAB): *m/z* (%) 704 (11) [M-(HCl), -(Cl⁻)]⁺, 740 (49) [M-(Cl⁻)]⁺, 1382 (9) [M+(L), -(Cl⁻)]⁺. HRMS (FAB): *m/z* (%) calcd for C₄₄H₅₈³⁵ClN₄Cu⁺ [M]⁺: 740.3646, found: 736.3624. IR (KBr): ν 3439, 2963, 2872, 1626, 1558, 1542, 1515, 1456, 1391, 1365, 1339, 1319, 1275, 1248, 1183, 1129, 1017. Anal. calcd for C₄₄H₅₈Cl₂CuN₄×1/6CHCl₃, C: 66.53 H: 7.35 N: 7.03. Found, C: 66.64 H: 7.46 N: 7.05.

1,1'-di(naphthalene-2-ylmethyl)-4,8,8'-trimethylbicyclo[2.2.1]-4,4',5,5',6,6',7,7'-octahydro-1*H*,1'*H*-3,3'-bipyrazole copper(II) chloride (70j**^(Cu)):**



Compound **70j**^(Cu) was prepared following the standard procedure using **69j** (54.1 mg, 0.086 mmol) and copper(II) chloride dihydrate (14.6 mg, 0.086 mmol) in 3 mL absolute ethanol to yield **70j**^(Cu) (59.5 mg, 0.078 mmol, 91%) as a fine, red powder. Mp. 131 – 138 °C; MS (FAB): *m/z* (%) 692 (9) [M-(HCl), -(Cl⁻)]⁺, 728 (44) [M-(Cl⁻)]⁺, 1358 (1) [M+(L), -(Cl⁻)]⁺. HRMS (FAB): *m/z* (%) calcd for C₄₄H₄₆³⁵ClN₄⁶³Cu⁺ [M]⁺: 728.2707, found: 728.2678. IR (KBr): ν 3431, 3053, 2963, 2873, 1634, 1510, 1455, 1390, 1370, 1330, 1287, 1275, 1248, 1185, 1126, 1102, 1017. Anal. calcd for C₄₄H₅₈Cl₂CuN₄×1/3CHCl₃, C: 64.78 H: 5.68 N: 6.79. Found, C: 64.91 H: 5.79 N: 6.97.

General procedure for the copper-free Wacker oxidations of terminal alkenes:



The catalyst[†] (5 mol%) was dissolved in a mixture of 2.5 mL of dimethyl acetamide and water (6:1) in a cap sealed vial, which was in turn evacuated at -78 °C and refilled with oxygen

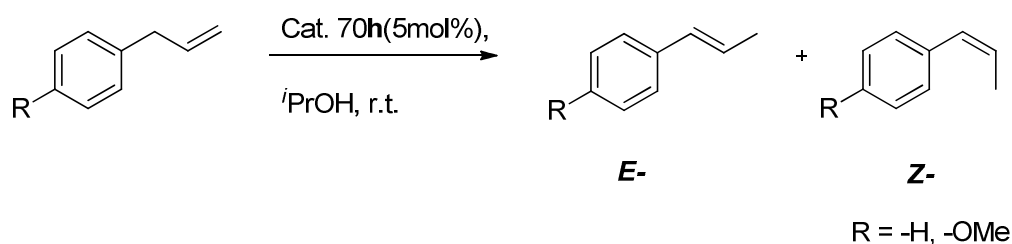
three times. The solution was allowed to warm up to room temperature and the appropriate alkene (0.89 mM) and 10 μ L of internal standard (undecane) were added. Reaction control samples were taken from the solution, extracted with diethyl ether, filtered through a short plug of neutral aluminum oxide to remove the catalyst and analyzed by GC- and GC-MS using a 25 m standard HP-5 MS column (film thickness 250 nm). Observed retention times of starting materials and products are depicted in table 1. For the oxidation without oxygen three equivalents of benzoquinone were added followed by the standard procedure.

[†] Pd(II)-2,2-bipyridine chloride **5** was synthesized from PdCl₂(MeCN)₂^[426] following the literature preparation.^[427]

Table 1: Observed retention times on a Agilent 25 m HP-5MS column using a temperature program (40 °C for 5 min, ramp 4 °C/min to 180 °C @ 80kPa He).

Substrate	RT [min]	Product	RT [min]
1-octene	8.3	octane-2-one	25.7
4-methylstyrene	17.8	4-methylbenzaldehyde	21.4
		1-(4-tolyl)ethanone	25.7
vinylcyclohexane	9.6	1-cyclohexylethanone	19.4

General procedure for the selective Isomerization of Allylbenzene and -anisole:



Catalyst **70h** (5 mol%) was dissolved in *iso*-propanol and the appropriate allylbenzenes (0.89 mM) and 10 μ L of internal standard (undecane) were added. Reaction control samples were taken from the solution, diluted with diethyl ether, filtered through a short plug of neutral aluminum oxide to remove the catalyst and analyzed by GC- and GC-MS using a 25 m standard HP-5MS column (film thickness 250 nm). Observed retention times of starting materials and products are depicted in table 2.

Table 2: Observed retention times on a Agilent 25 m HP-5MS column using a temperature program (100 °C for 5 min, ramp 4 °C/min to 180 °C @ 80kPa He).

Substrate	RT [min]	Product	RT [min]
allylbenzene	15.2	<i>cis</i> -propenylbenzene	17.3
		<i>trans</i> -propenylbenzene	18.8
allylanisole	11.5	<i>cis</i> -anethole	13.4
		<i>trans</i> -anethole	14.6

Preparation of authentic samples were carried out following the standard procedure using 1H, 1H-Heptafluoro-1-butanol as solvent. After the reaction was complete, the solution was extracted twice with pentane. The pentane layers were combined, filtered through neutral aluminum oxide and the solvent was allowed to evaporate at room temperature to yield the corresponding *E*-Isomers and traces of the *Z*-Isomers as shown in ¹H- and ¹³C-NMR spectroscopic measurements.

***trans*-propenylbenzene (72):**

¹H NMR (300.08 MHz, CDCl₃, TMS): δ 1.83 (dd, 3H, *J* = 6.5 Hz, ⁴*J* = 1.3 Hz, (-CH₃)), 6.18 (dq, 1H, *J*_{gem} = 15.6 Hz, ⁴*J* = 6.5 Hz, (-CHCH₃)), 6.35 (dd, 1H, *J*_{gem} = 15.7 Hz, ⁴*J* = 1.3 Hz, (-CHCHCH₃)), 7.11 – 7.15 (m, 1H, ArH), 7.20 – 7.29 (4H, 4×(ArH)) ppm. ¹³C NMR (75.46 MHz, CDCl₃, TMS): δ 18.5, 125.7, 125.8, 126.7, 128.4, 131.0, 137.9 ppm.

***trans*-anethole (73):**

¹H NMR (300.08 MHz, CDCl₃, TMS): δ 1.86 (dd, 3H, *J* = 6.5 Hz, ⁴*J* = 1.6 Hz, (-CH₃)), 3.80 (s, 3H, (-OCH₃)), 6.09 (dq, 1H, *J*_{gem} = 15.7 Hz, ⁴*J* = 6.5 Hz, (-CHCH₃)), 6.35 (dd, 1H, *J*_{gem} = 15.8 Hz, ⁴*J* = 1.5 Hz, (-CHCHCH₃)), 6.82 – 6.85 (m, 2H, 2×(ArH)), 7.26 – 7.28 (2H, 2×(ArH)) ppm. ¹³C NMR (75.48 MHz, CDCl₃, TMS): δ 18.4, 55.3, 113.9, 123.5, 126.9, 130.3, 130.8, 158.6 ppm.

UV-Vis spectra of palladium complexes 70h, 70j, 70d and 70k:

The solution spectra ($c = 0.03$ mM) of the palladium complexes were recorded in distilled tetrahydrofuran.

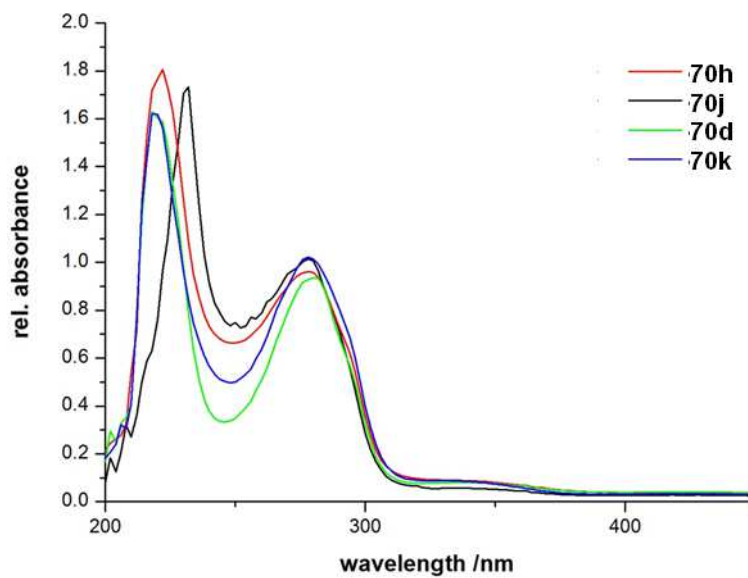
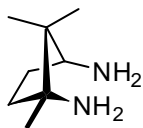


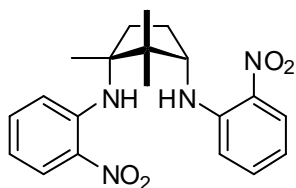
Figure 65 UV-Vis spectra of palladium complexes **70h**, **70j**, **70d** and **70k** in tetrahydrofuran.^[a]

Experimental Section – Chapter 3

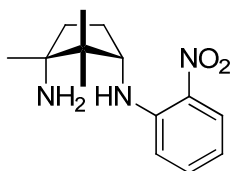
(1*R*,3*S*)-1,3-Diamino-1,2,2-trimethylcyclopentane (*R,S*-tmcp, **89**):



Caution: The reaction has to be performed very carefully due to danger of explosion. Strict control of the reaction conditions, addition cycles and monitoring of the reaction progress is crucial. It's explicitly advised to perform the reaction several times in a (sub-)gram scale prior to the amounts reported herein. Protecting equipment, like special gloves, a leather apron, a chest protector, a face shield as well as a bullet proof protective wall are recommended as well. This compound was prepared using a modified procedure of the reported one.^[349, 350] Camphoric acid (**88**, 36.0 g, 0.180 mol) and 1.2 L of ethanol-free chloroform were placed in a five liter round bottom flask under argon equipped with a mechanic stirrer and a 100 mL dropping-funnel. Sulfuric acid (90.0 mL, 98%) was slowly added and the mixture heated to 50 °C. A white gummy precipitate forms and after 30 min sodium azide (35.1 g, 0.540 mol) was added slowly in very small amounts starting with 1 g and later up to 3 g over a period of five hours (*caution*: hydrazoic acid generation). The mixture was stirred under argon for 18 h, cooled to 0 °C and poured slowly into 1 L of ice water. The chloroform layer was separated and discarded, the water layer adjusted to pH 12 with 3M sodium hydroxide (*caution*: carbon monoxide generation!) and extracted four times with dichloromethane (500 mL). Addition of sodium chloride may ease phase separation. The organic layers were combined and washed with brine. The organic layer was dried over sodium sulfate, the solvent evaporated and the product dried for 24 h under high vacuum to yield the title diamine **89** (24.1 g, 0.170 mol, 94%) as a white foam. The product can be stored under argon at low temperatures for several month without degradation. Mp. 127 – 129 °C; ¹H NMR (500.13 MHz, CDCl₃, TMS): δ 0.77 (s, 3H, -CH₃), 0.78 (s, 3H, -CH₃), 0.99 (s, 3H, -NH₂CCH₃), 1.23 – 1.31 (m, 1H, -CHCH₂-), 1.29 – 1.39 (bs, 4H, -NH₂), 1.54 – 1.66 (m, 2H, -CHCH₂-, -CH₃CCH₂-), 1.96 – 2.04 (m, 1H, -CH₃CCH₂), 2.95 (dd, *J* = 8.5 Hz, *J* = 9.0 Hz, 1H, -CHNH₂) ppm. ¹³C NMR (125.77 MHz, CDCl₃, TMS): δ 16.3, 22.2, 25.9, 30.3, 38.3, 46.2, 53.4, 60.8, 61.0 ppm. MS (CI): *m/z* (%) 71 (3), 83 (1), 110 (9) [M-2×NH₂]⁺, 143 [M+H]⁺. IR (KBr): ν 3282, 2960, 2869, 1594, 1472, 1371, 1316, 1209, 1165, 1093, 1043, 1018, 984, 877.

***N,N'*-Di(2-nitrophenyl)-(1*R*,3*S*)-diamino-tmcp (90):**

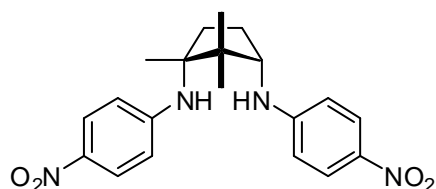
To a solution of *R,S*-tmcp (**89**, 6.00 g, 42.2 mmol) and freshly powdered potassium carbonate (11.67 g, 84.4 mmol) in 150 mL anhydrous dimethyl sulfoxide in a small reaction vessel (100 mL) was added 1-fluoro-2-nitrobenzene (12.50 g, 88.5 mmol) under vigorous stirring. The mixture turns immediately yellow and after stirring for 30 min the mixture was heated to 90 °C. At 2 h and 4 h freshly powdered potassium carbonate (11.67 g, 84.4 mmol) was added in one portion each. After stirring at 110 °C for 4 d the black, hot mixture was poured into 1.5 L water. The orange solid was filtered, washed five times with water, collected, dissolved in dichloromethane and dried over sodium sulphate. The solvent was evaporated and the residue was dried at 80 °C for one day and one day under high vacuum. The crude product was washed three times with diethyl ether to obtain the analytically pure product **90** (11.72 g, 30.5 mmol, 72%) as a bright orange-red, microcrystalline powder. Mp. 160 – 164 °C; ¹H NMR (300.13 MHz, CDCl₃, 25 °C): δ 1.18 (s, 3H, -CH₃), 1.24 (s, 3H, -CH₃), 1.51 (s, 3H, -NHCCCH₃), 1.67 – 1.79 (m, 1H, -CHCH₂-), 2.20 – 2.30 (m, 1H, -CHCH₂-), 2.35 – 2.48 (m, 2H, -CH₃CCH₂-), 4.02 (ddd, *J* = 8.4 Hz, *J* = 8.1 Hz, *J* = 8.1 Hz, 1H, -CH₂CHNH-), 6.60 - 6.67 (m, 2H, 2×ArH), 7.35 - 7.45 (m, 2H, 2×ArH), 8.17 - 8.22 (m, 2H, 2×ArH), 8.34 (bd, 1H, *J* = 8.4 Hz, -CHNH), 8.79 (bs, 1H, -CH₃CNH) ppm. ¹³C NMR (75.47 MHz, CDCl₃, TMS): δ 18.38, 21.6, 22.1, 29.1, 35.1, 49.7, 59.0, 64.3, 114.0, 115.2, 115.3, 115.8, 127.2, 127.6, 132.1, 132.7, 135.5, 136.2, 144.6, 145.5 ppm. MS (EI): *m/z* (%) 69 (23), 122 (13), 188 (29), 191 (13), 231 (16), 247 (100) [M-(2-nitroaniliny)]⁺, 384 (9) [M]⁺. HR-MS (EI, *m/z*): calc. for C₂₀H₂₄N₄O₄ [M]: 384.1798, found: 183.1771. IR (KBr): ν 3361, 2975, 1614, 1576, 1506, 1440, 1420, 1355, 1326, 1265, 1232, 1157, 1069, 1039, 1009, 857, 780, 742. Anal. calcd for C₂₀H₂₄N₄O₄, C: 62.49 H: 6.29 N: 14.57 O: 16.65. Found, C: 62.07 H: 5.81 N: 13.76.

(1*R*,3*S*)-1,2,2-trimethyl-*N*3-(2-nitrophenyl)cyclopentane-1,3-diamine (95):

This compound was prepared according to the procedure for the diarylation but with one equivalent of 1-fluoro-2-nitrobenzene (0.99 g, 7.0 mmol), *R,S*-tmcp (**89**, 1.00 g, 7.0 mmol) and freshly powdered potassium carbonate (1.95 g, 14.1 mmol) in 40 mL anhydrous dimethyl sulfoxide in a small reaction vessel (50 mL). After reacting for 2 d work-up followed according to the synthesis of the diarylation product *N,N'*-di(2-nitrophenyl)-(1*R*,3*S*)-diamino-tmcp to yield the title compound **95** as a bright, yellow solid (1.70 g, 6.4 mmol, 92%). Mp. 90 – 98 °C; ¹H NMR (300.13 MHz, CDCl₃, TMS): δ 0.96 (s,

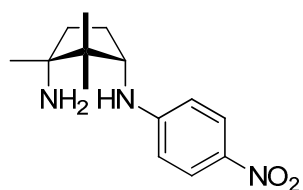
3H, -CH₃), 0.99 (s, 3H, -CH₃), 1.16 (s, 3H, -NHCCCH₃), 1.56 (bs, 3H, -NH₂), 1.62 – 1.72 (m, 2H, -CH₃CCH₂-, -CHCH₂-), 1.75 – 1.86 (m, 1H, -CHCH₂-), 2.24 – 2.37 (m, 1H, (-CH₃CCH₂), 3.80 (ddd, $J = 8.5$ Hz, $J = 8.5$ Hz, $J = 3.7$ Hz, 1H, -CH₂CHNH-), 6.85 (d, 1H, , $^4J_{\text{HAr-HAr}} = 8.7$ Hz, ArH), 6.55 - 6.50 (m, 1H, ArH), 7.40 - 7.32 (m, 1H, ArH), 8.13 (d, 1H, $^4J_{\text{HAr-HAr}} = 8.6$ Hz, $^4J_{\text{HAr-HAr}} = 1.6$ Hz, ArH), 8.15 (bd, 1H, $J = 8.2$ Hz, -NH-) ppm. ¹³C NMR (75.47 MHz, CDCl₃, TMS): δ 17.2, 24.2, 26.3, 29.4, 38.2, 47.5, 61.2, 62.0, 113.8, 114.1, 127.1, 131.5, 135.9, 145.3 ppm. MS (EI): m/z (%) 69 (17), 109 (8), 126 (100) [M-*o*-nitroaniliny]⁺, 231 (2), 246 (1) [M-NH₂]⁺, 263 (23) [M]⁺. HR-MS (EI, m/z): calc. for C₁₄H₂₁N₃O₂ [M]: 263.1634, found: 183.1631. ATR-FTIR: ν 3361, 2959, 1611, 1573, 1498, 1416, 1438, 1383, 1353, 1325, 1260, 1224, 1155, 1068, 1037, 948, 890, 856, 836, 780, 776, 739.

N,N'-Di(4-nitrophenyl)-(1*R*,3*S*)-diamino-tmcp (**97**):

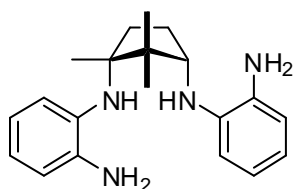


Method A: The compound was prepared similar to the diarylation to *N,N'*-di(2-nitrophenyl)-(1*R*,3*S*)-diamino-tmcp (**90**) using *R,S*-tmcp (**89**, 1.00 g, 7.0 mmol), 1-fluoro-4-nitrobenzene (2.28 g, 16.2 mmol) and freshly powdered potassium carbonate (3.89 g, 28.1 mmol) to yield the title compound **97** (506 mg, 1.3 mmol, 19%) as a bright yellow microcrystalline powder.

Method B: The compound was prepared using powdered caesium carbonate (9.16 g, 28.1 mmol) instead of potassium carbonate, *R,S*-tmcp (**89**, 2.00 g, 14.1 mmol) and 1-fluoro-4-nitrobenzene (4.36 g, 30.9 mmol) to yield the title compound **97** as a bright yellow microcrystalline powder (4.27 g, 11.1 mmol) in 79% yield. Mp. 79 – 82 °C; ¹H NMR (300.13 MHz, CDCl₃, TMS): δ 1.08 (s, 3H, -CH₃), 1.12 (s, 3H, -CH₃), 1.43 (s, 3H, -NHCCCH₃), 1.56 – 1.70 (m, 1H, -CHCH₂-), 2.06 – 2.16 (m, 1H, -CHCH₂-), 2.33 – 2.46 (m, 2H, -CH₃CCH₂-), 3.89 (ddd, $J = 8.4$ Hz, $J = 8.1$ Hz, $J = 8.1$ Hz, 1H, -CH₂CHNH-), 4.62 - 4.65 (m, 2H, 2×NH), 6.58 - 6.64 (m, 4H, 2×2ArH), 8.00 - 8.07 (m, 4H, 2×2ArH) ppm. ¹³C NMR (75.47 MHz, CDCl₃, TMS): δ 17.5, 21.1, 22.8, 29.2, 34.5, 49.6, 60.5, 64.6, 111.4, 113.4, 126.1, 126.5, 137.9, 151.9, 153.2 ppm. MS (EI): m/z (%) 69 (20), 109 (12), 321 (14) [M-CH₃]⁺, 247 (100) [M-*p*-nitroaniliny]⁺, 384 (8) [M]⁺. HR-MS (EI, m/z): calc. for C₂₀H₂₄N₄O₄ [M]: 384.1798, found: 183.1816. IR (KBr): ν 2967, 1596, 1504, 1472, 1377, 1309, 1187, 1114, 998, 835, 754, 700. Anal. calcd for C₂₀H₂₄N₄O₄, C: 62.49 H: 6.29 N: 14.57 O: 16.65. Found, C: 61.88 H: 6.24 N: 13.88.

(1*R*,3*S*)-1,2,2-trimethyl-*N*3-(4-nitrophenyl)cyclopentane-1,3-diamine (96):

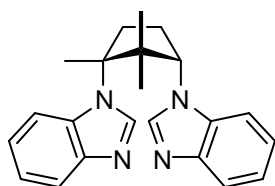
This compound was prepared according to the procedure for the diarylation but with one equivalent of 1-fluoro-4-nitrobenzene (0.50 g, 7.0 mmol), *R,S*-tmcp (**89**, 0.50 g, 3.50 mmol) and freshly powdered potassium carbonate (2.29 g, 7.0 mmol) in 40 mL anhydrous DMSO in a small reaction vessel (50 mL). After reacting for 2 d work-up followed according to the synthesis of the diarylation product *N,N'*-di(2-nitrophenyl)-(1*R*,3*S*)-diamino-tmcp (**90**) to yield the title compound **96** as a bright, yellow solid (0.93 g, 2.7 mmol, 78%). Mp. 90 – 98 °C; ¹H NMR (300.13 MHz, CDCl₃, TMS): δ 0.95 (s, 3H, -CH₃), 0.97 (s, 3H, -CH₃), 1.16 (s, 3H, -NHCCCH₃), 1.29 (bs, 2H, -NH₂), 1.58 – 1.71 (m, 2H, -CH₃CCH₂-, -CHCH₂-), 1.18 – 1.93 (m, 1H, -CHCH₂-), 2.18 – 2.32 (m, 1H, -CH₃CCH₂-), 3.66 (dd, *J* = 8.1 Hz, *J* = 7.8 Hz, 1H, -CH₂CHNH-), 6.43 - 6.47 (m, 2H, 2ArH), 4.64 (bd, *J* = 7.5 Hz, 1H, -CHNH-), 8.01 - 8.04 (m, 2H, 2ArH) ppm. ¹³C NMR (75.47 MHz, CDCl₃, TMS): δ 17.0, 25.5, 26.6, 29.4, 38.1, 47.9, 62.0, 63.3, 110.7, 126.7, 136.5, 153.5 ppm. MS (EI): *m/z* (%) 69 (12), 109 (10), 126 (100) [M-*p*-nitroaniliny]⁺, 164 (17), 231 (14), 246 (8) [M-NH₂]⁺, 263 (23) [M]⁺. HR-MS (EI, *m/z*): calc. for C₁₄H₂₁N₃O₂ [M]: 263.1634, found: 283.1650. ATR-FTIR: ν 3319, 2964, 2872, 1594, 1581, 1527, 1492, 1459, 1390, 1382, 1368, 1295, 1222, 1182, 1148, 1105, 1060, 1060, 996, 951, 926, 889, 822, 753.

***N*1,*N*1'-((1*R*,3*S*)-1,2,2-trimethylcyclopentane-1,3-diyl) di (benzyl-1,2-diamine) (91):**

To a solution of diaminoarylated-tmcp nitro compound **90** (1.00g, 2.60 mmol) in 50 mL anhydrous methanol under nitrogen was added palladium on charcoal (10% Pd, 277 mg). After addition the atmosphere was replaced by hydrogen two times. Hydrogen was constantly bubbled through the stirred mixture via a small syringe for two hours and the reaction progress monitored by thin-layer chromatography. The catalyst was removed by filtration (pore size 0.45 μm) and the solution was immediately evaporated to yield the tetramine title compound **91** (818 mg, 2.52 mmol, 97%) as a white foam. The product can be stored under argon and lower temperatures for some weeks. Decomposition of the compound due to oxidation is accompanied by a color-change from white to pale brown. ¹H NMR (300.13 MHz, CDCl₃, TMS): δ 1.10 (s, 3H, -CH₃), 1.20 (s, 3H, -CH₃), 1.33 (s, 3H, -NHCCCH₃), 1.53 - 1.65 (m, 1H, -CHCH₂-), 1.75 – 1.85 (m, 1H, -CHCH₂-), 2.30 – 2.42 (m, 1H, -CH₃CCH₂-), 2.50 – 2.62 (m, 1H, -CH₃CCH₂-), 3.53 - 3.93 (m, 7H, 2×-NH₂, 2×-NH-, -CHNH-), 6.62 - 6.89 (m, 8H, 2×4ArH) ppm. ¹³C NMR (75.47 MHz, CDCl₃, TMS): δ 17.3, 19.6, 25.1, 30.3, 32.6, 49.8, 62.1, 65.6, 112.1, 116.7, 117.1, 117.6, 118.2, 119.3, 120.0, 120.5, 134.5, 135.1, 137.6, 137.7 ppm. MS (EI): *m/z* (%) 69

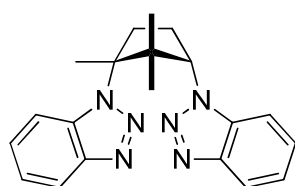
(20), 109 (12), 321 (14) $[M-CH_3]^+$, 247 (100) $[M-p\text{-nitroaniliny}]^+$, 384 (8) $[M]^+$. HR-MS (EI, m/z): calc. for $C_{20}H_{24}N_4O_4$ $[M]$: 384.1798, found: 183.1816. IR (KBr): ν 3054, 2968, 2872, 1620, 1597, 1504, 1454, 1391, 1371, 1342, 1294, 1266, 1238, 1148, 1101, 1059, 860, 821, 742.

1,1'-((1R,3S)-1,2,2-trimethylcyclopentane-1,3-diyl)di(1H-benzimidazole) (**92**):



Tetramine compound **91** (844 mg, 2.60 mmol) and triethyl orthoformate (7.0 mL, 42.1 mmol) were placed in a short distillation apparatus, two drops of formic acid were added and the reaction heated at 105 °C over night for distillation of ethanol. Triethyl orthoformate was decanted off, the residue dissolved in a small amount of dichloromethane and the product precipitated by addition of diethyl ether. The product was collected, washed with diethyl ether and the procedure repeated three times to yield 442 mg (1.28 mmol, 49%) of the title compound **92** as an off white powder. Mp. 120 – 127 °C; 1H NMR (500.13 MHz, $CDCl_3$, TMS): δ 0.60 (s, 3H, $-CH_3$), 1.36 (s, 3H, $-CH_3$), 2.00 (s, 3H, $-NHCCCH_3$), 2.31 – 2.36 (m, 1H, $-CHCH_2-$), 2.60 – 2.69 (m, 2H, $-CHCH_2-$, $-CH_3CCH_2-$), 3.37 – 3.50 (m, 1H, $-CH_3CCH_2-$), 4.90 (dd, $J = 9.0$ Hz, $J = 9.0$ Hz 1H, $-CH_2CHNH-$), 7.25 – 7.35 (m, 4H, 4ArH), 7.45 – 7.47 (m, 1H, ArH), 7.71 – 7.72 (m, 1H, ArH), 7.82 – 7.83 (m, 2H, 2ArH), 8.08 (s, 1H, $CHNCH-$), 8.19 (s, 1H, CH_3CNCH-) ppm. ^{13}C NMR (125.77 MHz, $CDCl_3$, TMS): δ 19.9, 23.6, 24.2, 26.0, 34.8, 50.5, 62.7, 69.3, 110.1, 113.9, 120.7, 120.9, 122.1, 122.4, 122.7, 123.1, 123.6, 133.7, 134.7, 141.7, 141.8, 143.4, 144.8 ppm. MS (EI): m/z (%) 69 (16), 109 (5), 119 (21), 145 (24), 159 (68), 173 (43), 211 (6), 227 (100) $[M\text{-benzimidazoly}]^+$, 329 (7) $[M-CH_3]^+$, 344 (58) $[M]^+$. HR-MS (EI, m/z): calc. for $C_{22}H_{24}N_4$ $[M]$: 344.2001, found: 344.1989. IR (KBr): ν 2976, 1734, 1636, 1559, 1540, 1506, 1490, 1457, 1386, 1284, 1229, 1133, 894, 779, 744. Anal. calcd for $C_{22}H_{24}N_4$, C: 76.71 H: 7.02 N: 16.27. Found, C: 76.12 H: 7.05 N: 16.06.

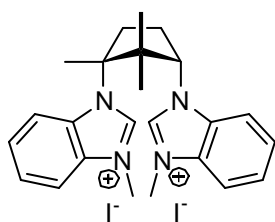
1,1'-((1R,3S)-1,2,2-trimethylcyclopentane-1,3-diyl)di(benzotriazole) (**99**):



The tetramine **91** (395 mg, 1.22 mmol) was dissolved in 25 mL anhydrous tetrahydrofuran, hypophosphorous acid (0.63 mL, 12.2 mmol) was added and the solution heated to 40 °C. *Tert*-butyl nitrite (377 mg, 3.66 mmol) dissolved in 5 mL anhydrous tetrahydrofuran was added dropwise over a period of 15 min and the reaction was stirred for 16 h at 40° C. The solution was allowed to cool down to room temperature and the solvent was evaporated under reduced

pressure. The residue was taken up in dichloromethane and washed two times with 10wt% aqueous sodium hydroxide solution. The organic layers were separated, combined and dried over sodium sulfate. The solvent was evaporated and the crude product purified by flash column chromatography (silica, hexane/ ethyl acetate = 10:1 to 1:1) to yield the title compound **99** as orange, needle-shaped crystals (314 mg, 0.91 mmol, 74%). Mp. 205 – 209 °C; ^1H NMR (300.13 MHz, CDCl_3 , TMS): δ 0.47 (s, 3H, $-\text{CH}_3$), 1.50 (s, 3H, $-\text{CH}_3$), 2.01 (s, 3H, $-\text{NHCCCH}_3$), 2.48 – 2.57 (m, 1H, $-\text{CHCH}_2-$), 2.58 – 2.71 (m, 1H, $-\text{CHCH}_2-$), 3.33 – 3.45 (m, 1H, $-\text{CH}_3\text{CCH}_2-$), 3.88 – 3.99 (m, 1H, $-\text{CH}_3\text{CCH}_2-$), 5.26 (dd, $J = 8.1$ Hz, $J = 10.0$ Hz, 1H, $-\text{CH}_2\text{CHNH}-$), 7.33 – 7.40 (m, 2H, $2\times\text{ArH}$), 7.43 – 7.53 (m, 2H, $2\times\text{ArH}$), 7.59 – 7.62 (m, 1H, ArH), 7.79 – 7.82 (m, 1H, ArH), 8.06 – 8.09 (m, 2H, $2\times\text{ArH}$) ppm. ^{13}C NMR (75.47 MHz, CDCl_3 , TMS): δ 19.7, 23.6, 24.9, 25.1, 34.4, 51.7, 66.6, 79.1, 110.0, 112.2, 120.2, 120.5, 123.5, 123.9, 127.1, 127.3, 133.1, 133.9, 146.0, 146.5 ppm. MS (EI): m/z (%) 76 (52), 118 (62), 158 (46), 184 (100), 198 (71), 227 (11), 331 (39) $[\text{M}-\text{CH}_3]^+$, 346 (77) $[\text{M}]^+$. HR-MS (EI, m/z): calc. for $\text{C}_{20}\text{H}_{22}\text{N}_6$ $[\text{M}]$: 346.1906, found: 344.1915. ATR-FTIR: ν 2962, 1610, 1582, 1481, 1447, 1466, 1390, 1373, 1352, 1313, 1286, 1224, 1185, 1163, 1133, 1072, 1051, 1034, 1009, 1001, 989, 945, 920, 900, 850, 779, 110, 160, 752, 740. Anal. calcd for $\text{C}_{20}\text{H}_{22}\text{N}_6$, C: 69.34 H: 6.40 N: 24.26. Found, C: 68.92 H: 6.44 N: 23.89.

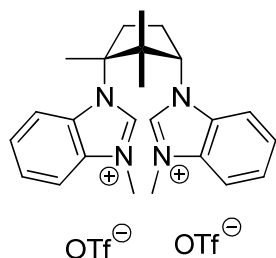
1,1'-((1R,3S)-1,2,2-trimethylcyclopentane-1,3-diyl) di (3-methyl-1H-benzimidazole-3-ium)iodide (93):



Dibenzimidazole **92** (400 mg, 1.16 mmol) was suspended in 25 mL anhydrous acetonitrile and methyl iodide (988 mg, 6.96 mmol) was added dropwise via syringe. After stirring for two hours the mixture was stirred at reflux temperature at 55 °C for one hour. The product **93** (675 mg, 1.07 mmol, 93%) was obtained as yellow crystals after evaporation of the solvent in vacuum. Mp. 201 – 209 °C; ^1H -NMR (500.13 MHz, $\text{DMSO}-d_6$): δ 0.65 (s, 3H, $-\text{CH}_3$), 1.26 (s, 3H, $-\text{CH}_3$), 2.09 (s, 3H, $-\text{NHCCCH}_3$), 2.35 – 2.41 (m, 1H, $-\text{CH}_2-$), 2.66 – 2.77 (m, 2H, $-\text{CH}_2-$), 3.35 – 3.42 (m, 1H, $-\text{CH}_2-$), 4.12 (s, 3H, $-\text{CH}_3$), 4.13 (s, 3H, $-\text{CH}_3$), 5.53 (t, $J = 9.2$ Hz, 1H, $-\text{CH}-$), 7.68 – 7.77 (m, 4H, ArH), 8.07 – 8.09 (m, 2H, ArH) 8.24 – 8.30 (m, 2H, ArH), 10.01 (s, 1H, $-(\text{CH})\text{N}-$), 10.19 (s, 1H, $-(\text{CH})\text{N}-$) ppm. ^{13}C -NMR (125.77 MHz, $\text{DMSO}-d_6$): δ 19.1, 22.1, 24.0, 25.49, 33.5, 33.8, 49.6, 63.4, 73.2, 113.7, 113.9, 114.1, 117.1, 126.2, 126.4, 126.5, 126.6, 130.9, 131.7, 132.0, 132.7, 142.8, 142.8 ppm. MS (ESI, pos. mode, arginin, m/z): m/z (%) 373 (8) $[\text{M}-\text{HI}, -\text{I}]^+$, 487 (8) $[\text{M}-\text{CH}_3, -\text{I}]^+$, 501 (100) $[\text{M}-\text{I}]^+$. HR-MS (ESI, pos. mode, arginin, m/z): calc. for $\text{C}_{24}\text{H}_{30}\text{I}_2\text{N}_4$ $[\text{M}]^+$: 501.1515, found: 501.1513. IR (KBr): ν 3138, 2966, 1609, 1567, 1461, 1393, 1348, 1320, 1263, 1212, 1143, 1100, 1023, 853, 758. Anal. calcd for $\text{C}_{24}\text{H}_{30}\text{I}_2\text{N}_4$, C: 45.88 H: 4.81 N:

8.92. Found C: 44.69 H: 4.99 N: 8.78.

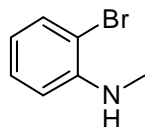
1,1'-((1*R*,3*S*)-1,2,2-trimethylcyclopentane-1,3-diyl) di (3-methyl-1*H*-benzimidazole-3-ium)triflate (94**):**



Dibenzimidazole **92** (400 mg, 1.16 mmol) was suspended in 25 mL anhydrous acetonitrile and methyl trifluoromethanesulfonate (391 mg, 2.38 mmol) was added dropwise via syringe. Upon addition the solid dissolved and the solution turned brown. After stirring for three hours at room temperature the solvent was removed in vacuum and the product **94** (694 mg, 1.03 mmol, 89%) was obtained as a white hygroscopic solid, which was stored at -20°C. ¹H-NMR (300.13 MHz, DMSO): δ 0.64 (s, 3H, -CH₃), 1.25 (s, 3H, -CH₃), 2.07 (s, 3H, -NHCCCH₃), 2.31 – 2.40 (m, 1H, -CH₂-), 2.63 – 2.71 (m, 2H, -CH₂-), 3.29 – 3.40 (m, 1H, -CH₂-), 4.10 (s, 3H; -CH₃), 4.11 (s, 3H; -CH₃), 5.49 (t, *J* = 9.3 Hz, 1H; -CH-), 7.66 – 7.78 (m, 4H; ArH), 8.06-8.09 (m, 2H; ArH) 8.20 – 8.26 (m, 2H; ArH), 9.93 (s, 1H; -(CH)N-), 10.05 (s, 1H; -(CH)N-) ppm. ¹³C-NMR (75.48 MHz, CDCl₃): δ 18.8, 22.0, 23.9, 25.4, 33.4, 33.7, 49.6, 63.3, 73.2, 113.7, 117.0, 126.3, 126.4, 126.6, 126.7, 131.0, 131.7, 132.2, 132.7, 142.8 ppm. HR-MS (ESI, pos. mode, arginin, *m/z*): calc. for C₂₅H₃₀F₃N₄O₃S [M]⁺: 523.1985, found: 523.1984. IR (KBr): ν 3415, 3157, 3092, 2986, 2576, 1708, 1651, 1572, 1466, 1408, 1258, 1226, 1162, 1030, 852, 759, 639, 573, 541, 517.

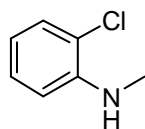
Experimental Section – Chapter 4

2-Bromo-*N*-methylaniline (**115**):^[420]



The compound was prepared following a procedure of Barluenga^[417] Therefore 2-bromoaniline (**113**, 6.74 g, 0.039 mol) was dissolved in 40 mL distilled, anhydrous tetrahydrofuran and as solution of *n*-butyllithium (2.2 M in *cyclo*-hexane, 9.80 mL, 0.039 mol) was slowly added at -50 °C (1 h). The resulting red mixture was stirred for 15 min at this temperature, cooled to -60 °C and iodomethane (1.22 mL, 0.039 mol) was added over a period of 30 min. The reaction mixture was allowed to warm up to room temperature and stirred for additional 16 h at room temperature. The reaction was quenched with 20 mL of water, the organic phase was separated and the aqueous phase extracted three times with 30 mL ethyl acetate. The organic layers were combined, washed with 50 mL aqueous, saturated sodium hydrogencarbonate solution, dried over sodium sulfate and the solvent was evaporated under reduced pressure. Purification by flash column chromatography (silica, hexane/ ethyl acetate = 100:1 to 50:1) yielded pure 2-bromo-*N*-methylaniline (**115**) as a colorless liquid (3.59 g, 0.019 mol, 49%). ¹H NMR (300.13 MHz, CDCl₃, TMS): δ 2.90 (d, 3H, *J* = 5.1 Hz, -CH₃), 4.35 (bs, 1H, NH), 6.55 – 6.60 (m, 1H, ArCH), 6.61 – 6.65 (m, 1H, ArCH), 7.18 – 7.24 (m, 1H, ArCH), 7.40 – 7.44 (m, 1H, ArCH) ppm. ¹³C NMR (75.47 MHz, CDCl₃, TMS): δ 30.6, 109.6, 110.7, 117.55, 128.6, 132.2, 145.9 ppm. MS (EI): *m/z* (%) 111 (2) [M-(NHCH₃)]⁺, 140 (100) [M-H]⁺, 141 (31) [M]⁺. HRMS (EI): *m/z* calcd for C₇H₈³⁵ClN: 141.0345. Found: 141.0317. ATR-FTIR: ν 3417, 3063, 2986, 2907, 2816, 1596, 1508, 1458, 1428, 1419, 1317, 1291, 1251, 1168, 1154, 1105, 1073, 1036, 1017, 923, 832, 802, 737, 706.

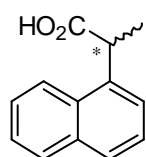
2-Chloro-*N*-methylaniline (**116**):^[418]



2-Chloro-*N*-methylaniline was prepared following the same procedure described for 2-Bromo-*N*-methylaniline by using 2-chloroaniline (**114**, 5.00 g, 0.039 mmol), *n*-butyllithium (2.2 M in *cyclo*-hexane, 9.80 mL, 0.039 mmol) and iodomethane (1.22 mL, 0.039 mmol). Purification by flash column chromatography (silica, hexane/ ethyl acetate = 100:1 to 50:1) yielded the title compound **116** as a colorless liquid (2.78 g, 0.020 mmol, 50%). ¹H NMR (300.13 MHz, CDCl₃, TMS): δ 2.91 (d, 3H, *J* = 5.0 Hz, -CH₃), 4.34 (bs, 1H, NH), 6.61 – 6.66 (m, 2H, ArCH), 7.14 – 7.20 (m, 1H, ArCH), 7.24 – 7.44 (m, 1H, ArCH) ppm. ¹³C NMR (75.47 MHz, CDCl₃, TMS): δ 30.4, 110.6, 117.0, 119.0, 127.8, 128.9, 145.0 ppm. MS (EI): *m/z* (%) 105 (18) [M-³⁵Cl]⁺, 184 (85) [M-H]⁺, 185 (100) [M]⁺. HRMS (EI): *m/z* calcd for C₇H₈⁷⁹BrN:

184.9840. Found: 184.9803. ATR-FTIR: ν 3432, 3067, 2991, 2934, 2911, 2873, 2818, 1601, 1516, 1461, 1426, 1322, 1295, 1251, 1168, 1114, 1075, 1033, 742.

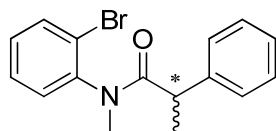
2-(Naphthalen-1-yl)propanoic acid (**118**):^[419]



Following the procedure of Thompson^[419], modified by Glorius^[393], *n*-butyllithium (2.2 M in cyclo-hexane, 47.85 mL, 0.190 mol) was added dropwise to a solution of freshly, distilled diisopropylamine (29.54 mL, 0.190 mol) in 150 mL tetrahydrofurane at -78 °C. The solution was stirred for 40 min at the same temperature and a solution of naphthylacetic acid (**117**, 8.10 g, 0.044 mol) in tetrahydrofurane was added slowly at -78 °C over a period of one hour. The solution was allowed to warm up to 0 °C, stirred for one hour at the same temperature and iodomethane (4.06 mL, 0.065 mol) was added in one portion. The deep yellow reaction mixture was allowed to warm up to room temperature overnight becoming a white suspension. Quenching by addition of 30 mL of water resulted in a clear yellow solution, which was concentrated under reduced pressure. The residue was taken up in 100 mL water, acidified with 1M hydrochloric acid (50 mL) and extracted six times with diethyl ether. The organic layers were combined, dried over sodium sulfate and the solvents evaporated under reduced pressure. Purification by flash column chromatography (silica, hexane/ ethyl acetate = 10:1 to 1:1) yielded pure 2-(naphthalen-1-yl)propanoic acid (**118**) as a colorless solid (7.94 g, 0.040 mol, 91%). ¹H NMR (300.13 MHz, CDCl₃, TMS): δ 1.68 (d, 3H, $J = 7.1$ Hz, -CH₃), 4.54 (q, 1H, $J = 7.1$ Hz, -CHCH₃), 7.43 – 7.57 (m, 4H, ArCH), 7.78 – 7.89 (m, 2H, ArCH), 8.08 – 8.11 (m, 1H, ArCH) ppm. ¹³C NMR (75.47 MHz, CDCl₃, TMS): δ 17.8, 41.0, 123.0, 124.6, 125.5, 125.7, 126.4, 128.0, 129.0, 131.3, 133.9, 135.9 ppm. MS (EI): m/z (%) 155 (100) [M-CO₂H]⁺, 200 (45) [M]⁺. HRMS (EI): m/z calcd for C₁₃H₁₂O₂: 200.0837. Found: 200.0843. ATR-FTIR: ν 3511, 3422, 3201, 3067, 3038, 2985, 2937, 2719, 2623, 1703, 1452, 1411, 1395, 1376, 1321, 1251, 1232, 922, 794, 778. **General procedure for the arylpropanamide synthesis:** The carboxylic acid (1.2 eq.) and thionyl chloride (2.4 eq.) were stirred at reflux temperature for 2 – 3 h until gas evolution had ceased. The mixture was cooled to room temperature, excess thionyl chloride was removed under high vacuum the residue was dissolved in dichloromethane (app. 0.28 M). Freshly, distilled triethylamine (2.0 eq.) and the appropriate 2-haloaniline derivative (1.0 eq.) were added and the mixture was stirred for 16 – 24 h at room temperature. The reaction mixture was diluted with diethyl ether (70 mL), quenched with saturated, aqueous ammonium chloride (100 mL) and the organic layer was separated. The aqueous layer was extracted with diethyl ether (2×20 mL), the layers were combined, washed with saturated, aqueous sodium carbonate and brine and dried over sodium sulfate. The pure arylpropanamides were obtained after flash

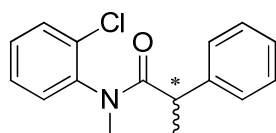
column chromatography (silica, hexane/ ethyl acetate) of the crude products. Enantiomeric excess was determined using chiral HPLC on a Chiralpak IA column. Product configuration was determined by retention times and elution order of reported compounds and referenced using chiral HPLC on a Chiralpak IB column.

***N*-(2-Bromophenyl)-*N*-methyl-2-phenylpropanamide (**121**):^[392]**



The title compound was obtained following the general procedure for the arylpropanamide formation by reaction of 2-phenylpropanoic acid (**119**) with thionyl chloride, treatment with 1, 2-bromo-*N*-methylaniline (**115**) and triethylamine. Purification by flash column chromatography (silica, hexane/ ethyl acetate = 50:1) yielded pure *N*-(2-bromophenyl)-*N*-methyl-2-phenylpropanamide (**121**) as a colorless, viscous oil (909 mg, 2.86 mmol, 43%). ¹H NMR (300.13 MHz, CDCl₃): δ 1.41 – 1.46 (m, 3H, -CHCH₃), 3.18 – 3.20 (m, 3H, NHCH₃), 3.36 (q, 0.72H, *J* = 6.8 Hz, -CHCH₃), 3.55 (q, 0.25H, *J* = 6.9 Hz, -CHCH₃), 6.70 – 6.73 (m, 0.72H, ArCH), 6.94 – 7.04 (m, 2H, ArCH), 7.15 – 7.30 (m, 4.75H, ArCH), 7.35 – 7.47 (m, 0.64H, ArCH), 7.57 – 7.61 (m, 0.26H, ArCH), 7.70 – 7.74 (m, 0.69H, ArCH) ppm. ¹³C NMR (75.47 MHz, CDCl₃): δ 20.1, 20.6, 36.1, 36.1, 43.2, 44.0, 123.6, 124.2, 126.6, 126.7, 126.9, 127.3 (3×), 127.4, 127.5, 128.0, 128.1, 128.2 (5×), 128.3 (2×), 128.4 (2×), 128.5 (5×), 128.6 (2×), 129.6, 129.7, 130.0, 130.7, 130.8, 133.5, 134.0, 140.5, 141.6, 142.2, 142.5 ppm. MS (FAB): *m/z* (%): 136 (18), 154 (21), 212 (12) [M-(C₈H₉)]⁺, 238 (31) [M-⁷⁹Br]⁺, 318 (100) [M+H]⁺. HRMS (FAB): *m/z* (%) calcd for C₁₆H₁₇⁷⁹BrNO⁺ [M+H]⁺: 318.04880. Found: 318.0435. ATR-FTIR: ν 3060, 3026, 2929, 2869, 1660, 1601, 1583, 1475, 1435, 1453, 1417, 1375, 1315, 1278, 1246, 1182, 1130, 1066, 1046, 1029, 1019, 988, 910, 866, 488, 764, 727.

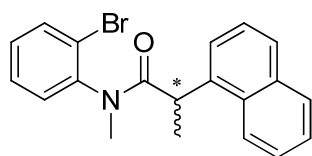
***N*-(2-Chlorophenyl)-*N*-methyl-2-phenylpropanamide (**122**):**



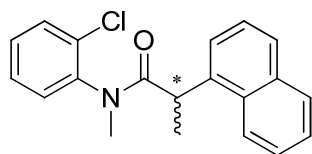
The title compound was obtained following the general procedure for the arylpropanamide formation by reaction of 2-phenylpropanoic acid (**119**) with thionyl chloride, treatment with 1, 2-chloro-*N*-methylaniline (**116**) and triethylamine. Purification by flash column chromatography (silica, hexane/ ethyl acetate = 50:1) yielded pure *N*-(2-chlorophenyl)-*N*-methyl-2-phenylpropanamide (**122**) as a colorless, viscous oil (794 mg, 2.90 mmol, 41%). ¹H NMR (500.13 MHz, CDCl₃): δ 1.40 – 1.43 (m, 3H, -CHCH₃), 3.17 (s, 3H, NHCH₃), 3.35 (q, 0.69H, *J* = 6.8 Hz, -CHCH₃), 3.55 (q, 0.29H, *J* = 6.8 Hz, -CHCH₃), 6.71 – 6.73 (m, 0.65H, ArCH), 6.96 – 6.97 (m, 1.88H, ArCH), 7.11 –

7.19 (m, 3.57H, ArCH), 7.29 – 7.37 (m, 2H, ArCH), 7.52 – 7.54 (m, 0.66H, ArCH) ppm. ^{13}C NMR (125.77 MHz, CDCl_3): δ 20.0, 20.5, 36.0, 36.2, 43.3, 43.9, 126.7, 127.4, 127.8, 127.8, 127.9, 128.2, 128.4, 129.4, 129.5, 130.0, 130.4, 130.8, 133.1, 133.9, 140.6, 140.8, 141.0, 141.7, 173.9, 174.0 ppm. MS (EI): m/z (%) 77 (10), 105 (45) $[\text{C}_8\text{H}_9]^+$, 141 (28) $[\text{M}-(\text{C}_9\text{H}_9\text{O})]^+$, 168 (42) $[\text{M}-(\text{C}_8\text{H}_9)]^+$, 238 (100) $[\text{M}-^{35}\text{Cl}]^+$. HRMS (EI): m/z calcd for $\text{C}_{16}\text{H}_{16}^{35}\text{ClNO}$: 273.0920. Found: 273.0927. ATR-FTIR: ν 3061, 3028, 2978, 2931, 1667, 1610, 1482, 1453, 1442, 1379, 1281, 1128, 1057, 755, 720, 700.

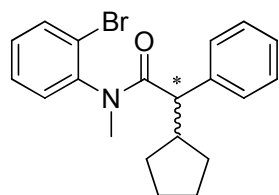
***N*-(2-Bromophenyl)-*N*-methyl-2-(naphthalen-1-yl)propanamide (124):**^[392]



The title compound was obtained following the general procedure for the arylpropanamide formation by reaction of 2-(naphthalen-1-yl)propanoic acid (**118**) with thionyl chloride, treatment with 1, 2-bromo-*N*-methylaniline (**115**) and triethylamine. Purification by flash column chromatography (silica, hexane/ ethyl acetate = 50:1) yielded pure *N*-(2-bromophenyl)-*N*-methyl-2-(naphthalen-1-yl)propanamide (**124**) as a colorless solid (2.30 g, 6.27 mmol, 89%). ^1H NMR (300.13 MHz, CDCl_3): δ 1.51 – 1.54 (m, 3H, $-\text{CHCH}_3$), 3.19 – 3.20 (m, 3H, NHCH_3), 4.17 (q, 0.82H, $J = 6.9$ Hz, $-\text{CHCH}_3$), 4.46 (q, 0.19H, $J = 6.9$ Hz, $-\text{CHCH}_3$), 6.06 – 6.09 (m, 0.76H, ArCH), 6.45 – 6.50 (m, 0.78H, ArCH), 6.85 – 6.90 (m, 0.79H, ArCH), 7.03 – 7.23 (m, 2.45H, ArCH), 7.31 – 7.40 (m, 2.41 H, ArCH), 7.44 – 7.51 (m, 1H, ArCH), 7.58 – 7.62 (m, 0.84H, ArCH), 7.64 – 7.69 (m, 1H, ArCH), 7.73 – 7.76 (m, 1H, ArCH) ppm. ^{13}C NMR (75.47 MHz, CDCl_3): δ 20.0, 36.2, 39.6, 121.9, 123.3, 124.5, 124.9, 125.2, 125.5, 125.6, 125.7, 127.1, 128.1, 128.5, 128.6, 129.2, 129.3, 130.0, 130.5, 130.6, 133.2, 133.7, 133.9, 138.5, 141.7, 174.1 ppm. MS (EI): m/z (%) 77 (8), 155 (100) $[\text{C}_{12}\text{H}_{11}]^+$, 212 (58) $[\text{M}-(\text{C}_6\text{H}_4^{79}\text{Br})]^+$, 288 (87) $[\text{M}-^{79}\text{Br}]^+$, 367 (48) $[\text{M}]^+$. HRMS (EI): m/z calcd for $\text{C}_{20}\text{H}_{18}^{79}\text{BrNO}$: 367.0572. Found: 367.0576. ATR-FTIR: ν 3055, 3013, 2974, 2932, 1657, 1584, 1475, 1457, 1442, 1430, 1412, 1396, 1381, 1275, 1129, 1049, 808, 799, 790, 774, 758, 724.

***N*-(2-Chlorophenyl)-*N*-methyl-2-(naphthalen-1-yl)propanamide (125):**^[392]

The title compound was obtained following the general procedure for the arylpropanamide formation by reaction of 2-(naphthalen-1-yl)propanoic acid (**118**) with thionyl chloride, treatment with 1, 2-chloro-*N*-methylaniline (**116**) and triethylamine. Purification by flash column chromatography (silica, hexane/ ethyl acetate = 50:1) yielded pure *N*-(2-bromophenyl)-*N*-methyl-2-(naphthalen-1-yl)propanamide (**125**) as a colorless solid (2.13 g, 6.58 mmol, 93%). ¹H NMR (300.13 MHz, CDCl₃): δ 1.50 – 1.54 (m, 3H, -CHCH₃), 3.20 (s, 3H, NHCH₃), 4.16 (q, 0.75H, *J* = 6.9 Hz, -CHCH₃), 4.47 (q, 0.23H, *J* = 6.9 Hz, -CHCH₃), 6.07 – 6.10 (m, 0.70H, ArCH), 6.42 – 6.47 (m, 0.72H, ArCH), 6.78 – 6.81 (m, 0.22H, ArCH), 6.93 – 7.00 (m, 0.73H, ArCH), 7.01 – 7.10 (m, 0.72H, ArCH), 7.14 – 7.44 (m, 5.90H, ArCH), 7.48 – 7.51 (m, 0.80H, ArCH), 7.64 – 7.69 (m, 1H, ArCH), 7.73 – 7.76 (m, 1H, ArCH) ppm. ¹³C NMR (75.47 MHz, CDCl₃): δ 19.9, 20.1, 36.1, 36.2, 38.8, 39.4, 121.9, 124.4, 124.9, 125.2, 125.4, 125.5, 125.6, 125.7, 127.0 (2×), 127.3, 127.8, 128.5, 128.6, 129.0, 129.1, 129.8, 130.1, 130.5 (2×), 130.6, 132.7, 133.7, 136.8, 138.5, 140.3, 174.2, 174.3 ppm. MS (EI): *m/z* (%) 77 (5), 155 (100) [C₁₂H₁₁]⁺, 167 (48), 182 (8), 288 (36) [M-³⁵Cl]⁺, 323 (36) [M]⁺. HRMS (EI): *m/z* calcd for C₂₀H₁₈³⁵ClNO: 323.1077. Found: 323.1090. ATR-FTIR: ν 3053, 3020, 2994, 2972, 2933, 1659, 1586, 1480, 1458, 1440, 1413, 1396, 1380, 1354, 1277, 1261, 1130, 1059, 809, 799, 791, 117, 156, 728.

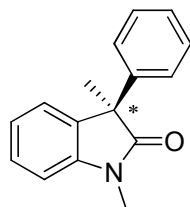
***N*-cyclo-pentyl-*N*-(2-bromophenyl)-2-phenylpropanamide (123):**

The title compound was obtained following the general procedure for the arylpropanamide formation by reaction of **120** with thionyl chloride, treatment with 1, 2-bromo-*N*-methylaniline (**115**) and triethylamine. Purification by flash column chromatography (silica, hexane/ethyl acetate = 50:1) yielded pure *N*-cyclo-pentyl-*N*-(2-bromophenyl)-2-phenylpropanamide (**123**) as a colorless, viscous oil (274 mg, 0.76 mmol, 72%). ¹H NMR (300.13 MHz, CDCl₃): δ 0.84 – 0.98 (m, 1.34H, -CH₂CH₂CH-), 1.20 – 1.27 (m, 1.34H, -CH₂CH₂CH-), 1.36 – 1.58 (m, 3.46H, -CH₂CH₂CH-), 1.63 – 1.73 (m, 2.10H, -CH₂CH₂CH-), 2.04 – 2.15 (m, 1.22H, -CH₂CH-), 2.60 – 2.80 (m, 1.04H, -CH₂CH-), 2.90 – 2.30 (m, 0.74H, -CH₂CHCH-), 3.14 – 3.18 (m, 0.30H, -CH₂CHCH-), 3.24 – 3.28 (m, 3H, NHCH₃), 6.58 – 6.62 (m, 0.73H, ArCH), 7.00 – 7.05 (m, 2H, ArCH), 7.18 – 7.44 (m, 5.24H, ArCH), 7.51 – 7.57 (m, 0.34H, ArCH), 7.64 – 7.67 (m, 0.27H, ArCH), 7.79 – 7.82 (m, 0.73H, ArCH) ppm. ¹³C NMR (75.47 MHz, CDCl₃): δ 24.4, 24.9, 30.3, 30.4, 32.0 (2×), 35.9 (2×), 44.7, 44.9, 55.0, 56.2, 123.1, 124.5,

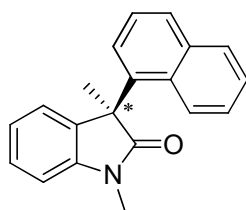
126.5, 127.9, 128.0 (2×), 128.1(3×), 128.2, 128.3, 128.4, 128.5, 129.5, 129.6 (2×), 130.7, 131.5, 133.5, 133.9, 138.9, 139.9, 141.9, 142.4, 172.9, 173.0 ppm. MS (FAB): m/z (%): 154 (31) $[C_6H_4^{79}Br]^+$, 212 (16), 292 (16) $[M-^{79}Br]^+$, 303 (11) $[M-(C_5H_9)]^+$, 372 (100) $[M+H]^+$. HRMS (FAB): m/z (%) calcd for $C_{20}H_{23}^{79}BrNO^+$ $[M+H]^+$: 372.0958. Found: 372.0968. ATR-FTIR: ν 3060, 3025, 2950, 2865, 1658, 1600, 1583, 1475, 1452, 1417, 1371, 1294, 1240, 1180, 1117, 1074, 1052, 1031, 949, 911, 815, 763, 750, 727, 718.

General procedure for the Pd-catalyzed, asymmetric oxindole synthesis: To a solution of starting material (0.3 mmol) and catalyst (2.5 mol%) in anhydrous dimethoxyethane (6 mL) was added sodium *tert*-butoxide (0.45 mmol) in one portion. The mixture was stirred at 50 °C, resp. 80 °C until all starting material was consumed (18 – 24 h). The mixture was diluted with 50 mL ethyl acetate, filtered and the solvent evaporated under reduced pressure. The crude product was absorbed on silica and purified by flash column chromatography (silica, hexane/EtOAc).

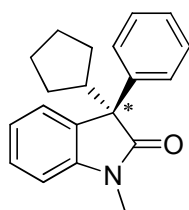
(*R*)-1,3-Dimethyl-3-phenylindolin-2-one^[396] (Table 15, entry 4):



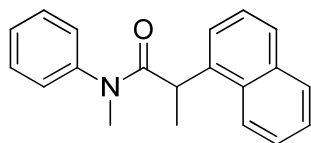
Following the general procedure for oxindole synthesis the title compound was obtained after flash column chromatography (silica, hexane/ ethyl acetate = 15:1 to 7:1) as pale oil (70 mg, 0.29 mmol, 98%). 1H NMR (500.13 MHz, $CDCl_3$): δ 1.75 (s, 3H, $-CHCH_3$), 3.20 (m, 3H, $-NHCH_3$), 6.87 – 6.88 (m, 1H, ArCH), 7.04 – 7.07 (m, 1H, ArCH), 7.14 – 7.16 (m, 1H, ArCH), 7.19 – 7.20 (m, 1H, ArCH), 7.21 – 7.30 (m, 5H, ArCH) ppm. ^{13}C NMR (125.77 MHz, $CDCl_3$): δ 23.7, 26.4, 52.1, 108.3, 122.7, 124.2, 126.6, 127.2, 128.1, 128.5, 134.8, 140.8, 143.2, 179.4 ppm. MS (EI): m/z (%) 77 (3), 165 (8), 194 (14), 208 (7) $[M-2\times(CH_3)]^+$, 222 (100) $[M-CH_3]^+$, 237 (99) $[M]^+$. HRMS (EI): m/z calcd for $C_{16}H_{15}NO$: 237.1154. Found: 237.1135. ATR-FTIR: ν 3055, 3024, 2969, 2931, 2870, 2245, 1708, 1610, 1491, 1470, 1444, 1418, 1372, 1342, 1302, 1258, 1157, 1144, 1115, 1099, 1078, 1054, 1023, 1002, 911, 860, 803, 748, 728. 63% ee [Chiralpak IA column, *n*-hexane/*i*-PrOH = 99:1, 1.0 mL/min, 210.5 nm; t_R = 17.21 min (minor) and 25.65 min (major)].

(R)-1,3-Dimethyl-3-(naphthalen-1-yl)indolin-2-one^[392] (Table 15, entry 6):

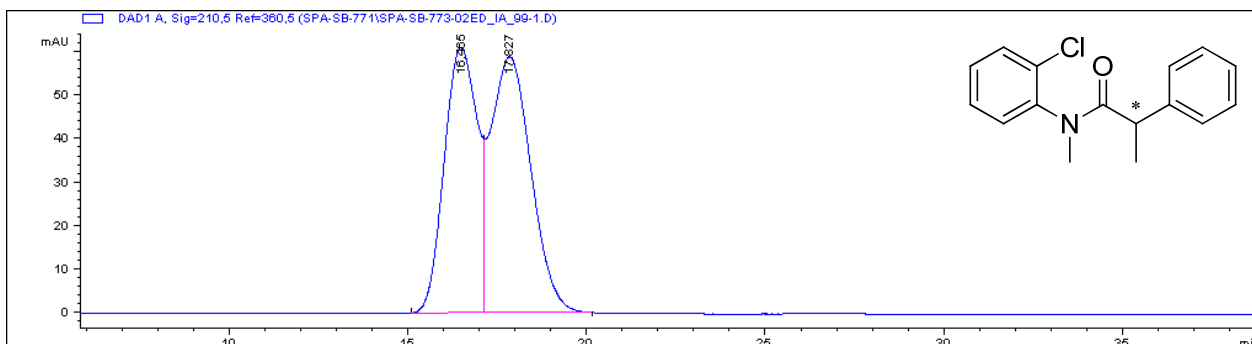
Following the general procedure for oxindole synthesis the title compound was obtained after flash column chromatography (silica, hexane/ ethyl acetate = 10:1 to 5:1) as pale oil (82 mg, 0.29 mmol, 95%). ¹H NMR (300.08 MHz, CDCl₃): δ 1.92 (s, 3H, -CHCH₃), 3.45 (m, 3H, -NHCH₃), 6.83 – 6.88 (m, 3H, ArCH), 7.04 – 7.07 (m, 1H, ArCH), 7.14 – 7.20 (m, 1H, ArCH), 7.29 – 7.36 (m, 2H, ArCH), 7.53 – 7.58 (m, 1H, ArCH), 7.80 – 7.88 (m, 3H, ArCH) ppm. ¹³C NMR (75.46 MHz, CDCl₃): δ 26.7, 26.8, 52.4, 108.6, 122.8, 123.1, 123.4, 125.0, 125.2, 126.2, 127.9, 129.0, 129.1, 131.3, 134.3, 135.1, 136.7, 142.2, 180.4 ppm. MS (ED): *m/z* (%) 83 (11), 136 (7), 160 (6) [M-naphthyl]⁺, 215 (11), 244 (14), 272 (59) [M-CH₃]⁺, 287 (100) [M]⁺. HRMS (EI): *m/z* calcd for C₂₀H₁₇NO: 287.1310. Found: 287.1293. ATR-FTIR: ν 3051, 2969, 2933, 2874, 2245, 1705, 1610, 1511, 1489, 1569, 1418, 1400, 1371, 1338, 1301, 1257, 1245, 1211, 1157, 1142, 1167, 1105, 1090, 1072, 1050, 1025, 983, 904, 776, 791, 725. 72% ee [Chiralpak IA column, *n*-hexane/*i*-PrOH = 99:1, 1.0 mL/min, 210.5 nm; *t_R* = 36.43 min (minor) and 56.04 min (major)].

(R)-1-cyclopentyl-3-methyl-3-phenylindolin-2-one (Table 15, entry 2):

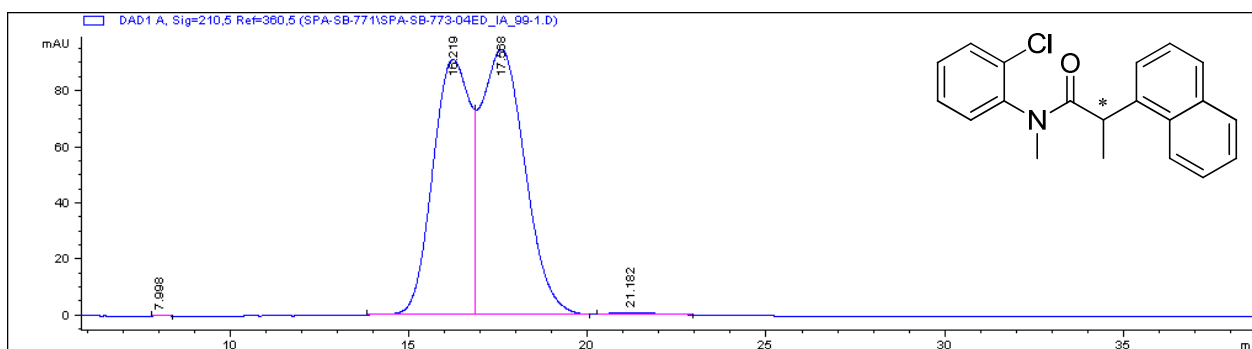
Following the general procedure for oxindole synthesis the title compound (0.25 mmol scale) was obtained after flash column chromatography (silica, hexane/ ethyl acetate = 20:1 to 10:1) as pale oil (69 mg, 0.24 mmol, 95%). ¹H NMR (500.13 MHz, CDCl₃): δ 0.74 – 0.84 (m, 1H), 1.28 – 1.61 (m, 7H), 2.97 – 3.07 (m, 1H), 3.11 (s, 3H, -NHCH₃), 6.80 – 6.82 (m, 1H, ArCH), 7.00 – 7.05 (m, 1H, ArCH), 7.10 – 7.26 (m, 4H, ArCH), 7.27 – 7.37 (m, 3H, ArCH) ppm. ¹³C NMR (125.77 MHz, CDCl₃): δ 25.2, 25.3, 26.2, 27.4, 29.7, 47.3, 57.8, 108.0, 122.2, 125.8, 126.6, 127.0, 127.5, 128.1, 128.3, 129.5, 130.9, 139.8, 144.3, 178.4 ppm. MS (ED): *m/z* (%) 91 (15), 107 (12), 134 (7), 159 (7), 194 (11), 223 (100) [M-cyclopentyl]⁺, 291 (22) [M]⁺. HRMS (EI): *m/z* calcd for C₂₀H₂₁NO: 291.1623. Found: 291.1615. ATR-FTIR: ν 3085, 3056, 3029, 2937, 2866, 1701, 1655, 1609, 1596, 1609, 1596, 1492, 1464, 1445, 1420, 1367, 1347, 1317, 1255, 1182, 1160, 1131, 1099, 1078, 1028, 1004, 952, 932, 914, 897, 885, 857, 839, 816, 752, 744, 721. 55% ee [Chiralpak IA column, *n*-hexane/*i*-PrOH = 99:1, 1.0 mL/min, 210.5 nm; *t_R* = 17.74 min (minor) and 19.68 min (major)].

***N*-phenyl-*N*-methyl-2-(naphthalen-1-yl)propanamide** (Table 15, entry 8):

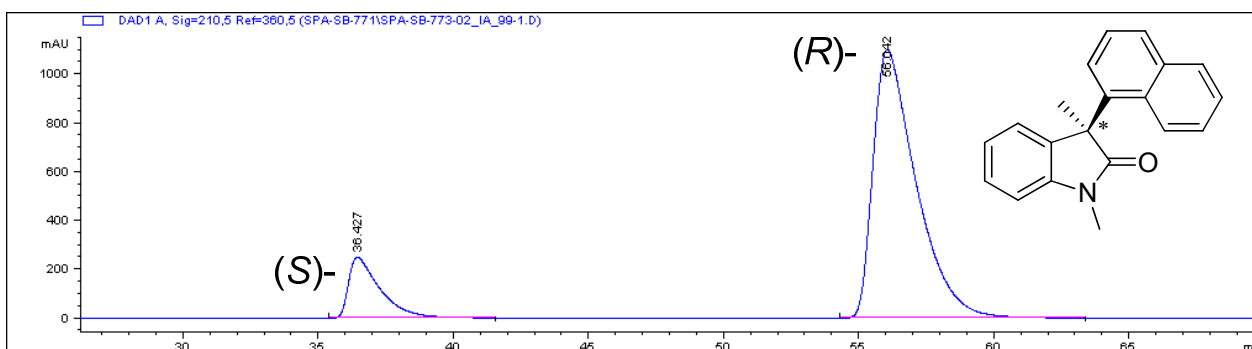
Following the general procedure for oxindole synthesis the dehalogenated title compound was obtained after flash column chromatography (silica, hexane/ethyl acetate = 15:1 to 5:1) as colorless oil (69 mg, 0.24 mmol, 91%). ^1H NMR (300.13 MHz, CDCl_3): δ 1.48 – 1.50 (m, 3H, $-\text{CHCH}_3$), 3.27 (s, 3H, NHCH_3), 4.41 (q, 1H, $J = 7.0$ Hz, $-\text{CHCH}_3$), 6.73 (bs, 2H, ArCH), 7.02 – 7.08 (m, 3H, ArCH), 7.18 – 7.21 (m, 1H, ArCH), 7.25 (s, 1H, ArCH), 7.34 – 7.41 (m, 2.42H, ArCH), 7.54 – 7.55 (m, 1H, ArCH), 7.68 – 7.69 (m, 1H, ArCH), 7.76 – 7.77 (m, 1H, ArCH) ppm. ^{13}C NMR (75.47 MHz, CDCl_3): δ 19.9, 29.7, 37.8, 38.8, 122.3, 124.7, 125.2, 125.6, 127.1, 127.4, 127.6, 128.6, 129.3, 133.7, 143.4, 174.3 ppm. MS (EI): m/z (%) 77 (9), 107 (16) [$\text{C}_7\text{H}_9\text{N}$] $^+$, 127 (7) [M-naphthyl] $^+$, 134 (87), 155 (100) [$\text{C}_{12}\text{H}_{11}$] $^+$, 182 (8), 289 (88) [M] $^+$. HRMS (EI): m/z calcd for $\text{C}_{20}\text{H}_{19}\text{NO}$: 289.1467. Found: 289.1461. MS (ESI): m/z (%) 290 (23) [$\text{M}+\text{H}$] $^+$, 312 (27) [$\text{M}+\text{Na}$] $^+$, 601 (100) [$2\text{M}+\text{Na}$] $^+$. HRMS (ESI, pos. mode, Arginin) m/z calcd for $\text{C}_{20}\text{H}_{20}\text{NO}$ [$\text{M}+\text{H}$] $^+$: 290.1539. Found: 290.1540. ATR-FTIR: ν 3058, 2967, 2928, 2868, 1652, 1594, 1510, 1495, 1452, 1418, 1378, 1351, 1310, 1269, 1245, 1167, 1124, 1096, 1071, 1031, 1002, 980, 903, 860, 796, 773, 733. (rac.) [Chiralpak IA column, *n*-hexane/*i*-propanol = 99:1, 1.0 mL/min, 210.5 nm; $t_R = 17.47$ min and 18.56 min].

HPLC-Data:

Chiralpak IA column, *n*-hexane/*i*-propanol = 99:1, 1.0 mL/min. DAD 1 A, Sig = 210.5 nm, Ref = 360.5 nm, t_R = 16.22 min and 17.57 min.

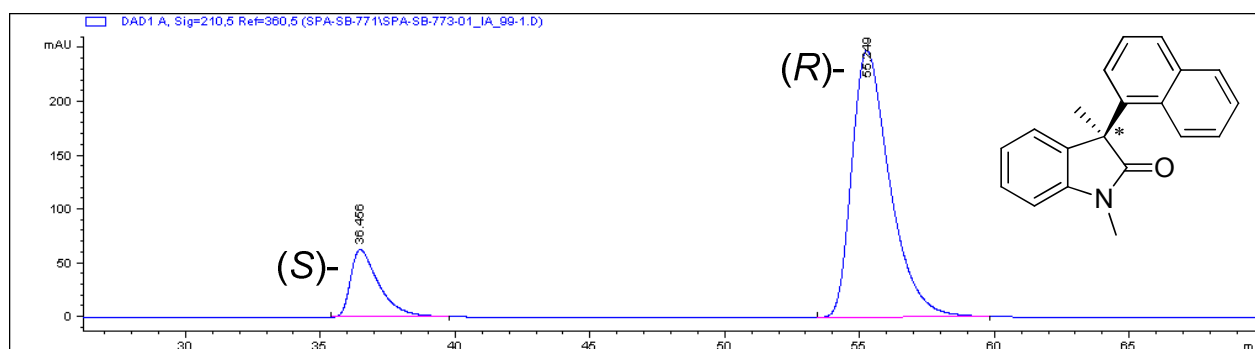


Chiralpak IA column, *n*-hexane/*i*-propanol = 99:1, 1.0 mL/min. DAD 1 A, Sig = 210.5 nm, Ref = 360.5 nm, t_R = 16.47 min and 17.83 min.

1,3-Dimethyl-3-(naphthalen-1-yl)indolin-2-one (Table 15, entry 6):

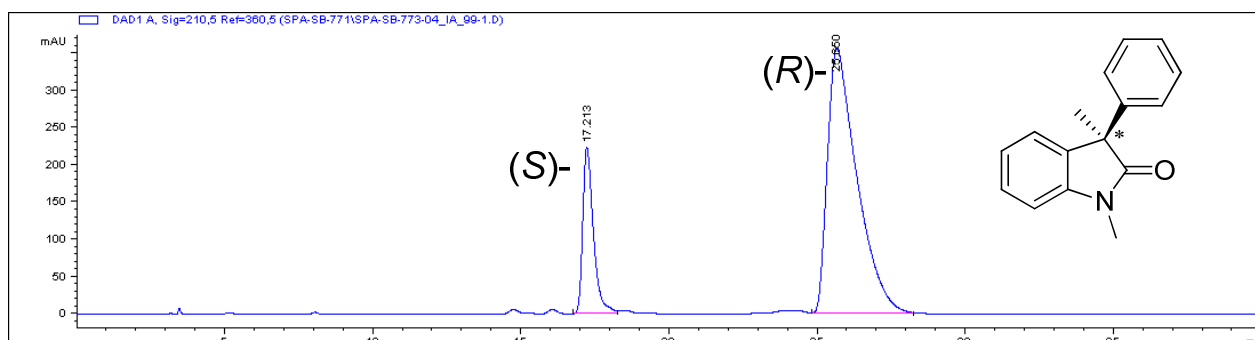
Chiralpak IA column, *n*-hexane/*i*-propanol = 99:1, 1.0 mL/min. DAD 1 A, Sig = 210.5 nm, Ref = 360.5 nm, t_R = 36.43 min (minor) and 56.04 min (major), 72% ee.

Peak	Area	Height	Width	Area%	Symmetry
36.427	20300.8	249.7	1.1806	14.214	0.345
56.042	122013.4	1101.2	1.6467	85.432	0.46

1,3-Dimethyl-3-(naphthalen-1-yl)indolin-2-one (Table 15, entry 5):

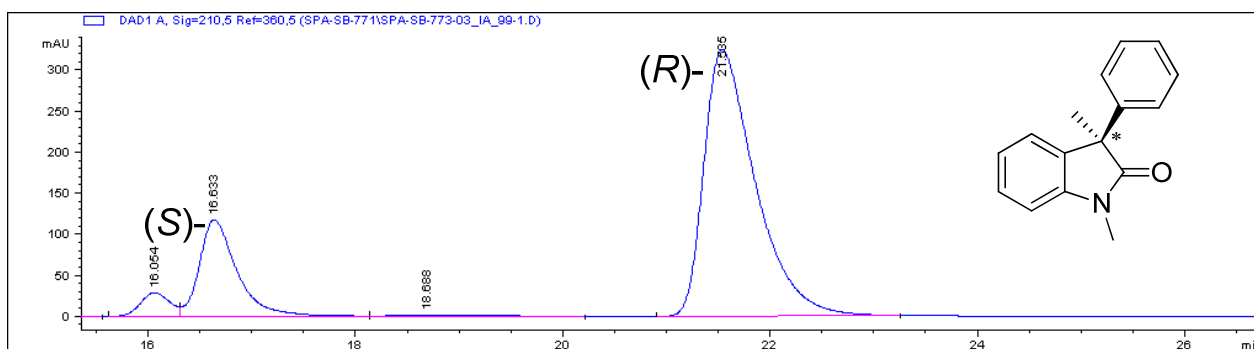
Chiralpak IA column, *n*-hexane/*i*-propanol = 99:1, 1.0 mL/min. DAD 1 A, Sig = 210.5 nm, Ref = 360.5 nm, t_R = 36.46 min (minor) and 55.25 min (major), 68% ee.

Peak	Area	Height	Width	Area%	Symmetry
36.456	4602.4	62.9	1.0756	15.759	0.474
55.249	24258.1	248.1	1.4846	83.063	0.615

1,3-Dimethyl-3-phenylindolin-2-one (Table 15, entry 4):

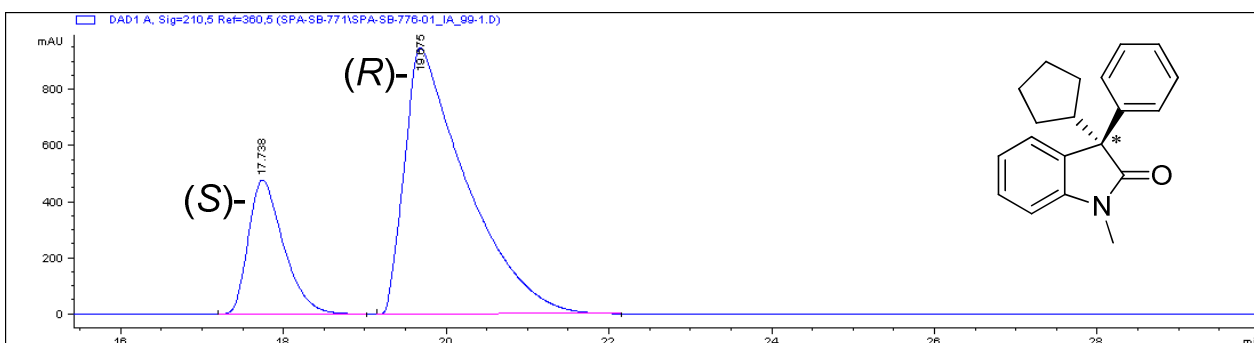
Chiralpak IA column, *n*-hexane/*i*-propanol = 99:1, 1.0 mL/min. DAD 1 A, Sig = 210.5 nm, Ref = 360.5 nm, t_R = 17.21 min (minor) and 25.65 min (major) 63% ee.

Peak	Area	Height	Width	Area%	Symmetry
17.213	5647.4	224.3	0.3777	18.673	0.578
25.650	24595.8	356.9	1.0161	81.327	0.433

1,3-Dimethyl-3-phenylindolin-2-one (Table 15, entry 3):

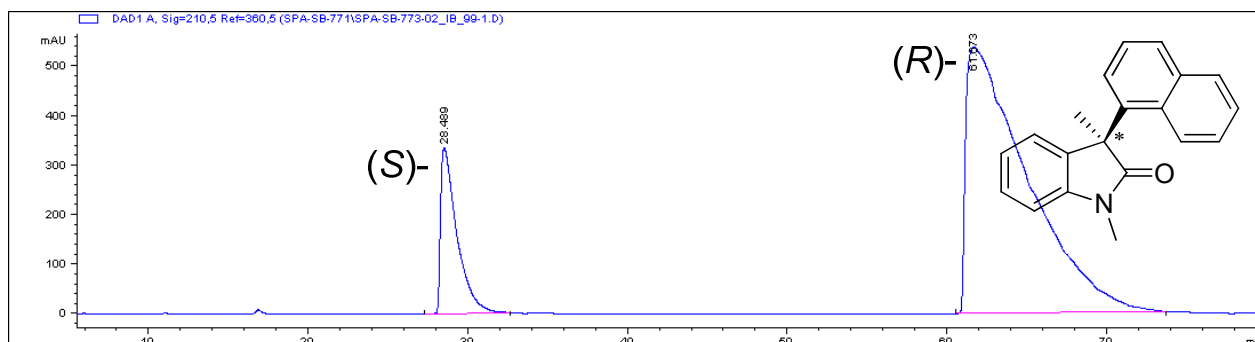
Chiralpak IA column, *n*-hexane/*i*-propanol = 99:1, 1.0 mL/min. DAD 1 A, Sig = 210.5 nm, Ref = 360.5 nm, t_R = 16.63 min (minor), 21.54 min (major) and 16.05 min (8% substrate), 58% ee.

Peak	Area	Height	Width	Area%	Symmetry
16.633	3018.9	118.2	0.3779	19.169	0.597
21.535	11294.2	325.5	0.5209	71.717	0.514

1-cyclo-pentyl-3-methyl-3-phenylindolin-2-one (Table 15, entry 2):

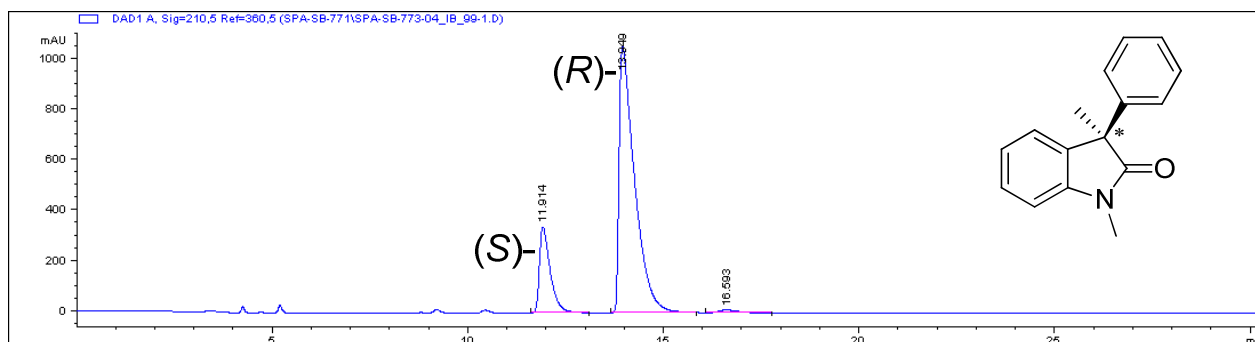
Chiralpak IA column, *n*-hexane/*i*-propanol = 99:1, 1.0 mL/min. DAD 1 A, Sig = 210.5 nm, Ref = 360.5 nm, t_R = 17.74 min (minor) and 19.68 min (major), 55% ee.

Peak	Area	Height	Width	Area%	Symmetry
17.738	14436.6	479.2	0.4575	22.376	0.632
19.675	50080.7	950.1	0.715	77.624	0.321

Determination of product configuration:^[393, 395, 396]**1,3-Dimethyl-3-(naphthalen-1-yl)indolin-2-one (reference on Chiralpak IB column equal to elution order reported):**

Chiralpak IB column, *n*-hexane/*i*-propanol = 99:1, 1.0 mL/min. DAD 1 A, Sig = 210.5 nm, Ref = 360.5 nm, t_R = 28.49 min (minor) and 61.67 min (major).

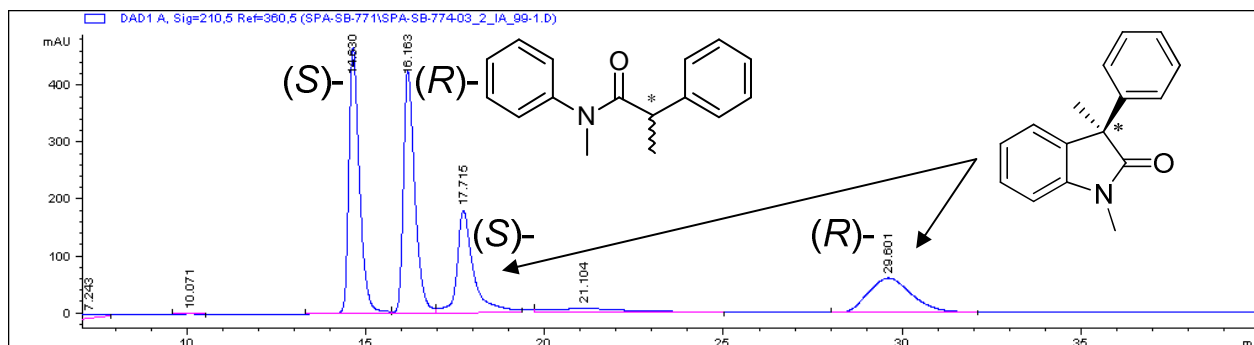
Peak	Area	Height	Width	Area%	Symmetry
28.489	23956.6	335.2	1.0859	14.297	0.259
61.673	143607	538.8	3.3677	85.703	0.14

1,3-Dimethyl-3-phenylindolin-2-one (reference on Chiralpak IB column equal to elution order reported):

Chiralpak IB column, *n*-hexane/*i*-propanol = 99:1, 1.0 mL/min. DAD 1 A, Sig = 210.5 nm, Ref = 360.5 nm, t_R = 11.91 min (minor) and 13.95 min (major).

Peak	Area	Height	Width	Area%	Symmetry
11.914	6582.1	339.9	0.2859	18.177	0.452
13.949	29241.3	1054	0.3977	80.753	0.271

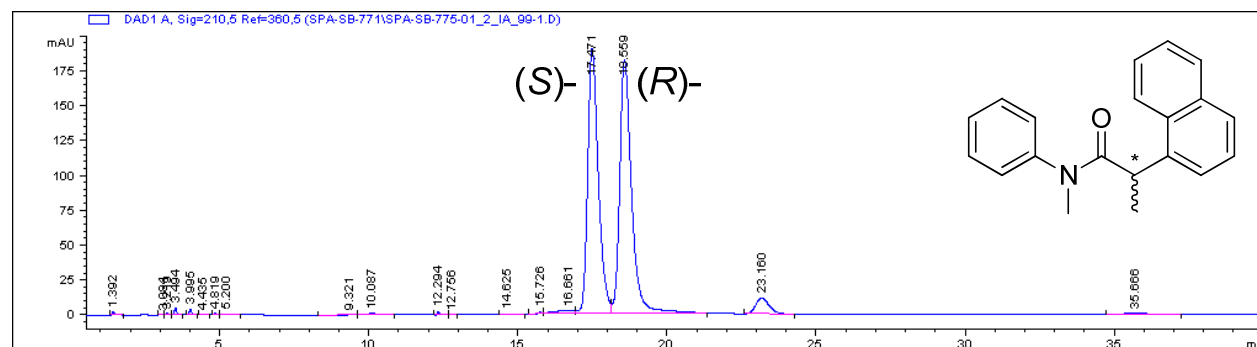
Dehalogenation products: *N*-methyl-*N*-diphenylpropanamide (A) and 1,3-Dimethyl-3-phenylindolin-2-one (B) (Table 15, entry 7):



Chiralpak IA column, *n*-hexane/*i*-propanol = 99:1, 1.0 mL/min. DAD 1 A, Sig = 210.5 nm, Ref = 360.5 nm, $t_{R, A} = 14.63$ min (A), 16.16 min (A) and $t_{R, B} = 17.72$ min (B), 29.60 min (B).

Peak	Area	Height	Width	Area%	Symmetry
14.630	9700.3	468	0.3118	26.772	0.604
16.163	9517.1	426.1	0.3366	26.267	0.592
17.715	5933.7	180.6	0.4713	16.377	0.57
29.601	5011.1	60.1	1.3246	13.830	0.827

***N*-phenyl-*N*-methyl-2-(naphthalen-1-yl)propanamide (Table 15, entry 8):**



Chiralpak IA column, *n*-hexane/*i*-propanol = 99:1, 1.0 mL/min. DAD 1 A, Sig = 210.5 nm, Ref = 360.5 nm, $t_R = 17.47$ min and 18.56 min and 23.16 min (3% substrate deriv.).

Peak	Area	Height	Width	Area%	Symmetry
17.471	4750.8	190.5	0.3769	44.904	0.671
18.559	5078.6	182.7	0.4163	48.004	0.618
23.16	371.7	11.7	0.4838	3.514	0.759
35.666	57.8	0.89	0.7718	0.546	0.869

References

- [1] K. W. Busch, M. A. Busch, *Chiral Analysis*, Elsevier, Amsterdam, **2006**.
- [2] W. G. McBride, *Lancet* **1961**, 2, 1358.
- [3] J. Christoffers, A. Baro, *Quaternary Stereocenters - Challenges and Solutions for Organic Synthesis*, Wiley-VCH, Weinheim, **2005**.
- [4] A. G. Jones, *Crystallization Process Systems*, Butterworth-Heinemann, Oxford, **2002**.
- [5] G. Subramanian, *Chiral Separation Techniques - A Practical Approach, 2nd, completely revised and updated edition*, Wiley-VCH, Weinheim, **2001**.
- [6] D. Enders, K.-E. Jaeger, *Asymmetric Synthesis with Chemical and Biological Methods*, Wiley-VCH, Weinheim, **2007**.
- [7] W. Wainer, *Trends Anal. Chem.* **1987**, 6, 125.
- [8] D. W. Armstrong, A. Alak, W. DeMond, W. L. Hinze, T. E. Riehl, *J. Liq. Chromatogr.* **1985**, 8, 261.
- [9] D. W. Armstrong, S. Chen, C. Chang, S. Chang, *J. Liq. Chromatogr.* **1992**, 15, 545.
- [10] W. H. Pirkle, D. W. House, *J. Org. Chem.* **1979**, 44, 1957.
- [11] W. H. Pirkle, J. M. Finn, J. L. Schreiner, B. C. Hamper, *J. Am. Chem. Soc.* **1981**, 103, 3964.
- [12] W. H. Pirkle, J. M. Finn, *J. Org. Chem.* **1981**, 46, 2935.
- [13] W. H. Pirkle, R. Däppen, *J. Chromatogr.* **1987**, 404, 107.
- [14] W. H. Pirkle, C. J. Welch, *J. Org. Chem.* **1984**, 49, 138.
- [15] W. H. Pirkle, J. M. Finn, *J. Org. Chem.* **1982**, 47, 4037.
- [16] W. H. Pirkle, M. H. Huyen, B. Banks, *J. Chromatogr.* **1984**, 316, 585.
- [17] Y. Okamoto, M. Kawashima, K. Yamamoto, K. Hatada, *Chem. Lett.* **1984**, 739.
- [18] Y. Okamoto, R. Aburatani, T. Fukumoto, K. Hatada, *Chem. Lett.* **1987**, 1857.
- [19] Y. Okamoto, T. Senoh, H. Nakane, K. Hatada, *Chirality* **1989**, 1, 216.
- [20] Y. Okamoto, M. Kawashima, K. Hatada, *J. Chromatogr.* **1986**, 363, 173.
- [21] A. Ichida, T. Shibata, Y. Okamoto, Y. Yuki, H. Namikoshi, Y. Toga, *Chromatographia* **1984**, 19, 280.

- [22] Y. Okamoto, R. Aburatani, Y. Kaida, K. Hatada, *Chem. Lett.* **1988**, 1125.
- [23] D. W. Armstrong, W. DeMond, A. Alak, W. L. Hinze, T. E. Riehl, K. H. Bui, *Anal. Chem.* **1985**, *57*, 234.
- [24] K. Fujimura, T. Ueda, T. Ando, *Anal. Chem.* **1983**, *55*, 446.
- [25] Y. Kawaguchi, M. Tanaka, M. Nakae, K. Funazo, T. Shono, *Anal. Chem.* **1983**, *55*, 1852.
- [26] G. Blaschke, *Chem. Ber.* **1974**, *107*, 237.
- [27] Y. Okamoto, R. Aburatani, S. Miura, K. Hatada, *J. Liq. Chromatogr.* **1987**, *10*, 1613.
- [28] V. A. Davankov, S. V. Rogozhin, *J. Chromatogr.* **1971**, *60*, 280.
- [29] V. A. Davankov, A. S. Bochkov, A. A. Kurganov, *Chromatographia* **1980**, *13*, 677.
- [30] V. A. Davankov, S. V. Rogozhin, V. A. Semechkin, T. P. Sachkova, *J. Chromatogr.* **1973**, *82*, 359.
- [31] V. A. Davankov, *Adv. Chromatogr.* **1980**, *18*, 139.
- [32] J. W. Dolan, L. R. Snyder, *Troubleshooting in LC Systems*, Human Press Inc., Totowa, New Jersey, **1989**.
- [33] D. Rodd, *The Troubleshooting and Maintenance Guide for Gas Chromatographers, Fourth, Revised and updated Edition*, Wiley-VCH, Weinheim, **2007**.
- [34] T. E. Beesley, R. P. W. Scott, *Chiral Chromatography*, John Wiley & Sons Ltd., Chichester, **1998**.
- [35] E. Gil-Av, B. Freibush, R. Charles-Sigler, *Tetrahedron Lett.* **1966**, *6*, 1009.
- [36] H. Frank, G. J. Graeme, E. Bayer, *J. Chromatogr. Sci.* **1977**, *15*, 174.
- [37] H. Frank, G. Nicholson, E. Bayer, *J. Chromatogr. Sci.* **1978**, *146*, 197.
- [38] I. Benecke, W. A. König, *Angew. Chem. Int. Ed. Engl.* **1982**, *21*, 709.
- [39] V. Schurig, *Angew. Chem. Int. Ed.* **1977**, *16*, 110.
- [40] T. Koscielski, D. Sybilska, *J. Chromatogr.* **1983**, *280*, 131.
- [41] G. Sicoli, Z. Jiang, L. Jicsinsky, V. Schurig, *Angew. Chem. Int. Ed.* **2005**, *44*, 4092.
- [42] V. Schurig, H.-P. Nowotny, *Angew. Chem. Int. Ed. Engl.* **1990**, *29*, 939.
- [43] V. Schurig, H.-P. Nowotny, *J. Chromatogr.* **1988**, *441*, 155.
- [44] V. Schurig, *Angew. Chem. Int. Ed.* **1989**, *28*, 736.
- [45] W. A. König, S. Lutz, G. Wenz, E. Bey, *J. High. Resolut. Chromatogr.* **1988**, *11*, 506.

- [46] W. A. König, S. Lutz, G. Wenz, *Angew. Chem. Int. Ed.* **1988**, 27, 979.
- [47] A. Dietrich, B. Maas, A. Mosandl, *J. High. Resolut. Chromatogr.* **1995**, 18, 152.
- [48] R. R. Fraser, M. A. Petit, J. K. Saunders, *Chem. Commun.* **1971**, 1450.
- [49] B. Freibush, M. F. Richardson, R. E. Sievers, C. S. J. Springer, *J. Am. Chem. Soc.* **1972**, 94, 6717.
- [50] T. J. Wenzel, B. T. Wenzel, *Chirality* **2009**, 21, 6.
- [51] V. Schurig, *Inorg. Chem.* **1972**, 11, 736.
- [52] V. Schurig, R. Weber, *J. Chromatogr.* **1981**, 217, 51.
- [53] V. Schurig, W. Bürkle, *J. Am. Chem. Soc.* **1982**, 104, 7573.
- [54] V. Schurig, W. Bürkle, *Angew. Chem. Int. Ed. Engl.* **1978**, 17, 132.
- [55] V. Schurig, D. Wistuba, *Tetrahedron Lett.* **1984**, 25, 5633.
- [56] V. Schurig, U. Leyrer, R. Weber, *Chromatogr. Commun.* **1985**, 8, 459.
- [57] V. Schurig, R. Weber, *Angew. Chem. Int. Ed.* **1983**, 22, 772.
- [58] V. Schurig, A. Ossig, R. Link, *Chromatogr. Commun.* **1988**, 11, 89.
- [59] V. Schurig, *J. Chromatogr. A* **2002**, 965, 315.
- [60] P. McMorn, G. J. Hutchings, *Chem. Soc. Rev.* **2004**, 33, 108.
- [61] M. Heitbaum, I. Glorius, I. Escher, *Angew. Chem. Int. Ed.* **2006**, 45, 4732.
- [62] I. F. J. Vankelecom, *Chem. Rev.* **2002**, 102, 3779.
- [63] M. J. Owen, *Silicon-Containing Polymers*, Kluwer Publishers, Dordrecht, Netherlands, **2000**.
- [64] C. J. Brinker, W. G. Scherer, *Sol-Gel Science - The Physics and Chemistry of Sol-Gel Processing*, Academic Press, San Diego, **1990**.
- [65] P. Fischer, R. Aichholz, U. Bözl, M. Juza, S. Krimmer, *Angew. Chem. Int. Ed. Engl.* **1990**, 19, 427.
- [66] V. Schurig, D. Schmalzing, U. Mühleck, M. Jung, M. Schleimer, P. Mussche, C. Duvekot, J. C. Buyten, *J. High Resol. Chromatogr.* **1990**, 13, 713.
- [67] V. Schurig, Z. Juvancz, G. J. Nicholson, D. Schmalzing, *J. High Resol. Chromatogr.* **1991**, 01, 58.
- [68] J. Dönnecke, W. A. König, O. Gyllenhaal, J. Vessman, C. Schultze, *J. High Resol. Chromatogr.* **1994**, 17, 779.

- [69] D. A. Armitage, *Comprehensive Organometallic Chemistry*, Vol. 2, Pergamon Press, Oxford, **1982**.
- [70] B. Marciniec, P. Krzyzanowski, *J. Organomet. Chem.* **1995**, 493, 261.
- [71] K. Takeshita, Y. Seki, K. Kawamoto, S. Murai, N. Sonoda, *J. Org. Chem.* **1987**, 52, 4864.
- [72] L. N. Lewis, J. Stein, Y. Gao, R. E. Colborn, G. Hutchins, *Platinum Metals Rev.* **1997**, 41, 66.
- [73] J. L. Speier, *Adv. Organomet. Chem.* **1979**, 17, 407.
- [74] B. D. Karstedt, US-A 3175452, in *US-A 3175452*, Vol. 3175452 (Ed.: U.-A. 3175452), US-A 3175452, US-A 3175452, **1973**.
- [75] P. Strohriegl, *Makromol. Chem. Rapid Commun.* **1987**, 7, 771.
- [76] P. Strohriegl, M. Lux, H. Höcker, *Makromol. Chem. Rapid Commun.* **1987**, 188, 811.
- [77] I. E. Markó, S. Stérin, O. Buisine, G. Magnani, P. Branlard, B. Tinant, J. P. Declercq, *Science* **2002**, 298, 204.
- [78] B.-H. Han, P. Boudjouk, *Organometallics* **1983**, 2, 769.
- [79] I. Agilent Technologies, *GC Columns: More than essential products. Reproducible results. - CP-Chirasil Val for Amino Acid Enantiomers, 2011*, Loveland, Colorado, United States, **2000 - 2011**.
- [80] T. Saeed, P. Sandra, M. Verzele, *J. Chromatogr.* **1979**, 29+, 611.
- [81] T. Saeed, P. Sandra, M. Verzele, *J. High Resol. Chromatogr.* **1980**, 3, 35.
- [82] V. Schurig, D. Schmalzing, M. Schleimer, *Angew. Chem. Int. Ed. Engl.* **1991**, 30, 987.
- [83] M. Fluck, Eberhard-Karls-Universität Tübingen (Tübingen), **1996**.
- [84] V. Schurig, R. Link, in *Proceedings of the International Meeting on Chromatography*, (Eds.: D. Stevenson, I. D. Wilson), Plenum Press, New York and London, University of Surrey, Guildford, 3 - 4 September 1987, **1988**, p. 91.
- [85] V. Schurig, R. Link, in *Proceedings of the International Meeting on Chromatography* (Eds.: D. Stevenson, I. D. Wilson), Plenum Press, New York and London, University of Surrey, Guilford 3 - 4, **1988**, p. 91.
- [86] G. Opitz, N. Fischer, *Angew. Chem. Int. Ed. Engl.* **1965**, 4, 70.
- [87] G. Opitz, *Angew. Chem. Int. Ed. Engl.* **1967**, 6, 107.
- [88] H. L. Goering, J. N. Eikenberry, G. S. Koermer, C. J. Lattimer, *J. Am. Chem. Soc.* **1974**, 96, 1493.

- [89] F. Keller, H. Weinmann, V. Schurig, *Chem. Ber./Recueil* **1997**, *130*, 879.
- [90] M. Schleimer, *Dissertation* **1992**, University of Tübingen.
- [91] B. O. Linn, C. R. Hauser, *J. Am. Chem. Soc.* **1956**, *78*, 6066.
- [92] K. R. Kopecky, D. Nonhebel, G. Morris, G. S. Hammond, *J. Org. Chem.* **1962**, *27*, 1036.
- [93] A. Togni, *Organometallics* **1990**, *9*, 3106.
- [94] A. Togni, G. Rist, G. Rihs, A. Schweiger, *J. Am. Chem. Soc.* **1993**, *115*, 1908.
- [95] M. Bednarski, S. Danishefsky, *J. Am. Chem. Soc.* **1983**, *105*, 6968.
- [96] M. Quimpère, K. Jankowski, *J. Chem. Soc., Chem. Commun.* **1984**, 676.
- [97] M. Bednarski, C. Maring, S. Danishefsky, *Tetrahedron Lett.* **1983**, *24*, 3451.
- [98] S. A. Matlin, W. J. Lough, L. Chan, D. M. H. Abram, Z. Zhou, *J. Chem. Soc., Chem. Commun.* **1984**, 1038.
- [99] S. Sandel, S. K. Weber, O. Trapp, *Chem. Eng. Sci.* **2011**, -, in press.
- [100] M. Felder, G. Giffels, *Tetrahedron: Asymmetry* **1997**, *8*, 1975.
- [101] Y.-R. Yang, W.-D. Z. Li, *J. Org. Chem.* **2005**, *70*, 8224.
- [102] S. d. l. M. Cerero, A. G. Martinez, E. T. Vilar, G. A. Fraile, B. L. Morato, *Journal of Organic Chemistry* **2003**, *68*, 1451.
- [103] A. G. Martinez, E. T. Vilar, G. A. Fraile, S. d. l. M. Cerero, B. L. Maroto, *Tetrahedron Lett.* **2001**, *42*, 6539.
- [104] A. G. Martinez, E. T. Vilar, G. A. Fraile, S. d. l. M. Cerero, B. L. Maroto, *Tetrahedron: Asymmetry* **2001**, *12*, 189.
- [105] A. G. Martinez, E. T. Vilar, G. A. Fraile, S. d. l. M. Cerero, P. M. Ruiz, *Tetrahedron: Asymmetry* **1998**, *9*, 1737.
- [106] B. L. Maroto, S. d. l. M. Cerero, A. G. Martinez, G. A. Fraile, E. T. Vilar, *Tetrahedron: Asymmetry* **2000**, *11*, 3059.
- [107] A. G. Martinez, E. T. Vilar, G. A. Fraile, S. d. l. M. Cerero, C. D. Morillo, *Tetrahedron* **2005**, *61*, 599.
- [108] A. G. Martinez, E. T. Vilar, J. O. Barcina, M. E. R. Herrero, S. d. l. M. Cerero, S. Hanack, L. R. Subramanian, *Tetrahedron: Asymmetry* **1993**, *4*, 2333.
- [109] A. G. Martinez, E. T. Vilar, G. A. Fraile, S. d. l. M. Cerero, J. M. Gonzales-Fleitas de Diego, L. R. Subramanian, *Tetrahedron: Asymmetry* **1994**, *5*, 1599.

- [110] P. Gosselin, M. Lelievre, B. Poissonnier, *Tetrahedron: Asymmetry* **2001**, *12*.
- [111] A. G. Martinez, E. T. Vilar, G. A. Fraile, S. d. I. M. Cerero, B. L. Maroto, *Tetrahedron: Asymmetry* **2002**, *13*, 17.
- [112] A. G. Martinez, E. T. Vilar, G. A. Fraile, S. d. I. M. Cerero, B. L. Maroto, C. D. Morillo, *Tetrahedron Lett.* **2001**, *42*, 8293.
- [113] A. G. Martinez, E. T. Vilar, G. A. Fraile, S. d. I. M. Cerero, B. L. Maroto, *Tetrahedron Lett.* **2001**, *42*, 5017.
- [114] A. G. Martinez, E. T. Vilar, G. A. Fraile, S. d. I. M. Cerero, B. L. Maroto, *Tetrahedron Lett.* **2002**, *43*, 1183.
- [115] A. G. Martinez, E. T. Vilar, G. A. Fraile, S. d. I. M. Cerero, P. M. Ruiz, C. D. Morillo, B. L. Maroto, *Tetrahedron Lett.* **2007**, *48*, 5981.
- [116] A. G. Martinez, E. T. Vilar, G. A. Fraile, S. d. I. M. Cerero, C. D. Morillo, R. P. Morillo, *Synlett* **2004**, 134.
- [117] A. G. Martinez, E. T. Vilar, M. G. Marin, C. R. Franco, *Chem. Ber.* **1985**, *118*, 1282.
- [118] A. G. Martinez, E. T. Vilar, G. A. Fraile, C. R. Franco, J. Soto, L. R. Subramanian, M. Hanack, *Synthesis* **1987**, 321.
- [119] A. G. Martinez, E. T. Vilar, J. O. Barcina, J. M. Alonso, M. E. R. Herrero, M. Hanack, L. R. Subramanian, *Tetrahedron Lett.* **1992**, *33*, 607.
- [120] J. E. H. Buston, I. Coldham, K. R. Mulholland, *J. Chem. Soc. Perkin Trans. 1* **1999**, 2327.
- [121] K. Bica, G. Gmeiner, C. Reichel, B. Lendl, P. Gaertner, *Synthesis* **2007**, *9*, 1333.
- [122] G. Chelucci, *Chem. Soc. Rev.* **2006**, *36*, 1230.
- [123] F. W. Lewis, G. Egron, D. H. Grayson, *Tetrahedron: Asymmetry* **2009**, 1531.
- [124] D. S. Tarbell, F. C. Loveless, *J. Am. Chem. Soc.* **1958**, *80*, 1963.
- [125] J. H. Hutchinson, T. Money, S. E. Piper, *Can. J. Chem.* **1986**, *64*, 854.
- [126] V. Schurig, W. Bürkle, K. Hintzer, R. Weber, *J. Chromatogr.* **1989**, *475*, 23.
- [127] J. S. McConaghy, J. J. Bloomfield, *J. Org. Chem.* **1968**, *33*, 3425.
- [128] O. Trapp, S. K. Weber, S. Bauch, *Angew. Chem. Int. Ed.* **2007**, *46*, 7307.
- [129] J. B. Perales, D. L. Van Vranken, *J. Org. Chem.* **2001**, *66*, 7270.
- [130] C. Pietraszuk, S. Rogalski, M. Majchrzak, B. Marciniak, *J. Org. Chem.* **2006**, *691*, 5476.

- [131] M. G. Voronkov, N. N. Vlasova, S. A. Bolshakova, S. V. Kirpichenko, *J. Organomet. Chem.* **1980**, *190*, 335.
- [132] G. Ertl, H. Knözinger, F. Schüth, J. Weitkamp, *Handbook of Heterogeneous Catalysis*, 2nd ed., Wiley-VCH, Weinheim, Germany, **2008**.
- [133] R. Schlögl, *Handbook of Heterogeneous Catalysis*, Wiley-VCH, Weinheim, **1997**.
- [134] G. V. Smith, F. Notheisz, *Heterogeneous Catalysis in Organic Chemistry*, Academic Press, San-Diego, **2000**.
- [135] M. R. Buchmeiser, *Polymeric Materials in Organic Synthesis and Catalysis*, Wiley-VCH, Weinheim, **2003**.
- [136] K. Burgess, *Solid-Phase Organic Synthesis*, Wiley-Interscience, New-York, **2000**.
- [137] R. W. Allington, M. Barut, O. Brüggemann, J. M. J. Frechet, S. Imamoglu, R. Necina, A. Podgornik, *Modern Advances in Chromatography*, Springer Berlin, Heidelberg, **2002**.
- [138] A. Hagemeyer, P. Strasser, A. F. J. Volpe, *High Throughput Screening in Chemical Catalysis*, Wiley-VCH, Weinheim, **2004**.
- [139] K. Grob, *Making and manipulating capillary columns for gas chromatography*, Huethig Jehle Rehm, Heidelberg, **1986**.
- [140] M. Schleimer, V. Schurig, *J. Chromatogr.* **1993**, *638*, 85.
- [141] A. Togni, S. D. Pastor, *Chirality* **1991**, *3*, 331.
- [142] R. Weber, Eberhardt-Karls-Universität Tübingen, *Dissertation* **1983**.
- [143] D. Shirotni, T. Suzuki, S. Kaizaki, *Inorg. Chem.* **2006**, *45*, 6111.
- [144] H.-J. Hübschmann, *Handbook of GC/MS: Fundamentals and Applications*, 2nd ed., Wiley-VCH, Weinheim, **2009**.
- [145] J. Cazes, R. P. W. Scott, *Chromatography Theory*, Marcel Dekker, Inc., New York, **2002**.
- [146] I. A. Fowles, *Gas Chromatography*, 2nd ed., John Wiley & Sons, Chichester, **1995**.
- [147] W. Jennings, E. Mittlefehldt, P. Stremple, *Analytical Gas Chromatography*, 2nd ed., Academic Press, San Diego, **1997**.
- [148] L. S. Ettre, *J. Chromatogr.* **1979**, *165*, 235.
- [149] V. Schurig, R. Schmidt, *J. Chromatogr. A* **2003**, *1000*, 311.
- [150] W. Francke, V. Heemann, B. Gerken, J. A. A. Renewick, J. P. Vité, *Naturwissenschaften* **1977**, *64*, 590.

- [151] C. Phillips, R. Jacobsen, B. Abrahams, H. J. Williams, L. R. Smith, *J. Org. Chem.* **1980**, *45*, 1920.
- [152] L. R. Smith, H. J. Williams, R. M. Silverstein, *Tetrahedron Lett.* **1978**, *35*, 3231.
- [153] for comprehensive data see, O. Trapp, V. Schurig, *Chem. Eur. J.* **2001**, *7*, 1495.
- [154] O. Trapp, V. Schurig, *Chem. Eur. J.* **2001**, *7*, 1495.
- [155] M. Schleimer, M. Fluck, V. Schurig, *Anal. Chem.* **1994**, *66*, 2893.
- [156] M. Jung, Eberhardt-Karls-Universität Tübingen **1993**.
- [157] V. Schurig, *J. Chromatogr. A* **2001**, *906*, 275.
- [158] O. Trapp, *Anal. Chem.* **2006**, *78*, 189.
- [159] O. Trapp, *Electrophoresis* **2006**, *27*, 534.
- [160] O. Trapp, *Electrophoresis* **2006**, *27*, 2999.
- [161] O. Trapp, *Chirality* **2006**, *18*, 489.
- [162] O. Trapp, *Electrophoresis* **2005**, *26*, 487.
- [163] O. Trapp, V. Schurig, *J. Chromatogr. A* **2001**, *911*, 167.
- [164] O. Trapp, V. Schurig, *Chirality* **2002**, *14*, 465.
- [165] for detailed informations see references [1], [7], [10 - 14] in, J. D. Dunitz, *Chemistry & Biology* **1995**, *2*, 709.
- [166] J. D. Dunitz, *Chemistry & Biology* **1995**, *2*, 709.
- [167] V. Schurig, J. Ossig, R. Link, *Angew. Chem. Int. Ed. Engl.* **1989**, *28*, 194.
- [168] E. J. Corey, A. W. Gross, *J. Org. Chem.* **1985**, *50*, 5391.
- [169] G. Chelucci, S. Baldino, *Tetrahedron: Asymmetry* **2006**, *17*, 1529.
- [170] T. C. Nugent, A. K. Ghosh, V. N. Wakchaure, R. R. Mohanty, *Adv. Synth. Catal.* **2006**, *348*, 1289.
- [171] T. C. Nugent, V. N. Wakchaure, A. K. Ghosh, R. R. Mohanty, *Org. Lett.* **2005**, *7*, 4967.
- [172] T. Ikenega, K. Matsushita, J. Shinozawa, S. Yada, Y. Takagi, *Tetrahedron* **2005**, *61*, 2105.
- [173] G. Knupp, A. W. Frahm, *Arch. Pharm.* **1985**, *318*, 250.
- [174] K. Kindler, G. Melamed, D. Matthies, *Justus Liebigs Ann. Chem.* **1961**, *644*, 23.

- [175] W. Hückel, P. Rieckmann, *Justus Liebigs Ann. Chem.* **1959**, 625, 1.
- [176] M. Santelli, J.-M. Pons, *Lewis Acids and Selectivity in Organic Chemistry*, CRC Press, New York, **1996**.
- [177] H. Yamamoto, *Lewis Acids in Organic Synthesis, Vol. 1*, Wiley-VCH, Weinheim, **2000**.
- [178] H. Yamamoto, *Lewis Acids in Organic Synthesis, Vol. 2*, Wiley-VCH, Weinheim, **2000**.
- [179] K. Narasaka, *Synthesis* **1991**, 1, 1.
- [180] J. Smidt, W. Hafner, R. Jira, R. Sieber, J. Sedlmeier, J. Sabel, *Angew. Chem. Int. Ed. Engl.* **1962**, 1, 80.
- [181] J. Hagen, *Industrial Catalysis: A Practical Approach*, 2nd ed., Wiley-VCH, Weinheim, Germany, **2006**.
- [182] J. Smidt, W. Hafner, R. Jira, J. Sedlmeier, R. Sieber, R. Rüttinger, H. Kojer, *Angew. Chem.* **1959**, 71, 176.
- [183] J. Tsuji, *Palladium in Organic Synthesis, Vol. 14*, **2005**.
- [184] J. Tsuji, *Palladium Reagents and Catalysts - New Perspectives for the 21st Century*, John Wiley & Sons Ltd., Chichester, England, **2004**.
- [185] R. Jira, *Angew. Chem. Int. Ed.* **2009**, 48, 9034.
- [186] B. J. Anderson, J. A. Keith, M. S. Sigman, *J. Am. Chem. Soc.* **2010**, 132, 11872.
- [187] A. Naik, L. Meina, M. Zabel, O. Reiser, *Chem. Eur. J.* **2010**, 19, 1624.
- [188] T. Mitsudome, T. Umetani, N. Nosaka, K. Mori, T. Mizugaki, K. Ebitani, K. Kaneda, *Angew. Chem. Int. Ed.* **2006**, 45, 481.
- [189] B. A. Steinhoff, S. R. Fix, S. S. Stahl, *J. Am. Chem. Soc.* **2002**, 124, 766.
- [190] S. Uchiumi, K. Ataka, T. Matsuzaki, *J. Organomet. Chem.* **1999**, 576, 279.
- [191] S. R. Fix, J. L. Brice, S. S. Stahl, *Angew. Chem. Int. Ed.* **2002**, 41, 164.
- [192] S. S. Stahl, J. L. Thorman, R. C. Nelson, M. A. Kozee, *J. Am. Chem. Soc.* **2001**, 123, 7188.
- [193] J. M. Takacs, X.-T. Jiang, *Current Organic Chemistry* **2003**, 7, 369.
- [194] J. A. Keith, P. M. Henry, *Angew. Chem. Int. Ed.* **2009**, 48, 2.
- [195] B. W. Michel, A. M. Camelio, C. N. Cornell, M. S. Sigman, *J. Am. Chem. Soc.* **2009**, 131, 6076.

- [196] R. M. Painter, D. M. Pearson, R. M. Waymouth, *Angew. Chem. Int. Ed.* **2010**, *49*, 9456.
- [197] J. A. Mueller, A. Cowell, B. D. Chandler, M. S. Sigman, *J. Am. Chem. Soc.* **2005**, *127*, 14817.
- [198] R. M. Trend, Y. K. Ramtohl, E. M. Ferreira, B. M. Stoltz, *Angew. Chem. Int. Ed.* **2003**, *42*, 2892.
- [199] C. N. Cornell, M. S. Sigman, *Org. Lett.* **2006**, *8*, 4117.
- [200] G.-J. t. Brink, I. W. C. E. Arends, M. Hoogenraad, G. Verspui, R. A. Sheldon, *Adv. Synth. Catal.* **2003**, *345*, 0.
- [201] G.-J. t. Brink, I. W. C. E. Arends, G. Papadogianakis, R. A. Sheldon, *Chem. Commun.* **1998**, *21*, 2359.
- [202] N. R. Conley, L. Labios, D. M. Pearson, C. C. L. McCrory, R. M. Waymouth, *Organometallics* **2007**, *26*, 5447.
- [203] G. W. Parshall, S. D. Ittel, *Homogeneous Catalysis*, 2nd ed., Wiley, New York, **1992**.
- [204] R. C. Larock, *Comprehensive Organic Transformations: A Guide to Functional Group Preparations*, 2nd ed., Wiley-VCH, New York, **1999**.
- [205] L. Canovese, C. Santo, F. Visentin, *Organometallics* **2008**, *27*, 3577.
- [206] I. S. Kim, G. R. Dong, Y. H. Jung, *Journal of Organic Chemistry* **2007**, *72*, 5424.
- [207] J. Yu, M. J. Gaunt, J. B. Spencer, *J. Org. Chem.* **2002**, *67*, 4627.
- [208] B. Cornils, W. A. Herrmann, *Applied Homogeneous Catalysis with Organometallic Compounds: A Comprehensive Handbook in Three Volumes*, 2nd ed., Wiley-VCH, New York, **2002**.
- [209] P. Kraft, K. A. D. Swift, *Current Topics in Flavour and Fragrance Research*, 1st ed., Hel. Chim. Acta, Zürich and Wiley-VCH, Weinheim, Germany, **2008**.
- [210] K. Bauer, D. Garbe, H. Surburg, *Common Fragrance and Flavour Materials: Preparation, Properties and Uses*, 5th ed., Wiley-VCH, Weinheim, Germany, **2006**.
- [211] H. R. Krieheldorf, O. Nuyken, K. A. D. Swift, *Handbook of Polymer Synthesis*, 2nd ed., Marcel Dekker, New York, **2005**.
- [212] S. K. Sharma, V. K. Srivastava, R. V. Jasra, *J. Mol. Catal. A* **2006**, *245*, 200.
- [213] D. Gauthier, A. T. Lindhardt, E. P. K. Olsen, J. Overgaard, T. Skrydstrup, *J. Am. Chem. Soc.* **2010**, *132*, 7998.
- [214] R. Jennerjahn, I. Piras, R. Jackstell, R. Franke, K.-D. Wiese, M. Beller, *Chem. Eur. J.* **2009**, *15*, 6383.

- [215] H. J. Lim, C. R. Smith, T. V. RajanBabu, *J. Org. Chem.* **2009**, *74*, 4565.
- [216] J. Fan, C. Wan, Q. Wang, L. gao, X. Zheng, Z. Wang, *Org. Biomol. Chem.* **2009**, *7*, 3168.
- [217] A. Scarso, M. Colladon, P. Sgarbossa, C. Santo, R. A. Michelin, G. Strukul, *Organometallics* **2010**, *29*, 1487.
- [218] B. Lastra-Barreira, J. Francos, P. Crochet, V. Cadierno, *Green Chem.* **2011**, *13*, 307.
- [219] S. Krompiec, N. Kuznik, M. Urbala, J. Rzepa, *J. Mol. Catal. A* **2006**, *248*, 198.
- [220] A. Salvini, F. Piacenti, P. Frediani, A. Devescovi, M. Caporali, *J. Organomet. Chem.* **2001**, *625*, 255.
- [221] T. J. Donohoe, T. J. C. O'Riordan, C. P. Rosa, *Angew. Chem. Int. Ed.* **2009**, *48*, 1014.
- [222] T. C. Morill, C. A. D'Souza, *Organometallics* **2003**, *22*, 1626.
- [223] I. R. Baxendale, A.-L. Lee, S. V. Ley, *J. Chem. Soc., Perkin Trans. I* **2002**, 1850.
- [224] C. J. Yue, Y. Liu, R. He, *J. Mol. Catal. A* **2006**, *259*, 17.
- [225] J. Zhang, H. Gao, Z. Ke, F. Bao, F. Zhu, Q. Wu, *J. Mol. Catal. A* **2005**, *231*, 27.
- [226] S. K. Sharma, V. K. Srivastava, P. H. Pandya, R. V. Jasra, *Catal. Commun.* **2005**, 205.
- [227] A. Quintard, A. Alexakis, C. Mazet, *Angew. Chem. Int. Ed.* **2011**, *50*, 2354.
- [228] L. Mantilli, D. Gérard, S. Torche, C. Besnard, C. Mazet, *Chem. Eur. J.* **2010**, *16*, 12736.
- [229] L. Mantilli, D. Gérard, S. Torche, C. Besnard, C. Mazet, *Angew. Chem. Int. Ed.* **2009**, *48*, 5182.
- [230] R. H. Crabtree, *The Organometallic Chemistry of the Transition Metals*, 4th ed., Wiley, New Jersey, **2005**.
- [231] S. Hanessian, S. Giroux, A. Larsson, *Org. Lett.* **2006**, *8*, 5481.
- [232] B. Schmidt, *Chem. Commun.* **2004**, 742.
- [233] M. Mirza-Aghayan, R. Boukherroub, M. Bolourtchian, *Appl. Organometal. Chem.* **2006**, *20*, 214.
- [234] M. Mirza-Aghayan, R. Boukherroub, M. Bolourtchian, M. Moseini, K. Tabar-Hydar, *Journal of Organometallic Chemistry* **2003**, *678*, 1.
- [235] S. H. Hong, D. P. Snaders, C. W. Lee, R. H. Grubbs, *J. Am. Chem. Soc.* **2005**, *127*, 17160.

- [236] P. S. Fordred, D. G. Niyadurupola, R. Wisedale, S. D. Bull, *Adv. Synth. Catal.* **2009**, *351*, 2310.
- [237] C. Kaes, A. Katz, M. W. Hosseini, *Chem. Rev.* **2000**, *100*, 3553.
- [238] G. Chelucci, R. P. Thummel, *Chem. Rev.* **2002**, *102*, 3129.
- [239] D. R. Boyd, N. D. Sharma, L. Sbirecea, D. Murphy, T. Belhocine, J. F. Malone, S. L. James, C. C. R. Allen, J. T. G. Hamilton, *Chem. Commun.* **2008**, 5535.
- [240] P. Kocovsky, A. V. Malkov, M. Bella, V. Langer, *Org. Lett.* **2000**, *2*, 3047.
- [241] H.-L. Kwong, H.-L. Yeung, W.-S. Lee, W.-T. Wong, *Chem. Commun.* **2006**, 4841.
- [242] A. V. Malkov, P. Kocovsky, M. Orsini, D. Pernazza, K. W. Muir, V. Langer, P. Meghani, *Org. Lett.* **2002**, *4*, 1047.
- [243] P. D. Wilson, M. P. A. Lyle, N. D. Draper, *Org. Lett.* **2005**, *7*, 901.
- [244] P. D. Wilson, M. P. A. Lyle, *Org. Lett.* **2004**, *6*, 855.
- [245] P. Kocovsky, A. V. Malkov, I. R. Baxendale, M. Bella, V. Langer, J. Fawcett, D. R. Russell, D. J. Mansfield, M. Valko, *Organometallics* **2001**, *20*, 673.
- [246] G. Chelucci, G. Chessa, G. Delogu, S. Gladiali, F. Soccolini, *J. Organomet. Chem.* **1986**, *304*, 217.
- [247] T. Jozak, D. Zabel, A. Schubert, Y. Sun, W. R. Thiel, *Eur. J. Inorg. Chem.* **2010**, 5135.
- [248] D. P. Fernando, A. R. Haight, K. A. Lukin, B. J. Kotecki, *Org. Lett.* **2009**, *11*, 947.
- [249] J. H. M. Hill, D. M. Berkowitz, K. J. Freese, *J. Org. Chem.* **1971**, *36*, 1563.
- [250] S. Trofimenko, *Chemical Reviews* **1972**, *72*, 497.
- [251] E. C. Constable, P. J. Steel, *Coord. Chem. Rev.* **1989**, *93*, 205.
- [252] J. Catalan, *Adv. Heterocycl. Chem.* **1987**, *41*, 2676.
- [253] G. Altenhoff, R. Goddard, C. W. Lehmann, F. Glorius, *J. Am. Chem. Soc.* **2004**, *126*, 15195.
- [254] L. Claisen, N. Stylos, *Ber. dt. chem. Ges.* **1888**, *21*, 1141.
- [255] A. Abiko, G.-q. Wang, *J. Org. Chem.* **1996**, *61*, 1164.
- [256] A. Abiko, G.-q. Wang, *Tetrahedron* **1998**, *54*, 11405.
- [257] Y. Sun, D. Rohde, Y. Liu, L. Wan, Y. Wang, W. Wu, C. Di, G. Yu, D. Zhu, *J. Mater. Chem.* **2006**, *16*, 4499.

- [258] M. Sugimoto, K. Matsushita, A. Furuhashi, *J. Soc. Anal. Chem.* **1977**, 26, 247.
- [259] M. Sugimoto, T. Matsushita, A. Furuhashi, *Fresenius Z. Anal. Chem.* **1978**, 290, 69.
- [260] B. Unterhalt, U. Pindur, *Arch. Pharm.* **1977**, 310, 264.
- [261] N. Nawar, *Qatar Univ. Sci. J.* **1994**, 14C, 105.
- [262] E. N. Kozminykh, N. M. Igidov, E. S. Berezina, G. A. Shavkunova, I. B. Yakovlev, S. A. Shelenkova, V. E. Kolla, E. V. Voronia, V. O. Kozminykh, *Pharm. Chem. J.* **1996**, 30, 458.
- [263] N. M. Igidov, E. N. Kozminykh, O. A. Sofina, T. M. Shironina, V. O. Kozminykh, *Chem. Heterocycl. Comp.* **1999**, 35, 1276.
- [264] V. O. Kozminykh, L. O. Konshina, N. M. Igidov, *J. Prakt. Chem.* **1993**, 335, 714.
- [265] T. M. Shironina, N. M. Igidov, E. N. Kozminykh, L. O. Kon'shina, Y. S. Kasatkina, V. O. Kozminykh, *Russian Journal of Organic Chemistry* **2001**, 37, 1486.
- [266] C. R. Noe, M. Knollmueller, P. Gaertner, K. Mereiter, G. Steinbauer, *Liebigs Ann. Chem.* **1996**, 6, 1015.
- [267] I. J. Hart, *Polyhedron* **1992**, 11, 729.
- [268] T. Eicher, S. Hauptmann, *The Chemistry of Heterocycles*, 2nd ed., Wiley-VCH, Weinheim, **2003**.
- [269] I. Bouabdallah, R. Touzani, I. Zidane, A. Ramdani, S. Radi, *ARKIVOC* **2006**, xiv, 46.
- [270] B. Kolp, D. Abeln, H. Stoeckli-Evans, A. Zelewsky, *Eur. J. Inorg. Chem.* **2001**, 1207 - 1220.
- [271] D. Lötscher, S. Rupprecht, P. Collomb, P. Belsler, H. Viebrock, A. Zelewsky, P. Burger, *Eur. J. Inorg. Chem.* **2001**, 40, 5675.
- [272] P. Kocovsky, A. V. Malkov, M. Bell, M. Orsini, D. Pernazza, A. Massa, P. Herrmann, P. Meghani, *J. Org. Chem.* **2003**, 68, 9659.
- [273] G. T. B. Storch, Ruprecht-Karls-Universität Heidelberg, *Advanced Internship Research Paper* **2011**.
- [274] P. Muller, *Pure & Appl. Chem.* **1994**, 66, 1077.
- [275] L. Ding, C. Liu, H. Wen, L. Yan, Z. Xiong, C. Liu, *New J. Chem.* **2011**, advance article, doi: 10.1039/c0nj00904k.
- [276] G. Tarrago, F. Mary, C. Marzin, S. Salhi, *Supramol. Chem.* **1993**, 3, 57.
- [277] A. V. Khripun, N. A. Bokach, S. I. Selivanov, M. Haukka, D. M. Revenco, V. Y. Kukushkin, *Inorg. Chem. Commun.* **2008**, 11, 1352.

- [278] L. El Ghayati, L. E. Ammari, L. T. Mohamed, E. M. Tjioua, *Acta Cryst.* **2011**, E67, m323.
- [279] Y.-Q. Wang, W.-H. Bi, X. Li, R. Cao, *Acta Cryst.* **2004**, E60, m876.
- [280] M. Fainerman-Melnikova, J. K. Clegg, A. A. H. Pakchung, P. Jensen, R. Codd, *Cryst. Eng. Comm.* **2010**, 12, 4217.
- [281] H. Jones, M. Newell, C. Metcalfe, S. E. Spey, H. Adams, J. A. Thomas, *Inorg. Chem. Commun.* **2001**, 4, 475.
- [282] S. Stockinger, Ruprecht-Karls-Universität Heidelberg, *Master Thesis* **2011**.
- [283] S. Stockinger, Ruprecht-Karls-Universität Heidelberg, *Advanced Internship Research Paper* **2011**.
- [284] M. Higuchi, S. Yamaguchi, T. Hirao, *Synlett* **1996**, 1213.
- [285] O. Trapp, *J. Chromatogr. A* **2008**, 1184, 160.
- [286] N. B. Debata, D. Tripathy, V. Ramkumar, D. K. Chand, *Tetrahedron Lett.* **2010**, 51, 4449.
- [287] R. G. Brown, R. V. Chaudhari, J. M. Davidson, *J. Chem. Soc., Dalton Trans.* **1977**, 183.
- [288] S. Liu, J. Xiao, *J. Mol. Catal. A* **2007**, 270, 1.
- [289] I. A. Shuklov, N. V. Dubrovina, A. Börner, *Synthesis* **2007**, 2925.
- [290] J.-P. Bégué, D. Bonnet-Delpon, B. Crousse, *Synlett* **2004**, 18.
- [291] P. Ballinger, F. A. Long, *J. Am. Chem. Soc.* **1960**, 82, 795.
- [292] P. Ballinger, F. A. Long, *J. Am. Chem. Soc.* **1959**, 81, 1050.
- [293] G. Erdogan, D. B. Grotjahn, *J. Am. Chem. Soc.* **2009**, 131, 10354.
- [294] W. A. Herrmann, B. Cornils, *Applied Homogeneous Catalysis with Organometallic Compounds*, Wiley-VCH, New York, **2000**.
- [295] I. I. Moiseev, T. A. Stromnova, M. N. Vargaftik, *J. Mol. Catal. A* **1994**, 86, 71.
- [296] D. Bingham, B. Hudson, D. E. Webster, P. B. Wells, *J. Chem. Soc. Dalt. Trans.* **1974**, 1521.
- [297] F. Ding, Y. Sun, F. Verpoort, *Eur. J. Inorg. Chem.* **2010**, 1536.
- [298] P. Kisanga, L. A. Goj, R. A. Widenhoefer, *J. Org. Chem.* **2001**, 66, 635.
- [299] K. L. Bray, J. P. H. Charmant, I. J. S. Fairlamb, G. C. Lloyd-Jones, *Chem. Eur. J.* **2001**, 7, 4205.

- [300] K. L. Bray, I. J. S. Fairlamb, G. C. Lloyd-Jones, *Chem. Commun.* **2001**, 187.
- [301] M. M. Kabat, L. M. Garofalo, A. R. Daniewski, S. D. Hutchings, W. Liu, M. Okabe, R. Radinov, Y. Zhou, *J. Org. Chem.* **2001**, *66*, 6141.
- [302] A. Heumann, L. Giordano, A. Tenaglia, *Tetrahedron Lett.* **2003**, *44*, 1515.
- [303] T. Hosokawa, T. Yamanaka, M. Itotani, S.-I. Murahashi, *J. Org. Chem.* **1995**, *60*, 6159.
- [304] E.-i. Negishi, *Handbook of Organopalladium Chemistry for Organic Synthesis, Vol. 2*, John Wiley & Sons, New York, **2002**.
- [305] F. Borchers, K. Levsen, H. Schwarz, C. Wesdemiotis, H. U. Winkler, *J. Am. Chem. Soc.* **1977**, *99*, 6359.
- [306] J. F. Hartwig, *Organotransition Metal Chemistry - From Bonding to Catalysis*, University Science Books, Sausalito, **2010**.
- [307] T. C. Morrill, C. A. D'Souza, *Organometallics* **2003**, *22*, 1626.
- [308] K. Burgess, W. A. Donk, T. B. Marder, S. A. Westcott, T. A. Baker, J. C. Calabrese, *J. Am. Chem. Soc.* **1992**, *114*, 9350.
- [309] A. C. Cooper, K. G. Caulton, *Inorg. Chim. Acta* **1996**, *251*, 41.
- [310] S. Fantasia, J. D. Egbert, V. Jurcik, C. S. J. Cazin, H. Jacobsen, L. Cavallo, M. Heinekey, S. P. Nolan, *Angew. Chem. Int. Ed.* **2009**, *48*, 5182.
- [311] K. Kudo, M. Hidai, Y. Uchida, *J. Organomet. Chem.* **1973**, *56*, 413.
- [312] K. M. Gligorich, S. A. Cummings, M. S. Sigman, *J. Am. Chem. Soc.* **2007**, *129*, 14193.
- [313] P. M. Henry, *J. Am. Chem. Soc.* **1972**, *94*, 7316.
- [314] R. Cramer, R. V. Lindsey, *J. Am. Chem. Soc.* **1966**, *88*, 3534.
- [315] S. Bhaduri, D. Mukesh, *Homogeneous Catalysis - Mechanisms and Industrial Applications*, John Wiley & Sons, New York, **2000**.
- [316] D. D. Beck, J. W. Sommers, C. L. DiMaggio, *Appl. Catal. B* **1994**, *3*, 205.
- [317] P. Albers, J. Pietsch, S. F. Parker, *J. Mol. Catal. A* **2001**, *173*, 275.
- [318] S. O. Ojwach, I. A. Guzei, J. Darkwa, *Journal of Organometallic Chemistry* **2009**, *694*, 1393.
- [319] L. Canovese, F. Visentin, C. Santo, A. Dolmella, *J. Organomet. Chem.* **2009**, *694*, 411.
- [320] M. Bovens, A. Togni, L. M. Venanzi, *J. Organomet. Chem.* **1993**, *451*, C28.

- [321] S. O. Ojwach, I. A. Guzei, J. Darkwa, S. F. Mapolie, *Polyhedron* **2007**, *26*, 851.
- [322] N. Arroyo, F. G.-d. I. Torre, F. A. Jalón, B. R. Manzano, B. Moreno-Lara, A. M. Rodríguez, *J. Organomet. Chem.* **2000**, *603*, 174.
- [323] K. Li, M. S. Mohlala, T. V. Segapelo, P. M. Shumbula, I. A. Guzei, J. Darkwa, *Polyhedron* **2008**, *27*, 1017.
- [324] J. A. Perez, J. Pons, X. Solans, M. Font-Bardia, J. Ros, *Inorg. Chim. Acta* **2005**, *358*, 617.
- [325] H. Mishra, A. Mukherjee, *J. Organomet. Chem.* **2010**, *695*, 1753.
- [326] H. Mishra, R. Mukherjee, *J. Organomet. Chem.* **2006**, *391*, 3545.
- [327] Z. Shirin, R. Mukherjee, J. F. Richardson, R. M. Buchanan, *J. Chem. Soc. Dalton Trans.* **1994**, 465.
- [328] S. O. Ojwach, I. A. Guzei, L. L. Benade, S. F. Mapolie, J. Darkwa, *Organometallics* **2009**, *28*, 2127.
- [329] P. Kaur, A. Sarangal, S. Kaur, *J. Coord. Chem.* **2008**, *61*, 3839.
- [330] M. Gennari, M. Lanfranchi, L. Marchio, *Inorg. Chim. Acta* **2009**, *362*, 4430.
- [331] E. A. B. Kantchev, C. J. O'Brien, M. J. Organ, *Angew. Chem. Int. Ed.* **2007**, *46*, 2768.
- [332] P. V. Simpson, B. W. Skelton, D. H. Brown, M. V. Baker, *Eur. J. Inorg. Chem.* **2011**, *12*, 1937.
- [333] M. V. Baker, D. H. Brown, P. V. Simpson, B. W. Skelton, A. H. White, *Eur. J. Inorg. Chem.* **2009**, *13*, 1977.
- [334] H. V. Huyun, J. H. H. Ho, T. C. Neo, L. L. Koh, *J. Organomet. Chem.* **2005**, *690*, 3854.
- [335] H. V. Huyun, T. C. Neo, G. K. Tan, *Organometallics* **2006**, *25*, 1298.
- [336] I. Ösdemir, M. Yigit, E. Cetinkaya, B. Cetinkaya, *Appl. Organometal. Chem.* **2006**, *20*, 187.
- [337] S. Gülcemal, S. Kahraman, J.-C. Daran, E. Cetinkaya, B. Cetinkaya, *J. Organomet. Chem.* **2009**, *649*, 3580.
- [338] A. Biffis, C. Tubaro, G. Buscemi, M. Basato, *Adv. Synth. Catal.* **2008**, *350*, 189.
- [339] S. K. U. Riederer, P. Gigler, M. P. Högerl, E. Herdtweck, B. Bechlars, W. A. Herrmann, F. E. Kühn, *Organometallics* **2010**, *29*, 5681.
- [340] C. H. Leung, C. D. Incarvito, R. H. Crabtree, *Organometallics* **2006**, *25*, 6099.

- [341] G. D. Frey, C. F. Rentzsch, D. Preysing, T. Scherg, M. Mühlhofer, E. Herdtweck, W. A. Herrmann, *J. Organomet. Chem.* **2006**, 691, 5725.
- [342] C. Radloff, H.-Y. Gong, C. Schulte to Brinke, T. Pape, V. M. Lynch, J. L. Sessler, F. E. Hahn, *Chem. Eur. J.* **2010**, 16, 13077.
- [343] F. E. Hahn, T. Fehren, T. Lügger, *Inorg. Chim. Acta* **2005**, 358, 4137.
- [344] Z. Liu, M. Shi, *Organometallics* **2010**, 29, 2831.
- [345] W. Wang, T. Zhang, M. Shi, *Organometallics* **2009**, 28, 2640.
- [346] T. Chen, J.-J. Jiang, Q. Xu, M. Shi, *Org. Lett.* **2007**, 9, 865.
- [347] M. Shi, H.-x. Quian, *Tetrahedron* **2005**, 61, 4949.
- [348] P. V. G. Reddy, S. Tabassum, A. Blanrue, R. Wilhelm, *Chem. Commun.* **2009**, 5910.
- [349] R. D. Gillard, P. D. Newman, R. S. Vagg, P. A. Williams, *Inorg. Chim. Acta* **1995**, 233, 79.
- [350] D. Jaramillo, D. P. Buck, J. G. Collins, R. R. Fenton, F. H. Stootman, N. J. Wheate, J. R. Aldrich-Wright, *Eur. J. Inorg. Chem.* **2006**, 4, 839.
- [351] J.-S. Yang, C.-W. Ko, *J. Org. Chem.* **2006**, 71, 844.
- [352] J.-S. Yang, J.-L. Yan, Y.-X. Jin, W.-T. Sun, M.-C. Yang, *Org. Lett.* **2009**, 11, 1429.
- [353] C. B. Gilley, Y. Kobayashi, *J. Org. Chem.* **2008**, 73, 4198.
- [354] S. Gonell, M. Poyatos, J. A. Mata, E. Peris, *Organometallics* **2011**, 30, 5985.
- [355] F. E. Hahn, M. Foth, *J. Organomet. Chem.* **1999**, 585, 241.
- [356] H. V. Huynh, J. H. H. Ho, T. C. Neo, L. L. Koh, *J. Organomet. Chem.* **2005**, 690, 3854.
- [357] M. Shi, H. Qian, *Tetrahedron* **2005**, 61, 4949.
- [358] T. A. P. Paulose, J. A. Olson, J. W. Quail, S. R. Foley, *J. Organomet. Chem.* **2008**, 693, 3405.
- [359] I. J. B. Lin, C. S. Vasam, *Coord. Chem. Rev.* **2007**, 251, 642.
- [360] for entries 4 - 11 see: C. Böhling, Ruprecht-Karls-Universität Heidelberg, *Advanced Internship Research Paper* **2011**.
- [361] H. W. Wanzlick, *Angew. Chem. Int. Ed.* **1960**, 1, 75.
- [362] H. W. Wanzlick, H. J. Kleiner, *Angew. Chem.* **1961**, 73, 493.
- [363] H. W. Wanzlick, F. Esser, H. J. Kleiner, *Chem. Ber.* **1963**, 96, 1208.

- [364] H. W. Wanzlick, H. J. Schönherr, *Angew. Chem. Int. Ed.* **1968**, *7*, 141.
- [365] K. J. Öfele, *Organomet. Chem.* **1968**, *12*, 42.
- [366] A. J. Arduengo, III, R. L. Harlow, M. J. Kline, *J. Am. Chem. Soc.* **1991**, *113*, 2801.
- [367] F. Glorius, *Topics in Organometallic Chemistry, Vol. 21*, Springer, Berlin, **2010**.
- [368] S. P. Nolan, *N-Heterocyclic Carbenes in Synthesis*, Wiley-VCH, Weinheim, **2006**.
- [369] W. A. Herrmann, *Angew. Chem. Int. Ed.* **2002**, *41*, 1290.
- [370] F. E. Hahn, M. C. Jahnke, *Angew. Chem. Int. Ed.* **2008**, *47*, 3122.
- [371] S. Díez-González, S. P. Nolan, *Coord. Chem. Rev.* **2007**, *251*, 874.
- [372] H. Clavier, A. Correa, L. Cavallo, E. C. Escudero-Adán, J. Benet-Buchholz, A. M. Z. Slawin, S. P. Nolan, *Eur. J. Inorg. Chem.* **2009**, *27*, 1767.
- [373] A. Poater, B. Cosenza, A. Correa, S. Giudici, F. Ragone, V. Scarano, L. Cavallo, *Eur. J. Inorg. Chem.* **2009**, *27*, 1759.
- [374] C. A. Tolman, *Chem. Rev.* **1977**, *77*, 313.
- [375] C. M. Crudden, D. P. Allen, *Coord. Chem. Rev.* **2004**, *248*, 2247.
- [376] V. César, S. Bellemin-Laponnaz, L. H. Gade, *Chem. Soc. Rev.* **2004**, *33*, 619.
- [377] R. E. Douthwaite, *Coord. Chem. Rev.* **2007**, *251*, 702.
- [378] D. Rix, S. Labat, L. Toupet, C. Crévisy, M. Mauduit, *Eur. J. Inorg. Chem.* **2009**, *13*, 1989.
- [379] A. O. Larsen, W. Leu, C. N. Oberhuber, J. E. Campbell, A. H. Hoveyda, *J. Am. Chem. Soc.* **2004**, *126*, 11130.
- [380] D. G. Gillingham, O. Kataoka, S. B. Garber, A. H. Hoveyda, *J. Am. Chem. Soc.* **2004**, *126*, 12288.
- [381] D. R. Snead, H. Seo, S. Hong, *Curr. Org. Chem.* **2008**, *12*, 1370.
- [382] L. G. Bonnet, R. E. Douthwaite, R. Hodgson, *Organometallics* **2003**, *22*, 4384.
- [383] M. Iglesias, D. J. Beetstra, J. C. Knight, L.-L. Ooi, A. Stasch, S. Coles, L. Male, M. B. Hursthouse, K. J. Cavell, A. Dervisi, I. A. Fallis, *Organometallics* **2008**, *27*, 3279.
- [384] J. Li, I. C. Stewart, R. H. Grubbs, *Organometallics* **2010**, *29*, 3765.
- [385] X. Luan, R. Mariz, M. Gatti, C. Costabile, A. Poater, L. Cavallo, A. Linden, R. Dorta, *J. Am. Chem. Soc.* **2008**, *130*, 6848.

- [386] W. A. Herrmann, D. Basakakov, E. Herdtweck, S. D. Hoffmann, T. Bunlaksananusorn, F. Rampf, L. Rodefeld, *Organometallics* **2006**, *25*, 2449.
- [387] H. Seo, D. Hirsch-Weil, K. A. Abboud, S. Hong, *J. Org. Chem.* **2008**, *73*, 1983.
- [388] S. Würtz, F. Glorius, *Acc. Chem. Res.* **2008**, *41*, 1523.
- [389] F. Bellina, R. Rossi, *Chem. Rev.* **2010**, *110*, 1082.
- [390] U. Christmann, R. Vilar, *Angew. Chem. Int. Ed.* **2005**, *44*, 366.
- [391] J. E. M. N. Klein, R. J. K. Taylor, *Eur. J. Org. Chem.* **2011**, *34*, 6821.
- [392] S. Lee, J. F. Hartwig, *J. Org. Chem.* **2001**, *66*, 3402.
- [393] S. Würtz, C. Lohre, K. Bergander, F. Glorius, *J. Am. Chem. Soc.* **2009**, *131*, 8344.
- [394] X. Luan, R. Mariz, C. Robert, M. Gatti, S. Blumentritt, A. Linden, R. Dorta, *Org. Lett.* **2008**, *10*, 5569.
- [395] Y.-X. Jia, D. Katayev, G. Bernardinelli, T. M. Seidel, E. P. Kündig, *Chem. Eur. J.* **2010**, *16*, 6300.
- [396] E. P. Kündig, T. M. Seidel, Y.-X. Jia, G. Bernardinelli, *Angew. Chem. Int. Ed.* **2007**, *46*, 8484.
- [397] Y.-X. Jia, J. M. Hillgren, E. L. Watson, S. P. Marsden, E. P. Kündig, *Chem. Commun.* **2008**, 4040.
- [398] L. Liu, N. Ishida, S. Ashida, M. Murakami, *Org. Lett.* **2011**, *13*, 1666.
- [399] F. Glorius, G. Altenhoff, R. Goddard, C. W. Lehmann, *Chem. Commun.* **2002**, 2704.
- [400] A. Binobaid, M. Iglesias, D. J. Beetstra, B. Kariuki, A. Dervisi, I. A. Fallis, K. J. Cavell, *Dalton Trans.* **2009**, 7099.
- [401] M. Mayr, K. Wurst, K.-H. Ongania, M. R. Buchmeiser, *Chem. Eur. J.* **2004**, *10*, 1256.
- [402] U. Siemeling, C. Färber, M. Leibold, C. Bruhn, P. Mücke, R. Winter, B. Sarkar, M. Hopffgarten, G. Frenking, *Eur. J. Inorg. Chem.* **2009**, *31*, 4607.
- [403] P. Bazinet, G. P. A. Yap, D. S. Richeson, *J. Am. Chem. Soc.* **2003**, *125*, 13314.
- [404] V. César, N. Lugan, G. Lavigne, *J. Am. Chem. Soc.* **2008**, *130*, 11286.
- [405] P. Bazinet, T.-G. Ong, J. S. O'Brien, N. Lavoie, E. Bell, G. P. A. Yap, I. Korobkov, D. S. Richeson, *Organometallics* **2007**, *26*, 2885.
- [406] P. D. Newman, K. J. Cavell, B. M. Kariuki, *Organometallics* **2010**, *29*, 2724.
- [407] C. C. Scarborough, I. A. Guzei, S. S. Stahl, *Dalton Trans.* **2009**, 2284.

- [408] M. Iglesias, D. J. Beetstra, B. M. Kariuki, K. J. Cavell, A. Dervisi, I. A. Fallis, *Eur. J. Inorg. Chem.* **2009**, *13*, 1913.
- [409] C. C. Scarborough, M. J. W. Grady, I. A. Guzei, B. A. Gandhi, E. E. Bunel, S. S. Stahl, *Angew. Chem. Int. Ed.* **2005**, *44*, 5269.
- [410] W. Y. Lu, K. J. Cavell, J. S. Wixey, B. Kariuki, *Organometallics* **2011**, *asap*.
- [411] D. Riedel, Ruprecht-Karls-Universität Heidelberg, *Dissertation*, to be submitted **2012**.
- [412] A. S. K. Hashmi, C. Lothschütz, *N-heterocyclic Carbene Complexes, their Preparation and Use*, 2010-10-28, patent application.
- [413] A. S. K. Hashmi, C. Lothschütz, C. Böhling, T. Hengst, C. Hubbert, F. Rominger, *Adv. Synth. Catal.* **2010**, *352*, 3001.
- [414] A. S. K. Hashmi, C. Lothschütz, C. Böhling, F. Rominger, *Organometallics* **2011**, *30*, 2411.
- [415] A. S. K. Hashmi, C. Lothschütz, K. Graf, T. Häffner, A. Schuster, F. Rominger, *Adv. Synth. Catal.* **2011**, *353*, 1407.
- [416] A. S. K. Hashmi, T. Hengst, C. Lothschütz, F. Rominger, *Adv. Synth. Catal.* **2010**, *352*, 1315.
- [417] F. J. Fananas, A. Granados, R. Sanz, J. M. Ignacio, J. Barluenga, *Chem. Eur. J.* **2001**, *7*, 2896.
- [418] J. Barluenga, F. J. Fananas, R. Sanz, Y. Fernandez, *Chem. Eur. J.* **2002**, *8*, 2034.
- [419] H. W. Thompson, S. Y. Rashid, *J. Org. Chem.* **2002**, *67*, 2813.
- [420] U. S. Sorensen, E. P.-Villar, *Helv. Chim. Acta* **2004**, *87*, 82.
- [421] T. Dröge, F. Glorius, *Angew. Chem. Int. Ed.* **2010**, *49*, 6940.
- [422] H. E. Gottlieb, V. Kotlyar, A. Nudelmann, *J. Org. Chem.* **1997**, *62*, 7512.
- [423] F. Dallacker, U. Klaus, L. Maria, *Liebigs Ann. Chem.* **1963**, *667*, 50.
- [424] F. Dallacker, J. Alrogen, H. Krings, B. Lauris, M. Lipp, *Liebigs Ann. Chem.* **1961**, *647*, 26.
- [425] W. Hüchel, P. Rieckmann, *Justus Liebigs Ann. Chem.* **1959**, *625*, 1.
- [426] M. A. Andrews, T. C.-T. Chang, C.-W. Cheng, T. J. Emge, K. P. Kelly, T. F. Koetzle, *J. Am. Chem. Soc.* **1984**, *106*, 5913.
- [427] W. Duczmal, N. Malgorzata, E. Sliwinska, *Trans. Met. Chem.* **2003**, *28*, 756.

Appendix

Erklärung

Die vorliegende Arbeit entstand unter Anleitung von Herrn Prof. Dr. Oliver Trapp am Organisch-Chemischen Institut der Ruprecht-Karls-Universität Heidelberg in der Zeit von Januar 2009 bis Dezember 2011.

Gemäß § 8 (3) b) und c) der Promotionsordnung der Ruprecht-Karls-Universität Heidelberg für die Naturwissenschaftlich-Mathematische Gesamtfakultät erkläre ich hiermit, dass ich die vorgelegte Dissertation selbst verfasst und mich keiner anderen als der von mir ausdrücklich bezeichneten Quellen bedient habe und dass ich an keiner anderen Stelle ein Prüfungsverfahren beantragt bzw. die Dissertation in dieser oder anderer Form bereits anderswertig als Prüfungsarbeit verwendet oder an einer anderen Fakultät als Dissertation vorgelegt habe.

Heidelberg, den 14.02.2012

.....

Markus J. Spallek

Academic Teachers

My academic teachers:

Prof. Dr. T. Bein, Prof. Dr. T. Carell, Prof. Dr. J. Evers, Prof. Dr. M. Heuschmann, Prof. Dr. D. Johrendt, Prof. Dr. K. Karagiosoff, Prof. Dr. T. M. Klapötke, Prof. Dr. P. Klüfers, Prof. Dr. P. Knochel, Prof. Dr. A. Kornath, Prof. Dr. H. Langhals, Prof. Dr. I.-P. Lorenz, Prof. Dr. M. T. Reetz, Prof. Dr. H. Mayr, Prof. Dr. H. R. Pfändler, Prof. Dr. W. Schnick, Prof. Dr. K. Sünkel, Prof. Dr. F. Schüth, Prof. Dr. O. Trapp, Prof. Dr. R. de Vivie-Riedle, Prof. Dr. W. Thiel, Prof. Dr. J. Winterlin, Prof. Dr. H. Zipse.